Proceedings of the 17th International Students Conference "Modern Analytical Chemistry"

Prague, 16—17 September 2021

Edited by Karel Nesměrák

FACULTY OF SCIENCE
Charles University

Prague 2021

Proceedings of the
17th International Students Conference
"Modern Analytical Chemistry"

Proceedings of the 17th International Students Conference "Modern Analytical Chemistry"

Prague, 16—17 September 2021

Edited by Karel Nesměrák

FACULTY OF SCIENCE
Charles University

Prague 2021

KATALOGIZACE V KNIZE – NÁRODNÍ KNIHOVNA ČR

Modern Analytical Chemistry (konference) (17. : 2021 : Praha, Česko)
Proceedings of the 17th international students conference "Modern Analytical Chemistry" : Prague, 16–17 September 2021 / edited by Karel Nesměrák. – 1st edition. – Prague : Faculty of Science, Charles University, 2021. – vi, 249 stran
Obsahuje bibliografie a rejstříky

ISBN 978-80-7444-089-2 (brožováno)

* 543 * (062.534)
– analytická chemie
– sborníky konferencí

543 - Analytická chemie [10]

The electronic version of the Proceedings is available at the conference webpage:
http://www.natur.cuni.cz/isc-mac/

ISBN 978-80-7444-089-2

Preface

Although scientific research has been significantly affected by the Covid-19 pandemic for over a year, the possibility to present their scientific achievements and share the experience made brought sixty young analytical chemists from five countries to Prague, Czech Republic, to attend the 17th International Student Conference "Modern Analytical Chemistry". Being the embodiment of the future of analytical chemistry, the representatives of thirteen European universities actively engaged in vivid discussions exchanging their ideas and accomplishments made in the fields of our science. The zeal of their presentations painted the most promising and very encouraging picture of the future development of analytical science. In addition, participation in the conference further cultivated the presentation and language skills of the participants.

A total of forty-one conference participants decided to publish the full texts of their papers, which thus form these proceedings. The contributions are sorted by the delivery date and supplemented by indexes allowing easy navigation through the pages. The topics of the papers cover all three areas of instrumental analysis (i.e., electrochemical, separation, and spectral methods) and their application to solving tasks for human society, but touch also on general issues of analytical chemistry. Hopefully, the reader will get interesting, beneficial, and enjoyable reading.

As in previous years, the Division of Analytical Chemistry of the European Chemical Society and the Working Group of Analytical Chemistry of the Czech Chemical Society shield the conference.

We are very grateful to our sponsors, not only for their kind sponsorship making the conference possible but also for all their cooperation and support in many of our other activities.

doc. RNDr. Karel Nesměrák, Ph.D., *editor*

Sponsors

The organizers of 17th International Students Conference "Modern Analytical Chemistry" gratefully acknowledge the generous sponsorship of following companies:

cz.vwr.com

www.thermofisher.cz

www.lach-ner.com

www.metrohm.com

www.optikinstruments.cz

www.quinta.cz

www.2theta.cz

www.waters.com

www.zentiva.cz

Contents

Characterization and functionalization of biosilica composite

Hussam AL Saoud[a,*], Michał Kawalec[a], Boguslaw Buszewski[b]

[a] *Bialystok University of Technology, Faculty of Mechanical Engineering, Department of Materials Engineering and Production, Wiejska 45C, 15-351, Bialystok, Poland* ✉ *h.alsaoud@pb.edu.pl*
[b] *Nicolaus Copernicus University, Interdisciplinary Centre of Modern Technologies, Wileńska 4, 87-100 Toruń, Poland*

Keywords
biosilica
characterize
diatom
functionalization

Abstract
Biosilica is an inorganic polymer formed by orthosilicate units of organisms such as diatoms or silica sponges, in which two groups of silanol are bound together to form a single bond or siloxane. Biosilica has been used in various uses, such as water treatment systems, pharmaceutical applications, and as a tool for drug delivery systems. The surface of the amorphous silica exhibits high levels of free reactive hydroxyl groups (−OH) which can be used to modify the frustule with chemical groups ($-NH_2$, −COOH, −SH, and −CHO). These groups are suitable for the binding of various biomolecules to diatoms (i.e., enzymes, proteins, antibodies, peptides, DNA). The aim of this study characterizes bare diatoms shells and functionalization by various physical-chemical techniques comprising scanning electron microscopy, transmission electron microscopy, FTIR, and Raman spectroscopy.

1. Introduction

The Diatoms are single-celled, eukaryotic, photosynthetic algae common in water ecosystems [1]. Diatoms can be easily obtained from the environment, their culture requires environmental conditions and does not involve any expensive media or costly instruments, as well as being able to be transported in small quantities and proliferated from that scratch to a desirable confluence, so they are an outstanding cost-effective industrial raw material [2]. There are 10 000 diatoms organisms, and they have special silica (hydrated silicon dioxide) cell walls called frustules [3]. The most attractive features of frustules are that they have a porous structure, a high specific surface area, special optical effects, and high mechanical strength [4]. Diatom Biosilica consists primarily of amorphous, hydrated SiO_2 (silica) containing a small proportion of organic macromolecules long-speculated for the control of silica deposition and nanopatterns [5]. Diatom biosilica consists of two distinct building blocks: valves produced during cell division and girdle bands generated during interphase processes [6]. Biosilica is

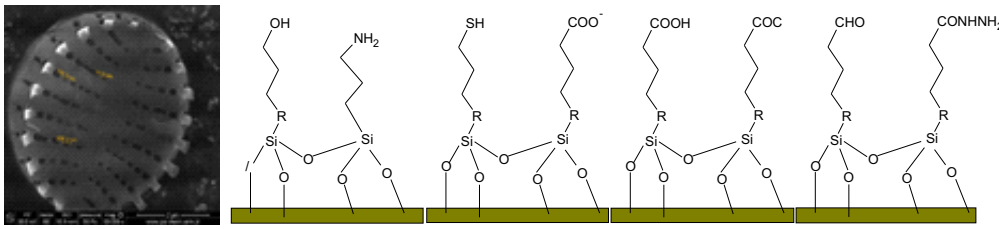

Fig. 1 (a) Bare diatom biosilica, (b) diatom structure with scheme their surface functionalization's using different organosilanes. Amoxicillin was used as a model drug.

an inorganic polymer formed by orthosilicate units of organisms such as diatoms or silica sponges, in which two groups of silanol are bound together to form a single bond or siloxane [7]. Amoxicillin is a phenolic agent used internationally to treat serious respiratory, gastrointestinal, urinary, and skin infections as an antibiotic [8]. This antibiotic includes a number of functional groups, including hydroxyl, carbonyl, and amino groups, which can interact with the biosilica surface [9]. In this work, we detect the characterization of bare diatom silica shells using different physical-chemical techniques like microscopy (scanning electron microscopy, SEM, transmission electron microscopy, TEM), FTIR, and Raman spectroscopy. The second step of this study was functionalization of the surface by different modifiers and introducing new interaction side Fig. 1.

2. Experimental

2.1 Procedures of cleaning diatom frustules

The diatoms culture was separated from the culture media after eight days by decantation and washed five times with distilled water using centrifuged at 3000 rpm for 10 minutes to remove dissolved salts. After that, the diatom biomass was dried at 80 °C without being allowed to completely dry. After that, 30% (v/v) aqueous hydrogen peroxide was applied and left for 2 hours at 80 °C to oxidize the organic matter of diatom cells, with a few drops of 37% (v/v) HCl added at the end of the process to remove the residual hydrogen peroxide and carbonates [10, 11].

2.2 Methods

The scanning electron microscopy (SEM/FIB – Quanta 3D FEG) has studied the morphological and structural characteristics of diatom biosilica.

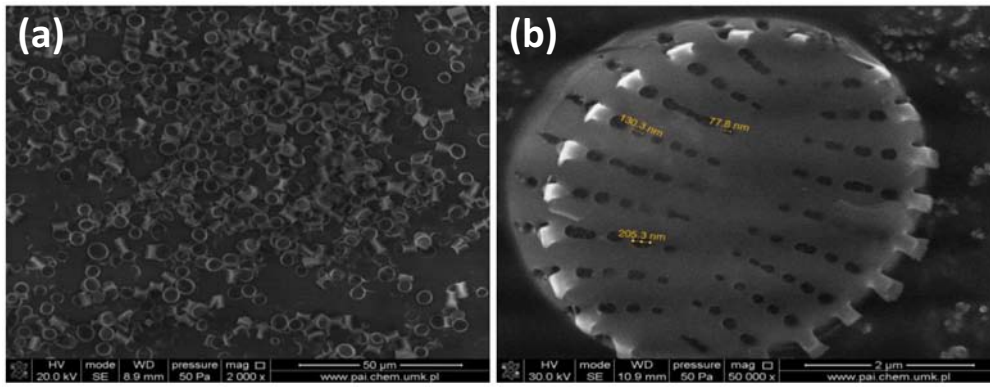

Fig. 2 Scanning electron microscopy images of diatom biosilica at (a) 2 000× magnicicatiion, and (b) 50 000× magnification

3. Results and discussion

3.1 The morphology, structure, and elemental composition

Scanning electron microscopy offered a description of the arrangement and morphology of a diatom biosilica at various magnifications (Fig.2). Fig. 2a shows a macroscopic image of the dried diatom frustules (biosilica). Fig. 2b presents reveal the intricate design of the external surface of a single diatom valve and the pore size is in the range of 77.8–205.3 nm. Sprynskyy et al. [12] was studied the characteristic of biosilica by scanning electron microscopy and they found the pore size is in the range of 150–200 nm.

3.2 Surface functionalization of diatom biosilica

Silica and other supports can be functionalized with various functional groups utilizing substitution reactions among the organosilanes, and silanol moieties present on the silica surface [13]. Adding polar functional groups to the silica sorbent surface, such as cyano-, amine-, and diol-, results in normal phase sorbents that extract the polar analyte from the polar medium through hydrophilic interaction [14]. Fig. 3 depicts a regular diatom biosilica structure as well as a schematic diagram of proposed surface modifications, including self-assembled organic monolayers based on various organosilanes. Organosilanes with amino functional groups, such as 3-aminopropyltriethoxy silane was chosen because they are popular surface modification agents with a broad range of applications in promoting steady adsorption between organic compounds (proteins, drugs) and silica substrates [15].

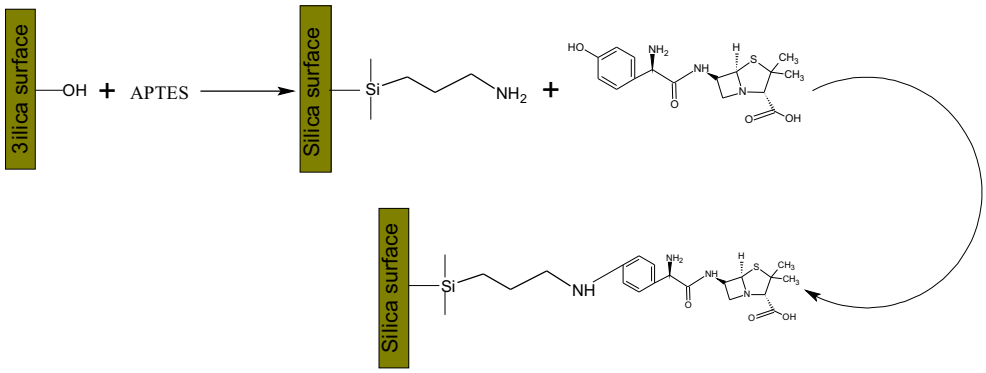

Fig. 3 Synthetic process of amoxicillin – 3-aminopropyltriethoxy silane

4. Conclusions

As the result of the functionalization of bare diatom silica, we obtain a new composite material that will be used as packing of solid-phase extraction and chromatographic column. The study result clearly revealed that diatom biosilica is considering a very useful material as a drug carrier because of its highly organized shapes, wide surface areas, high mechanical resistance, as well as biodegradability, and biocompatibility.

Acknowledgments

This work financed by the BIOG-NET project (POIR.04.04.00-IW.04-00-TN1/18).

References

[1] Medarević Đ., Losić D., Ibrić S.: Diatoms-nature materials with great potential for bioapplications. *Hem. Ind.* **70** (2016), 613–627.

[2] Mishra M., Arukha A.P., Bashir T., Yadav D., Prasad G.B.K.S.: All new faces of diatoms: potential source of nanomaterials and beyond. *Front. Microbiol.* **8** (2017), 1239.

[3] Venkatesan J., Lowe B., Kim S.K.: Application of diatom biosilica in drug delivery. In: *Handbook of Marine Microalgae*. S.K. Kim (ed.). Amsterdam, Elsevier 2015, p. 245–254.

[4] Jiang W., Luo S., Liu P., Deng X., Jing Y., Bai C., Li J.: Purification of biosilica from living diatoms by a two-step acid cleaning and baking method. *J. Appl. Phycol.* **26** (2013), 1511–1518.

[5] Adams L.A., Essien E.R., Adesalu A.T., Julius M.L.: Bioactive glass 45S5 from diatom biosilica. *J. Sci.: Adv. Mater. Devices* **2** (2017) 476–482.

[6] Görlich S., Pawolski D., Zlotnikov I., Kröger N.: Control of biosilica morphology and mechanical performance by the conserved diatom gene Silicanin-1. *Commun. Biol.* **2** (2018), 1–8.

[7] Müller W.E., Schröder H.C., Burghard Z., Pisignano D., Wang X.: Silicateins–A novel paradigm in bioinorganic chemistry: Enzymatic synthesis of inorganic polymeric silica. *Chem. – Eur. J.* **19** (2013), 5790–5804.

[8] Marra M.C., Cunha R.R., Muñoz R.A.A., Batista A.D., Richter E.M.: Single-run capillary electrophoresis method for the fast simultaneous determination of amoxicillin, clavulanate, and potassium. *J. Sep. Sci.* **40** (2017), 3557–3562.

[9] Rogowska A., Rafińska K., Pomastowski P., Walczak J., Railean-Plugaru V., Buszewska-Forajta M., Buszewski B.: Silver nanoparticles functionalized with ampicillin. *Electrophoresis* **38** (2017), 2757–2764.

[10] Jeffryes C., Gutu T., Jiao J., Rorrer G.L.: Two-stage photobioreactor process for the metabolic insertion of nanostructured germanium into the silica microstructure of the diatom *Pinnularia* sp. *Mater. Sci. Eng, C* **28** (2017), 107–118.

[11] Xiong Z., Li T.: Cleaning of marine sediment samples for large diatom stable isotope analysis. *J. Earth Sci.* **23** (2012), 161–172.

[12] Sprynskyy M., Pomastowski P., Hornowska M., Król A., Rafińska K., Buszewski B.: Naturally organic functionalized 3D biosilica from diatom microalgae. *Mater. Des.* **132** (2017), 22–29.

[13] Žuvela P., Skoczylas M., Jay Liu J., Bączek T., Kaliszan R., Wong M.W., Buszewski B.: Column characterization and selection systems in reversed-phase high-performance liquid chromatography. *Chem. Rev.* **119** (2019), 3674–3729.

[14] Buszewski B., Szultka M.: Past, present, and future of solid phase extraction: A review. *Crit. Rev. Anal. Chem.* **42** (2012), 198–213.

[15] Aw M.S., Bariana M., Yu Y., Addai-Mensah J., Losic D.: Surface-functionalized diatom microcapsules for drug delivery of water-insoluble drugs. *J. Biomater. Appl.* **28** (2012), 163–174.

Determination of antibiotic resistance using different analytical methods

Dominika Błońska[a, *], Michał Złoch[b],Paweł Pomastowski[a, b], Małgorzata Szultka-Młyńska[a], Bogusław Buszewski[a, b]

[a] *Nicolaus Copernicus University in Toruń, Faculty of Chemistry, Department of Environmental Chemistry and Bioanalytics, Gagarina 7, 87 100 Toruń, Poland* ✉ *dominikab10@gmail.com*
[b] *Nicolaus Copernicus University in Toruń, Centre for Modern Interdisciplinary Technologies, Wileńska 4, 87 100 Toruń, Poland*

Keywords
antibiotic resistance
bacteria
carbapenems
E-test
MALDI-TOF/MS

Abstract
Inappropriate use and overuse of antibiotics, e.g., carbapenems, has led to the rapid emergence of antibiotic resistance among microorganisms around the world, which causes problems with selecting an appropriate treatment for patients suffering from bacterial infections. Identification of pathogens and rapid detection of drug resistance are crucial for the fast diagnosis and effective treatment and can be carried out after obtaining pure cultures if bacterial isolate from clinical specimens such as urine, blood, saliva, or wound swabs. For pathogens identification and drugs resistance indication, different methods like E-test strips, Matrix-assisted laser desorption-/ionization time-of-flight mass spectrometry (MALDI-TOF/MS) and Polymerase Chain Reaction (PCR) are used. Therefore, the main objective of the present study was to analyze drug resistance among various *Enterobacterales* and *P. aeruginosa* strains using two different methods: E-test strips and MBT-STAR Carba assay (MALDI-TOF/MS technique).

1. Introduction

Antibiotics are chemicals produced by living organisms, mainly microorganisms, that are used to treat infections caused by pathogens. The overuse and inadequate use of antimicrobials have resulted in the development of numerous mechanisms in bacteria that made them resistant to antibiotics [1]. Carbapenems, e.g., imipenem, meropenem, belonging to the group of β-lactam antibiotics, exhibit a broad spectrum of antimicrobial activity and are less susceptible to most of the β-lactam resistance mechanisms, making them considered the most reliable last resort antibiotics. For these reasons, the emergence of resistance to carbapenems (mainly in Gram-negative bacteria), is a global problem, that threatens human health and life. In order to quickly diagnose and select the appropriate therapy, it is

necessary to analyze and identify both bacteria and antibiotic resistance markers [2]. For this purpose, methods such as E-test, Matrix - assisted laser desorption/-ionization with a time-of-flight analyzer combined with mass spectrometry (MALDI-TOF/MS), or Polymerase Chain Reaction (PCR) are used [3]. The most frequently used methods in routine clinical laboratories include classical techniques with the inoculation of bacteria on selective media and/or with the performance of appropriate biochemical tests. These include, for example, strip tests: E-test, which use strips coated with predefined concentrations of antibiotics, and the corresponding interpretive minimum inhibitory concentration (*MIC*) ranges are marked on its surface. E-test enables defining whether the analyzed bacteria is resistant to a given drug and to determine the *MIC* value [4]. The other method used as an identification tool in clinical diagnosis is MALDI-TOF/MS. Identification of microorganisms by this method is based on the analysis of proteins, mainly ribosomal, in the presence of a matrix. Analyzing proteins are ionized to measure their mass to charge (*m/z*) ratio, resulting in a characteristic spectrum (protein profile), which is then compared with the spectra present in the reference database, making it possible to identify the bacteria [5]. Polymerase Chain Reaction, called PCR, is a method of amplifying genetic material and is used for the rapid identification of specific nucleic acid sequences, e.g. in pathogens. Using PCR, copies of very small amounts of DNA sequences are exponentially amplified over a series of temperature cycles. The polymerase chain reaction enables the determination of antibiotic resistance genes found in bacteria [6]. Both E-test, the MALDI-TOF/MS, and the PCR can be used for the identification and effective determination of antibiotic resistance in pathogens. Spectroscopic and molecular biology methods are characterized by a much shorter analysis time than in the case of E-test, with the MALDI-TOF/MS technique being the least time-consuming, which is also less expensive than the PCR.

2. Experimental

2.1 Microorganisms

Eight *Enterobacterales* and one *P. aeruginosastrains* (nine in total), previously characterized in view of presence of different β-lactamases coding genes, were used for both: E-test technique and the MALDI-TOF/MS analysis using the MBT-STAR Carba Kit. Based on the previous PCR analysis, four bacterial strains (3, 4, 6 and 8) indicated a presence of β-lactamases from Class A in Ambler Classification among which strains 6 and 8 demonstrated carbapenemase activity (KPC producers). Four strains (strains: 3, 4, 6, 8) showed an activity of extended-spectrum β-lactamases ESBL (strains 3,6, 8 - TEM, strain 4 – unknown genes). Five strains (1–3, 5, and 9) demonstrated the presence of β-lactamases from Class B (Metallo-β-Lactamases: VIM, NDM, IMP), which have a ability to hydrolyse

imipenem. Two strains showed the presence of genes coding both ESBLs and carbapenemases: strain 3 – NDM, TEM, strain 6 – KPC, TEM.

2.2 Preparation of samples for E-test detection of Metallo β-Lactamases (MBL) in Gram-negative bacteria (IP/IPI)

Bacteria for E-test analysis were cultured on Muller Hinton Agar (Sigma Aldrich, Germany)and incubated in 37 °C for 18–24 hours in CO_2 incubator (Memmert, Germany). Isolated colonies were suspended in 0.85% sodium chloride (Sigma Aldrich, Germany) to achieve a turbidity equivalent to 0.5 McFarland standard using the densitometer DEN-1B (Biosan, Latvia). Cotton swabs were used to transfer the bacteria from solution to the agar plates. E-test MBL strips (bioMérieux, France) with imipenem–IP (in concentration range: 4–256 µg/ml) and imipenem overlaid with EDTA (IPI)(in concentration range: 1–64 µg/ml) were applied on plates with inoculated bacteria.

2.3 Preparation of samples for MALDI-TOF/MS analysis of carbapenamase activity in bacteria using MBT-STAR Carba Kit

Bacteria for MALDI-TOF/MS analysis were isolated on ColumbiaBlood Agar (Oxoid, United Kingdom) and then 1–5 isolated colonies were collected using 1µl microbial loop and suspended in MBT STAR-Carba Antibiotic Reagent (reconstituted in MBT STAR Buffer) from MBT-STAR Carba Kit (Bruker Daltonik, Germany). Prepared samples were subjected to incubation for 30–35 minutes in (35±2) °C with mixing (600–900 rpm) using Thermomixer Compact (Eppendorf, Germany. After incubation samples were centrifuged (2 min., 13 000 rpm) and 1 µl of supernatants were deposited onto the MALDI target plate (MTP 384 ground steel) and after air drying overlaid with MBT STAR Matrix solution. For each sample prepared two spots. Analyzes were conducted using ultrafleXtreme MALDI-TOF/TOF mass spectrometer (Bruker Daltonik GmbH, Germany), equipped with the smart beam-II-laser-positive mode and obtained mass spectra were subjected to smoothing and baseline correction procedure using the program flexControl (Bruker Daltonik GmbH, Germany). The collected data was analyzed using the MBT-STAR-BL Prototype (RUO) online program (Bruker, Germany). Ultrapure water for MBT STAR Calibrator was purified using the Milli-Q Reference A+ system (Bedford, USA). All samples were centrifuged on Vortex LabDancer (IKA®) or Vortex-2 Genie (Scientific Industries).

3. Results and discussion

3.1 E-test detection of Metallo β-Lactamases (MBL) in Gram-negative bacteria (IP/IPI)

In the E-test analysis for detection of Metallo β-Lactamases (MBL), after overnight incubation of investigated bacteria with E-test strips, the agar plates were observed for IP and IPI minimum inhibitory concentration values showed by the respective inhibition ellipses that intersect the strip. The bacterial strain was considered positive for MBL when the IP/IPI ratio was more than eight.

The results of E-test showed that in six of all analysed strains (strains: 2–6, 8) no MBL activity was detected (IP/IPI ratio <8, in four strains (2–5) IP/IPI = 0, strain 6: IP/IPI = 1, strain 8: IP/IPI = 4), in two of them (strains: 1, 7) the presence of MBL was indicated (IP/IPI ratio: 16, 8) and in one strain (strain 9) the MBL activity was not determinable (IP > 256, IP/IPI ratio: >128). The results are shown in Fig. 1 and Table 1.

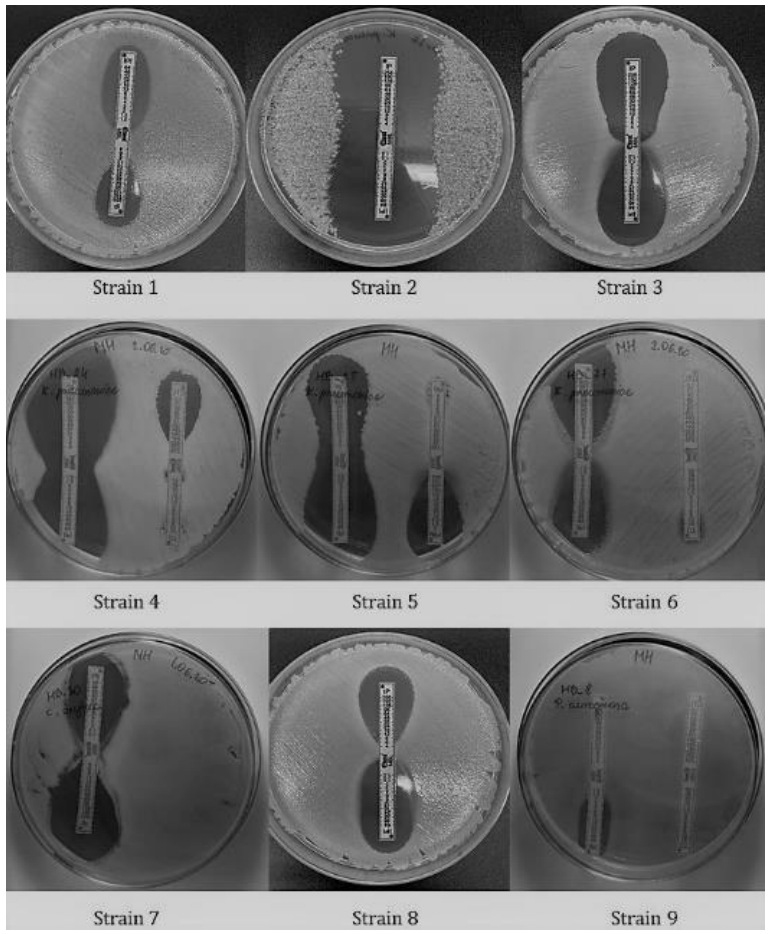

Fig. 1 Results of carbapenem-resistance detection among investigated bacteria

Table 1
Results of carbapenem-resistance detection among investigated bacteria

Strain	Species	β-lactamases	IP	IP/IPI
1	*Enterobacter cloacae*	VIM	16	16
2	*Klebsiella pneumoniae*	NDM	0	0
3	*Providencia stuartii*	NDM, TEM	0	0
4	*Klebsiella pneumoniae*	ESBL	0	0
5	*Klebsiella pneumoniae*	NDM	0	0
6	*Klebsiella pneumoniae*	KPC, TEM	4	1
7	*Klebsiella oxytoca*	KPC	8	8
8	*Klebsiella pneumoniae*	TEM	4	4
9	*Pseudomonas aeruginosa*	IMP	>256	128

IP/IPI Ratio	Result
>8	Positive
<8	Negative
>256/>64 or <4/<1	Not Determinable

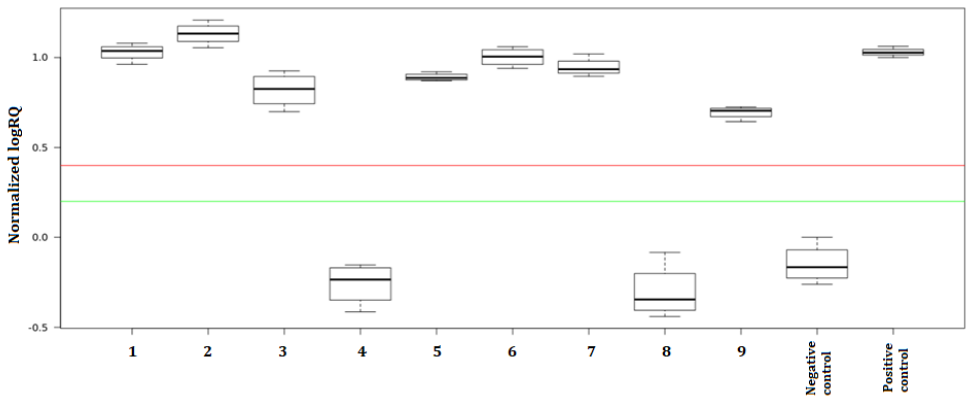

Fig. 2 Graph showing the results of carbapenemase activity level (normalized log *RQ*) among investigated bacterial strains determined using MBT STAR-Carba Kit. The graph area between the green and red lines (0.2–0.4 normalized log *RQ* values) determines the range of the unclear results of hydrolytic activity. Values: above red line (0.4) – hydrolysis; below green line (0.2) – no hydrolysis.

3.2 MALDI-TOF/MS analysis of carbapenamese activity in bacteria using MBT-STAR Carba Kit

The MALDI-TOF/MS analysis of investigated bacteria using MBT-STAR Carba Kit and data analysis by MBT STAR-BL Prototype (RUO) online program allowed to obtain the results showing the level of carbapenemase activity among the bacteria. As shown in the Fig. 2., seven of analysed bacteria strains (strains: 1–3, 5–7, and 9) show a carbapenemase activity (positive result), and only two of them (strain: 4, 8) gave a negative result of the analysis, which indicates no carbapene-

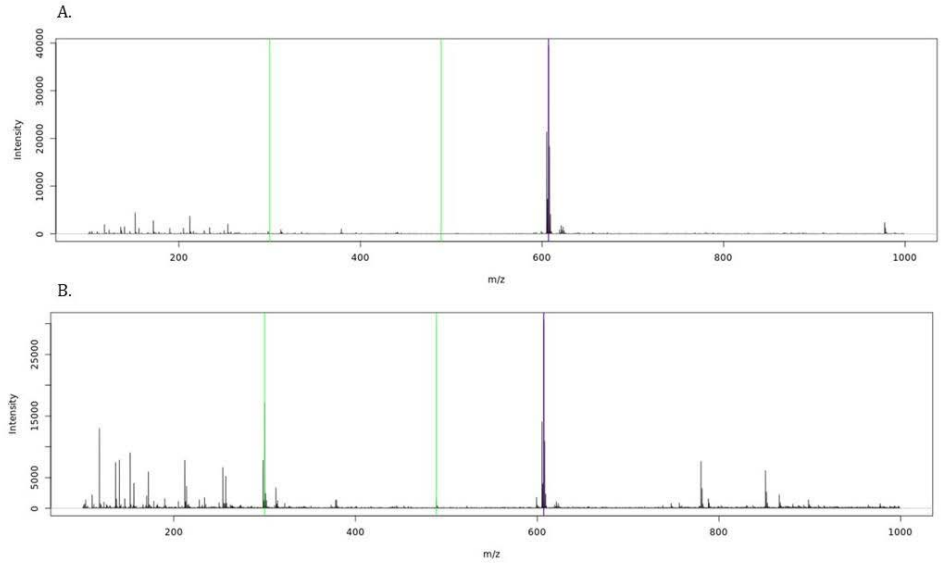

Fig. 3 Exemplary mass spectra of the investigated (A) positive (strain 2) and (B) negative (strain 4) bacterial strains obtained from MBT STAR-BL Prototype (RUO) online program

Table 2
Investigated β-lactamase-producing bacteria with marked type of β-lactamases and hydrolytic activity value obtained using MBT STAR-Carba assay (Δ controls: quality control of the results calculated by subtracting the highest calculated original log *RQ* value of the acquired negative control spectra from the lowest calculated original log *RQ* value of the acquired positive control spectra; ≥ 0.7 means that the assay results are evaluated as accepted)

Strain	Species	β-lactamases	Mean ± SD
1	*Enterobacter cloacae*	VIM	1.03 ± 0.05
2	*Klebsiella pneumoniae*	NDM	1.13 ± 0.07
3	*Providencia stuartii*	NDM, TEM	0.82 ± 0.10
4	*Klebsiella pneumoniae*	ESBL	−0.26 ± 0.12
5	*Klebsiella pneumoniae*	NDM	0.89 ± 0.02
6	*Klebsiella pneumoniae*	KPC, TEM	1.00 ± 0.05
7	*Klebsiella oxytoca*	KPC	0.85 ± 0.05
8	*Klebsiella pneumoniae*	TEM	−0.30 ± 0.16
9	*Pseudomonas aeruginosa*	IMP	0.69 ± 0.04
Negative control	*E. coli* ATCC 25922		−0.15 ± 0.11
Positive control	*K. pneumoniae* ATCC BAA-1705		1.03 ± 0.03
Δ controls			1.39

mase activity. The results are shown in Table 2. Exemplary mass spectra of the investigated positive and negative bacteria are presented in Fig. 3.

Resistance for imipenem was indicated in two samples (1, 7) by E-test method and in 7 samples (1–3, 5–7 and 9) by MALDI-TOF/MS. Strains 1 and 7 were considered positive by both methods. Strains 2 – 6 and 8 gave a negative result by E-test

analysis, but only strains 4 and 8 didn't indicate carbapenemase activity by MALDI-TOF/MS technique (strains 2, 3, 5, 6 gave a positive result). One strain (9 - Pseudomonas aeruginosa) was not determinable because of the IP and IP/IPI ratio by strip test, but showed a carbapenemase activity using MBT-STAR CARBA analysis.

4. Conclusions

Both the E-test method and the MALDI-TOF/MS method with the use of MBT-STAR Carba KIT enable the detection of antibiotic resistance in bacteria, but in the case of the MALDI technique, resistance to imipenem was identified in a larger number of bacteria which proves the greater accuracy of the method. Moreover, the MALDI-TOF/MS is much less time consuming than the E-test method. Sample preparation and analysis can take barely a few hours, which enables quick diagnosis and selection of the appropriate therapy of bacterial infections.

Acknowledgments

This study was supported by SONATINA 2 project No. 2018/28/C/ST4/00434 from Nation Science Centre, Poland.

References

[1] Spellberg B, Gilbert D.N.: The future of antibiotics and resistance: A tribute to a career of leadership by John Bartlett. *Clin. Infect. Dis.* **59** (2014), 71–75.

[2] Meletis G.: Carbapenem resistance: overview of the problem and future perspectives. *Ther. Adv. Infect. Dis.* **3** (2016), 15–21.

[3] Vrioni G., Tsiamis C., Oikonomidis G., Theodoridou K., Kapsimali V., Tsakris A.: MALDI-TOF mass spectrometry technology for detecting biomarkers of antimicrobial resistance: Current achievements and future perspectives. *Ann. Transl. Med.* **6** (2018), 240–240.

[4] Khan Z.A., Siddiqui M.F., Park S.: Current and emerging methods of antibiotic susceptibility testing. *Diagnostics (Basel)* **9** (2019), 49.

[5] Złoch M., Pomastowski P., Maślak E., Monedeiro F., Buszewski B.: Study on molecular profiles of *Staphylococcus aureus* strains: Spectrometric approach. *Molecules* **25** (2020), 4894.

[6] Pereckaite L., Tatarunas V., Giedraitiene A.: Current antimicrobial susceptibility testing for beta-lactamase-producing *Enterobacteriaceae* in clinical settings. *J. Microbiol. Methods* **152** (2018), 154–164.

Identification of the mechanisms of antibiotic resistance on the basis of specific *m/z* values

Daria Janiszewska[a,*], Małgorzata Szultka-Młyńska[a], Michał Złoch[b], Paweł Pomastowski[b], Bogusław Buszewski[a]

[a] *Nicolaus Copernicus University in Toruń, Faculty of Chemistry, Department of Environmental Chemistry and Bioanalytics, Gagarina 7, 87 100 Toruń, Poland*
✉ *janiszewska_daria@doktorant.umk.pl*
[b] *Nicolaus Copernicus University in Toruń, Centre for Modern Interdisciplinary Technologies, Wileńska 4, 87 100 Toruń, Poland*

Keywords
antibiotic resistance
bacterial virulence
MALDI TOF-MS

Abstract
Currently, antibiotic resistance of bacteria is an extremely big problem, and infections caused by such pathogens are a threat to the health and life of patients. Depending on the therapeutic group to which they belong, antibacterial agents may affect the bacterial cell wall, inhibit replication, as well as adversely affect protein biosynthesis. By comparing the protein profiles of bacterial isolates from patients not treated with antibiotics to those who have used antibiotic therapy, it is possible to predict the mechanism of action of antibiotics, as well as confirm the presence of proteins in response to the antibacterial agents, based on the absence or presence of specific signals. The approach used may be an appropriate tool for the detection of antibacterial drug resistance. Moreover, microbiological proteomics is an important tool, not only in basic research but also provides guidelines in clinical diagnostics and antimicrobial therapy.

1. Introduction

Antibiotic resistance is the ability of microorganisms to either neutralize the action of antibiotics or remove them from their cells. Resistance can be an intrinsic or acquired trait when a bacterium that was previously sensitive to antibiotics develops resistance by mutating or acquiring foreign DNA [1]. One of the main reasons for the emergence of antimicrobial resistance is easy access, which often leads to their abuse [2]. It is extremely important to quickly identify drug-resistant bacteria as well as to learn about the mechanisms of antibiotic resistance and the mechanisms of action of the newly developed antibiotics [3]. For this purpose, the matrix-assisted laser desorption ionization time-of-flight mass spectrometry (MALDI TOF-MS) technique is used. Depending on the group of

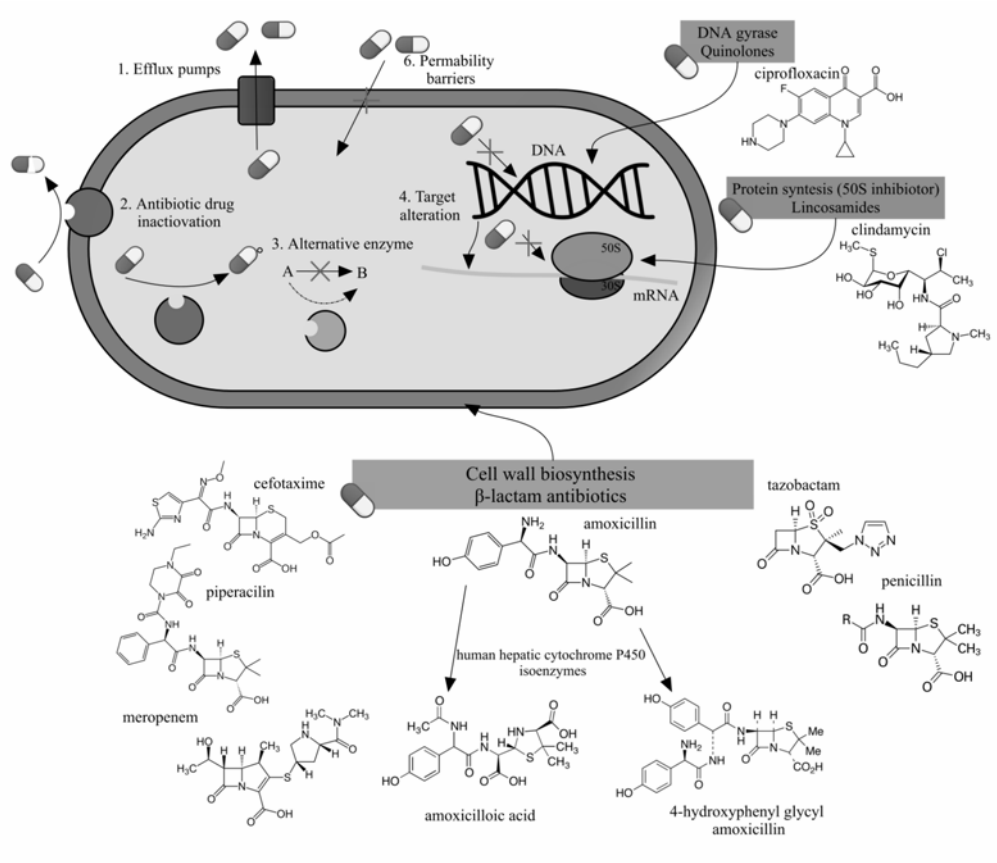

Fig. 1 Target sites and mechanisms of action of studied antibiotic in bacteria, metabolites of one of the antibiotics and the mechanisms of bacterial resistance to antibiotics

antibiotics, they may exhibit various bacteriostatic and bactericidal effects, such as inhibition of cell wall biosynthesis, interaction with ribosomal subunits, or with the genetic material of bacteria [4]. Figure 1 shows examples of antibiotics and their mechanisms of action. MALDI TOF-MS is the simplest form of mass spectrometry, successfully applied for the effective detection of bacteria in clinical samples. Identification based on MALDI TOF-MS consists of generating mass spectra representing surface proteins (analysis of whole bacterial cells) or extracted from whole cells, mainly ribosomal proteins [5]. In addition to identifying previously unknown proteins, the MALDI TOF-MS technique is successfully used in research to determine the mass of proteins and peptides [6].The aim of the research was to compare the generated protein profiles of strains derived from control patients (no antibiotic treatment) and that of subjected to antibiotic therapy based on the presence/absence of specific signals in order to predict the mechanism of action of the antibacterial drug used. For this purpose, the UniProt database was used, which allows characterizing the proteins corresponding to the signals and their potential functions.

2. Experimental

2.1 Reagents and chemicals

Non-selective media (Brain Heart Infusion Agar, Miller-Hilton Agar), and selective media (Glucose Bromocresol Purple Agar, and Vancomycin Resistance Enterococci Agar Base) were used for bacterial isolation (all from Sigma-Aldrich, Germany). HPLC-grade water, formic acid, acetonitrile, ethanol, and trifluoroacetic acid (Sigma-Aldrich, Germany) were used to prepare protein extracts of bacteria. For MALDI TOF-MS analysis acid α-cyano-4-hydroxycinnamic (Sigma-Aldrich, Switzerland) and Bacterial Test Standard (Bruker, Germany) were used.

2.2 Instrumentation

The research was carried out using the MALDI MTP 384 polished steel target (BrukerDaltonik, Germany), the MLADI Ultraflextreme II mass spectrometer (Bruker, Germany), and the FlexControl software-ultraflex TOF/TOF with the FlexAnalysys tool, the Biotyper 3.0 database (Bruker, Germany), and Universal Protein (UniProt) available online.

2.3 Sample characterization

The biological samples were superficial swabs from postoperative wounds collected from patients of the Provincial Polyclinic Hospital in Toruń. The patients treated with antibiotics (cefotaxime, clindamycin, meropenem, ciproflaxacin, metronidazole, piperacillin, tazobactam, penicillin, amoxicillin) were test samples. Patients who did not take antibiotics were control samples.

2.4 Bacteria isolation

The swabs were placed in the transport medium. Bacteria were isolated by spreading samples (100 µl) in Petri dishes containing four different growth media: Brain Heart Infusion Agar, Miller-Hilton Agar, Glucose Bromocresol Purple Agar, and Vancomycin Resistance Enterococci Agar Base. The plates were incubated at 37 °C for 24 hours. Then, the bacterial colonies were purified by the reducing method.

2.5 MALDI-TOF MS Analysis

Bacterial extracts were prepared using ethanol, formic acid, and acetonitrile. The obtained bacterial isolates were analyzed using the MALDI technique according to the Bruker protocol. After centrifugation, 1 µl of the supernatant was transferred to a MALDI target spot, dried in the air, and α-cyano-4-hydroxycinnamic matrix

Table 1
Summary of signals observed on MALDI-TOF MS spectra with characterized *m/z* values, according to the database of Universal Protein (UniProt).

m/z	Control sample	Test sample	Protein	Putative function
E. faecalis (β-lactam antibiotics: piperacillin comined with tazobactam)				
2443.330	–	+	Attenuator leader peptide	response to antibiotic
5016.225	+	–	Zinc ribbon-containing protein	inactivate β-lactams [6]
E. faecalis (quinolon with nitroimidazoles antibioiotics: ciprofloxacin combined with metronidazol)				
3343.957	+	–	Nucleotide-binding protein	nucleotide-binding
7037.987	+	–	Integrase catalytic domain-containing protein	DNA integration
8106.457	+	–	Helix-turn-helix domain-containing protein	DNA binding
E. faecalis (β-lactam antibiotic: meropenem)				
5016.225	+	–	Zinc ribbon-containing protein	inactivate β-lactams [6]

solution was applied to the same spot. Calibration was performed on the basis of Bacterial Test Standard. The generated mass spectra were analyzed using the MALDI BioTyper database in the range of 200–20 000 *m/z* values. The *m/z* values of bacteria from control patients and those treated with antibiotics were compared on the basis of the presence or absence of specific signals. Using the UniProt database, the corresponding *m/z* values of protein and their probable function in antibiotic resistance, virulence, or related to the mechanism of action of antibiotics were identified.

3. Results and discussion

Table 1 shows the specific signals identified on MALDI TOF-MS and their corresponding proteins and predicted functions from the UniProt database. The signals generated for *Enterococcus faecalis* (Fig. 2) from the control patient were compared with those obtained from patients treated with different antibiotics (piperacillin combined with tazobactam, meropenem, and ciprofloxacin combined with metronidazole).

No zinc ion binding protein signal (*m/z* = 5016.23) was observed after the use of β-lactam antibiotics. Some bacterial β-lactamases use Zn^{2+} to inactivate β-lactams [7]. The lack of this protein likely leads to a failure to develop antibiotic resistance. Additionally, after applying piperacillin with tazobactam in the test sample, a signal characteristic of the attenuator leader peptide protein (*m/z* = 2443.33) was noticed, which appears as a response to the antibiotics used.

Comparing the signals from bacterial isolates from control patients to those from patients receiving ciprofloxacin with metronidazole showed that three

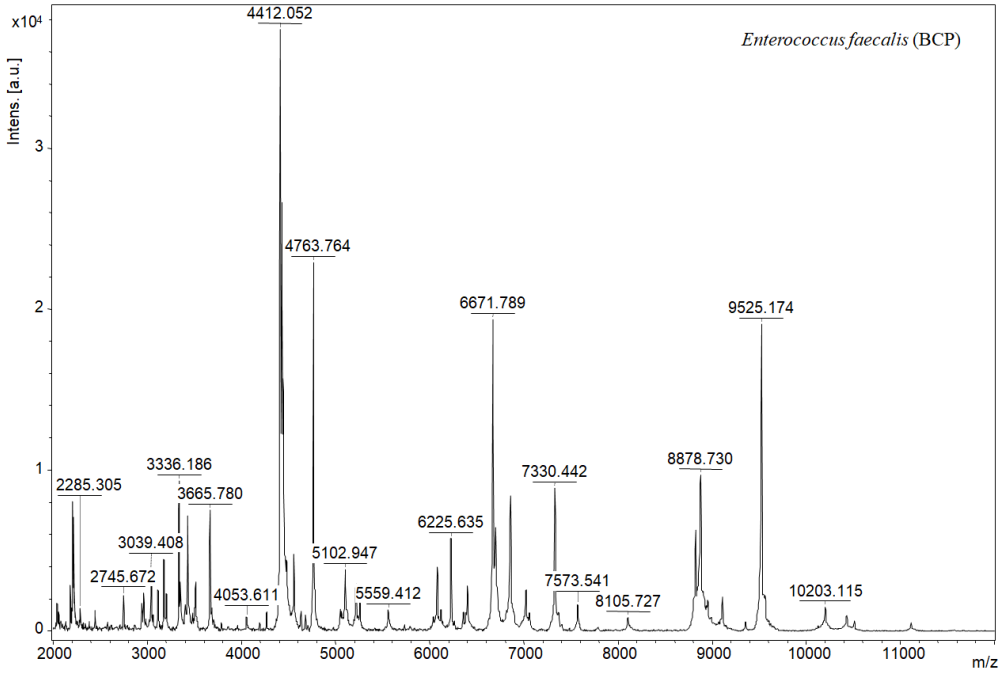

Fig. 2 A characteristic mass spectrum for *E. faecalis* generated using the MALDI TOF-MS technique

signals corresponded to three proteins: nucleotide-binding protein (*m/z* = = 3343.96), integrase catalytic domain-containing protein (*m/z* = 7037.987), the function of which is the integration of DNA, and helix-turn-helix domain-containing protein (*m/z* = 8106.457) responsible for the correct folding of the DNA helix. Ciprofloxacin and metronidazole are antibiotics that act on DNA. Ciprofloxacin is an inhibitor of DNA gyrase and topoisomerase II and thus disrupts the process of replication of genetic material, similarly to metronidazole, it disrupts and causes the loss of the helical DNA structure of bacteria [8–9].

4. Conclusions

Thanks to the use of the MALDI-TOF MS technique to generate mass spectra of proteins of bacterial isolates obtained from clinical samples and the use of the UniProt database, it is possible to identify probable similar mechanisms of antibiotic action and proteins responding to the antibiotics used. However, more research is needed to analyze more bacterial strains and antibiotics belonging to different therapeutic groups. This knowledge will allow the creation of new antibiotics with both narrow and broad action and improvement of the treatment of patients. Moreover, by using MALDI-TOF MS it is possible to predict the action of newly emerging antibiotics belonging to different therapeutic groups.

References

[1] Tomasz A., Munoz R.: β-Lactam antibiotic resistance in gram-positive bacterial pathogens of the upper respiratory tract: a brief overview of mechanisms. *Microb. Drug. Resist.* **1** (1995), 103–109.
[2] Read A.F., Woods R.J.: Antibiotic resistance management. *Evol. Med. Public. Health* **2014** (2014), 147.
[3] Kłodzińska E., Kupczyk W., Jackowski M., Buszewski B.: Capillary electropforesis in the diagnosis of surgical site infections. *Electrophoresis* **34** (2013), 3206–3213.
[4] Pauter K., Szultka-Młyńska M., Buszewski B.: Determination and identification of antibiotic drugs and bacterial strains in biological samples. *Molecules* **25** (2020), 2556.
[5] Pomastowski P., Buszewski B.: Complementarity of matrix- and nanostructure-assisted laser desorption/ionization aproaches. *Nanomaterials (Basel)* **9** (2019), 260.
[6] Dingle T.C., Butler-Wu S.M.: MALDI-TOF mass spectrometry for microorganism identifi-cation. *Clin. Lab. Med.* **33** (2013), 589–609.
[7] Bebrone C.: Metallo-β-lactamases (classification, activity, genetic, organization, structure, zinc coordination) and their superfamily. *Biochem. Pharmacol.* **74** (2007), 1686–1701.
[8] Albornoz E., Tijet N., De Belder D., Gomez S., Martino F., Corso A., Melano R.G., Petroni A.: QnrE1, a member of a new family of plasmid-located quinolone resistance genes, originated from the chromosome of enterobacter species. *Antimicrob. Agents Chemother.* **61** (2017), 1–8.
[9] Tocher J.H., Edwards D.I.: The interaction of reduced metronidazole with DNA bases and nucleosides. *Int. J. Radiat. Oncol. Biol. Phys.* **22** (1992), 661–663.

Spectrometry approach in study of cytokines by applicationmatrix-assisted laser desorption/ionization

Anna Kuźniewska[a, b, *], Paweł Pomastowski[b], Renata Gadzała-Kopciuch[a, b], Bogusław Buszewski[a, b]

[a] *Nicolaus Copernicus University in Toruń, Faculty of Chemistry, Department of Environmental Chemistry and Bioanalytics, Gagarina 7, 87 100 Toruń, Poland* ✉ *kuzniewskaa@gmail.com*
[b] *Nicolaus Copernicus University in Toruń, Centre for Modern Interdisciplinary Technologies, Wileńska 4, 87 100 Toruń, Poland*

Keywords
breast milk
cytokines
immunity
interleukin
MALDI

Abstract
Breast milk is a secretion with a unique composition, therefore it is perfectly adapted to the needs of each newborn in terms of nutrients. Cytokines with anti-inflammatory and immunomodulatory properties, i.e., interleukin 8 (IL-8) and cachectin (TNF-α), play a key role in the life of a newborn, but their dysregulated production can have a detrimental effect on the functioning of the organism – the appearance of inflammation or disease. The isolation of cytokines from different biological matrices and their identification is important in order to understand and deepen the understanding of immunology, disease course, and possible treatment strategy. The preparation of samples for further analysis and identification is an integral part of the analytical procedure. Therefore, MALDI and antibody-based techniques such as ELISA will allow the identification and determination of cytokines in human milk. The aim of this work is to select spectrometric conditions for the identification of selected cytokines using MALDI.

1. Introduction

Breast milk contains many molecules, i.e. proteins, carbohydrates, vitamins, and therefore it provides newborns with basic building blocks which are essential for further functioning and development of the child. These compounds facilitate digestion, participate in immunological protection and stimulate the proper development of the child [1]. It consists mainly of water, macronutrients, and microelements: 7% carbohydrates, 4% lipids, 1% proteins, and others [2]. Breast milk changes with the lactation period and can therefore be divided into: colostrum (milk produced after birth), mature milk (from 5 to 15 days after birth), mature milk. However, it is important to remember that each woman's transition

of a particular type of milk can be different and quite individual. Human milk contains more than 400 different proteins that have different functions. They can be divided into the following groups:

- casein–insoluble proteins, are an excellent source of amino acids and provide calcium and phosphate;
- whey proteins–insoluble, are involved in immunological processes, e.g., cytokines;
- mucins–constitute a small percentage of the total protein content of milk [2, 3].

Human milk also contains cytokines that play a role in immunoprotective and anti-inflammatory activities in an auto- and paracrine manner. Such cytokines include IL-6, IL-8, IFN-γ, TNF-α [1, 4]. Their levels depend on the lactation period, and elevated cytokine levels are associated with inflammation or disease progression, so measuring their levels becomes important to monitor disease progression or the effects of its treatment [2, 5]. Due to the fact that cytokines present in milk are present in low concentrations, the sample preparation step becomes a key element, while the identification method must be highly selective and specific. Among others, proteins can be detected and determined by ELISA, an enzyme-linked immunosorbent assay. The enzyme is covalently linked to a specific antibody, which ultimately recognizes the antigen. The antibody-enzyme complex binds to the antigen present in the well, and when a substrate is added, the enzyme catalyses the reaction to form a coloured product. ELISA is a fast and convenient technique for detecting proteins [6]. However, when it comes to the MALDI method, the sample is mixed with a small-molecule matrix compound before measurement. The purpose of the matrix is to ionise particles, which may not absorb the laser radiation. Therefore, the selection of an appropriate type of matrix is of fundamental importance for the success of the experiment [7]. In this case, two matrices for cytokine template samples were used for comparison. The results obtained will allow further research towards the detection of specific cytokines in human milk.

The aim of the study is identification and determination of cytokines classes such as interleukin 8 (IL-8) and cachectin (TNF-α) by application of MALDI TOF MS approachin linear positive mode.

2. Experimental

2.1 Reagents and chemicals

All materials and solvents were purchased from Sigma-Aldrich (Germany).

2.2 Instrumentation

To investigate the effect of different matrices on MALDI-TOF MS spectra, the same sample preparation method was used. Namely, dilutions of cytokine standards

(IL-8, TNF-α) were prepared by taking 1 µL of sample and dissolving in 9 µL of 0.1% trifluoroacetic acid. Serial dilutions (1:10 – C_1, 1:100 – C_2, 1:1000 – C_3, 1:10 000 – C_4) for standards with initial concentrations: IL-8: 0.5 mg/ml, TNF-α: 1 mg/mL. HCCA (α-cyano-4-hydroxy-cinnamic acid) and DHB (2,5-dihydroxy-benzoic acid) matrices dissolved in TA30 (30:70 mixture of acetonitrile: trifluoroacetic acid (0,1 %) were also prepared. The analyte was then mixed 1:1 with the matrix solution and 1µLwas applied in triplicate to a 96-well MALDI plate. The dried plate was inserted into the chamber of a MALDI Biotyper mass spectrometer, where the proteins were desorbed and ionised under laser irradiation and then moved in an electric field. They were separated according to molecular weight, charge, and different transit time. Calibration was also carried out, where a bacterial test standard from Bruker was used, and mass spectra were processed using software supplied by the manufacturer - flexControl and flexAnalysis.

3. Results and discussion

Selection of the best matrix and optimisation of parameters are crucial to obtain the highest quality mass spectra for each sample. For this purpose, it was decided to select appropriate spectrometric conditions to identify selected cytokines. For the previously prepared IL-8 and TNF-α dilutions for two matrices: DHB and

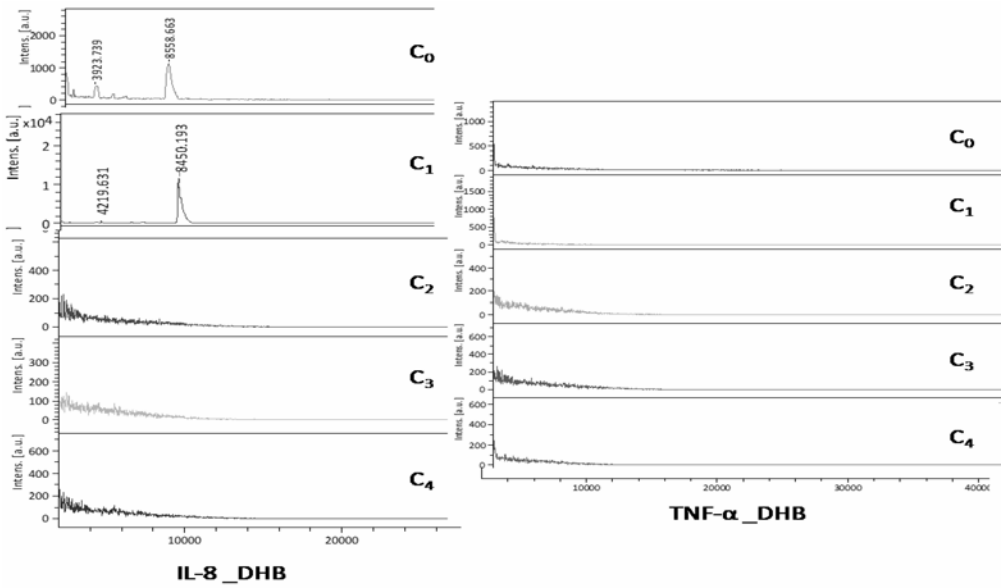

Fig. 1 Spectra for the cytokines IL-8 and TNF-α (with corresponding concentrations from C_0 to C_4) using the DHB matrix.

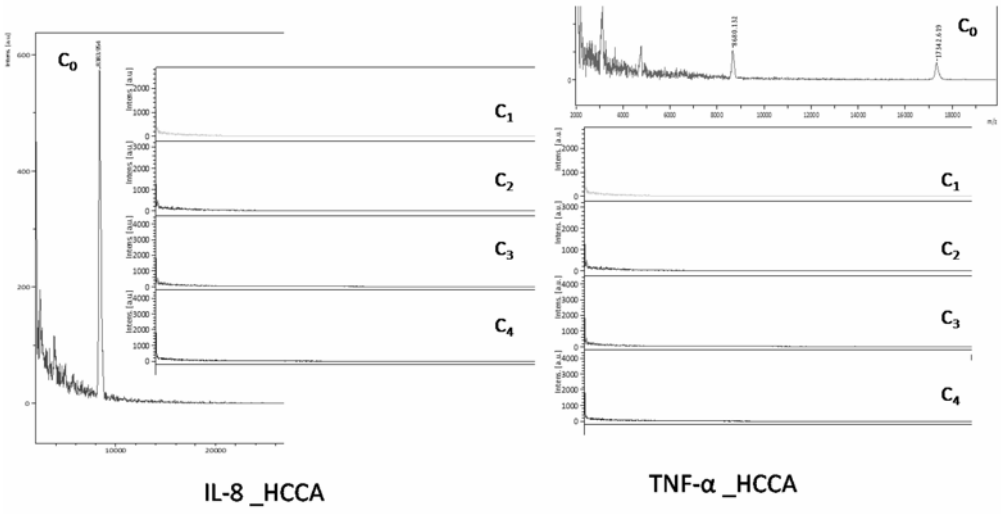

Fig. 2 Spectra of IL-8 and TNF-α cytokines (with corresponding C_0 to C_4 concentrations) for HCCA matrix

Table 1
Reference and experimental masses for IL-8 and TNF-α.

Cytokine	*M* / Da		
	Reference	Matrix	
		DHB	HCCA
IL-8	8 400	8 550.39 ± 94.48	8 399.32 ± 26.67
TNF-α	17 000	–	17 363.58 ± 49.33

HCCA, the following spectra were obtained (Fig.1, and Fig.2) by MALDI-TOF/MS technique. In the case of DHB matrix, results were obtained only for IL-8 (initial concentration: C_0 and 10-fold dilution of C_1), for cachectin no signal was observed on the mass spectrum. As for the HCCA matrix, signals were obtained for both cytokines in the range of their reference masses. For IL-8 the molecular mass is estimated within 8.4 kDa [8], while TNF-α is 17 kDa [9]. The following table summarises the *m/z* obtained together with the standard deviation and the reference masses (Table 1).

4. Conclusions

The results obtained illustrate that the MALDI technique allows direct determination of *m/z* for a molecular ion of a given sample. Regarding the matrices used, in this case, the use of the HCCA matrix gives a better signal quality, since for both cytokines a signal within their reference masses was observed.

HCCA effectively crystallises on the test sample, while DHB produces small or imperceptible crystals. The dilution effect allowed us to visualise the concentration levels for the cytokines in question and to use them for further studies on the identification of these cytokines in real samples - in human milk, using the ELISA technique.

Acknowledgments

This work was financially supported by the National Science Centre within the framework of Opus 15 project No.2018/29/B/ST4/01681 (2019–2022)

References

[1] Lis J., Orczyk-Pawiłowicz M., Katnik-Prastowska I.: Proteins of human milk involved in immunological processes. *Postepy Hig. Med. Dosw.* **67** (2013), 529–547 (In Polish).
[2] Pajewska-Szmyt M., Sinkiewicz-Darol E., Gadzała-Kopciuch R.: The impact of environmental pollution on the quality of mother's milk. *Environ. Sci. Pollut. Res.* **26** (2019), 7405–7427.
[3] Rico Y., Bidegain J.C.: Magnetostratigraphy and environmental magnetism in a sedimentary sequence of Miramar, Buenos Aires, Argentina. *Quat. Int.* **317** (2013), 53–63.
[4] Hurley W.L., Theil P.K.: Perspectives on immunoglobulins in colostrum and milk. *Nutrients* **3** (2011), 442–474.
[5] Stenken J.A., Poschenrieder A.J.: Bioanalytical chemistry of cytokines – A review. *Anal. Chim. Acta* **853** (2015), 95–115.
[6] Berg J.M., Stryer L., Ttmoczko J.L, Gatto G.J.: *Biochemia.* Warszawa, Wydawnictwo Naukowe PWN 2019 (In Polish).
[7] Kraj A., Drabik A., Silberring J.: *Proteomika i metabolomika.* Warszawa, Wydawnictwo Naukowe PWN 2010 (In Polish).
[8] Beutler B., Manhoney J., Le Trang N, Pekala P., Cerami A.: Purification of cachectin, a lipoprotein lipase-suppresssing hormone secreted by endotoxin-induced raw 264.7 cells. *J. Exp. Med.* **161** (1985), 984–995
[9] https://www.sigmaaldrich.com/catalog/product/SIGMA/I1645?lang=pl&region=PL (accessed 21st March, 2021)

Short-incubation method for rapid identification of bacterial pathogens via MALDI TOF MS technique

Ewelina Maślak[a,*], Michał Złoch[b], Paweł Pomastowski[b], Bogusław Buszewski[b]

[a] *Nicolaus Copernicus University in Toruń, Faculty of Chemistry, Department of Environmental Chemistry and Bioanalytics, Gagarina 7, 87 100 Toruń, Poland* ✉ *e_maslak@doktorant.umk.pl*
[b] *Nicolaus Copernicus University in Toruń, Centre for Modern Interdisciplinary Technologies, Wileńska 4, 87 100 Toruń, Poland*

Keywords
bacteria
diabetic foot infection
MALDI
short-incubation method

Abstract
The aim of this study was to investigate the usefulness of four different liquid culture media for reducing the incubation time of microorganisms needed to obtain reliable MALDI identification. The study was conducted on 10 different bacterial species regarded as the frequent causative agents of diabetic foot infections. The short-incubation method used was based on the analysis of the protein extracts obtained after 3, 6, 9, and 24 hours of incubation in investigated liquid media followed by bacteria identification via MALDI Biotyper 3.0 platform.

1. Introduction

The last decades have seen a significant development of analytical techniques applicable in microbiological diagnostics. Particular attention is focused on the techniques enabling the rapid and reliable identification of pathogens responsible for the infection, such as Matrix-Assisted Laser Desorption/Ionization (MALDI) technique [1]. It has become an easy-to-use, fast, and highly sensitive pathogen identification method for routine microbiology laboratories [2, 3]. The principle of this method is based on the generation and analysis of the unique protein profile of the microorganism and its comparison with that included in the reference spectrum database [4]. During analysis, the matrix plays a key role by absorbing the laser radiation, thus, leading to the desorption and ionization of the sample molecules. Obtained ions are accelerated in the electric field and then transferred to the detector which generates the mass spectrum [3, 5]. The generated mass spectra are unique for individual microorganisms because they consist mainly of highly evolutionarily conserved ribosomal proteins [4]. The process of identifying individual strains using the MALDI technique itself does not

exceed a few minutes [2]. However, it is preceded by the incubation step, which depends on the growth rate of microorganisms. Usually, before the analysis is performed, it is necessary to incubate the microorganisms for 24 hours, which significantly extends time-to-result [6]. By reducing this time, results will be obtained more quickly allowing the faster introduction of appropriate treatment. This is especially important in the treatment of chronic wounds such as the diabetic foot, as their microbial composition changes over time [7]. Given the rapidly growing number of people suffering from diabetes, the rapid identification of microorganisms that infect diabetic feet can protect them from serious complications such as amputation of the lower limbs.

2. Experimental

2.1 Chemicals and culture media

Chemicals for the MALDI TOF MS analysis (acetonitrile, trifluoroacetic acid, formic acid 70%, and α-cyano-4-hydroxycinnamic acid) were supplied at the highest commercially available purity by Sigma Aldrich (Germany). Water (for LC-MS grade, ⩾99,99%) was purchased from VWR Chemicals, USA. Four liquid microbiological media (Peptone Water, Mueller Hinton Broth, Tryptic Soy Broth, Brain Heart Infusion Broth) were purchased from Sigma Aldrich (Germany). Solid culture media, Columbia Agar Base, was obtained from Oxoid (Great Britain). All culture media were prepared according to the manufacturer's guidelines.

2.2 Bacterial strains

Ten reference strains purchased as Kwik-stik (Pol-Aura, Poland) were used in the study. The species that are most often responsible for causing infections in the diabetic foot were selected, i.e., *Acinetobacter baumannii* ATCC BAA-1605, *Escherichia coli* ATCC 10536, *Enterococcus faecalis* ATCC 51575, *Enterococcus faecium* ATCC 700221, *Klebsiella pneumoniae* ATCC 700603, *Pseudomonas aeruginosa* ATCC 15442, *Proteus mirabilis* ATCC 29245, *Staphylococcus aureus* ATCC BAA-44, *Staphylococcus epidermidis* ATCC 51625, *Streptococcus dysgalactiae* ATCC 12388.

2.3 Sample preparation and protein extraction

All reference strains were transferred to Columbia Agar Base medium plates and incubated at 37 °C for 24 hours under aerobic conditions. After this time, another passage of microorganisms was performed, from which bacterial suspensions were prepared in liquid media (Peptone Water, Mueller Hinton Broth, Tryptic Soy Broth, Brain Heart Infusion Broth) with the optical density of 0.5 McFarland each – initial suspensions. Then, 100 µl of the prepared stock suspensions were added to

the test tubes containing 9900 µl of sterile liquid media and mixed thoroughly by vortexing.

A volume of 125 µL of pure medium and 125 µL of bacterial suspension prepared in the same medium were added to each well of 96-well plates intended for cell culture. The whole was mixed by pipetting. Plates were incubated in a microplate incubator (Incubating Microplate Shaker, VWR) at 37 °C for 24 hours under aerobic conditions. After 3, 6, 9, and 24 hours, the cultures from four wells containing the same medium in a total volume of 1 ml were transferred to a sterile Eppendorf tube. The procedure was performed twice for each culture.

Before preparing protein extracts, each sample was centrifuged (13 000 rpm, 5 minutes), the supernatant was discarded and the remaining pellet was washed with 100 µL of water (LC-MS grade). The samples were re-centrifuged (13 000 rpm, 5 minutes) and the supernatant was discarded. Afterward, the protein extraction procedure was started. Extracts were prepared using the protein extraction method according to the protocol provided by the manufacturer of the MALDI Biotyper system (Bruker Daltonik, Germany). For this purpose, 150 µl of water (LC-MS purity) was added to the pellet, mixed and 450 µl of 96% ethanol was mixed and mixed again. The samples were centrifuged, the supernatant was discarded and the pellet was dried using a vacuum centrifuge. After drying, 10 µl of 70% formic acid and 10 µl of acetonitrile were added to the precipitate. After centrifugation, 1 µl of the prepared extracts were transferred onto the MALDI target plate and covered with the same volume of α-cyano-4--hydroxycinnamic acid matrix and were left to air dry. For each sample prepared two spots (4 measurements per sample in total). Ready target plates were analyzed using ultrafleXtreme MALDI–TOF/TOF mass spectrometer (Bruker Daltonik, Germany) equipped with the smartbeam-II laser–positive mode according to the procedure described in detail in a work [8]. Obtained spectra were subjected to smoothing and baseline corrections as well as calibration with BTS (Bruker Bacterial Test Standard, Bruker Daltonik, Germany) in quadratic mode using the manufacturer software, flexAnalysis.

3. Results and discussion

After comparing the collected spectra with the spectra in the reference database, the correct identification was obtained for most of the samples; the obtained match values allowed for a probable identification at least to the genus (score value > 1.7). Figure 1 shows an exemplary mass spectrum recorded during identification with the MALDI technique. The incubation time of the tested strains and the composition of the culture medium influenced the identification result. Table 1 shows the mean score values calculated from the four replicates.

After 3 hours of incubation, correct bacterial identification was achieved in 18/40 (45%) of the samples, most of which were gram-negative bacteria (12 samples). In the case of the remaining samples, due to the insufficient amount

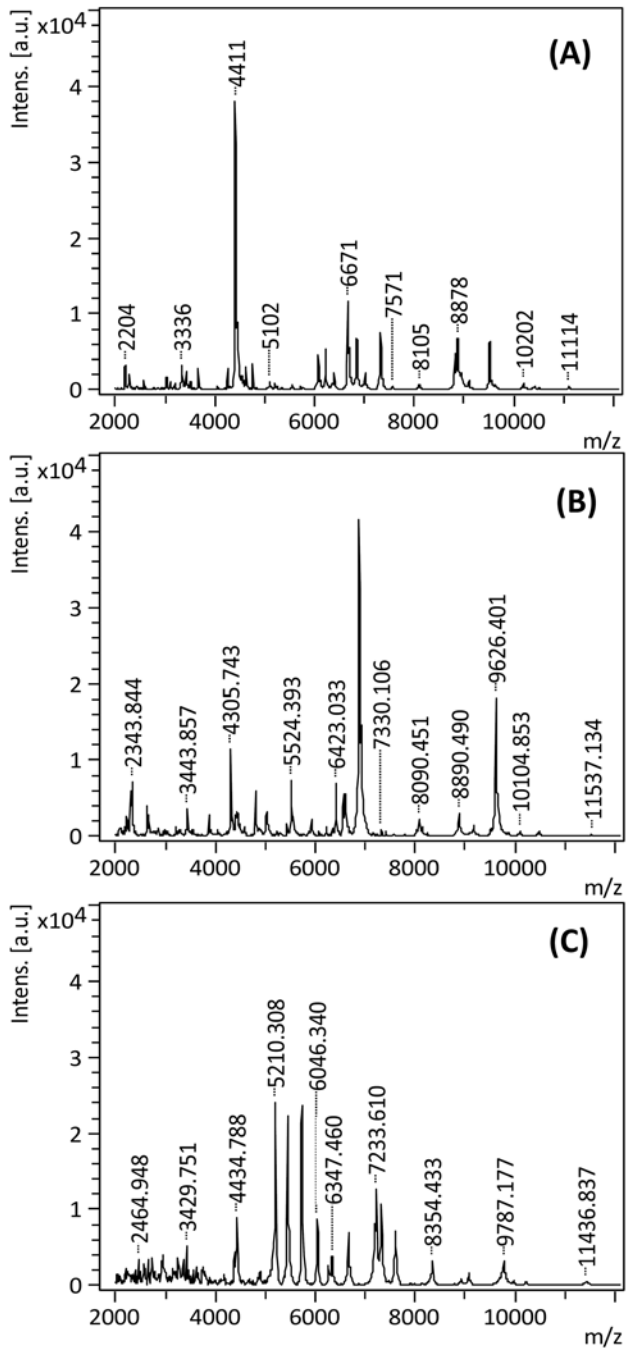

Fig. 1 Exemplary mass spectra recorded during identification with the MALDI technique after 6 hour of incubation: (A) *Enterococcus faecalis*, (B) *Staphylococcus aureus*, (C) *Pseudomonas aeruginosa*

Table 1
Score values (mean ± deviation) for the tested strains grown in Mueller Hinton Broth, Brain Heart Infusion Broth, peptone water, and Tryptic Soy Broth medium after different incubation times.

Strain	Incubation time / h			
	3	6	9	24
Mueller Hinton Broth				
A. baumannii	no spectrum	2.11 ± 0.04	2.05 ± 0.08	2.01 ± 0.17
E. coli	1.80 ± 0.31	2.25 ± 0.08	2.32 ± 0.08	2.29 ± 0.05
E. faecalis	1.81 ± 0.29	2.16 ± 0.12	1.81 ± 0.45	2.29 ± 0.07
E. faecium	no spectrum	1.90 ± 0.39	1.91 ± 0.21	1.73 ± 0.27
K. pneumoniae	2.22 ± 0.05	2.22 ± 0.14	2.29 ± 0.06	1.98 ± 0.18
P. aureginosa	no spectrum	2.27 ± 0.03	2.31 ± 0.06	1.98 ± 0.18
P. mirabilis	no spectrum	2.45 ± 0.07	2.43 ± 0.03	2.33 ± 0.13
S. aureus	1.86 ± 0.69	2.19 ± 0.07	2.28 ± 0.04	2.26 ± 0.10
S. epidermidis	no spectrum	1.78 ± 0.13	1.91 ± 0.07	1.96 ± 0.08
S. dysgalactiae	1.77 ± 0.15	2.19 ± 0.20	2.19 ± 0.05	2.16 ± 0.26
Brain Heart Infusion Broth				
A. baumannii	1.80 ± 0.17	2.05 ± 0.20	1.98 ± 0.15	1.99 ± 0.06
E. coli	1.98 ± 0.11	2.20 ± 0.08	2.21 ± 0.16	1.90 ± 0.23
E. faecalis	2.13 ± 0.10	2.06 ± 0.10	2.06 ± 0.06	2.14 ± 0.16
E. faecium	1.46 ± 0.16	1.83 ± 0.23	1.99 ± 0.24	2.11 ± 0.07
K. pneumoniae	2.21 ± 0.05	1.94 ± 0.26	2.03 ± 0.01	1.74 ± 0.10
P. aureginosa	1.49	2.19 ± 0.04	2.06 ± 0.24	1.80 ± 0.20
P. mirabilis	2.10 ± 0.05	2.12 ± 0.03	1.88 ± 0.39	1.99 ± 0.06
S. aureus	no spectrum	2.20 ± 0.09	2.35 ± 0.05	2.27 ± 0.06
S. epidermidis	1.35 ± 0.12	1.72 ± 0.05	1.77 ± 0.33	1.61 ± 0.31
S. dysgalactiae	1.45 ± 0.17	2.15 ± 0.12	2.03 ± 0.04	1.87 ± 0.23
Peptone Water				
A. baumannii	1.78 ± 0.12	2.16 ± 0.10	2.13 ± 0.08	2.07 ± 0.20
E. coli	1.97 ± 0.08	2.16 ± 0.08	2.33 ± 0.08	2.32 ± 0.03
E. faecalis	1.28 ± 0.18	1.93 ± 0.13	1.73 ± 0.22	2.00 ± 0.12
E. faecium	1.30 ± 0.11	1.55 ± 0.32	1.84 ± 0.24	1.99 ± 0.12
K. pneumoniae	2.19 ± 0.05	2.24 ± 0.08	2.23 ± 0.12	2.11 ± 0.11
P. aureginosa	no spectrum	2.27 ± 0.03	2.28 ± 0.08	1.97 ± 0.09
P. mirabilis	1.98 ± 0.18	2.33 ± 0.10	2.34 ± 0.14	2.34 ± 0.07
S. aureus	1.90 ± 0.33	2.28 ± 0.07	2.21 ± 0.13	2.18 ± 0.10
S. epidermidis	1.43 ± 0.01	1.74 ± 0.35	2.03 ± 0.06	1.99 ± 0.07
S. dysgalactiae	1.53 ± 0.14	1.57 ± 0.25	1.75 ± 0.29	1.52 ± 0.08
Tryptic Soy Broth				
A. baumannii	no spectrum	2.07 ± 0.04	2.11 ± 0.01	2.03 ± 0.11
E. coli	1.29 ± 0.09	2.25 ± 0.05	2.21 ± 0.12	2.24 ± 0.10
E. faecalis	1.43 ± 0.37	2.26 ± 0.13	2.12 ± 0.05	2.17 ± 0.04
E. faecium	no spectrum	2.04 ± 0.21	2.07 ± 0.16	2.30 ± 0.03
K. pneumoniae	2.15 ± 0.08	2.13 ± 0.06	2.09 ± 0.09	2.12 ± 0.13
P. aureginosa	no spectrum	1.95 ± 0.52	2.31 ± 0.05	1.55 ± 0.07
P. mirabilis	2.04 ± 0.11	2.42 ± 0.07	2.24 ± 0.10	2.19 ± 0.16
S. aureus	2.06 ± 0.12	2.35 ± 0.06	2.46 ± 0.10	2.38 ± 0.12
S. epidermidis	1.15 ± 0.25	1.51 ± 0.20	1.42 ± 0.24	1.77 ± 0.13
S. dysgalactiae	1.61 ± 0.23	2.19 ± 0.06	2.12 ± 0.08	2.13 ± 0.08

Table 2
Media giving the highest identification values of a given strain after a certain time (* – score value > 2.0, ** – score value > 2.3). Abbreviations: BHIB – Brain Heart Infusion Broth, MHB – Mueller Hinton Broth, TSB – Tryptic Soy Broth, and WP – peptone water.

Group	Strain	Incubation time / h			
		3	6	9	24
G(+)	*S. aureus*	TSB*	TSB**	TSB**	TSB**
	S. epidermidis	WP	MHB	MHB*	WP*
	S. dysgalactiae	MHB	TSB*	MHB*	TSB*
	E. faecalis	BHIB*	TSB*	TSB*	MHB*
	E. faecium	BHIB	TSB*	TSB*	TSB**
G(–)	*P. aeruginosa*	–	MHB*/WP*	MHB**/TSB**	MHB/WP
	P. mirabilis	BHIB*	MHB**/TSB**	MHB**	MHB**/WP**
	E. coli	BHIB/WP	MHB*/TSB*	MHB**/WP**	WP**
	A. baumanii	BHIB	WP*	WP*/TSB*	WP*
	K. pneumoniae	BHIB*/MHB*	MHB*/WP*	MHB*	MHB*

of bacterial sediment obtained, it was not possible to record the mass spectra or the obtained values of the match were too low. Most often, correct identification was obtained for *S. aureus* in the case of gram-positive bacteria, and in the case of gram-negative bacteria for *E. coli*, *K. pneumoniae*, and *P. mirabilis*. Contrary, *P. aureginosa* was the species for which no spectra were obtained after 3 hours using most of the media.

Regardless of the medium used, 6 hours of incubation was sufficient to obtain the spectra of all tested strains, and the obtained mean values of the match allowed for the correct identification of 37/40 (92.5%) samples (Table 1). After 9 hours, correct identification was achieved for 39/40 (97.5%), and after 24 hours for 37/40 (92.5%) samples. After 6, 9, and 24 hours, the value of the match was most often above 2, i.e., some identification to genus and probable to species was obtained. In most cases, the identification values obtained after 6 and 9 hours were very similar and were often higher than those obtained for the control samples, after 24 hours. The mean identification values of gram-negative bacteria in most cases after 6 and 9 hours of incubation were higher than those of gram-positive bacteria. For most species, identification results worsened with increasing incubation times, regardless of the culture medium used.

From the obtained identification values using the Statistica software, the box plots were generated on the basis of which Table 2 was created. This table shows the media that give the best identification results for the tested strains after a certain time. After 3 hours of incubation for most species, the highest identification results were obtained on the enriched medium: Brain Heart Infusion Broth. This is due to the fact that the cultivation of bacteria in highly nutritious liquid media allows faster and more abundant growth of bacterial biomass, which enables analysis at early time points. After 6 hours, the best adjustments of spectra were obtained with Tryptic Soy Broth, after 9 hours Mueller Hinton Broth,

and after 24 hours Peptone Water. Overall, the highest identification values after 3, 6, and 9 hours were obtained on Tryptic Soy Broth and Mueller Hinton Broth media, with gram-positive bacteria having significantly better results on Tryptic Soy Broth, and in the case of gram-negative bacteria on Mueller Hinton Broth. Thus, based on the results, it can be concluded that the most beneficial in this study was the use of universal substrates. However, the use of selective media could give better results when analyzing clinical samples (and not pure cultures as in the experiment).

4. Conclusions

The MALDI technique can be used to speed up bacterial identification based on early bacterial growth analysis. In this approach, it is essential to select a medium that promotes rapid bacterial growth to obtain reliable identification. In the case of the species that most frequently cause infections of the diabetic foot, the use of an enriched liquid medium (Brain Heart Infusion Broth) allowed the identification of the majority of gram-negative species after 3 hours of incubation. The 6-hour incubation was sufficient for the correct identification of all tested species. Tryptic Soy Broth medium gave the highest identification values for G (+) species, and Mueller Hinton Broth for G (−) species.

Acknowledgments

This study was supported by SONATINA 2 project No. 2018/28/C/ST4/00434 from National Science Centre, Poland.

References

[1] Franco-Duarte R., Cernáková L., Kadam S., Kaushik K., Salehi B., Bevilacqua A., Rosaria Corbo M., Antolak H., Dybka-Stępień K., Leszczewicz M., Relison Tintino S., de Souza V., Sharifi-Rad J., Coutinho H., Martins N., Rodrigues C.: Advances in chemical and biological methods to identify microorganisms: From past to present. *Microorganisms* **7** (2019), 130.

[2] De Carolis E., Vella A., Vaccaro L., Torelli R., Spanu T., Fiori B., Posteraro B., Sanguinetti M.: Application of MALDI-TOF mass spectrometry in clinical diagnostic microbiology. *J. Infect. Dev. Ctries.* **8** (2014) 1081–1088.

[3] Buszewski B., Rogowska A., Pomastowski P., Złoch M., Railean-Plugaru V.: Identification of microorganisms by modern analytical techniques. *J. AOAC Int.* **100** (2017), 1607–1623.

[4] Sauget M., Valot B., Bertr X., Hocquet D.: Can MALDI-TOF mass spectrometry reasonably type bacteria? *Trends Microbiol.* **5** (2017), 447–455.

[5] Lartigue M.F.: Matrix-assisted laser desorption ionization time-of-flight mass spectrometry. *Infect. Genet. Evol.* **13** (2013), 230–235.

[6] Kohlmanna R., Hoffmannb A., Geis G., Gatermann S.: MALDI-TOF mass spectrometry following short incubation on a solid medium is a valuable tool for rapid pathogen identification from positive blood cultures. *Int. J. Med. Microbiol.* **305** (2015), 469–479.

[7] Mendes J., Neves J.: Diabetic foot infections: current diagnosis and treatment. *Journal of Diabetic Foot Complications* **4** (2012), 26–45.

[8] Pomastowski P., Złoch M., Rodzik A., Ligor M., Kostrzewa M., Buszewski B.: Analysis of bacteria associated with honeys of different geographical and botanical origin using two different identification approaches: MALDI-TOF MS and 16S rDNA PCR technique. *PLoS ONE* **14** (2019), e0217078.

Application of ultrasound-assisted solvent extraction of porous membrane packed liquid samples for polyphenols determination in wine samples

Magdalena Fabjanowicz[a,*], Alicia Robles[b], Justyna Płotka-Wasylka[a]

[a] *Gdańsk University of Technology, Faculty of Chemistry, Department of Analytical Chemistry, 11/12 Narutowicza Street, 80-233 Gdańsk, Poland* ✉ *plotkajustyna@gmail.com*
[b] *National University of Mar del Plata, Faculty of Exact and Natural Sciences, Department of Chemistry, 3350 Funes Street, 7600 Mar del Plata, Provincia de Buenos Aires, Argentina*

Keywords
extraction
polyphenols
wine

Abstract
Polyphenols play a crucial role in proper human health maintenance as well as their presence very often correspond to the quality assessment of products like wine. Thus, their monitoring is of high interest. However, as they occur in complex matrices their extraction is very often necessary prior to the analysis. Herein, new ultrasound-assisted solvent extraction of porous membrane packed liquid sample technique has been optimized for the determination of polyphenols in wine samples as an alternative for existing methods used prior GC-MS analysis. The achieved accuracy is in the range of 100.7–108.3 while recovery between 97–110% from spiked samples at 5 to 10 ppm concentration range. Limit of detection 0.174–1.99 $\mu g\,mL^{-1}$ while limit of quantitation 0.522–5.97 $\mu g\,mL^{-1}$.

1. Introduction

Increased awareness of the society about the positive influence of the application of a healthy and well balanced diet is a driving force for scientists looking for bioactive compounds promoting human health as well as factors influencing their occurrence and availability. Natural antioxidants are the subject of high interest during the last decade. The most widely studied group of compounds having desired properties are polyphenols. Apart from antioxidant properties, they exhibit other health beneficial effects like anti-inflammatory, antimutagenic, anticarcinogenic as well as they help to prevent age-related diseases [1]. It is well known, that polyphenols are widely abundant in fruits especially blueberries, grapes, and products made from them. Thus, wine is considered as one of the sources of given compounds, where they play a crucial role, being responsible for

the aesthetic and organoleptic character of this alcoholic beverage. Thus, it is important to monitor the content of polyphenols to control the quality of wine products. There are plenty of methods of polyphenols determination described in the literature. However, mostly they are based on high performance liquid chromatography and capillary electrophoresis. Gas chromatography was applied only in few cases. This is due to the physico-chemical properties of given compounds and thus a more complex sample preparation process than in HPLC, since extraction of preferable analytes and their derivatization should be performed[2]. Herein, in a given study a new, promising extraction technique is presented an ultrasound-assisted solvent extraction of porous membrane packed liquid sample. The following work is focused on catechin, rersveratrol and pterostilbene determination in the red wines that originated in Poland.

2. Experimental

2.1 Reagents and chemicals

All standards were of high purity, suitable for the GC analysis. (+)-Catechin was purchased from Sigma-Aldrich. Resveratrol and pterostilbene were delivered from Extrashynthese (France). Additionally, the derivatization reagent 1% trimethyl chlorsilane and *N,O*-bis(trimethylsilyl)trifluoroacetamide were supplied by Sigma Aldrich. Polypropylene (PP) flat membrane sheet (Type PP 1E (R/P), pore size: 0.1 μm, wall thickness: 100 μm) was purchased from Membrana (Germany). Deionized water from the Milli-Q Direct 8 Water Purification System (Merc Millipore) for the sample (pre)treatment and sample dilution was used.

2.2 Samples

Ten bottles of red wines originated from Polish vineyards.

2.3 Instrumentation

Analysis was performed with 7890A GC System (Agilent Technologies, USA) coupled to an electron ionization ion source and a 5975C single quadrupole mass spectrometer (Agilent Technologies, USA), by which resveratrol, pterostilbene, and catechin concentration were investigated.

2.3 Extraction and derivatization procedure

A new, alternative extraction technique procedure is presented in Fig. 1. Firstly, the membrane bag with the sample needs to be prepared. Secondly, the porous membrane bag is subjected to solvent extraction assisted by the ultrasounds bath for 25 min and thirdly, it is evaporated in the stream of nitrogen. Afterward, the

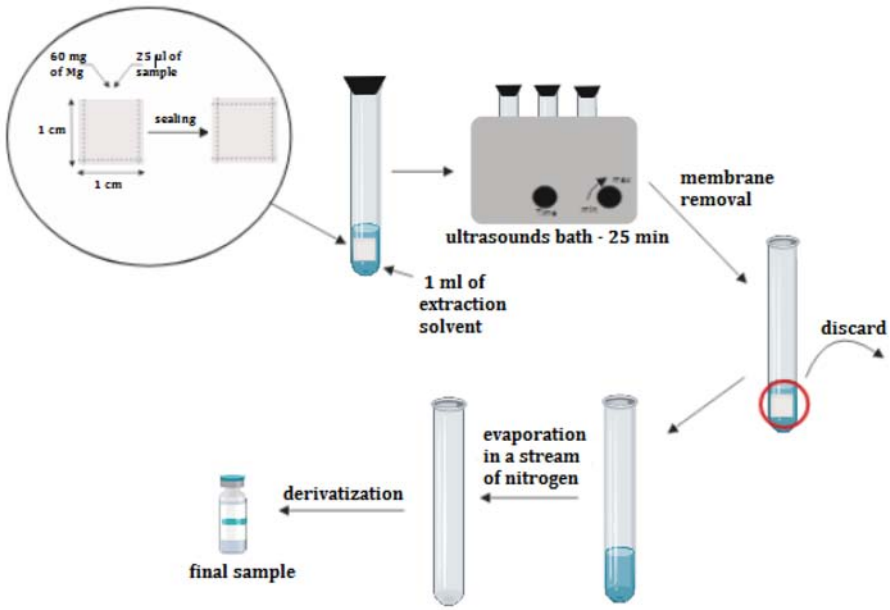

Fig. 1 Scheme of the ultrasound-assisted solvent extraction of porous membrane packed liquid samples extraction process

derivatization process should be performed in order to enhance the volatility, thermal stability of analytes as well as to improve resolution and detection of the gas chromatography performance. During the derivatization process, 30 µL of *N,O*-bis(trimethylsilyl)trifluoroacetamide was added in the vial and vortex for 30 s. Then the solution was heated for 30 min in a temperature of 35 °C. At the end, 170 µL of extraction solvent was added and heated again at the same condition for 15 min prior analysis.

3. Results and discussion

Matrices of wine samples are very diverse apart of polyphenols contains sugars, tannins, vitamins, organic acids, minerals, aromatic compounds, and many others that disturb the analysis of selected compounds. Due to this fact sample preparation is a very crucial aspect. Up till now, there were several extraction techniques applied, like: Solid Phase Extraction, Solid Phase Microextraction, Stir Bar Sorptive Extraction or Dispersive Liquid-Liquid Microextraction [3–7]. However, there is no unique technique that can be applied to each kind of matrix so still there is a place for a new one.

Presented in this paper, the new extraction technique is easy in sample and extraction device preparation and consumes a minimal amount of solvent. There were several parameters optimized like the type of extraction solvent, its volume (1 ml of ethylacetate:dichloromethane 1:1), the time required for sufficient

Table 1
Method validation parameters.

Compound	Linear range / μg mL^{-1}	r^2	*LOD* / μg mL^{-1}	*LOQ* / μg mL^{-1}
Pterostilbene	0.58–29	0.9979	0.174	0.522
Resveratrol	0.987–24	0.9966	0.329	0.987
Catechin	5.97–14.18	0.9884	1.99	5.97

Table 2
Method precision and recovery.

Compound	Intra-day precision Accuracy (precision) (n = 7, c = 10 μg mL^{-1})	Recovery (n = 3) %R ± U%R (k =2)		ME Accuracy (precision) (n = 5, c = 5 μg mL^{-1})
Pterostilbene	100.7 (9.0)	5 ppm:	102.3±2.9	102.2 (5.0)
		10 ppm:	110.0±11.7	
Resveratrol	105.0 (7.5)	5 ppm:	99.2±16.6	114.7 (7.9)
		10 ppm:	106.0±13.1	
Catechin	108.3 (6.8)	5 ppm:	95.8±11.2	106.5 (2.3)
		10 ppm:	97.2±12.3	

extraction, and ultrasounds power. After optimization of given parameters, developed extraction technique gives significant improvements over the published method, having promising results expressed in the validation parameters as well as precision and recovery presented in Table 1 and Table 2. The limit of detection is in the range between 0.174–0.329 μg mL^{-1} while the limit of quantitation is within 0.522–5.97 μg mL^{-1}. Moreover, accuracy is in the range of 102.2–114.7 while recovery between 95.8–110%. Those are very good analytical figures of merit, showing reliable and reproducible results in terms of polyphenols determination.

Additionally, there is no need for special solvent to be used. Extraction and desorption are possible within one single step. There is no need for salt addition and pre-condition treatment to Solid Phase Microextraction device what in total makes this technique economically favourable. As every extraction technique also this one has some limitations since once used the membrane bag cannot be used again. Special care needs to be taken while processing, because the Solid Phase Microextraction device can break during the extraction process. Up-till now, automated procedures for device fabrication, extraction, and its online application with analytical instruments are not available yet. However, it is possible to couple ultrasound-assisted solvent extraction of porous membrane packed liquid sample technique with different quantification techniques.

4. Conclusions

Wine is a complex matrix rich in many different groups of compounds thus extraction of desired analytes is a crucial aspect in the context of wine sample analysis. There are several extraction techniques already available nevertheless there is no one uniqueness, ideal for each kind of analytes extraction from a sample thus the door is still open for new techniques which may eliminate limitations previously appearing. Presented extraction techniques of polyphenols from wine matrices is a promising tool for the complex matrix sample preparation prior to the gas chromatography analysis. The validation process of a given technique clearly shows that method can be successfully used for the quantitative measurements of polyphenols in wine samples, giving reliable and reproducible results.

References

[1] Jurikova T., Sochor J., Rop O., Mlček J., Balla Š., Szekeres L., Žitný R., Zitka O., Adam V., Kizek R.: Evaluation of polyphenolic profile and nutritional value of non-traditional fruit species in the Czech Republic – A Comparative Study. *Molecules* **17** (2012), 8968–8981.

[2] Fabjanowicz M., Płotka-Wasylka J., Namieśnik J.: Detection, identification and determination of resveratrol in wine: Problems and challenges. *Trends Anal. Chem.* **103** (2018), 21–33.

[3] Gawlik M., Nowak Ł., Baran M.: Analiza właściwości win produkcji polskiej. *Bromat. Chem. Toksykol.* **41** (2008), 15–20 (In Polish).

[4] Montes R., García-López M., Rodríguez I., Cela R.: Mixed-mode solid-phase extraction followed by acetylation and gas chromatography mass spectrometry for the reliable determination of trans-resveratrol in wine samples. *Anal. Chim. Acta* **673** (2010), 47–53.

[5] Cai L., Koziel J., Dharmadhikari M., van Leeuwen J.: Rapid determination of trans-resveratrol in red wine by solid-phase microextraction with on-fiber derivatization and multidimensional gas chromatography–mass spectrometry. *J. Chromatogr. A* **1216** (2009), 281–287.

[6] Arslan G., Yilmaz N.: Determination of trans-resveratrol levels in different fruits, vegetables and their skin by HPLC. *Asian J. Chem.* **25** (2013), 1225–1228.

[7] Rodríguez-Cabo T., Rodríguez I., Cela R.: Determination of hydroxylated stilbenes in wine by dispersive liquid-liquid microextraction followed by gas chromatography mass spectrometry. *J. Chromatogr A.* **1258** (2012), 21–29.

Development of methodology for study of interactions between shikimic acid and bovine serum albumin

Tetiana Dyrda-Terniuk[a,*], Magdalena Buszewska-Forajta[b], Paweł Pomastowski[c], Bogusław Buszewski[a, c]

[a] *Nicolaus Copernicus University in Toruń, Faculty of Chemistry, Department of Environmental Chemistry and Bioanalytics, Gagarina 7, 87 100 Toruń, Poland* ✉ *tania25dyrda@gmail.com*
[b] *Nicolaus Copernicus University in Toruń, Faculty of Biological and Veterinary Sicences, Institute of Veterinary Medicine, Lwowska 1, 87 100 Torun, Poland*
[c] *Nicolaus Copernicus University in Toruń, Centre for Modern Interdisciplinary Technologies, Wileńska 4, 87 100 Toruń, Poland*

Keywords
Bovine Serum Albumin
cyclitol
interactions
mechanism

Abstract
Learning the mechanism of interactions between the target molecule and ligand allows us to understand the nature of molecular recognition, functions, and biological activity of the protein-ligand complex. In the present work, non-specific interactions between model protein (Bovine Serum Albumin) and cyclitol (shikimic acid) were under investigation. Various analytical methods including chromatographic and spectroscopic ones were applied to determine the molecular mechanism of protein-cyclitol interactions.

1. Introduction

Cyclitols are secondary metabolites considered as one of the most abundant phytochemicals [1]. Among them, shikimic acid is an important precursor in the biosynthesis of lignin, aromatic amino acids, and alkaloids. Naturally, it occurs in plants and microorganisms. Shikimic acid and its derivatives have anti-inflammatory, antioxidant, antithrombotic, anticoagulant properties, thus it could have many applications in pharmacy [2]. It can be also considered as a ligand, which can bind to the molecular target like protein. One of the model proteins for the study of protein-ligand interactions is bovine serum albumin, because of its medical importance, easy availability, and high binding affinity to various ligands.

Bovine Serum Albumin is a large globular protein, with a molecular weight of 66430 Da. The single polypeptide chain of its protein is composed of 583 amino acids [3]. Its native 3D structure is determined by a variety of non-covalent interactions between amino acid residues and solvent molecules. Functions and biological activity of bovine serum albumin can be influenced by the binding ligand to a particular site on the protein [4].

The aim of the present work was to study the mechanism of interactions between bovine serum albumin and shikimic acid with the use of complementary instrumental techniques including high performance liquid chromatography coupled with tandem mass spectrometry (HPLC-MS/MS) and spectroscopic methods (fluorescence spectroscopy, FTIR).

2. Experimental

2.1 Materials

Bovine serum albumin, shikimic acid, formic acid were purchased from Sigma-Aldrich (Germany). Isopropanol and water (LC-MS grade) were obtained from Supelco (USA).

Bovine serum albumin powder was dissolved in a 2 mL Eppendorf tube to the concentration of 1 mg mL^{-1}.

Shikimic acid solutions were prepared in such a concentration that after adding to protein solution the protein-cyclitol molar ratio was ranging 1:1–1:10, 1:100, and 1:1000.

2.2 Fluorescence spectroscopy

Fluorescence 3D analysis of bovine serum albumin was determined with the Spectrofluorometer FP-8300 (Jasco, Japan) was used. The concentration of protein was set as 0.05 mg mL^{-1}. The excitation wavelength and emission wavelength were, respectively, in range λ_{ex} = 200–735 nm in 5 nm increments, and λ_{em} = 210–750 nm.

Fluorescence intensity was carried out a Varioscan LUX at values of absorption and emission determined from the 3D-fluorimetric spectrum of bovine serum albumin. The protein solution was used with a constant concentration of 1 mg mL^{-1} and shikimic acid concentration varied from 5.24×10^{-3} mg mL^{-1} to 5.24 mg mL^{-1}.

2.3 FTIR spectroscopy

The infrared spectrums of the protein control sample and protein with bonded shikimic acid were measured in the range 1700–950 cm^{-1} (Perkin Elmer, USA) with the use of CaF_2 optical window and thin layer method. Data was collected with 20 scans and resolution was set as 8 cm^{-1}.

2.4 HPLC-MS/MS analysis

Qualitative and quantitative profiling of shikimic acid and its complexes with protein was done using high pressure liquid chromatography coupled with mass spectrometry. HPLC-MS system (LCMS-8050 SHIMADZU, Japan) including ESI

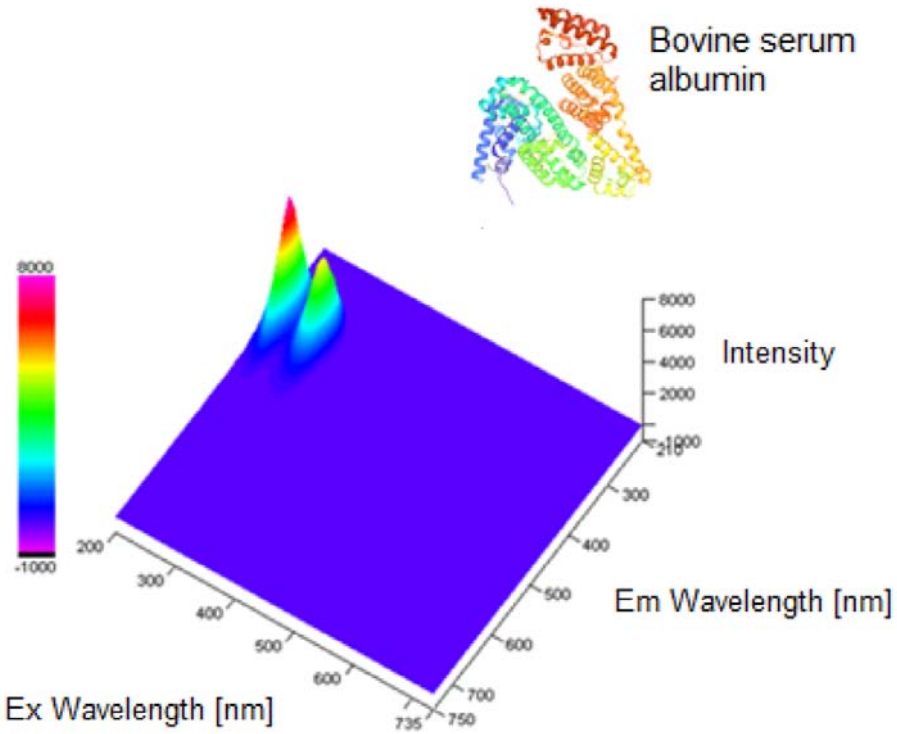

Fig. 1 3D fluorescence spectrum of bovine serum albumin

source and triple quadrupole analyzer. Cyclitol was analyzed using the column packed with BSA particles (RESOLVOSIL BSA-7, Macherey-Nagel, Germany) at 30 °C. Analysis protein-cyclitol interactions were done with the use of eight mobile phases composed of water, isopropanol, and the addition of formic acid. Mass spectrometry parameters were as follows: ion source temperature 230 °C, flow rate 0.5 mL min^{-1}, nebulizing gas 2 L min^{-1}, capillary voltage 4 kV. Scans were recorded ranging *m/z* 50 to 400.

Quantitative analysis was carried out without a column. Free cyclitol, as well as its unbounded fraction (complexes 1:2, 1:5, and 1:7 protein-cyclitol), were determined at SIM mode. Mobile phase was composed of 0.1% (v/v) formic acid-water (A) and acetonitrile (B) at 75:25 (v/v).

3. Results and discussion

3.1 Fluorescence spectroscopy

Figure 1 shows that excitation of bovine serum albumin occurs at two wavelengths λ_{ex} = 225 nm and λ_{ex} = 280 nm and wavelength of emission were recorded at 340 nm. Excitation at 225 nm is characteristic for carbonyl bonding C=O of

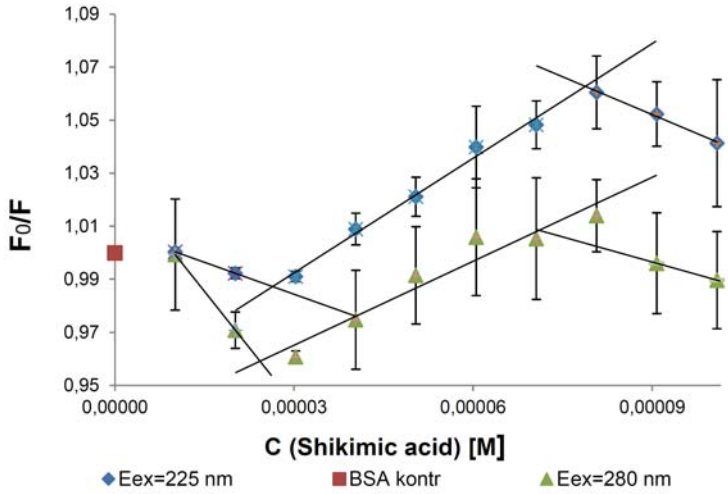

Fig. 2 Stern-Volmer plot for protein-cyclitol complex (in the range of 1:1–1:10 molar ratio)

α-helix polypeptide backbone and as a result of π → π* electronic transition. Strong absorption at 280 nm is caused by n → π* electronic transition of the indole ring of tryptophan [5].

Occurring fluorescence phenomena was described by the Stern-Volmer equation, presented in the graphical plot in Fig. 2 for protein-cyclitol complex in the range of molar ratio from 1:1 to 1:10. Figure 2 shows interactions between bovine serum albumin and shikimic acid. Firstly, the fluorescence intensity increased, then decreased, and finally increased again. This, in turn, confirms that the polarity of the environment of aromatic amino acid residues has changed dynamically. Negative values of Stern-Volmer constant ($\boldsymbol{K}_{SV\ (225\ nm)}$ = −103.76 M^{-1}, $\boldsymbol{K}_{SV\ (280\ nm)}$ = −800.45 M^{-1}) shows that cyclitol had stabilizing effect on protein structure and its environment became more hydrophobic. Stabilization may be caused by preferential hydration, where cyclitol molecule could be excluded from the surface of the macromolecule. However, the hydration shell stayed preserved. Thus, nonpolar groups are hidden into protein structure that provides an enhancing of hydrophobic interactions [6, 7].

3.2 FTIR spectroscopy

Figure 3 shows changes in characteristic bands of active functional groups of bovine serum albumin that are involved in interactions. Higher frequencies of the Amide I band (Fig. 3 (1 and 2)) in presence of cyclitol proved the increasing content of α-helix in protein secondary structure [8]. Shifting of the amide II band towards higher frequencies (Fig. 3 (3 and 4)) indicates the formation of new hydrogen bounds. Bands presented in Fig. 3 (5) are responsible for C–H stretching and in-plane banding vibrations. Amide III band can be applied to analyze the type of secondary structure. For control sample band (Fig. 3 (6)) is characteristic for

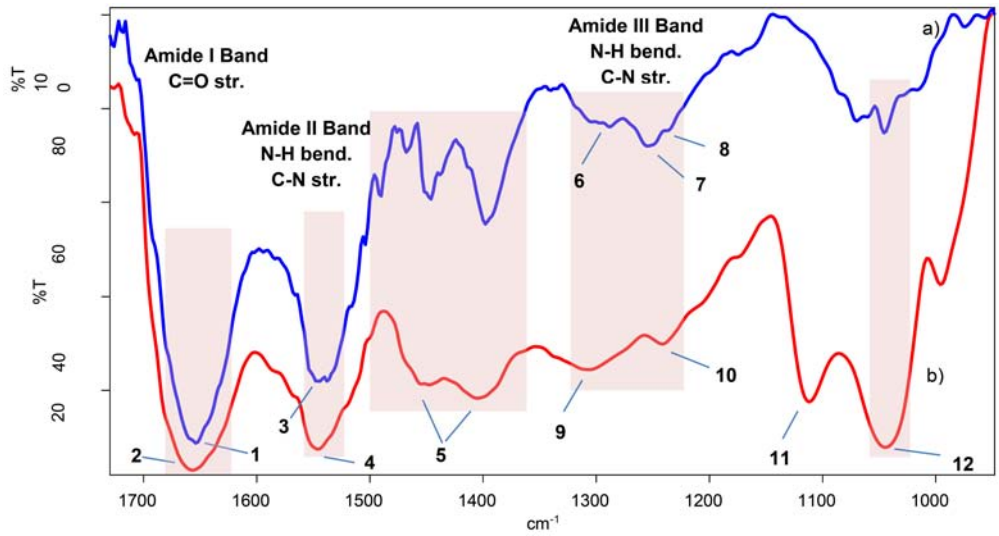

Fig. 3 FTIR spectrum in range: 1700–950 cm^{-1}: a) bovine serum albumin; b) bovine serum albumin-shikimic acid complex

α-helix structure and bands at Fig. 3 (7 and 8) can be assigned to the random coil and β-sheet structure, respectively. For complex appeared bands at Fig. 3 (9 and 10) that can be assigned to α-helix and β-sheet structure, respectively [9]. Intensive bands at Fig. 3 (11 and 12) for the protein-cyclitol complex are characteristic for C–O, and C–OH stretching vibrations of cyclitol. Thus, as a result of cyclitol-protein backbone chain interactions, the conformation of bovine serum albumin changes, increases the amount of intermolecular hydrogen and protein structure became more folded.

3.3 HPLC-MS/MS

HPLC-MS/MS method was used in order to investigate the quantitative relationship of protein-cyclitol. Shikimic acid was detected in negative ionization mode. It was found, that only mobile phases with the addition of formic acid enable detection of the analyte. Obtained retention times of pseudo-molecular ion are following:

- Water + 0.1 % (v/v) formic acid: t_r = 5.099 minutes.
- Water + 0.1 % (v/v) formic acid + 0.5 % (v/v) isopropanol: t_r = 5.064 minutes.
- Water + 0.1 % (v/v) formic acid + 1 % (v/v) isopropanol: t_r = 5.060 minutes.
- Water + 0.1 % (v/v) formic acid + 2 % (v/v) isopropanol: t_r = 5.057 minutes.

For the determination of unbounded cyclitol, a mobile phase composed of water with 0.1 % (v/v) formic acid was selected. The calibration curve of shikimic acid with a regression equation is shown in Fig. 4. Electrostatic interactions, between a deprotonated carboxylic group of cyclitol with charged groups of protein as well

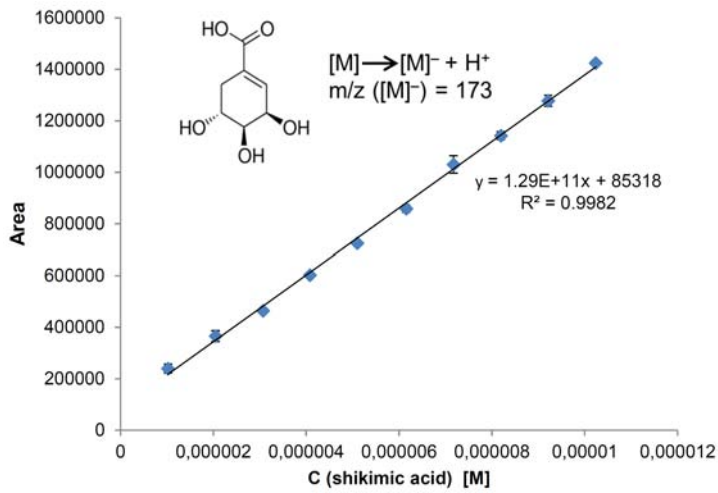

Fig. 4 Calibration curve of shikimic acid

Table 1
Quantitative analysis of cyclitol binded with bovine serum albumin.

Molar ratio of protein-cyclitol	Initial molar concentration of shikimic acid / M	Percent of binded cyclitol with protein	SD %
1:2	6.02×10^{-5}	92.52	1.49
1:5	1.50×10^{-4}	54.98	1.77
1:7	2.11×10^{-4}	45.70	0.33

as π – π stacking interaction of cyclitol ring with aromatic amino acids, occurs in the column. In the case of a higher concentration of shikimic acid, a relatively lower amount of cyclitol is bound to a macromolecule (Table 1). It is caused by saturation of bovine serum albumin binding sites with cyclitol which blocks electrostatic interaction between molecules [10].

4. Conclusions

The aim of the present work was to study the interaction between model protein and shikimic acid. The conducted research allowed us to make the following conclusions: 1) results obtained by fluorescence spectroscopy proved that protein-cyclitol binding is a dynamic process. Cyclitol had a stabilization effect on protein structure. It was preferentially excluded from the protein surface and hydrophobic effect was enhanced; 2) FTIR spectra showed that shikimic acid induced folding of protein structure as a result of cyclitol-polypeptide backbone chain interactions; 3) HPLC-MS/MS analysis shows that cyclitol bind to bovine serum albumin mainly because of electrostatic and π – π stacking interactions.

Protein-cyclitol binding affinity tends to decrease at high concentrations of shikimic acid, thus these types of interactions were inhibited. To summarize, interactions between bovine serum albumin and shikimic acid had a non-specific character and could be described as a kind of solvation phenomenon – preferential exclusion.

Acknowledgments

This work was financially supported in the framework of the project "Advanced Biocomposites for Tomorrow's Economy BIOG-NET" (FNP POIR.04.04.00-00-1792/18-00).

References

[1] Al-Suod H., Ligor M., Ratiu I. A., Rafińska K., Górecki R., Buszewski B.: A window on cyclitols: Characterization and analytics of inositols. *Phytochem. Lett.* **20** (2017), 507–519.

[2] Singh P., Gupta E., Mishra P: Shikimic acid as intermediary model for the production of drugs effective against influenza virus. In: *Phytochemicals as Lead Compounds for New Drug Discovery.* C. Egbuna, S. Kumar, J.C. Ifemeje, S.M. Ezzat, S. Kaliyaperumal (eds.). Elsevier 2020, p. 245–256.

[3] Vishwas D. S., Laxman S. W.: Spectroscopic analysis on the binding interaction of biologically active pyrimidine derivative with bovine serum albumin. *J. Pharm. Anal.* **6** (2016), 56–63.

[4] Dechang L., Baohua J.: Protein conformational transitions coupling with ligand interactions: Simulations from molecules to medicine. *Med. Nov. Technol. Devices.* **3** (2019), 1–10.

[5] Metrick M. A., Temple J. E., Macdonald G.: The effects of buffers and pH on the thermal stability, unfolding and substrate binding of RecA. *Biophys. Chem.* **184** (2013), 29–36.

[6] Liu X., Zhou P., Tran A., Labuza T. P.: Effects of polyols on the stability of whey proteins in intermediate-moisture food model systems. *J. Agric. Food Chem.* **57** (2009), 2339–2345.

[7] Gekko K., Science F., Culture M.: Preferential Polyhydric Hydration of Bovine Serum Albumin in of polyhydric alcohols (ethylene glycol, glycerol, xylitol, sorbitol, mannitol, and inositol) was investigated by a densimetric method with the application of multicom ponent theory. *Biochem. J.* **90** (1981), 39–50.

[8] Sukumaran S.: Protein secondary structure elucidation using FTIR spectroscopy. https://assets.thermofisher.com/TFS-Assets/MSD/Application-Notes/AN52985-protein-secondary-structure-elucidation-using-ftir-spectroscopy.pdf

[9] Barth A.: Infrared spectroscopy of proteins. *Biochim. Biophys. Acta* **1767** (2007),1073–1101.

[10] Bodzioch K., Durand A., Kaliszan R., Baczek T, Vander Heyden Y.: Advanced QSRR modeling of peptides behavior in RPLC. *Talanta* **81** (2010), 1711–1718.

Analytical methods in the identification and isolation of 2-aminoimidazoline-2 derivatives

Dominik Straszak*, Dariusz Matosiuk

Medical University of Lublin, Faculty of Pharmacy, Department of Synthesis and Chemical Technology of Pharmaceutical Substances, Chodźki 4a, 20-093 Lublin, Poland
✉ *dominik.straszak@gmail.com*

Keywords
NOESY
tautomers
ureas

Abstract
2-Imidazoline derivatives are an extremely important group of compounds with a broad spectrum of biological activity. Many of them exhibit anticancer, antimicrobial, anti-inflammatory, antiviral, cytotoxic, antidepressant, antihypertensive, and antispasmodic effects. A series of 2-substituted 2-imidazolines acting on imidazoline, adrenergic, and/or histamine receptors are an important class of therapeutic agents used in clinical practice. In addition urea derivatives of 2-imidazoline exhibit opioid receptors agonist properties. Like all 2-imidazolines containing an amino substituent in the 2-position on the ring, they can exist in the two forms of tautomers: 2-aminoimidazoline-2 and 2-iminoimidazolidine. In our work, a series of known 1-(arylimidazolin-2-yl)-3-benzylureas was synthesized and isolated by a new method. The structures of the obtained compounds, with particular emphasis on the double bond system on the C2 carbon of the imidazoline ring, were confirmed by analytical experimental methods.

1. Introduction

Imidazolines are a group of five-membered, heterocyclic, organic imidazole derivatives with one double bond and two nitrogen atoms in their structure. Due to the partial hydrogenation of the ring, we distinguish three isomers of imidazoline: 2-imidazoline and 3-imidazoline containing the imino group, and 4-imidazoline containing the alkene group. The location of the double bond is crucial to the physical, chemical, and biological properties. Among the three mentioned isomers, 2-imidazoline, and in particular, its derivatives containing the amino-, alkoxy-, mercapto-, and alkyl- substituent in the 2-position, are the most important in medicinal chemistry. Chemically, they can exist in tautomeric forms where the double bond is located in the imidazoline ring or between the carbon and the 2-substituent. Over the years, many methods of synthesizing the 2-imidazoline system have been developed. The vast majority of them are based on the cyclization of ethylenediamines, aziridines, isocyanides, cyanides,

amidines, amides, or imines with aldehydes, nitriles, carboxylic acids, and other carbon donor nucleophiles [1].

2-Imidazolines show diversified biological activity and are part of the structure of a large number of drug candidates. They act as inhibitors of the proteasome [2], selective cyclooxygenase-2 inhibitors [3], P2X purinoreceptor-7 antagonists [4], estrogen receptor agonists [5], glycoprotein IIb / IIIa inhibitors [6]. 2-imidazoline derivatives also inhibit interactions between human homolog of double minutes-2 (MDM2) and tumor suppressor protein p53 [7], many of them also exhibit antibacterial and antiprotozoal properties [8, 9]. The reason for the activity of the imidazoline ring is, inter alia, their ability to interact with aspartate and glutamate acids, which are present in the structure of many molecular targets. Another important cause is the presence of imidazoline receptors in the human body that specifically bind to the imidazoline ring [10, 11]. The 2-imidazoline derivatives currently used in pharmacotherapy have a similar structure consisting of a 2-imidazoline ring connected by a methylene or amine bridge or directly to an aryl moiety. Xylometazoline, naphazoline, oxymetazoline, and tetryzoline are α-adrenomimetics used externally as nasal vasoconstrictors. Clonidine, moxonidine, tizanidine are agonists at α2-adrenergic and imidazoline receptors. Other 2-imidazoline derivatives widely used in medicine are the non-selective α-adrenergic receptor antagonist–tolazoline, the first generation histamine H1 receptor antagonist–antazoline, and α-adrenergic antagonist –phentolamine [12].

Obtained by Matosiuk and co-workers urea derivatives with analgesic activity are a very promising group of 2-substituted 2-imidazolines [13, 14]. They structurally fit the non-classical pharmacophore model of opioid receptors and the activity of these compounds has been confirmed by biological tests. They showed an affinity for the μ-opioid receptor at the micromolar level and a strong antinociceptive effect in animal tests. The aim of this study was to synthesize and isolate 2-imidazoline urea derivatives by the new method and to perform their structural analysis using the available experimental methods.

2. Experimental

2.1 Reagents and chemicals

Reagents used for the synthesis of 1-(arylimidazolin-2-yl)-3-benzylureas were obtained from Sigma-Aldrich (USA), and solvents from POCh Gliwice (Poland). Toluene and ethyl acetate (HPTLC grade) applied for chromatography were purchased from Merck (Darmstadt, Germany) and used without further purification. Dimethyl sulfoxide-d_6 was purchased from VWR International (USA).

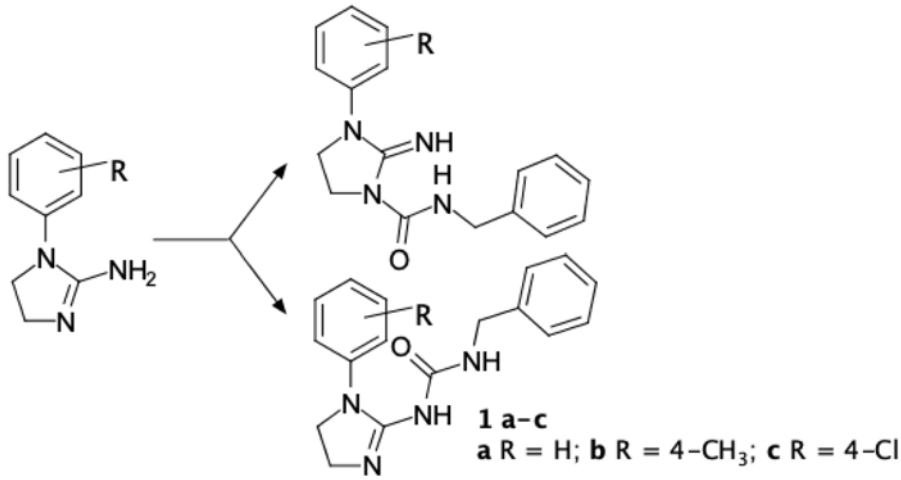

Fig. 1 Scheme of the synthesis of compounds **1a**–**1c**.

2.2 Instrumentation

Isolation of 1-(arylimidazolin-2-yl)-3-benzylureas was performed by FLASH (DCVC) using a puriFlash 430 apparatus and using PF-15SIHP puriFlash commercial columns from Interchim (Montluçon, France). The chromatograms were developed under the light of UV lamp (λ = 254 nm). MS spectra were obtained by electrospray ionization method using a Bruker microTOF-Q II mass spectrometer. NMR spectra were recorded on a Bruker Ascend™ 600 MHz spectrometer in dimethyl sulfoxide-d_6 as a solvent. Tetramethylsilane was used as an internal standard. Elemental analysis was carried out by a Perkin-Elmer analyser.

3. Results and discussion

3.1 Synthesis and isolation

Urea derivatives were synthesized as previously reported: benzylamine (1 eq.), triphosgene (0.33 eq.) and triethylamine (10 ml) were stirred for 2 hours in dry toluene (100 ml), then the appropriate 1-aryl-2-iminoimidazolidine (1 eq.), and triethylamine (10 ml) were added dropwise and the mixture was heated for 6 hours at 100 °C. Then, the precipitate was filtered from the reaction mixture, and the filtrate's solvent was distilled off. The oily residue was recrystallized from isopropanol. The obtained white solid was composed of two urea imidazoline derivatives: 1-(arylimidazolin-2-yl)-3-benzylurea and 1-aryl-2-imino-3-benzyl-aminocarbonylimidazolidine as a by-product (Fig. 1). The isomer mixture was separated by FLASH (DCVC) on a normal-phase chromatography system. Hexane:ethyl acetate was used as the mobile phase in a 6:4 volume ratio.

Table 1
Experimental NMR chemical shifts of synthesized compounds **1a**–**1c**.

Compound, molecular formula	^{1}H NMR	^{13}C NMR
1a, $C_{17}H_{18}N_4O$	8.64 (s, 1H, NH), 7.76 (t, *J* = = 2.5 Hz, 1H, NH), 7.35–7.23 (m, 8H, Ar-H), 7.03 (tt, *J* = = 7.7, 1.3, 2H, Ar-H), 4.21 (d, *J* = 6.2 Hz, 2H, CH_2), 3.85 (dd, *J* = 9.5, 7.5 Hz, 2H, CH_2), 3.55 (dd, *J* = 9.3, 6.9 Hz, 2H, CH_2)	159.6, 154.1, 141.7, 139.2, 129.6, 128.5, 127.7, 127.3, 124.9, 121.0, 50.6, 48.0, 42.8
1b, $C_{18}H_{20}N_4O$	8.60 (s, 1H, NH), 7.39–7.32 (m, 5H, Ar-H), 7.28–7.27 (m, 2H, Ar-H), 7.27–7.11 (m, 2H, Ar-H), 6.46 (t, *J* = 7.9 Hz, 1H, NH), 4.22 (d, *J* = 6.6 Hz, 2H, CH_2), 3.84 (dd, *J* = 9.5, 7.0 Hz, 2H, CH_2), 3.57 (dd, *J* = 9.4, 7.0 Hz, 2H, CH_2), 2.25 (s, 3H, CH_3)	159.6, 154.1, 140.0, 139.2, 135.1, 129.7, 128.5, 127.7, 127.3, 120.7, 50.6, 48.0, 42.8, 20.7
1c, $C_{17}H_{17}ClN_4O$	8.66 (s, 1H, NH), 7.84 (t, *J* = = 2.9 Hz, 1H, NH), 7.35 (ddd, *J* = 8.1, 1.5, 0.5 Hz, 2H, Ar-H), 7.32–7.20 (m, 7H, Ar-H), 4.21 (d, *J* = 6.4 Hz, 2H, CH_2), 3.84 (dd, *J* = 9.6, 7.0, 2H, CH_2), 3.55 (dd, *J* = 9.4, 7.1 Hz, 2H, CH_2)	159.5, 154.1, 140.4, 139.2, 130.1, 129.4, 128.5, 127.7, 127.3, 123.4, 50.6, 48.0, 42.8

3.2 Structural analysis

The structures of the compounds were confirmed by analytical methods. The protonated molecular ions were in the range of ±4 ppm. The obtained results of the elemental analysis differed from the theoretical values by ±0.4%. All proton and carbon resonances of 1-(arylimidazolin-2-yl)-3-benzylureas were assigned using one- and two-dimensional NMR techniques (^{1}H–decoupled, ^{13}C NMR, Phase sensitive NOESY, ^{1}H–^{13}C multiplicity edited ^{1}H–^{13}C HSQC with gradient selection, ^{1}H–^{13}C HMBC with gradient selection). ^{1}H NMR spectral characteristic of the examined compounds revealed two double-doublets signals of 2-imidazoline methylene hydrogens (C4 and C5) at ca. 3.6 and 3.8 ppm, respectively, with the coupling constants of *J* ca. 9.5 and *J'* ca. 7.0 Hz, one dublet signal of benzyl methylene protons (C9) at ca. 4.2 ppm with the coupling constant *J* ca. 6.4 Hz and widely separated hydrogens signals of two aromatic rings in the 7.2–7.8 ppm range. The nitrogen-bounded hydrogen atoms (N6 and N8) were represented by a singlet signal of the chemical shift values of ca. 8.6 ppm (N6 hydrogens) and triplet signal between 7.8–6.5 ppm (N8 hydrogens). ^{1}H NMR spectra were recorded at three temperatures: 0, 20, and 40 °C. They showed no major changes in the distribution and structure of proton signals. The ^{13}C NMR spectra of compounds in the

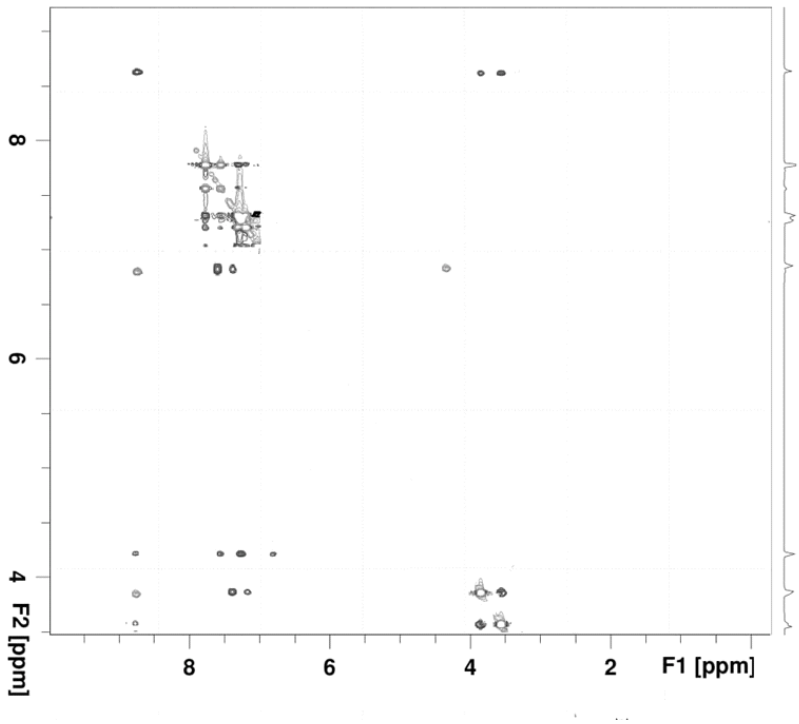

Fig. 2 NOESY spectrum of compound **1a**.

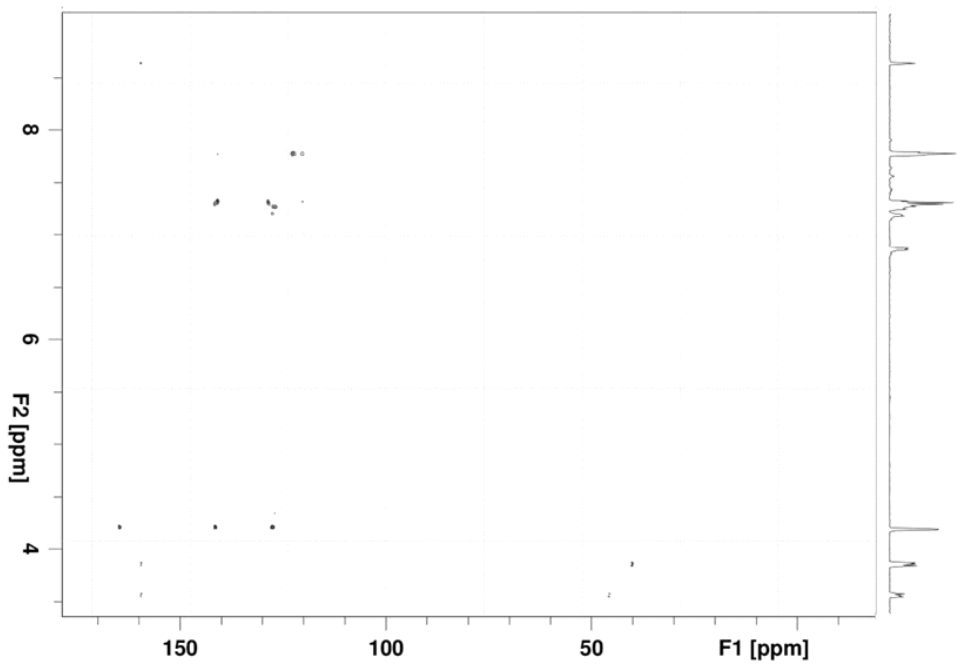

Fig. 3 $^{1}H–^{13}C$ HMBC spectrum of compound **1a**.

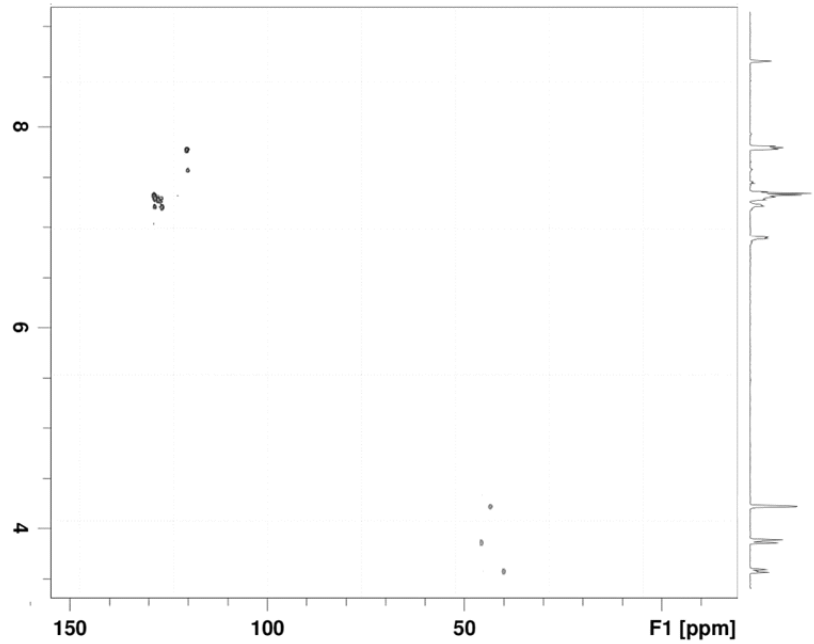

Fig. 4 $^{1}H–^{13}C$ HSQC spectrum of compound **1a**.

aliphatic range revealed signals of three methylene carbon atoms (C4, C5 C9) with the values of the chemical shift, respectively: 48.0, 50.6, 42.8 ppm. The carbonyl (C7) and carbimine (C2) carbon atoms signals were located at ca. 154.1 (C7) and 159.6 ppm (C2). NMR spectra confirmed the presence of signals for all hydrogen and carbon atoms of analyzed 1-(arylimidazolin-2-yl)-3-benzylureas. ^{1}H and ^{13}C NMR data are presented in Table 1. To learn more about the structure of the compounds, the NOESY experiment was performed which correlates protons through dipolar couplings. Cross-peak of C9/N6 hydrogens at ca. 8.6/4.2 ppm corresponding to the form of 2-aminomidazoline-2 derivatives, rather than 2-iminoimidazolidine (Fig. 2). Additionally, the $^{1}H–^{13}C$ HMBC and $^{1}H–^{13}C$ HSQC techniques were used to confirm the position of protonated carbons in the structure of the obtained compounds. The experimental spectra of compound **1a** are shown in Fig. 3 and 4.

4. Conclusions

The synthesis and purity of 2-amino-imidazoline derivatives have been confirmed by analytical methods. The results of the spectral analysis indicate that the obtained compounds in dimethyl sulfoxide solution exist in the form of 1-(aryl-imidazolin-2-yl)-3-benzylureas. The finding is essential to molecular docking and structure-activity relationship studies.

References

[1] Mehedi M.S., Tepe J.J.: Recent advances in the synthesis of imidazolines (2009–2020). *Adv. Synth. Catal.* **362** (2020), 4189–4225.

[2] Azevedo L.M., Lansdell T.A., Ludwig R.A, Mosey R.A., Woloch D.K., Cogan D.P., Patten G.P., Kuszpit M.R., Fisk J.S., Tepe J.: Inhibition of the human proteasome by. imidazoline scaffolds. *J. Med. Chem.* **56** (2013), 5974–5978.

[3] Khanna I.K., Weiler Y., Yu X., Xu X.D., Koszyk F.J., Collins P.W., Koboldt C.M., Veenhuizen A.W., Perkins W.E., Casper J.J., Masferrer J.L., Zhang Y.Y., Gregory S.A., Seibert K., Isakson P.C.: 1,2-Diarylimidazoles as potent, cyclooxygenase-2 selective, and orally active anti-inflammatory agents. *J. Med. Chem.* **40** (1997), 1634–1647.

[4] Merriman H.H., Ma L., Shum P., McGarry D., Volz F., Sabbel J.S., Gross A., Zhao Z., Rampe D., Wang L., Wirtz-Brugger F., Harris B.A., Macdonald D.: Synthesis and SAR of novel diarylimidazolines as potent P2X7 receptor antagonists. *Bioorg. Med. Chem. Lett.* **15** (2005), 435–438.

[5] Gust R., Beurgermeister T., Mannschreck A., Schoenenberger H.: Aqua[1-(2,3-dichloro-4-hydroxyphenyl)-2-phenylethylenediamine](sulfato)platinum(II) complexes with variable substituents in the 2-phenyl ring. 1. Synthesis and anti tumor and estrogenic properties. *J. Med. Chem.* **33** (1990), 2535–2544.

[6] Zabłocki J., Miyano M., Garland R.B., Pireh D., Schretzman L., Rao S.N., Lindmark R.J., Panzer-Knodle S.G., Nicholson N.S., Taite B.B., Salyers A.K., King L.W., Campion J.G., Feigen L.P.: Potent in vitro and in vivo inhibitors of platelet aggregation based upon the Arg-Gly-Asp-Phe sequence of fibrinogen. A proposal on the nature of the binding interaction between the Arg-guanidine of RGDX mimetic and the platelet GP IIb-IIa receptor. *J. Med. Chem.* **36** (1993), 1811–1819.

[7] Tovar C., Graves B., Packman K., Filipovic Z., Higgins B., Xia M., Tardell C., Garrido R., Lee E., Kolinsky K., To K., Linn M., Podlaski F., Wovkulich P., Vu B., Vassilev L.T.: MDM2 small-molecule antagonist RG7112 activates P53 signaling and regresses human tumors in preclinical cancer models. *Cancer Res.* **73** (2013), 2587–2597.

[8] Donkor I.O., Clark A.M.: In vitro antimicrobial activity of aromatic diamidines and diimidazolines related to pentamidine. *Eur. J. Med. Chem.* **34** (1999), 639–643.

[9] Altameemi H.A., Askar F.W., Nie O.A.: Synthesis and biologiical evaluation of some imidazoline derivatives. *Conf. Ser.: Mater. Sci. Eng.* **871** (2020), 012030.

[10] Krasavin M.: Biologically active compounds based on the privileged 2-imidazoline scaffold: The world beyond adrenergic/imidazoline receptor modulators. *Eur. J. Med. Chem.* **97** (2015), 525–537.

[11] Rasach W., Schafer U., Chun J., Dominiak P.: Biological significance of agmatine, an endogenous ligand at imidazoline binding sites. *Br. J. Pharmacol.* **133** (2001), 755–780.

[12] Ritter J., Lewis L., Mant T., Ferro A.: *A Textbook of Clinical Pharmacology and Therapeutics.* 5nd ed. London, CRC Press 2008.

[13] Matosiuk D., Fidecka S., Antkiewicz-Michaluk L., Dybała I., Kozioł A.E.: Synthesis and pharmacological activity of new carbonyl derivatives of 1-aryl-iminoimidazolidine. Part 1. Synthesis and pharmacological activity of chain derivatives of 1-aryl-2-iminoimidazolidine containing urea moiety. *Eur. J. Med. Chem.* **36** (2001), 783–797.

[14] Szacoń E., Rządkowska M., Kaczor A.A., Kędzierska E., Fidecka S., Matosiuk D.: Synthesis, central nervous system activity and structure-activity relationships of novel 1-(1-alkyl-4-aryl-4,5-dihydro-1*H*-imidazo)-3substituted urea derivatives. *Molecules* **20** (2015), 3821–3840.

Investigation of the oxidation behaviour of cysteine by means of electrochemistry hyphenated to capillary electrophoresis and mass spectrometry

Johannes Eidenschink*, Frank-Michael Matysik

University of Regensburg, Faculty of Chemistry and Pharmacy, Institute of Analytical Chemistry, Chemo- and Biosensors, Universitätsstraße 31, 93053 Regensburg, Germany
✉ *johannes.eidenschink@chemie.uni-regensburg.de*

Keywords
capillary electrophoresis
electrochemistry
mass spectrometry
redox studies
screen-printed electrodes

Abstract
Classical electrochemical techniques are limited in the identification of reaction product species. By hyphenating electrochemistry (EC) to mass spectrometry (MS) this limitation can be overcome and a potent method for redox studies is established. A further enhancement can be achieved through the implementation of a separation technique in-between. In this contribution, we investigated the oxidation behaviour of cysteine with EC coupled directly to MS or via capillary electrophoresis (CE) for analyte separation prior to introduction into the mass spectrometer. Measurements were conducted on carbon-based screen-printed electrodes (SPEs), which performed well in preliminary experiments. Cystine, cysteine sulfinic acid and cysteic acid were found as electrogenerated products. These product species were identified based on their migration behaviour in CE, mass-to-charge ratios and isotopic patterns.

1. Introduction

Since its introduction by Bruckenstein and Gadde in 1971 [1], EC-MS became a powerful method for qualitative as well as quantitative studies of redox reactions [2]. A common mode of EC-MS is the direct coupling of an electrochemical flow cell to the MS. Such a system is characterised by a fast transfer of electrogenerated species to the MS. Thus, it is capable of detecting even short-lived intermediates [3]. Information on the potential-dependent product formation is generated by applying a potential sweep and simultaneous recording of MS spectra. Since there is no separation taking place between the redox reaction at the electrode surface and the detection in the MS, all components in the solution reach the detector at the same time. This may lead to discrimination of analytes, e. g., due to ion suppression effects in electrospray ionization, and thus, limits the

generation of quantitative information [4]. Matysik proposed a solution to this limitation in 2003 [5] by the hyphenation of EC to CE, which was termed electrochemically assisted injection (EAI). In 2011, Scholz et al. [6] achieved the first combination of EAI-CE to MS with a manually controlled device. Further improvement by Palatzky et al. [7] resulted in the development of a fully automated injection cell.

In this contribution, we applied this combination of techniques to analyse the oxidation products of cysteine. Cysteine is an electrochemically active amino acid. Due to a thiol group in its side chain several oxidation states are possible. The amino acid is involved in a variety of biological processes, e. g., in the antioxidant gluthathione. Together with its dimer, cystine, it also has a major impact on the structure of proteins by formation of disulfide bonds [8]. Other oxidation products, such as cysteine sulfinic and cysteic acid, are topic of current research, e. g., in metabolic studies [9].

2. Experimental

2.1 Reagents and chemicals

The following chemicals were used, all of analytical grade: 0.1 M sodium hydroxide solution, ammonia, ammonium acetate, formic acid (Merck, Germany), acetic acid, L-cysteic acid, L-cysteine, L-cysteine sulfinic acid (Sigma Aldrich, USA), caffeine (ABCR, Germany), isopropanol (Roth, Germany), L-cystine (Mann Research, USA). Solutions were prepared with ultra-pure water provided by a Milli-Q Advantage A10 system (Merck, Germany).

2.2 Instrumentation

2.2.1 Consumables

Within this work, fused silica capillaries (Polymicro Technologies, USA) with an outer diameter of 360 µm and an inner diameter of 50 µm were used. At both ends, 0.5 cm of the polyimide coating was removed. The detection side was polished to a plane edge, while the tip at the injection side was polished at a 15-degree angle. Prior to each measurement session, separation capillaries were conditioned applying the following protocol: At first, the capillary was flushed for 10 min with 0.1 M sodium hydroxide solution, then for 5 min with ultra-pure water and finally for at least 30 min with 500 mM acetic acid. Electrochemical measurements were carried out with disposable SPEs (Metrohm DropSens, Spain) of the type DRP-110 with working and counter electrode based on carbon and a silver quasi-reference electrode. All mentioned potentials refer to this electrode system.

2.2.2 Setup for direct EC-MS

Electrochemical conversion of cysteine in EC-MS experiments was carried out in a commercially available flow cell (Metrohm DropSens, Spain) for SPEs. The potential was controlled with a μStat 200 potentiostat (Metrohm DropSens, Spain). The flow of the sample solution was achieved by a syringe pump of type UMP3 with a Micro2T pump controller (World Precision Instruments, USA). The pump was equipped with a 1 mL glass syringe. For detection, a micrOTOF time-of-flight MS (Bruker Daltonics, Germany) equipped with a grounded CE-ESI-MS sprayer interface (Agilent Technologies, Germany) was used. The flow cell and the MS were connected via a fused silica capillary with a length of 21 cm installed in the ESI interface. Three sample solutions containing 1 mM cysteine and 50 mM ammonium acetate were prepared with different pH values. One solution was adjusted to pH = 5 with acetic acid, the second solution had a pH of 7 and the third one was adjusted to pH = 9 with ammonia. The sheath liquid used for the operation of the ESI interface consisted of isopropanol, water, and formic acid (49.9/49.9/0.2, *v/v/v*). It was provided at a constant flow rate of 8 μL min^{-1} by a syringe pump (KD Scientific, USA). The flow rate of sample solution was 16 μL min^{-1}. Linear sweep voltammograms were carried out in a potential range from 0.0 to 2.0 V with a scan rate of 10 mV s^{-1} and mass spectra were recorded simultaneously. The MS detection parameters were: positive ion mode, mass range 50–500 *m/z*, spectra rate 5 Hz, nebulizer gas 1.0 bar, dry gas 4.0 L min^{-1}.

2.2.3 Online EC-CE-MS setup

For online EC-CE-MS experiments, an automated, custom-made system for CE developed by Palatzky et al. in 2013 [7] was used. The setup is shown schematically in Fig. 1. Main part of the system is a horizontally movable desk made of Teflon with positions for a buffer vial and a SPE. A Pt electrode connected to a high voltage source is inserted into the buffer vial. The separation capillary can be installed via a sleeve and is movable in vertical direction. Potentiostat and detector were identical to the EC-MS setup. The separation capillary had a length of 35 cm. Two sample solutions were used, the first one consisted of 1 mM cysteine, 50 mM ammonium acetate and 250 μM caffeine as electroosmotic flow marker. The second solution additionally contained 100 μM cysteine sulfinic acid and 100 μM cysteic acid. For measurements, 50 μL of sample solution were placed on the electrode and the oxidation was started by applying a constant potential for 15 s. The hydrodynamic sample injection was initiated 5 s after the start of the oxidation by an automated movement of the capillary tip into the sample droplet for 10 s. Afterwards, the capillary was moved back into the buffer vial and the separation was started by applying a voltage of 20 kV. The separation buffer was a 500 mM acetic acid solution. The MS detection parameters and sheath liquid composition were identical to the EC-MS measurements.

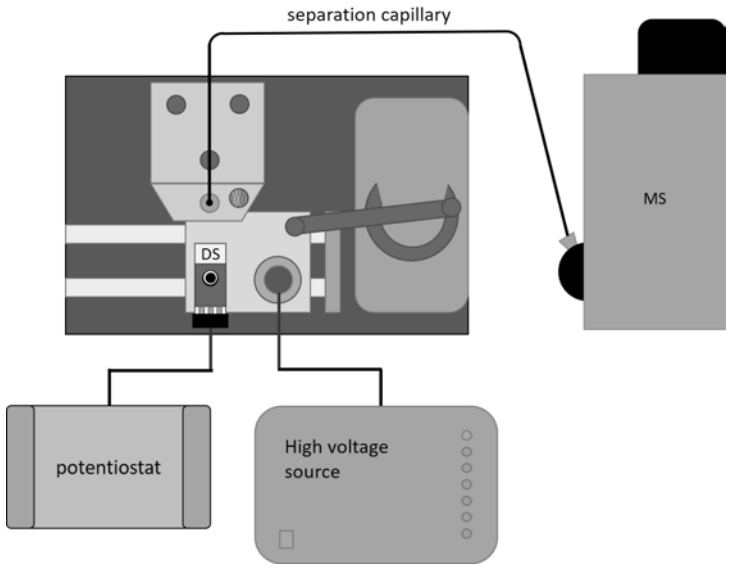

Fig. 1 Schematic illustration of the EC-CE-MS setup. The main component of the system is a movable desk with slots for a buffer vial and a SPE. The potential at the SPE is controlled via a potentiostat. Inside the buffer vial is a Pt electrode, which is connected to a high voltage source. One end of the separation capillary is installed in the movable desk via a sleeve and the other end is inserted into the ESI interface of the mass spectrometer.

3. Results and discussion

To obtain information on the potential-dependent formation of oxidation products of cysteine, direct EC-MS measurements were performed. Mass voltammograms resulting from experiments with a cysteine solution adjusted to acidic, neutral, or basic pH are shown in Fig. 2.

In the measurement of the cysteine solution adjusted to pH = 5 (Fig. 2A), two additional oxidation products besides from cystine were found. The generation of a species with *m/z* of 154.02 started at an applied potential of 0.4 V. Another product with *m/z* of 170.01was formed beginning at a potential of 0.8 V. Both species were also found in the measurements of cysteine solutions at neutral and basic pH (Fig. 2B and C). Under basic conditions, the formation of cystine started at lower potentials and resulted in higher signal intensities. Therefore, we conclude that cystine generation is more favourable at higher pH values. In contrary, the generation of the other two products started at lower potentials and resulted in higher signal intensities in the acidic cysteine solution. The signals of these two product species were assigned to cysteine sulfinic acid (*m/z* 154.02) and cysteic acid (*m/z* 170.01). This assignment was confirmed by online EC-CE-MS experiments. In these comparative measurements, the *m/z*, the migration times and the isotopic patterns of electrogenerated species matched with the reference substances. The measured *m/z* with the corresponding product species and their potential ranges of formation are summarized in Table 1.

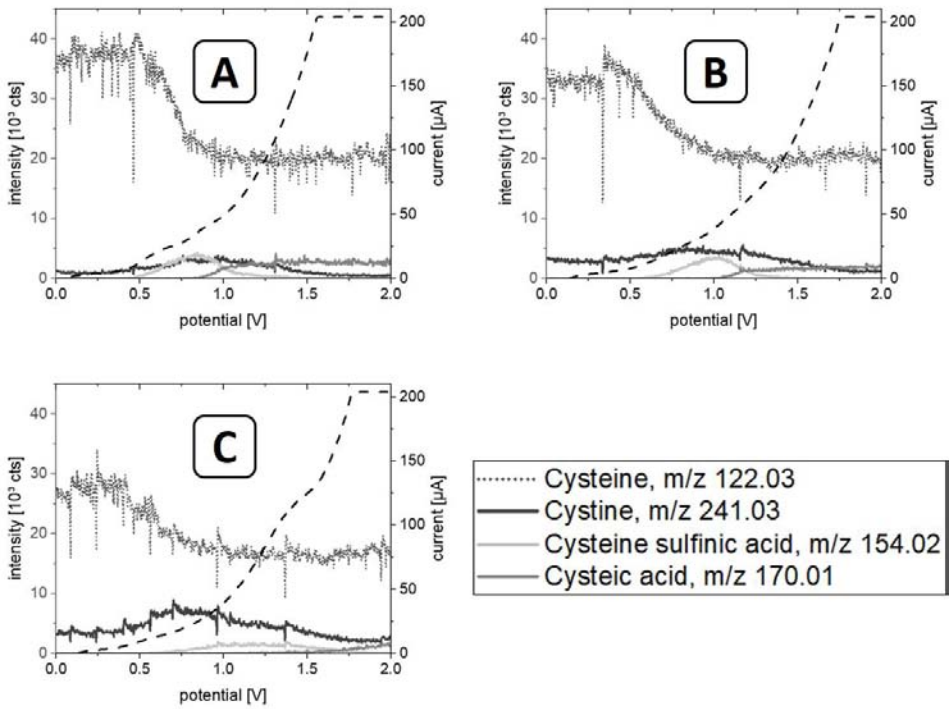

Fig. 2 Mass voltammograms of a 1 mM cysteine solution with 50 mM ammonium acetate adjusted to (A) pH = 5, (B) pH = 7, and (C) pH = 9. The measurements were conducted on a carbon-based SPE. Linear potential sweeps were performed from 0.0 to 2.0 V at a scan rate of 10 mV s^{-1}. Currents recorded during measurements are shown as dashed line. The flow rate of sample solutions was 16 µL min^{-1}. The transfer capillary had an inner diameter of 50 µm and a length of 21 cm.

Table 1
Proposed oxidation products of cysteine and potential ranges of their formation at the respective pH.

m/z	Oxidation product	Potential range of product formation / V		
		pH = 5	pH = 7	pH = 9
241.03	Cystine	0.5–1.4	0.4–1.4	0.3–1.5
154.02	Cysteine sulfinic acid	0.4–1.6	0.5–1.6	0.6–2.0
170.01	Cysteic acid	0.8–2.0	1.0–2.0	1.1–2.0

4. Conclusions

Electrochemical oxidation of cysteine was possible with the described setup. It was shown in direct EC-MS measurements, that two additional oxidation products apart from cystine were formed. The potential-dependent formation of product species was investigated for acidic, neutral, and basic pH conditions. Cystine was

shown to be the predominant oxidation product under basic conditions, while cysteine sulfinic and cysteic acid were found to be more preferred at acidic pH. These products were also electrogenerated and separated in an online EC-CE-MS approach. Electrochemically formed cysteine sulfinic and cysteic acid were identified based on their migration behaviour in CE, measured *m/z* and isotopic patterns in comparison to corresponding reference substances.

References

[1] Bruckenstein S., Gadde R.: Use of a porous electrode for in situ mass spectrometric determination of volatile electrode reaction products. *J. Am. Chem. Soc.* **93** (1971), 793–794.

[2] Mark J., Scholz R., Matysik F.-M.: Electrochemical methods in conjunction with capillary and microchip electrophoresis. *J. Chromatogr. A.* **1267** (2012), 45–64.

[3] Herl T., Matysik F.-M.: Recent developments in electrochemistry-mass spectrometry. *ChemElectroChem.* **7** (2020), 2498–2512.

[4] Karst U.: Electrochemistry/mass spectrometry (EC/MS)-A new tool to study drug metabolism and reaction mechanisms. *Angew. Chem., Int. Ed.* **43** (2004), 2476–2478.

[5] Matysik F.-M.: Electrochemically assisted injection – a new approach for hyphenation of electrochemistry with capillary-based separation systems. *Electrochem. Commun.* **5** (2003), 1021–1024.

[6] Scholz R., Matysik F.-M.: A novel approach for the separation of neutral analytes by means of electrochemically assisted injection coupled to capillary electrophoresis-mass spectrometry. *Analyst* **136** (2011), 1562–1565.

[7] Palatzky P., Zöpfl A., Hirsch T., Matysik F.-M.: Electrochemically assisted injection in combination with capillary electrophoresis-mass spectrometry (EAI-CE-MS) – Mechanistic and quantitative studies of the reduction of 4-nitrotoluene at various carbon-based screen-printed electrodes. *Electroanalysis* **25** (2013), 117–122.

[8] Berg J.M., Tymoczko J.L., Gatto Jr. G.J., Stryer L.: *Stryer Biochemie*, 8th ed. Heidelberg, Springer 2018

[9] Tramonti A., Contestabile R., Florio R., Nardella C., Barile A., Di Salvo M.L.: A novel, easy assay method for human cysteine sulfinic acid decarboxylase. *Life* **11** (2021), 438.

Bioluminescence determination of caspase-3/7 in single osteosarcoma cells

Michael Killinger[a, b, *], Eva Matalová[c], Karel Klepárník[a]

[a] *Institute of Analytical Chemistry of Czech Academy of Science, Department of Bioanalytical Instrumentation, Veveří 97, 602 00Brno, Czech Republic* ✉ *killinger@iach.cz*
[b] *Masaryk University, Faculty of Science, Department of Chemistry, Kotlářská 2, 611 37 Brno, Czech Republic*
[c] *Institute of Animal Physiology and Genetics of Czech Academy of Science, Laboratory of Odontogenesis and Osteogenesis, Veveří 97, 602 00 Brno, Czech Republic*

Keywords
apoptosis
bioluminescence
cancer
single-cell analysis

Abstract
The knowledge of the accurate quantity of relevant proteins at the cellular level is essential for the correct diagnostic and therapeutic interpretation of analytical results. Some low copy number proteins are associated with physiological, but also pathological processes including cancer. This is likely to apply also for caspases, cysteine proteases traditionally associated with cell death via apoptosis. Their deregulation is observed in severe cancers. Here, we developed miniaturized instrumentation, and ultrasensitive and highly selective methodology based on bioluminescence photon-counting to quantify activated caspase-3/7 in individual cells. By comparison of the caspase-3/7 amounts of healthy and cancer cells, the results indicate an increase of caspase-3/7 activation in osteosarcoma cells, probably due to non-apoptotic functions of caspases in cancer. The developed instrumentation can potentially serve as a sensitive tool for diagnostics and anti-cancer strategies, where are single-cell analyses crucial to distinguish tumor and surrounded healthy tissue cells.

1. Introduction

Caspases are the group of cysteine-aspartic acid proteases with a crucial role during programmed cell death (apoptosis) and inflammation. Executioner caspases-3/7 are the final proteases activated before apoptosis, leading to cleavage of upwards of a thousand proteins and cell degradation [1]. Although they have been considered as the major switch between cell life and death, their role is also connected with cell differentiation [2]. The cell pro-differentiation effects of caspase-3 have been noted in diverse cell types that display minimal apoptotic-like features [3, 4]. Non-apoptotic effects of caspases are also recently emphasized in osteogenesis [5, 6]. Surprisingly, higher amounts of activated caspase-3 is observed in severe tumor tissues. Moreover, the deficiency of

caspase-3 either in tumor cells or in tumor stroma caused significant tumor sensitivity to radiotherapy in xenograft or mouse tumors [7].

The objective of the project is the development and application of an ultrasensitive and highly selective bioluminescence method to quantify proteins level heterogeneity in individual cells. Our previous study has already revealed a different level of active caspase-3/7 in the mouse osteoblast cells (MC3T3-E1) and mouse osteosarcoma cells (DUNN) in proliferating and apoptotic conditions. Moreover, the level heterogeneity of active caspase-3/7 in individual cells was established. This can be used for distinguishing tumors from surrounding healthy tissue cells in many clinical applications.

2. Experimental

2.1 Reagents and chemicals

A cell line of mouse osteoblastic precursors, MC3T3-E1, was obtained from the European Collection of Cell Culture (c.n. 99072810), mouse osteosarcoma cells, DUNN, were kindly provided by Dr. Lucia Knopfova from the Department of Experimental Biology, Masaryk University, Czech Republic. Proliferation conditions were obtained by cultivation the cells in MEM Alpha medium (Gibco, USA) enriched by 10% FBS (BioTech, CZ), penicillin/streptomycin (100 U/ml, 100μg/ml). Apoptosis was induced by 100μM cisplatin treatment overnight. Cells were suspended using trypsin (0.25 %, Gibco, Life Technologies), followed by centrifugation to remove trypsin and re-suspended in fresh PBS (BioTech, CZ) buffer for further bioluminescence analyses.

In our experiments, we used commercially available kit Caspase-Glo (Promega) providing a homogeneous single-step assay based on a luciferin-luciferase bioluminescent system [8]. Here, amino luciferin conjugated with a caspase-specific DEVD-peptide is inaccessible for luciferase. However, after the cleavage of the peptide attached to luciferin moiety by an active caspase, the free amino luciferin is immediately oxidized by firefly luciferase resulting in photon emission (Fig. 1; next page).

2.2 Instrumentation

Bioluminescence signal is registered by PMT head with cooled photocathode (Hamamatsu 7421-40, Japan). The bioluminescence reactions take place in eight 7 μl microvials made of glass tubes of sizes i.d./o.d. 1.3/1.9 mm (Hirschmann Laborgeräte, Germany). The microvials are placed in a carousel holder mounted on the body of PMT and sealed by a rubber O-ring. The temperature of the assembly is kept at a standard value of 37 °C. The signal of 7 μl of Caspase-Glo® lysis substrate in each microvial was taken as a blank.

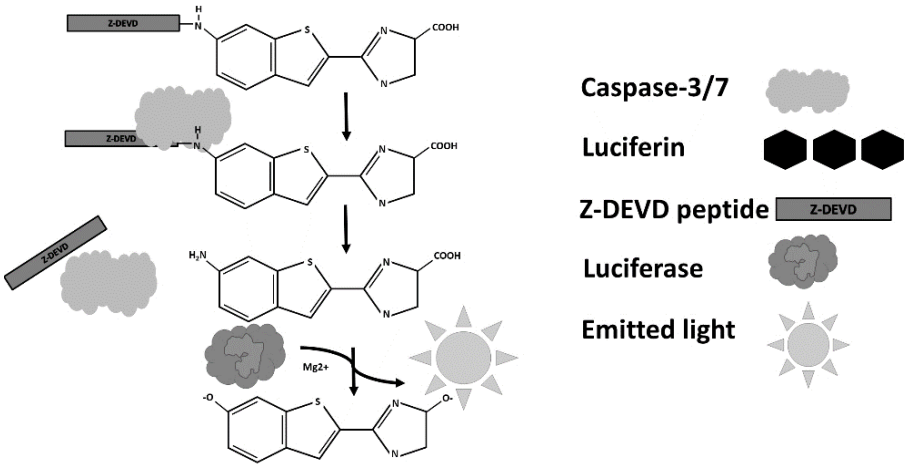

Fig. 1 Scheme of homogeneus single-step assay based on bioluminescent Caspase-Glo® reagents. Caspase-3/7 cleaving the specific DEVD peptide, resulting in immediate oxidation by luciferase and photon emission.

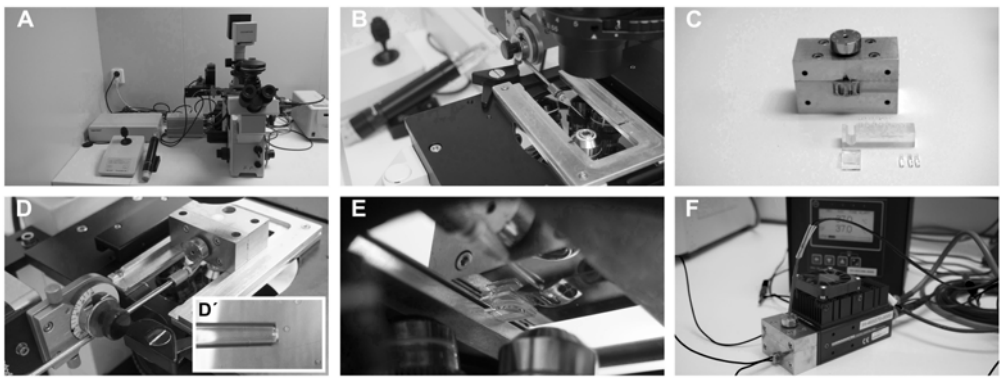

Fig. 2 Cell filling process: (A) The whole process take place on table of inverted microscope. (B) Prepared microcapillary is attached to in vitro manipulator. (C) Microvials filled with reagent are positioned into carousel body and the cell suspension is transferred into glass C-holder. (D) Carousel with filled microvials and attached C-holder is placed on microscope table and (D') individual cell are collected. (E) The C-holder with the cell suspension is attached to the carousel next to the microvials holder and cells are moved into the microvials filled by substrate. (F) A heated stainless-steel carousel attached to the body of the PMT.

To capture a single cell from suspension, we used micromanipulator ISCI (Eppendorf). The cell suspension is injected into a glass C-holder made of microscope slide enabling transparent choice of cells, free movement of the capillary, fast and easy capturing. Cells were transferred into microvials filled with Caspase-Glo® 3/7 lysis substrate placed in the carousel holder. The whole process is described in Fig. 2.

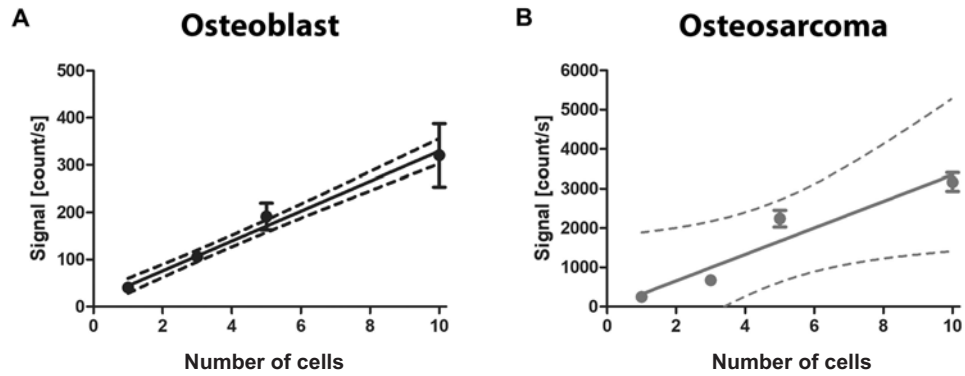

Fig. 3 Dependence of bioluminiscence signal on the number of cells. Mean values and SD were calculated from 3 individual measurements after subtraction of the blank signal. The osteosarcoma cells (B) showed increased level of activity of caspase-3/7 to control osteoblast cells (A). Dashed curves represent 95% interval of confidence for obtained results.

3. Results and discussion

To prove the reliability of the transfer of cells into the detection vials and purity of cultivation buffers, the bioluminescence signal was measured in vials with one, three, five, and ten cells sterilely transferred into caspase-3/7 Glo substrate and lysis agent. As shown in Fig. 3, the linearity of the dependences of the mean of signal values on the number of injected cells together with their plot inside the 95% confidence interval is a confirmation of the injection reliability. The quantities of caspase-3/7 in proliferating osteoblast and osteosarcoma cells are compared. The proliferating osteosarcoma cells comprise about the five-times higher amount of caspase-3/7 than osteoblast cells.

Determination of low copy number proteins in a single-cell level can reveal important processes of life phenomena. For determining the variability of caspase-3/7 level in single cells, we repeatedly measured bioluminescence signal in osteoblast and osteosarcoma cells in proliferating and apoptotic conditions. As shown in Fig.4 (next page), the level of active caspases in osteosarcoma cells was significantly higher than in osteoblast cells. Under the apoptotic conditions, the osteosarcoma cells exhibited enormous increases of active caspase-3/7. The ratio of amounts of caspase-3/7 between proliferating and apoptotic osteoblast cells and proliferating and apoptotic osteosarcoma cells was the same, approximately five-time higher. Interestingly, the caspases levels in proliferating osteosarcoma cells were similar to normal osteoblast in apoptotic conditions. (Fig. 4).

The increased activation of caspase-3/7 in apoptotic osteosarcoma cells can indicate, that the same treatment of cisplatin induces stronger induction of apoptosis, but the high level of active caspase was observed also in proliferating cancer cells. The increased level of caspases in osteosarcoma compared to osteoblast cells indicate a specific function of these executors in osteosarcoma,

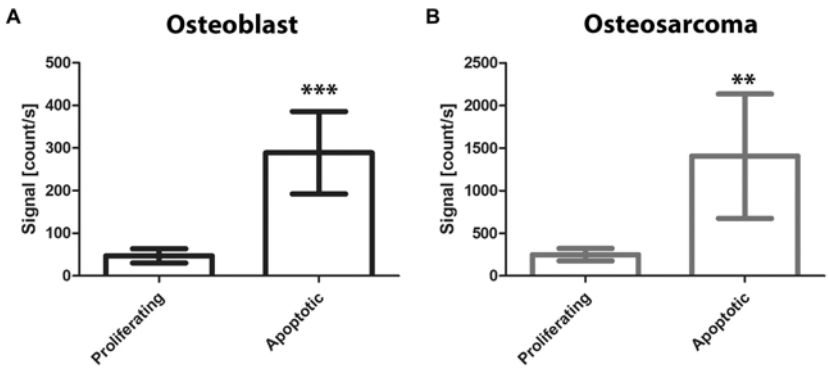

Fig. 4 The level of active caspase-3/7 in proliferating and apoptotic osteoblasts and osteosarcoma single cells. Osteosarcoma cells exhibited five time higher expression of active caspase-3/7 than physiological osteoblasts. The apoptotic cell content is more than five-times higher than in the proliferating cells in both cell lines. The apoptotic osteoblasts exhibited the same level of active caspase-3/7 like proliferating osteosarcoma cells. The differences were tested by *t*-test, $P < 0.05$.

that remains unknown. Generally, a high number of caspases observed in the mouse osteosarcoma can relate to the stimulation of non-apoptotic tumor cells to proliferate and survive under stress conditions. Moreover, surviving of the cells with caspase-3 activation causes significantly elevated levels of genetic instability and oncogenic transformation [9]. Due to this controversy of caspase-driven apoptosis-induced proliferation and cell instability can contribute to the development of extreme bone tumor masses in vivo [10]. More importantly, in some cases, a higher amount of activated caspase-3 in tumor tissues is also correlated with a markedly increased rate of recurrence and death in humans [11, 12].

4. Conclusions

The presented results indicate that the miniaturized bioluminescence instrumentation can potentially serve as a sensitive tool for diagnostics at a single cell level. As our method is simple and universal, it could be further widely used for other kinds of cellular research. The increased levels of active caspases in proliferating osteosarcoma cells could be a result of a specific function of caspase-3/7 in osteosarcoma tumor cells. The pilot result can also help to understand mechanisms why the bone represents a great niche for metastasis spreading.

Acknowledgments

The research was supported by the Grant Agency of the Czech Republic, project no. 20-00726S. MK is Brno PhD. Talent Scholarship Holder funded by the Brno City Municipality.

References

[1] Julien O., Wells J.A.: Caspases and their substrates. *Cell Death Differ.* **24** (2017), 1380–1389.
[2] Bell R.A.V., Megeney L.A.: Evolution of caspase-mediated cell death and differentiation: twins separated at birth. *Cell Death Differ.* **24** (2017), 1359–1368.

[3] Szymczyk K.H., Freeman T.A., Adams C.S., Srinivas V., Steinbeck M.J.: Active caspase-3 is required for osteoclast differentiation. *J. Cell. Physiol.* **209** (2006), 836–844.

[4] Miura M., Chen X.D., Allen M.R., Bi Y., Gronthos S., Seo B.M., Lakhani S., Flavell R.A, Feng X.H., Robey P.G., Young M., Shi S.: A crucial role of caspase-3 in osteogenic differentiation of bone marrow stromal stem cells. *J. Clin. Invest.* **114** (2004), 1704–1713.

[5] Svandova E., Vesela B., Tucker A.S., Matalova E.: Activation of pro-apoptotic caspases in non-apoptotic cells during odontogenesis and related osteogenesis. *Front. Physiol.* **9** (2018), 174.

[6] Kratochvílová A., Veselá B., Ledvina V., Švandová E., Klepárník K., Dadáková K., Beneš P., Matalová E.: Osteogenic impact of pro-apoptotic caspase inhibitors in MC3T3-E1 cells. *Sci. Rep.* **10** (2020):7489.

[7] Huang Q., Li F., Liu X., Li W., Shi W., Liu F.F., O'Sullivan B., He Z., Peng Y., Tan A.C., Zhou L., Shen J., Han G., Wang X.J., Thorburn J., Thorburn A., Jimeno A., Raben D., Bedford J.S., Li C.Y.: Caspase 3-mediated stimulation of tumor cell repopulation during cancer radiotherapy. *Nat. Med.* **17** (2011), 860–866.

[8] O'Brien M.A., Daily W.J., Hesselberth P.E., Moravec R.A., Scurria M.A., Klaubert D.H., Bulleit R.F.,, Wood K.V.: Homogeneous, bioluminescent protease assays: caspase-3 as a model. *J. Biomol. Screen.* **10** (2005), 137–148.

[9] Liu X., He Y., Li F., Huang Q., Kato T.A., Hall R.P., Li C.Y.: Caspase-3 promotes genetic instability and carcinogenesis. *Mol. Cell.* **58** (2015), 284–296.

[10] Fogarty C.E., Bergmann A.: Killers creating new life: caspases drive apoptosis-induced proliferation in tissue repair and disease. *Cell Death Differ.* **24** (2017), 1390–1400.

[11] Cheng J., He S., Wang M., Zhou L., Zhang Z., Feng X., Yu Y., Ma J., Dai C., Zhang S., Sun L., Gong Y., Wang Y., Zhao M., Luo Y., Liu X., Tian L., Li C., Huang Q.: The Caspase-3/PKCδ/Akt/VEGF-A signaling pathway mediates tumor repopulation during radiotherapy. *Clin. Cancer Res.* **25** (2019). 3732–3743.

[12] Liu P.F., Hu Y.C., Kang B.H., Tseng Y.K., Wu P.C., Liang C.C., Hou Y.Y., Fu T.Y., Liou H.H., Hsieh I.C., Ger P.L., Shu C.W.: Expression levels of cleaved caspase-3 and caspase-3 in tumorigenesis and prognosis of oral tongue squamous cell carcinoma. *PLoS One* **12** (2017), e0180620.

Application of chromogenic dye in biogenic amines determination using spectrophotometry

Kaja Kalinowska*, Marek Tobiszewski

Gdańsk University of Technology, Faculty of Chemistry, Department of Analytical Chemistry, 11/12 Gabriela Narutowicza Street, 80-233 Gdańsk, Poland ✉ *kaja.kalinowska@pg.edu.pl*

Keywords
biogenic amines
chromogenic dye
food analysis
spectrophotometry

Abstract
Biogenic amines content can be the source of information in the field of freshness and suitability of certain foods for consumption. However, most analytical methods for their determination require complicated sample preparation and expert knowledge. Because of that, a novel approach based on chromogenic dye application was proposed. After the S_N1 reaction of an amine with S 0378 dye, the absorbance of the solution was measured using spectrophotometry. With the proposed methodology, it was possible to determine total biogenic amines content in the range of 0.5–100 $\mu g\,L^{-1}$ with a determination coefficient exceeding 0.98.

1. Introduction

The quality and safety evaluation is one of the most important aspects of food analysis. In order to ensure consumers' satisfaction, the quality of products is assessed both at the industrial and retail level. However, while typical levels of contaminants such as pesticides or pharmaceuticals are well-known and regulated, data concerning e.g. biogenic amines content is scarce. Biogenic amines are low molecular weight organic compounds formed as a result of metabolic processes occurring in animal, plant, or bacterial cells [1]. Since they are precursors of various compounds, they can be found in many protein-rich food matrices [2]. Because the concentrations of individual biogenic amines are significantly influenced by numerous external factors, such as microbial activity or time and storage conditions, biogenic amines content can be used in the assessment of freshness and suitability of certain foods for consumption [9–10]. In addition, since the high content of certain amines in food products can be the result of poor quality raw materials, inadequate food processing, and contamination [5], the determination of biogenic amines can prove to be useful information on spoilage and overall sanitary quality of food products [8]. However, the determination of biogenic amines in food is important primarily due

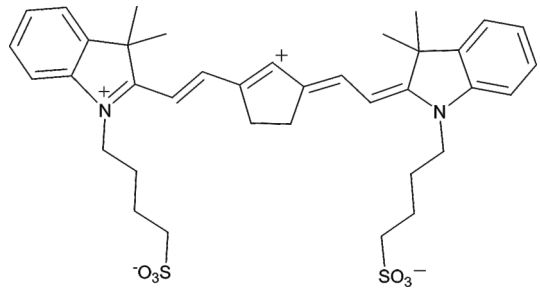

Fig. 1 Chemical structure of S 0378 dye.

to the negative impact that their excessive consumption may have on the health of the consumer. Based on the literature data, it can be concluded that these compounds are potential substrates for the formation of carcinogenic *N*-nitroso compounds. Primary amines react with nitrosating agents to form alkylating compounds that can react with other ingredients present in food [6]. In addition, in foods containing a large amount of fat, the formation of *N*-nitrosopyrrolidine from putrescine or spermidine is possible [1, 4, 7].

There are numerous methods of biogenic amines determination with the use of gas or liquid chromatography, however, their application is often associated with time-consuming and complicated sample preparation, as well as highly trained staff. An alternative approach would be to determine biogenic amines using spectrophotometric methods, which are relatively fast and easy to apply. What is more, most spectrophotometers are rather inexpensive and portable, which means that they can be used by producers, retailers, and consumers. While biogenic amines are weak absorbers of visible light, which makes their optical detection challenging [3], labelling them with a chromophore enables their spectrophotometric determination. S 0378 dye (Fig. 1) is a water-soluble cyanine dye, which reacts with primary amines by means of a unimolecular nucleophilic substitution mechanism (S_N1). During this reaction, the conjugate is formed, which results in a colour change from green to blue. The aim of this study is to evaluate whether S 0378 dye can be applied in the spectrophotometric determination of biogenic amines.

2. Experimental

2.1 Reagents and chemicals

Standard of putrescine was obtained from Merck. High-purity grade methanol was supplied by Avantor Performance Materials Poland. S 0378 dye was obtained from FEW Chemicals.

2.2 Instrumentation

Spectrophotometric measurements were performed with the use of the DR 3900 Hach Lange spectrophotometer. Absorbance was measured at 650 nm.

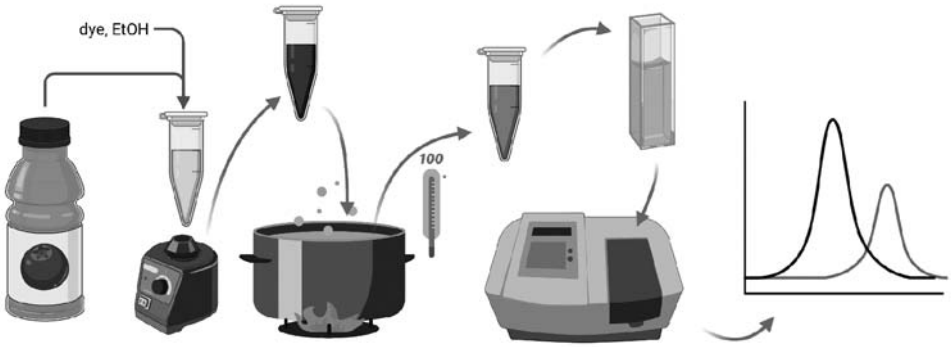

Fig. 2 Proposed procedure for biogenic amines determination.

3. Results and discussion

During the course of an experiment, it was evaluated whether biogenic amines can be determined using spectrophotometric methods. Because of that, the response of chromogenic dye to biogenic amines was tested using the procedure depicted in Fig. 2. First, a series of putrescine solution at a concentration ranging from 0.5 to 100 μg L^{-1} was prepared. Each of them was mixed with ethanol and green S 0378 dye. The mixtures were vortexed and then placed in a water bath for 2 h, during which dye reacted with putrescine forming blue conjugate. Solutions were then analysed using a spectrophotometer.

As can be seen in Fig. 3, it was possible to obtain a linear response in the range of 0.5–100 μg L^{-1}. What, is more, the determination coefficient exceeded 0.98, which suggests that this methodology might be applied for the determination of biogenic amines in real samples.

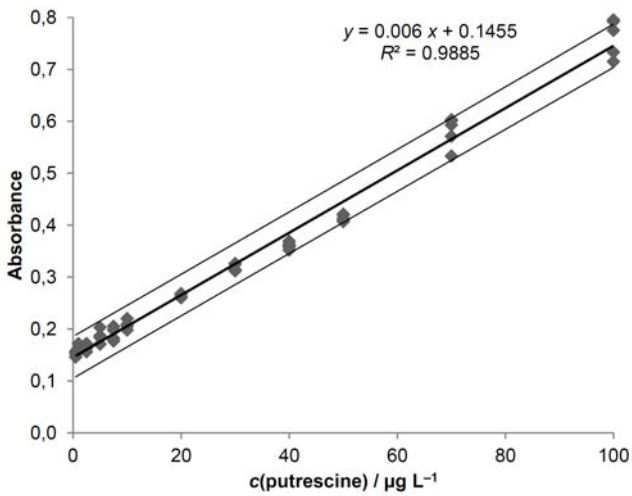

Fig. 3 Absorbance of S 0378 dye after reaction with different putrescine amounts.

4. Conclusions

Based on the results of the experiment it was possible to conclude that chromogenic dye can be applied in the determination of total biogenic amines content. The proposed methodology is relatively simple and not requiring expert knowledge. This suggests that it could be applied not only in the analytical laboratory but also could be used in production and distribution centres.

References

[1] Mayer H. K., Fiechter G., Fischer E.: A new ultra-pressure liquid chromatography method for the determination of biogenic amines in cheese. *J. Chromatogr. A* **1217** (2010), 3251–3257.
[2] Karovičová J., Kohajdová Z.: Biogenic amines in food. *Chem. Pap.* **59** (2005), 70–79.
[3] Mobarez S. N., Wongkaew N., Simsek M., Baeumner A. J., Duerkop A.: Dipsticks with reflectometric readout of an NIR dye for determination of biogenic amines. *Chemosensors* **8** (2020), 99–114.
[4] Nowak A. Libudzisz Z.: Karcynogeny w przewodzie pokarmowym człowieka. *Żywność. Nauk. Technol. Jakość* **4** (2008), 9–25. (In Polish.)
[5] Önal A.: A review: Current analytical methods for the determination of biogenic amines in foods. *Food Chem.* **103** (2007), 1475–1486.
[6] Papageorgiou M., Lambropoulou D., Morrison C., Namieśnik J., Płotka-Wasylka J., Kłodzińska E.: Literature update of analytical methods for biogenic amines determination in food and beverages. *TrAC - Trends Anal. Chem.* **98** (2018), 128–142.
[7] Reddy B. S.: *Diet, Nutrition and Cancer: A Critical Evaluation: Volume II.* CRC Press, 2018.
[8] Triki M., Herrero A., Jiménez-Colmenero F., Ruiz-Capillas C.: Quality assessment of fresh meat from several species based on free amino acid and biogenic amine contents during chilled storage. *Foods* **7** (2018), 132–147.
[9] Veciana-Nogués M. T., Mariné-Font A., Vidal-Carou M. C.: Biogenic amines as hygienic quality indicators of tuna. Relationships with microbial counts, ATP-related compounds, volatile amines, and organoleptic changes. *J. Agric. Food Chem.* **45** (1997), 2036–2041.
[10] Wojnowski W., Kalinowska K., Majchrzak T., Płotka-Wasylka J., Namieśnik J.: Prediction of the biogenic amines index of poultry meat using an electronic nose. *Sensors (Switzerland)* **19** (2019), 1580–1589.

Development of new methodologies for rapid determination of oxidizable and reducible organic compounds using batch injection analysis

Pavel Dvořák*, Vlastimil Vyskočil

Charles University, Faculty of Science, Department of Analytical Chemistry, UNESCO Laboratory of Environmental Electrochemistry, Hlavova 8, 128 43 Prague 2, Czech Republic
✉ *dvorakpav@natur.cuni.cz*

Keywords
amperometry
batch injection analysis
chlorpromazine
oxygen removal

Abstract
Batch injection analysis (BIA) offers many advantages, e.g., rapid analysis, high reproducibility, sufficient selectivity, and minimal sample and reagent consumption. The development of a new method using BIA with amperometric detection (BIA-AD) for sensitive determination of chlorpromazine is described in this contribution. The following parameters were optimized within the method development: pH of media (supporting electrolyte), detection potential, rate of dispense, and volume of dispense. Under the optimized conditions (pH = 6, detection potential of 700 mV, dispense rate of 286.3 μL s^{-1}, injected volume of 50 μL), a linear calibration dependence of chlorpromazine was measured at a screen-printed carbon electrode in the concentration range 1–1000 μmol L^{-1}, with a limit of quantification 2.7 μmol L^{-1}. Applicability of the newly developed method was verified on determination of chlorpromazine in pharmaceutical formulation Plegomazine with satisfactory results. It is worth mentioning that air oxygen needs to be removed in BIA-AD from analyzed solutions while reducible compounds are determined. One possible solution to overcome this complication is shown in experiments with metronidazole, where adding solid sodium sulfite as a reductive agent shows comparable results to the traditional oxygen removal with nitrogen gas.

1. Introduction

Today's advances in both technology and analytical chemistry allows development of fully automatized procedures that can process large number of samples in short period of time while maintaining all important analytical parameters such as accuracy, sensitivity, selectivity, or reproducibility. During 1980s, analytical technique called flow injection analysis (FIA) was developed and introduced. This

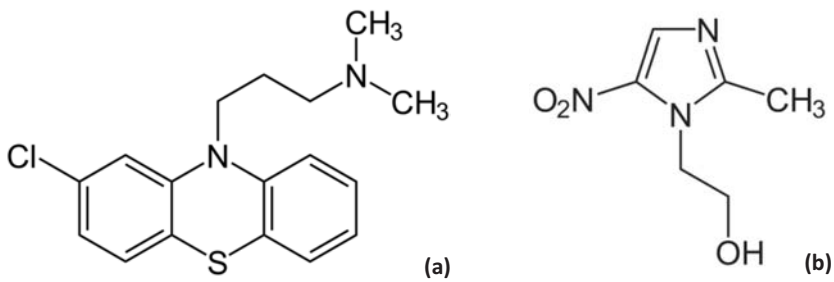

Fig. 1 Structural formula of (a) chlorpromazine, and (b) metronidazole.

technique is based on injection of sample plug to a flowing stream of carrier solution which takes sample towards detector [1]. Flow injection analysis has found a wide use in analysis of environmental and industrial samples as well as analysis of pharmaceutical substances, mainly due to its versatile use, high precision, and reproducibility. In 1991, Wang and Taha [2] introduced alternative technique called batch injection analysis (BIA). Batch injection analysis allows to perform a quick analysis with minimal sample consumption. If amperometry is used as a detection technique in BIA, then this technique (BIA-AD) is based on injection of a sample through a micropipette tip directly onto a working electrode surface (wall-jet configuration) which is immersed in a large volume of blank solution. This arrangement prevents passivation of the working electrode. Batch injection analysis provides similar properties as flow injection analysis, namely sensitivity, speed of analysis, small sample consumption, or reproducibility [3]. However, BIA offers some improvements, e.g., elimination of a typical drawback associated with pump and valves of FIA system. Batch injection analysis apparatus is consisting of all battery-powered components, which turns BIA into an easily portable analytical system [4–8].

Chlorpromazine (Fig. 1a) belongs to phenothiazine derivatives. Until nowadays, it is still used by psychiatric patients suffering from schizophrenia, states of psychomotor discomfort, hallucinations, anxiety, and obsessive neuroses [9]. The phenothiazine ring could be easily electrochemically oxidized [10], and this property of chlorpromazine was thus used for its electrochemical detection.

Metronidazole (Fig. 1b) belongs to nitroimidazole derivatives. It is used as an antibiotic drug to treat endocarditis, bacterial vaginosis, or pelvic inflammatory disease. Its structure contains a nitro group which could be electrochemically reduced [11]. For working in reduction potentials, oxygen needs to be removed from the analysed solution. A traditional way is bubbling the analysed sample with pure nitrogen gas which is time consuming and expensive. Less common approach is adding sodium sulphite as commonly used reductive agent [12, 13].

The aim of this work was to develop of new methods for the rapid determination of oxidizable and reducible drugs using BIA-AD with various arrangements of detection cells.

2. Experimental

2.1 Reagents and chemicals

Chlorpromazine hydrochloride (≥ 98% purity) and metronidazole (≥ 100% purity) (both Sigma-Aldrich) were used as test substances. pH of stock solutions has been adjusted using a 0.04 mol L^{-1} Britton-Robinson (BR) buffer. Acidic part of the BR buffer was prepared by mixing 2.69 mL of 85% phosphorus acid (p.a.; Lach-Ner, Czech Republic) and 2.27 mL of 99% acetic acid (p.a.; Penta, Czech Republic), dissolving 2.75 g of boric acid (p.a.; Lachema, Czech Republic), and adding deionized water to a 1 L final volume. Basic part of the BR buffer was prepared by dissolving 8.0 g of solid sodium hydroxide (p.a.; Lach-Ner, Czech Republic) in deionized water of a 1 L final volume. The buffer of requested pH was made by mixing the acidic and basic part of the BR buffer. Sodium sulfite (p.a.; Lach-Ner, Czech Republic) was used for oxygen removal. Deionized water was produced by a Millipore Milli-Q Plus System (Millipore, USA).

2.2 Instrumentation

Batch injection analysis with amperometic detection experiments with chlorpromazine were performed in a BIASPE02 set (DropSens, Spain) consisting of an electrochemical cell (DropSens, Spain) and a programmable electronical pipette Gilson PIPETMAN M (Gilson, USA). Pipetting Mode Builder (Gilson, USA) software was used for setting the pipette.

An electrochemical analyser Autolab PGSTAT 10 (Metrohm Autolab, The Netherlands) was used in case of chlorpromazine. Nova 1.11 (Metrohm Autolab, The Netherlands) software was used to conduct electrochemical measurements which were performed in a three-electrode system using screen-printed carbon electrodes DRP-110 (DropSens, Spain).

Determination of metronidazole was performed at a boron-doped diamond electrode (type D-653-SA, Windsor Scientific, UK), and electrochemical measurements were conducted with PSTrace 5.8 (PalmSens, The Netherlands) software using a PalmSens1 electrochemical analyser (PalmSens, The Netherlands).

Exact values of pH were measured on a digital pH meter Jenway 3510 (Jenway, UK) with a combined glassy electrode (type 924 005). The instrument was calibrated using standard calibration buffers.

3. Results and discussion

Firstly, optimal pH of the medium for chlorpromazine determination needed to be found. Britton-Robinson buffer solutions in the pH range from 2 to 12 were prepared for this purpose. Using cyclic voltammetry (start potential of 0 mV, stop potential of 1200 mV, step potential of 5 mV, and scan rate of 100 mV s^{-1}), peak

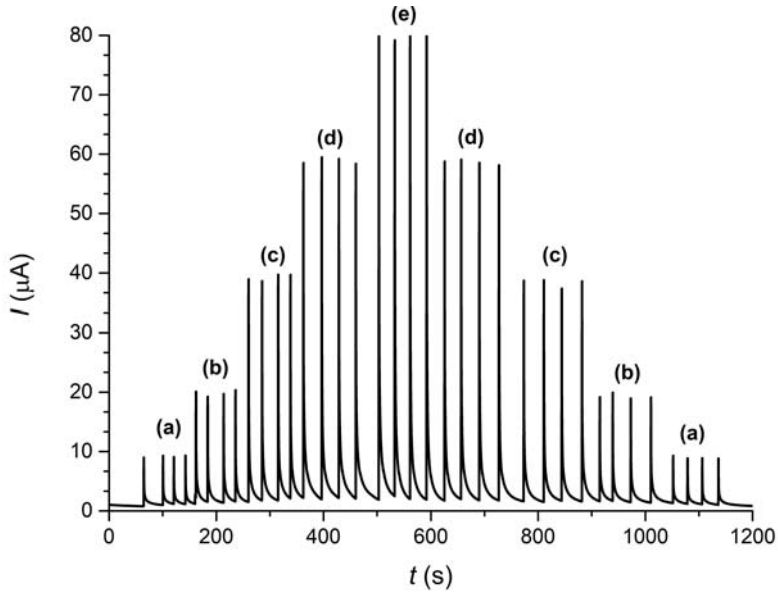

Fig. 2 Batch injection analysis amperometric responses recorded on a screen-printed carbon electrode (n = 4) for solutions containing chlorpromazine of following concentrations: (a) 100 μmol L^{-1}, (b) 250 μmol L^{-1} , (c) 500 μmol L^{-1} , (d) 750 μmol L^{-1}, and (e) 1000 μmol L^{-1}. Electrolyte: Britton-Robinson buffer pH = 6; detection potential 700 mV; dispense rate 286.3 μL s^{-1}; injected volume 50 μL.

current in a 1×10^{-1} mol L^{-1} chlorpromazine solution was measured. The highest peak current was recorded in a medium with pH = 8, although already at pH = 7, white crystals started to form in the solution (probably as products of chlorpromazine hydrolysis). The crystal formation did not allow to obtain reproducible results, and, therefore, pH of 6 was chosen as optimal.

The second optimized parameter was the detection potential for AD. Peak current was measured in a 1×10^{-3} mol L^{-1} chlorpromazine solution of pH = 6 at inserted detection potentials between 600 and 1000 mV. A potential of 700 mV was selected as optimal.

Next, the settings of electronic pipette were optimized. The peak current of 1×10^{-3} mol L^{-1} chlorpromazine was measured while dispensed volume was changed in the range between 20 and 100 μL. A volume of 50 μL was selected as optimal, because four assays from full pipette tip can be realized, and the value of peak current was optimal as well.

Lastly, the optimal setting of dispense rate was determined. The rate 1–6 (which corresponds to the flow rate between 7.5 and 286.3 μL s^{-1}) was set on the pipette, and the peak current of 1×10^{-3} mol L^{-1} chlorpromazine was measured. Fastest rate was selected, as the peak current reached its maximum values while this rate was used.

When optimal conditions were found (pH = 6, detection potential of 700 mV, dispensed volume of 50 μL, dispense rate of 286.3 μL s^{-1}), chlorpromazine

Table 1
Comparison of results for the determination of chlorpromazine using BIA-AD and UV-VIS.

Method	Concentration / μmol L^{-1}	Concentration / mg per 5 mL	Recovery / %
Manufacturer declares	141	25	100
BIA-AD	200	35	140
UV-VIS	152	27	108

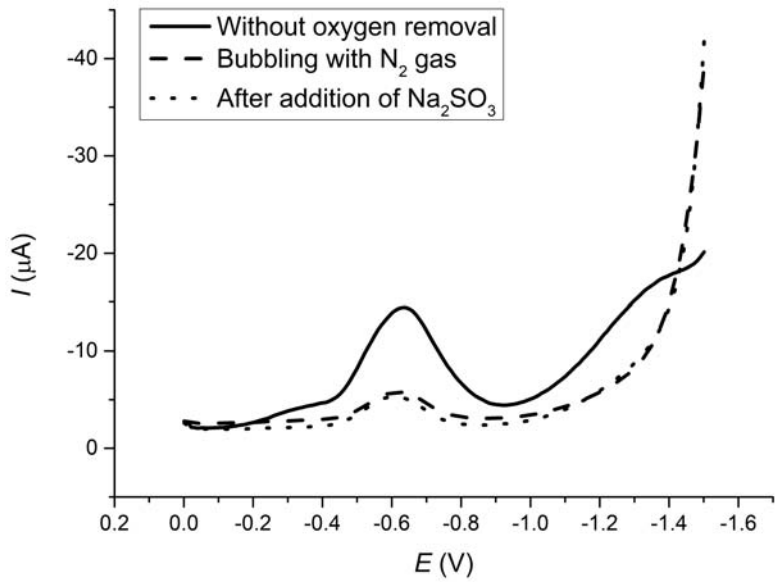

Fig. 3 Differential pulse voltammograms of 1×10^{-4} mol L^{-1} metronidazole at a boron-doped diamond electrode without oxygen removal (solid line), after 5 minutes of pure nitrogen gas bubbling (dashed line), and after addition of solid sodium sulfite with its final concentration of 0.01 g mL^{-1} (dotted line). Conditions were as follows: Britton-Robinson buffer pH = 10, E_{step} = 10 mV, E_{pulse} = 200 mV, t_{pulse} = 0.02 s, and scan rate 100 mV s^{-1}.

solutions in the concentration range between 1 and 1000 μmol L^{-1} were prepared, pH was adjusted using BR buffer of pH = 6, and the volumetric flasks were wrapped in aluminium foil. Corresponding BIA-AD recordings are shown in Fig. 2. Linear trend throughout the whole examined concentration range, with the obtained limit of quantification of 2.7 μmol L^{-1}, showed the usability of the newly developed method.

Practical applicability of the newly developed method was tested in determination of chlorpromazine in the pharmaceutical formulation Plegomazine. Standard addition method was used, and obtained results were compared with a UV-VIS technique. The sumarized results are shown in Table 1.

Optimization of the BIA-AD procedure for reducible compounds was performed in a similar way. However, prior to the analysis, dissolved oxygen needs to be removed. Differential pulse voltammograms of a 1×10^{-4} mol L^{-1} metronidazole

solution without any oxygen removal, after 5 minutes of bubbling with pure nitrogen gas, and after addition of solid sodium sulfite (for its final concentration of 0.01 g mL^{-1}) are shown in Fig. 3 as the pilot results showing the applicability of this approach for further research in this field.

4. Conclusions

In this contribution, the process of developing BIA-AD method for rapid determination of organic compounds, both oxidizable and reducible, was shown. Conditions to optimize are as follows: pH of the working media (supporting electrolyte), detection potential, dispense rate of the sample, and injected volume of the sample. Drug chlorpromazine was selected as an electrochemically oxidizable analyte in this study. Under the optimized conditions (pH = 6, detection potential of 700 mV, dispense rate of 286.3 μL s^{-1}, and injected volume of 50 μL), a linear calibration dependence was measured at the screen-printed carbon electrode in the concentration range 1–1000 μmol L^{-1}, with a limit of quantification of 2.7 μmol L^{-1}. Applicability of the newly developed methodology was successfully verified on the determination of chlorpromazine in Plegomazine. Dissolved air oxygen needs to be removed from the analysed solution when electrochemical reductions are studied at cathodic potentials. Electrochemically reducible drug metronidazole was selected as model analyte for the pilot electrochemical experiments perfor-med at the boron-doped diamond electrode. The use of sodium sulphite is a promising way how to replace the use of pure nitrogen gas.

Acknowledgments

This research was supported by the Specific University Research (Project SVV260440) and by the Czech Science Foundation (GA CR Project 20-01417J).

References

[1] Růžička J., Hansen E.H.: Flow injection analyses: Part I. A new concept of fast continuous flow analysis. *Anal. Chim. Acta* **78** (1975), 145–157.
[2] Wang J., Taha Z.: Batch injection analysis. *Anal. Chem.* **63** (1991), 1053–1056.
[3] Rocha D.P., Cardoso R.M., Tormin T.F., de Araujo W.R., Munoz R.A.A., Richter E.M., Anges L.: Batch-injection analysis better than ever: New materials for improved electrochemical detection and on-site applications. *Electroanalysis* **30** (2018), 1386–1399.
[4] Quintino M.S.M., Anges L.: Batch injection analysis: An almost unexplored powerful tool. *Electroanalysis* **16** (2004), 513–523.
[5] Tormin T.F., Cunha R.R., da Silva R.A.B., Munoz R.A.A., Richter E.M.: Combination of screen-printed electrodes and batch injection analysis. A simple, robust, high-throughput and portable electrochemical system. *Sens. Actuators B Chem.* **202** (2014), 93–98.
[6] Stefano J.S., Tormin T.F., da Silva J.P., Richter E.M., Munoz R.A.A.: Amperometric determination of omeprazole on screen-printed electrode using batch injection analysis. *Microchem. J.* **133** (2017), 398–403.
[7] Dvořák P., Vyskočil V.: Vsádková injekční analýza a možnosti jejího využití v novém tisíciletí. *Chem. Listy* **113** (2019), 703–709. (In Czech.)

[8] Barek J., Pecková K., Vyskočil V.: Kam směřují moderní elektroanalyticé metody 50 let po udělení Nobelovy ceny za polarografii. *Chem. Listy* **103** (2009), 889–893. (In Czech.)
[9] *Český lékopis 2017*. Praha , Grada 2017. (In Czech.)
[10] Nesměrák K., Červený V., Hraníček J., Rychlovský P.: A spectrofluorimetric determination of phenothiazine derivates after their photooxidation or chemical or electrochemical oxidation in a flow injection arrangement. *Microchem. J.* **106** (2013), 226–232.
[11] Lu S., Wu K., Dang X., Hu S.: Electrochemical reduction and voltametric determination of metronidazole at a nanomaterial thin film coated glassy carbon electrode. *Talanta* **63** (2004), 653–657.
[12] Pastor F.T., Dejmková H., Zima J., Barek J.: Determination of chloramohenicol by differential pulse voltammetry at carbon paste electrodes – The use of sodium sulfite for removal of oxygen from electrode surface. *Collect. Czech Chem. Commun.* **76** (2011), 383–397.
[13] Hájková A., Vyskočil V., Josypčuk B., Barek J.: A miniaturized electrode system for voltammetric determination of electrochemically reducible environmental pollutants. *Sens. Actuators B Chem.* **227** (2016), 263–270.

Abacavir: comparison of oxidation mechanisms

Filip Vymyslický[a,*], Tomáš Křížek[a], Jakub Heřt[b]

[a] *Charles University, Faculty of Science, Department of Analytical Chemistry, Hlavova 8/2030, 128 43 Prague 2, Czech Republic* ✉ *f.vymyslicky@gmail.com*
[b] *Zentiva Group, a.s., U Kabelovny 130, 102 37 Prague 10, Czech Republic*

Keywords
abacavir
forced degradation studies
oxidation mechanism

Abstract
During forced degradation studies that are a part of the drug product development, an active substance is exposed to extreme conditions. The effect of humidity, light, pH and oxidation on the active substance is studied. The most common way to study the effect of oxidation is to expose active substance to a 0.1–3.0% solution of hydrogen peroxide. Another possibility is to use radical initiators or metal ions. An alternative method is electrochemical oxidation. The oxidation of an active substance is not only affected by the oxidation agent but also depends on the solvent. In this study, the abacavir oxidation in different solvents by different approaches is investigated. The electrochemical oxidation in flow cell was compared with peroxide mediated, radical and metal ions oxidation. Electrochemical oxidation yielded the largest variety of oxidation products from all the tested approaches.

1. Introduction

Abacavir sulphate, {(1*S*,4*R*)-4-[2-amino-6-(cyclopropylamino)-9H-purin-9-yl]cyclopent-2-en-1-yl}methanol sulfate (2:1), is nucleoside reverse transcriptase inhibitor used to treat human immudeficieny virus [1, 2]. The formula of abacavir is $C_{14}H_{18}N_6O$, the structure of abacavir is in Fig. 1. Abacavir is sold under the tradename Ziagen. Abacavir is distributed either as a 20 mg ml^{-1} solution or as tablets containing 300 mg of abacavir.

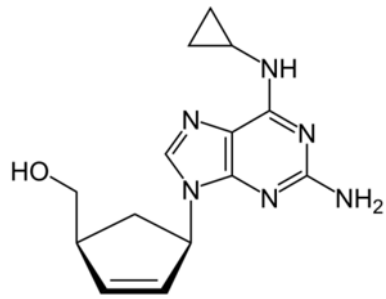

Fig. 1 Chemical structure of abacavir.

Forced degradation studies are a part of drug product development. In forced degradation studies, active pharmaceutical ingredient or drug product is exposed to extreme chemical and physical conditions. The forced degradation studies studied the effect of oxidation, humidity, light, and pH on active pharmaceutical ingredient or drug product [3]. Many authors have already published the forced

degradation studies of abacavir. In these studies, abacavir was subjected to photolytic, thermal, oxidation, and hydrolysis stress. In all studies, stressed samples were analyzed by high performance liquid chromatography and impurities and degradation products were characterized by mass spectrometry [4–6]. The effect of oxidation is studied using a 0.1–3.0% hydrogen peroxide solution at room or elevated temperature [7]. Another way is to use radical initiators such as 2,2′-azobis(2-methylpropionitrile) at elevated temperatures, which initiates the oxidation of active pharmaceutical ingredient. Another way is to expose the active pharmaceutical ingredient or drug product to oxygen present in the air. The least used method is the metal ions such as iron(III) [8]. An alternative method is the electrochemical oxidation of active pharmaceutical ingredient. The working electrolyte with active pharmaceutical ingredient is inserted into the electrochemical flow cell, where a constant potential is applied to the working electrode and the active pharmaceutical ingredient is oxidized.

2. Experimental

2.1 Reagents and chemicals

Abacavir sulfate (Zentiva, Czech Republic), 99.9% methanol (Honeywell, Germany), 99.9% acetonitrile (Honeywell, Germany), 99% ammonium hydrogen carbonate (Merck, Gemany), 99% ammonium acetate (Merck, Gemany), 30% hydrogen peroxide (Lachner, Czech Republic), 97% iron(III) chloride (Sigma-Aldrich, USA), 98% 2,2′-azobis(2-methylpropionitrile) (Sigma-Aldrich, USA), 98% sodium perchlorate (Sigma-Aldrich, USA), water for chromatography was obtained by purifying demineralised water using Millipore type Synergy UV purification instrument.

2.2 Instrumentation

An Acquity H-class UPLC system (Waters, USA) with high pressure pump, autosampler, thermostat, DAD and QDA detectors was used for all experiments. The Acquity UPLC HSS SB C18 column (100×2.1 mm, 1.8 μm; Waters, USA) was used for separation. In the UPLC method, 10 mM ammonium hydrogen carbonate buffer pH = 7.8 was used as component A and acetonitrile as component B of the mobile phase. The gradient program was set as follows: *t*(min)/% B: 0/5, 1.5/5, 10/70, 12/5, 15/5. The flow rate of the mobile phase was 0.3 ml min^{-1} and the injection volume was 0.5 μl. The detector operated at a wavelength of 284 nm. The autosampler temperature was set at 20 °C and the column temperature at 40 °C. The Empower software was used for evaluation. For electrochemical oxidation, electrochemical flow cell from ALS (Japan) was used. Glassy carbon electrode (diameter 6 mm) and silver/silver chloride electrode were used as working and reference electrode, respectively. The scheme of electrochemical flow cell is in

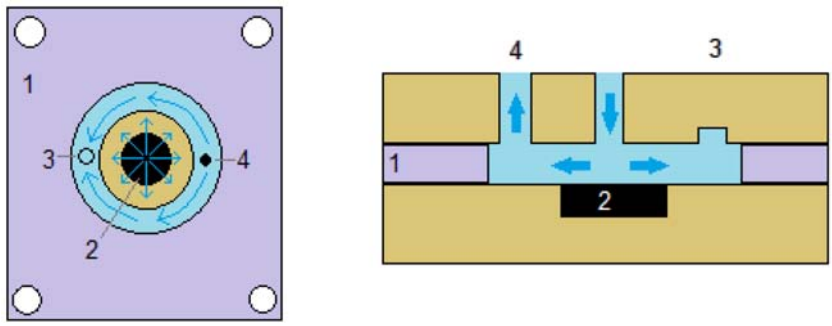

Fig. 2 Schematic diagram of the electrochemical flow cell: (1) gasket, (2) working electrode, (3) inlet, (4) outlet.

Fig. 2. Electrodes were connected with potentiostat PalmSens 3 from PalmSens (Netherlands). An Elmasonic S15H ultrasonic bath from Elma (Germany) was used for sample preparation. For pH measurements pH meter Jenway 3540 from Jenway (United Kingdom) was used.

2.3 Electrochemical oxidation

Electrochemical oxidation of abacavir was performed by chronoamperometry in an electrochemical flow cell in static mode. A glassy carbon electrode, silver/silver chloride were used as the working and reference electrode, respectively. Electrochemical oxidation duration is 5 hours and cell size was set to 2000 µm. The volume of the reactor was 127 µL. The working potential was set to 1.3 V. Concentration of abacavir in all experiments was 1 mg/ml. Electrochemical oxidation study was performed in three media: 0.5 M ammonium acetate (pH = 7), 0.5 M ammonium acetate (pH = 7) / MeOH (1:1) and MeOH with 0.1 M $NaClO_4$.

3. Results and discussion

Figure 3A shows a comparison of the sums of impurities formed by electrochemical oxidation in 5 hours. It can be seen that most impurities were formed in 0.5 M ammonium acetate (pH = 7) (4.76%) and the least in methanol solution with 0.1 M $NaClO_4$ (2.91 %). This difference is in part due to the conductivity of the used media. Figure 3B, we can see the representation of oxidation products formed in individual media. In all media, an impurity *m/z* 247 was formed primarily. In media containing 0.5 M ammonium acetate (pH = 7), impurities with *m/z* 319 were formed, on the contrary, the formation of these impurities in methanol with 0.1 M $NaClO_4$ was suppressed. Furthermore, we can observe the formation of impurity with *m/z* 299, which occurred only in the environment containing methanol.

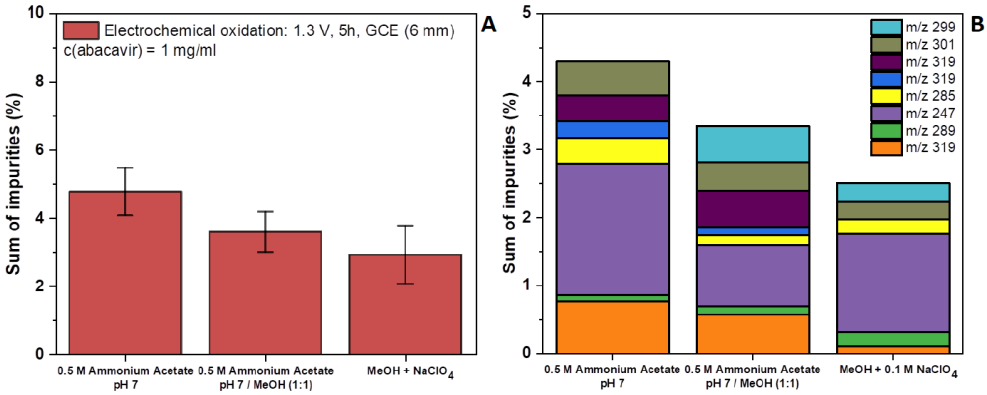

Fig. 3 (A) Total amounts of impurities electrochemically formed in 5 hours (n = 3). (B) Profile of electrochemically formed impurities in different media in 5 hours.

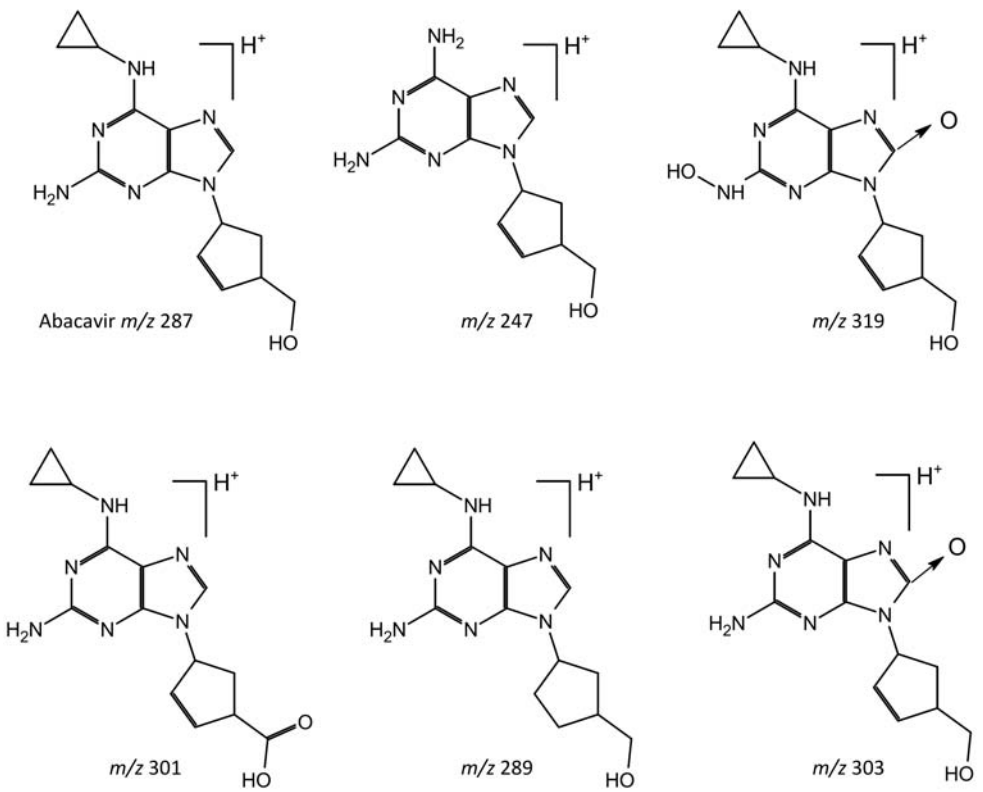

Fig. 4 Structures of abacavir and known impurities with their m/z.

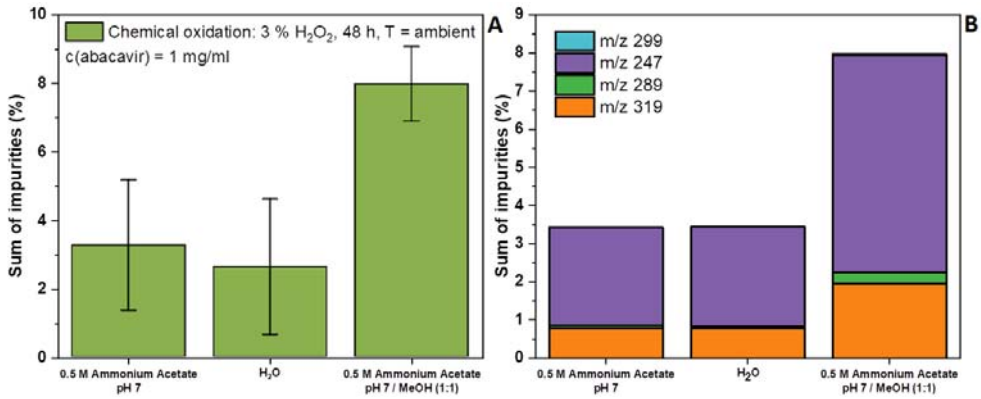

Fig. 5 (A) Total amounts of impurities formed by peroxide mediated oxidation in 48 hours (n = 3). (B) Profile of impurities formed by peroxide mediated oxidation in different media in 48 hours.

Figure 4 shows abacavir and its known degradation products, which were formed during oxidation experiments with their *m/z* values. During the oxidation, impurities with m/z 285, 299 and 343 also appeared. Their structures are not known [9].

To compare the oxidative mechanisms of degradation, electrochemical oxidation and the effect of solvent on the oxidation of abacavir, the degradation studies were performed using the radical initiator, metal ions and H_2O_2 solution. A 3% H_2O_2 solution was used for peroxide mediated oxidation of abacavir for 48 hours at ambient temperature in three different media: 0.5 M ammonium acetate (pH = 7), H_2O and 0.5 M ammonium acetate (pH = 7)/MeOH (1:1). Fig. 5A presents the sums of impurities formed by peroxide mediated oxidation in 48 hours. Most oxidation products were formed in 0.5 M ammonium acetate (pH = 7)/MeOH (1:1) (7.97%). A comparable amount of impurities formed in H_2O (2.61%) and 0.5 M ammonium acetate (pH = 7) (3.27%). In Fig. 5B, we can see the representation of oxidation products that were formed in individual media. As in the case of electrochemical oxidation, the main degradation product is the impurity with *m/z* 247. In all three media, the impurity with *m/z* 319 was formed and impurity with *m/z* 289 occurred. As with electrochemical oxidation in methanol containing media, an impurity with *m/z* 299 was formed.

For another experiment, the radical initiator 2,2′-azobis(2-methylpropionitrile) was used with a concentration of 20 mol% of abacavir. The radical oxidation was performed for 7 days at 50 °C in three media: H_2O, MeOH and H_2O/MeOH (1:1). Fig. 6A compares the sums of impurities formed. It can be seen that radical oxidation produced significantly more impurities than other approaches. Most impurities were formed in MeOH (34.27%) and then in H_2O (23.70%) and the least in the cosolvent H_2O/MeOH (1.73%). Fig. 6B presents oxidation products formed in individual media by radical oxidation. In the aqueous medium, as in the case of electrochemical and chemical oxidation, the

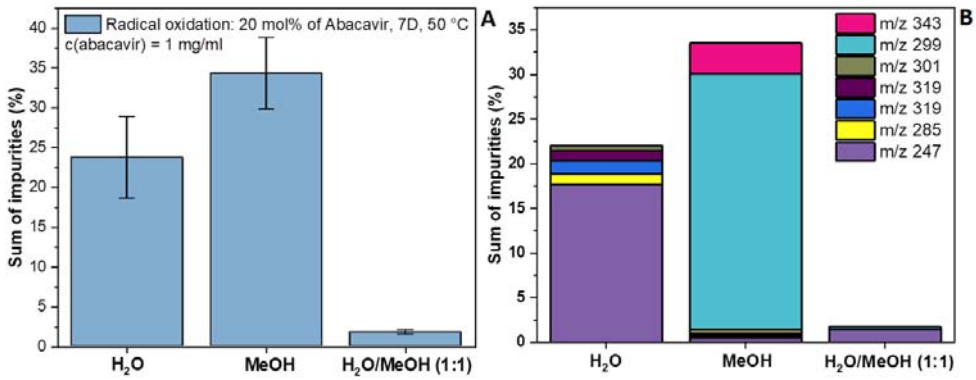

Fig. 6 (A) Total amounts of impurities formed by radical oxidation in 7 days (n = 3). (B) Profile of impurities formed by radical oxidation in different media in 7 days.

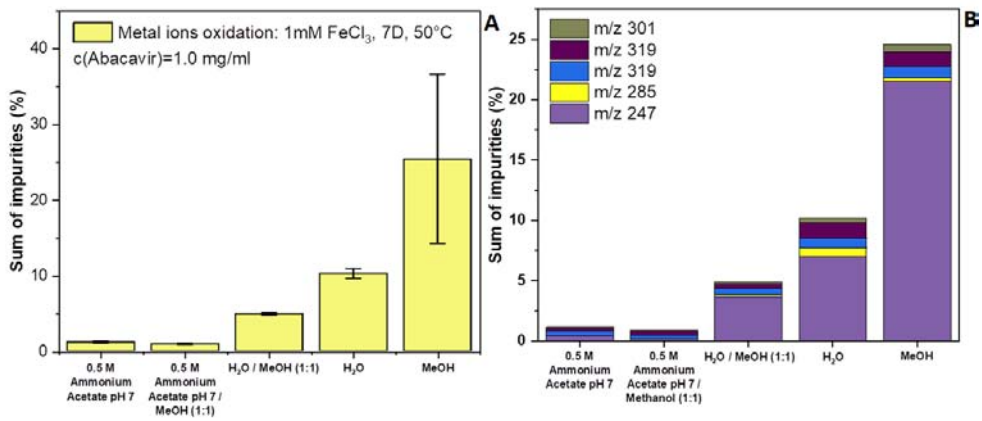

Fig. 7 (A) Total amounts of impurities formed by oxidation using metal ions in 7 days (n = 3). (B) Profile of impurities formed by oxidation using metal ions in different media in 7 days.

impurity with *m/z* 247 was formed primarily. In the non-aqueous medium, almost only the impurity with *m/z* 299 and the impurity with *m/z* 343 were formed. The cosolvent formed predominantly an impurity with *m/z* 247 and a small amount of impurity with *m/z* 299, which forms in methanol containing media.

Oxidation using metal ions was used as the last approach. Anhydrous $FeCl_3$ with a concentration of 1 mmol l^{-1} was used for the oxidation for 7 days at 50 °C. Oxidation using metal ions was performed in 5 media: 0.5 M ammonium acetate (pH = 7), H_2O, H_2O/MeOH (1:1), 0.5 M ammonium acetate (pH = 7)/MeOH (1:1) and MeOH. Fig. 7A compares the sums of impurities formed. The highest amount of oxidation products was achieved in MeOH (25.37%). In contrast, the lowest degree of oxidation was achieved in media containing 0.5 M ammonium acetate (pH = 7), where the oxidation was probably suppressed by the content of ammonium acetate. Two times more oxidation products were formed in H_2O (10.22%) as in H_2O/MeOH (4.89%). Fig. 7B, we see oxidation products formed in

individual media by oxidation using metal ions. As in the other types of oxidation studied, the main oxidation product is the impurity with *m/z* 247. Furthermore, the oxidation with metal ions formed impurities with *m/z* 258, 319, and 301. The difference in oxidation with metal ions is that impurity with *m/z* 299, which occurred in all other studied approaches in presence of MeOH, was not formed, which is probably due to the mechanism of oxidation by metal ions.

4. Conclusions

An alternative study of the effect of oxidation on abacavir was performed using an electrochemical flow cell. This study was compared with the three approaches used to study the effect of oxidation on the active pharmaceutical ingredient. Electrochemical oxidation of abacavir yielded the most diverse oxidation products from all tested.

Acknowledgments

This work has been supported by Charles University SVV260560 project and pharmaceutical applied research center (The Parc).

References

[1] Gallant J.E.: Initial therapy of HIV infection. *J. Clin. Virol.* **25** (2002), 317–333.
[2] Hervey P.S., Perry C.M.: Abacavir: A review of its clinical potential in patients with HIV infection. *Drugs* **60** (2000), 447–479.
[3] Baertshi S.W., Alsante K.M., Reed R.A.: *Pharmaceutical Stress Testing: Predicting Drug Degradation.* 2nd Ed. London, Informa Healthcare 2011.
[4] Rao R.N., Vali M.R., Ramacahndra B., Raju S.S.: Separation and characterization of forced degradation products of abacavir sulphate by LC–MS/MS. *J. Pharm. Biomed. Anal.* **54** (2011), 279–285.
[5] Vukkum P. , Deshpande G.R., J Moses Babu J.M.,Muralikrishna R., Jagu P.: Stress degradation behavior of abacavir sulfate and development of a suitable stability-indicating UHPLC method for the determination of abacavir, its related substances, and degradation products. *Sci. Pharm.* **80** (2012), 903–921.
[6] Prakash A., Teotia A.K., Farooqi A.J., Singh G.N.: Forced degradation study of abacavir sulfate under the frame of genotoxic impurity. *Indian J. Chem.* **55B** (2016), 213–219.
[7] Venkatarama S., Manasa M.: Forced degradation studies: Regulatory guidance, characterization of drugs, and their degradation products – A review. *Drug Invent. Today* **10** (2018), 137–146.
[8] Alsante K.M., Ando A., Brown R., Ensing J., Hatajik T.D. Kong W., Tsuda Y.: The role of degradant profiling in active pharmaceutical ingredients and drug products. *Drug Deliv. Rev.* **59** (2007), 29–37.
[9] Kurmi M., Sahu A., Singh S.: Stability behaviour of antiretroviral drugs and their combinations. 5: Characterization of novel degradation products of abacavir sulfate by mass and nuclear magnetic resonance spectrometry. *J. Pharm. Biomed. Anal.* **134** (2017), 372–384.

Novel analytical approach for real-time monitoring of volatile Maillard reaction products emitted from the sugar-amino acid model system using proton transfer reaction mass spectrometry

Anna Banaszkiewicz*, Tomasz Majchrzak

Gdańsk University of Technology, Faculty of Chemistry, Department of Analytical Chemistry, Gabriela Narutowicza 11/12, 80-233 Gdańsk, Poland ✉ *s165588@student.pg.edu.pl*

Keywords
food processing
Maillard reaction
model systems
PTR-MS
UV/Vis
volatiles

Abstract
In the presented research, volatile Maillard reaction products formation in the two sugar-amino acid model systems, namely glucose-lysine and ribose-lysine model systems were investigated using proton transfer reaction mass spectrometry. Obtained data were supported by the reference method, i.e., UV/Vis spectrometry. A number of volatile organic compounds were selected based on the correlation of the effect of Maillard reaction conditions and model system concentration with the emission of characteristic volatiles. It was demonstrated that the ribose-lysine model system was more reactive than the glucose-lysine model system which resulted in the high concentration of volatiles, such as acetonitrile, acetaldehyde, and 2,3-pentanedione. Characteristic volatile Maillard reaction products were observed only in the ribose–lysine model system: 2,3-butanedione and 3-methylbutanal, while methylfuran was characteristic for the glucose–lysine model system. Absorbance measurements revealed a correlation between the browning of the model systems and the emission of selected volatile Maillard reaction products.

1. Introduction

Maillard reaction, also known as a non-enzymatic browning reaction, is one of the main chemical processes responsible for the aroma, taste, appearance, as well as texture of thermally processed foodstuffs. Maillard reaction is driven by the condensation of reducing sugar with compounds having a free amino group, namely amino acids, proteins, and peptides, among others [1]. Then, it is followed by a series of chemical reactions leading to the formation of brownish products, melanoidins. The key products of the Maillard reaction are also volatile Maillard

reaction products, such as methylpyrazines, pyrrole-2-carboxaldehyde, acetaldehyde, butanedione, and acetol to name a few [2, 3], which are responsible for the characteristic bread crust-like aroma.

Although a general Maillard reaction mechanism is commonly known [7], there is still a need for deeper research for a better understanding of the exact pathway of volatile Maillard reaction products formation in different reaction scenarios. Over the last decade, due to the development of MS-based analytical techniques, volatile Maillard reaction products formation and emission are gaining the attention of food analysts. New methods based on gas chromatography-mass spectrometry or direct mass spectrometry methods, such as atmospheric pressure chemical ionization mass spectrometry or proton transfer reaction mass spectrometry (PTR-MS) can be found in the literature [4].

The last of these techniques, PTR-MS, is a promising tool for real-time identification and quantification of volatile Maillard reaction products. This technique, due to the rapid measurement and kinetics-driven quantification, could find a place in food processing monitoring [4, 5]. In Maillard reaction studies PTR-MS was, for example, used by Nestle Research for on-line monitoring of acrylamide formation [5], and more recently in the monitoring of the bread making process [6]. However, most of the studies related to the application of the PTR-MS in food processing monitoring are focused on food matrices, rather than strictly controllable, simplified model systems.

The aim of the research was to identify and trace selected volatile Maillard reaction products in two sugar-amino acid model systems, namely glucose–lysine and ribose–lysine model systems, using PTR-MS. Data were supported by the measurements using a reference technique, i.e., UV-VIS spectrometry. In the presented research, the emphasis was placed on the impact of amino acid and sugar concentration, temperature, and time of the reaction on the emission characteristic of volatile Maillard reaction products.

2. Experimental

2.1 Reagents and chemicals

Two aqueous sugar-amino acid model systems, namely ribose-lysine and glucose-lysine with equimolar concentrations of 50 mM, 100 mM, and 200 mM were heated to 90 °C, 75 °C, 60 °C for 10 min, 30 min, and 60 min. All of the reagents were purchased in Sigma Aldrich (USA).

2.2 Instrumentation

In order to compare concentrations of selected volatile Maillard reaction products measured with PTR-MS the standard method, namely UV/Vis spectroscopy was used. Absorbance was measured at 294 nm as an indication of early-stage

Table 1
The juxtaposition of selected volatile Maillard reaction products emitted from different 200mM model systems heated to 90 °C for 60 minutes (*n.d.* – not determined).

Model	Absorbance		Concentration / ppb_v						
	294 nm	420 nm	m42	m45	m59	m63	m83	m87	m101
Glucose–lysine	3.20	0.39	673.8	71.8	32.0	2.4	18.3	1.9	2.8
Ribose–lysine	>3.50	>3.50	1407.0	557.9	66.3	16.3	3.7	30.5	32.0
Glucose	<0.10	<0.10	*n.d.*	*n.d.*	*n.d.*	*n.d.*	*n.d.*	*n.d.*	1.8
Ribose	0.18	<0.10	*n.d.*	43.9	7.2	*n.d.*	3.00	*n.d.*	5.2
Lysine	0.52	<0.10	*n.d.*	25.5	11.0	*n.d.*	4.9	*n.d.*	9.7

Maillard reaction products at 420 nm as an indication of advanced glycation end products in the late stage of Maillard reaction [1]. Two UV/Vis spectrometers were used, namely, Spectroquant® Prove 600 (Merck, USA) for UV wavelength and DR3900 (Hach Lange, USA) for VIS wavelength.

PTR TOF1000 ultra proton transfer reaction mass spectrometer (Ionicon) was used in this study. A reduced field E/N of 100 Td was maintained during the measurement. Into a 20 ml headspace, 1 ml of the model system was placed vial and kept at 40 °C prior to the analysis. The IoniTOF v3.0 (Ionicon) and PTR-MS Viewer v3.3.7 (Ionicon) software was used for data acquisition and processing, respectively. For Maillard reaction products quantification, reaction rate coefficient k was set to 2.0×10^{-9} cm^3 s^{-1}.

3. Results and discussion

The comparison of selected volatile Maillard reaction products concentration in both glucose-lysine and ribose-lysine model systems, as well as glucose, ribose, and lysine alone are shown in Table 1. All of these samples contained a 200 mM aqueous solution of each substrate and were heated for 60 minutes at 90 °C. According to the UV/VIS data, the most reactive sample was ribose-lysine which turned to intense brownish color and gained a bread crust-like aroma. It was shown that water solutions of glucose, ribose, and lysine were unreactive in terms of the Maillard reaction.

Using PTR-MS it was possible to tentatively identify volatile Maillard reaction products such as acetaldehyde (m45), acetone (m59), methylfuran (m83), and 2,3-pentanedione (m101). These compounds were reported in other papers [7–10] and are found to be Maillard reaction products. The ribose-lysine model system was represented by the highest total volatile organic compounds emission, where acetonitrile (m42), acetaldehyde (m45), and acetone (m59) were dominant. Some of the volatile Maillard reaction products were specific for the ribose-lysine model system, such as m63 (unknown) or m83 (2,3-butanedione or 3-methylbutanal [10]). The methylfuran (m83) seems to be the characteristic volatile Maillard reaction products for glucose-lysine.

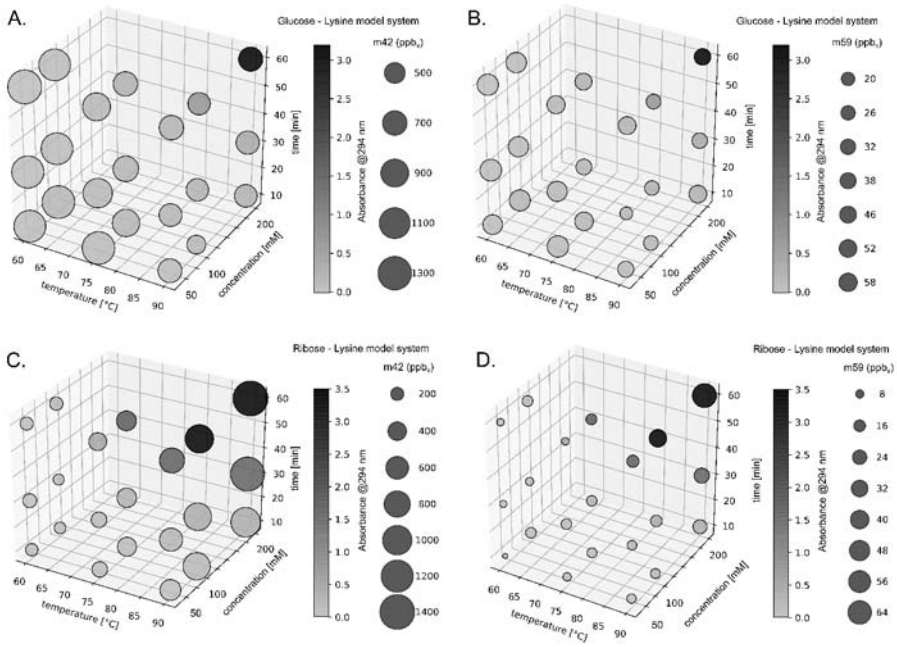

Fig. 1 The emission of acetonitrile (m42) and acetone (m59) in glucose-lysine (A and B) and ribose-lysine (C and D) model systems in different Maillard reaction conditions, namely concentration of model system, heating temperature and reaction time. The size of the bubbles represents the volatile Maillard reaction products concentration (ppb_v) and the greyscale describes the absorbance of the model system at 294 nm.

The effect of Maillard reaction condition and model system concentration on the volatile Maillard reaction product emission was presented in Fig. 1. It can be seen that for ribose-lysine the concentration of acetonitrile (Fig. 1C) and acetone (Fig. 1D) follow the change of UV absorbance, whereas for the glucose-lysine model system the correlation is unclear. The concentrations for both acetonitrile (Fig. 1A) and acetone (Fig. 1B) were the highest in low glucose-lysine model system concentration (50 mM), 90 °C, and 10 minutes of heating. Whereas, in the ribose-lysine model system, the concentrations for both acetonitrile (Fig. 1C) and acetone (Fig. 1D) were the highest in 200 mM ribose-lysine model system concentration, 60°C, and 60 minutes of heating. Thus, it can be concluded that both acetone and acetonitrile could be indicators of the progression of Maillard reaction only in the ribose-lysine model system due to the directly proportional relationship of time, the concentration of the model system, and temperature of heating with the volatile Maillard reaction products emission.

4. Conclusions

Using PTR-MS it was possible to determine volatile Maillard reaction products which were emitted from different sugar-amino acid model systems. It is possible to correlate volatile Maillard reaction products emission with the absorbance in the UV spectrum only for the ribose-lysine model system. What is more, it is possible to find a correlation between Maillard reaction conditions such as concentration of the model system, time, temperature of heating, and the selected volatile Maillard reaction products emission. In the next step, the real-time measurement of volatile Maillard reaction products using PTR-MS should be performed.

References

[1] Kim J., Lee Y.: Study of Maillard reaction products derived from aqueous model systems with different peptide chain lengths. *Food Chem.* **116** (2009), 846–853.
[2] Kagami K., Onda K., Oka K., Hirano T.: Suppression of blood lipid concentrations by volatile Maillard reaction products. *Nutrition* **24** (2008), 1159–1166.
[3] Nursten H.E.: *The Maillard Reaction: Chemistry, Biochemistry and Implications.* London, The Royal Society of Chemistry 2005.
[4] Fay L., Brevard H.: Contribution of mass spectrometry to the study of the Maillard reaction in food. *Mass Spectrom. Rev.* **24** (2005), 487–507.
[5] Pollien P., Lindinger C., Yeretzian C., Blank I.: Proton transfer reaction mass spectrometry, a tool for on-line monitoring of acrylamide formation in the headspace of Maillard reaction systems and processed food. *Anal. Chem.* **88** (2003), 5488–5494.
[6] Makhoul S., Romano A., Capozzi V., Spano G., Aprea A., Cappellin L., Benozzi E., Scampicchio M., Märk T., Gasperi F., El-Nakat H., Guzzo J., Biasioli F.: Volatile compound production during the bread-making process: effect of flour, yeast and their interaction. *Food Bioprocess Technol.* **8** (2015), 1925–1937.
[7] Amrani-Hemaimi M., Cerny C., Fay L.: Mechanisms of formation of alkylpyrazines in the Maillard reaction. *J. Agríc. Food Chem.* **43** (1995), 2818–2822.
[8] Zhu C.Z., Zhao J.L., Tian W., Liu Y.X., Li M.Y., Zhao G.M.: Contribution of histidine and lysine to the generation of volatile compounds in Jinhua Ham exposed to ripening conditions via Maillard reaction. *Food Chem.* **83** (2018), 46–52.
[9] Märk J., Pollien P., Lindinger C., Blank I., Märk T.: Quantitation of furan and methylfuran formed in different precursor systems by proton transfer reaction mass spectrometry. *J. Agric. Food Chem.* **54** (2006), 2786–2793.
[10] Cerny C.: The aroma side of the Maillard reaction. *Ann. N. Y. Acad. Sci.* **1126** (2008), 66–71.

Solid state ion-selective electrode based on silver nanoparticles

Karolina Pietrzak[a,*], Nikša Krstulović[b], Cecylia Wardak[a], Szymon Malinowski[c]

[a] *Maria Curie-Sklodowska University, Faculty of Chemistry, Institute of Chemical Sciences, Department of Analytical Chemistry, Maria Curie-Sklodowska Sq. 3, 20-031 Lublin, Poland*
✉ *karolina.pietrzak@poczta.umcs.lublin.pl*
[b] *Institute of Physics, Bijenička cesta 46, 10 000 Zagreb, Croatia*
[c] *Lublin University of Technology, Faculty of Civil Engineering and Architecture, Nadbystrzycka 40, 20-618 Lublin, Poland*

Keywords
ion-selective electrodes
potassium
potentiometry
silver nanoparticles

Abstract
The research on the use of silver nanoparticles as an ion to electron transducer in ion-selective electrodes with solid contact sensitive to potassium ions was described. Silver nanoparticles were obtained using the laser ablation technique. Basic analytical parameters were determined for electrodes with two thicknesses of silver nanoparticles placed between the electrode material and the membrane. The obtained modified electrodes had a very good slope of the characteristic curve (56.16 mV dec^{-1}), fast response (< 6 s), good potential stability (0.32 mV h^{-1}), and long life time (> 5 months). In the case of modified electrodes, a significant improvement in the stability of the potential and an increase in life time compared to unmodified electrodes have been noticed.

1. Introduction

All modifications in the design of ion-selective electrodes are aimed at improving their most important analytical parameters, including increasing the slope of the calibration curves, extending the linearity ranges, and lowering the detection limit, which will enable the determination of ions at lower concentration levels. Apart from the above, a very important parameter, which has been improved in recent years, characterizing the ion-selective electrodes is their selectivity, i.e., their ability to determine the selected main ion to which the ion-selective membrane is sensitive, in the presence of other interfering ions in the sample [1]. In addition, in the case of potentiometric sensors, the stability of the measured potential over time and under various, also changing environmental conditions (change of the light intensity, pH of the sample, presence of O_2 and CO_2) is very important, which favors their subsequent use in environmental analysis and measurements in the in situ environment. In addition to changing the active ingredients of ion-selective membranes, in the case of solid contact ion-selective

electrodes, intermediate layers and additional membrane components acting as solid contact are also used. Due to the elimination of the internal solution, these electrodes can be miniaturized, their shape can be modified, they are easier to transport and store, and they are much more mechanically resistant and durable [2].

Nanomaterials have found applications in many fields of science and industry. Recently, they have been successfully used to construct electrochemical sensors, including ion-selective electrodes. So far, carbon nanomaterials (carbon nanotubes [3, 4], graphene [5], fullerenes [6], carbon black [7]) and metal nanoparticles (Ag [8], Au [9], Pt [10]) have already been used for this purpose.

2. Experimental

2.1 Reagents and chemicals

Ion selective membrane components were obtained from Aldrich (potassium ionophore-valinomycin, and low molecular weight poly(vinylchloride)) and Fluka (potassium tetrakis(*p*-chlorophenyl)borate and bis(2-ethylhexyl)sebacate). Salts of the highest purity available (pure pro analysis) and freshly deionized water were used for the preparation of aqueous ion solutions. These substances were mainly obtained from Fluka. Silver nanoparticles (precisely silver nanoparticles in water) were obtained using the laser ablation in liquid method at the Institute of Physics in Zagreb.

2.2 Instrumentation

All potentiometric measurements were made for a cell consisting of an Ag/AgCl reference electrode (Metrohm 6.0750.100) and the tested ion-selective electrodes (unmodified electrodes containing only the membrane and electrodes with an intermediate layer of silver nanoparticles of different thickness). The tests were carried out at room temperature in mixed solutions. A 16-channel data acquisition system (Lawson Labs, USA) connected to a computer was used to collect and process the results.

2.3 Preparation of solid contact ion-selective electrodes

The qualitative and quantitative composition of the membrane was as follows: 3% valinomycin, 1% potassium tetrakis(*p*-chlorophenyl)borate, 32% poly(vinylchloride), 64% bis(2-ethylhexyl)sebacate. Weighing amounts of 0.3 g of the ingredients were weighed, followed by the addition of 3 ml of tetrahydrofuran. Everything was homogenized with an ultrasonic water bath. The surface of glassy carbon electrodes with a diameter of 3 mm was polished with sandpaper and an alumina powder (size 0.3 μm). Then the electrodes were rinsed with distilled

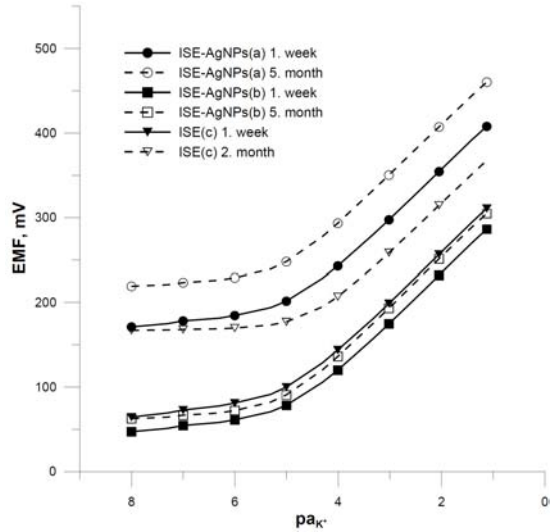

Fig. 1 Calibration curves of electrodes determined after 1 week and 5 months of electrode operation (for electrodes with silver nanoparticles).

water and additionally an ultrasonic water bath was used to get rid of the residual abrasive material. The electrodes were immersed in tetrahydrofuran to degrease the surface and allowed to dry. Small volumes of nanoparticles in water were then spotted (500 and 100 μL in total) and allowed to dry again. Finally, a membrane mix was spotted on the previously prepared electrodes (3×30 μL of the mixture with an interval of half an hour), and the next day, after complete drying, they were immersed in a conditioning solution (1×10^{-3} mol L^{-1} KNO_3). For comparison, apart from electrodes with intermediate layers of nanoparticles (500 μL – AgNPs (a), and 100 μL - AgNPs (b)), unmodified electrodes, containing only the ion-selective membrane (c) were also made.

3. Results and discussion

The cell electromotive force measurements were performed in KNO_3 solutions in the concentration range of 10^{-8}–10^{-1} mol L^{-1}. On the basis of the obtained calibration curves (Fig. 1), the values of the basic analytical parameters were determined: slopes and linear ranges of calibration curve as well as detection limits for all sensors (Table 1).

The reversibility of the potential of the tested sensors in 10^{-5}, 10^{-4}, and 10^{-3} mol L^{-1} solutions was also investigated. The numerical values including the average potentials and standard deviations for five repetitions are presented in Table 2. In each case, the values of the standard deviation were lower for the modified electrodes as compared to the unmodified ones, which proves the beneficial effect of silver nanoparticles intermediate layer on the reversibility of the electrode potential.

Table 1
Selected analytical parameters obtained for the tested electrodes (*LOD* – limit of detection; 5. month – for ISE-Ag(a) and ISE-Ag(b) electrodes; 2. month – for ISE(c)).

Parameter	ISE-Ag(a)	ISE-Ag(b)	ISE(c)
Slope / mV dec^{-1}			
1. week	–55.51	–56.16	–55.03
5./2. month	–55.17	–56.60	–54.79
Linear range / mol L^{-1}			
1. week	10^{-5}–10^{-1}	10^{-5}–10^{-1}	10^{-5}–10^{-1}
5./2. month	10^{-5}–10^{-1}	10^{-5}–10^{-4}	10^{-4}–10^{-1}
LOD /mol L^{-1}			
1. week	5.38×10^{-6}	5.17×10^{-6}	5.86×10^{-6}
5./2. month	7.58×10^{-6}	5.05×10^{-6}	1.93×10^{-5}
Short term potential drift / mV h^{-1}	1.85	0.32	5.17
Long term potential drift / mV day^{-1}	0.38	0.15	1.1
Response time / s	< 6	< 6	< 8

Table 2
Mean values of potentials (*E*) and standard deviations (SD) obtained for the tested electrodes for five measurements.

$c(K^+)$ / mol L^{-1}	Parameter	ISE-Ag(a)	ISE-Ag(b)	ISE(c)
10^{-5}	*E* / mV	220.25	78.12	123.44
	SD / mV	4.22	5.06	6.36
10^{-4}	*E* / mV	268.61	136.30	166.71
	SD / mV	0.93	1.52	2.68
10^{-3}	*E* / mV	324.45	182.23	223.66
	SD / mV	0.75	0.46	1.76

The selectivity of the tested electrodes was estimated thanks to the determination of the selectivity coefficients by the method of separate solutions. The selectivity coefficients obtained for selected metal cations (Na^+, Ca^{2+}, Mg^{2+}, Co^{2+}, Zn^{2+}, Cu^{2+}, Cd^{2+}, Pb^{2+}) were compared. For the ion sequences given above, the log *K* are respectively: for the ISE-AgNPs electrode (a) [–5.03; –4.30; –5.40; –4.08; –4.85; –4.82; –4.77; –5.06], for the ISE-Ag electrode (b) [–4.90; –4.37 –5.46; –3.86; –5.19; –5.18; –5.14; –5.46] and for the ISE electrode [–4.75; –4.76; –4.82; –3.75; –5.04; –5.11; –4.95; –5.13]. No significant influence of the modification of the electrodes on their selectivity was noticed, as the values of all obtained selectivity coefficients were comparable for all types of electrodes. Slightly better selectivity coefficients for the tested electrodes were obtained for Mg^{2+} and Co^{2+} cations.

The short and long term stability of the electrode potential was also investigated. The short-term stability of the potential was measured for 3 h in a KNO_3 solution with a concentration of 10^{-1} mol L^{-1}. Figure 2 shows a graph of electrode potential change versus time. Modified electrodes are characterized by better

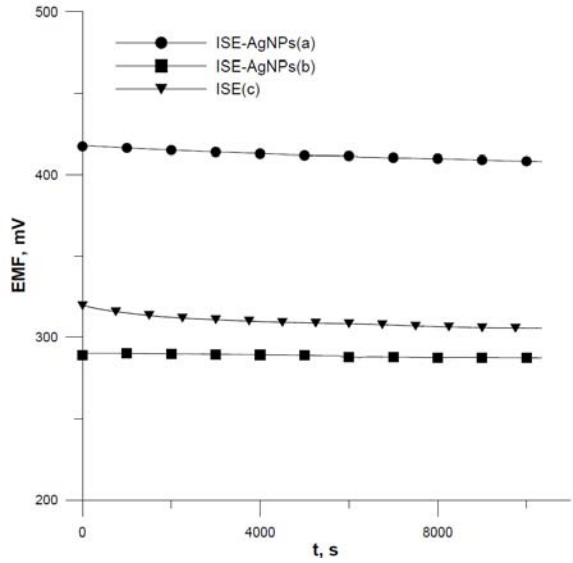

Fig. 2 Short-term stability of the electrode potential in a solution of 10^{-1} mol L^{-1} KNO_3.

potential stability, while the lowest potential change over time is shown by electrodes with a thinner layer of silver nanoparticles.

In order to determine the long-term stability of the electrode potential and their lifetime, electrodes were tested for 5 months. Figure 1 shows a comparison of calibration curves for each type of electrode determined for one week and five months old electrode. During this time, both the slope and the linearity range did not change much, and the modified electrodes continued to function properly. In the case of unmodified electrodes, the linearity range of the calibration curve decreased by an order of magnitude (from 10^{-5}–10^{-1} mol L^{-1} to 10^{-4}–10^{-1} mol L^{-1}). Moreover, modified electrodes showed much better long term potential stability. Change of E°_{st} was much smaller for modified electrodes compared to unmodified ones. The electrodes with a thinner layer of nanoparticles showed the lowest long term potential drift over time.

4. Conclusions

Modification of the electrodes mainly influenced the improvement of the stability and reversibility of the electrode potential and their durability compared to electrodes without an intermediate layer. The electrodes with an additional layer of silver nanoparticles worked properly for over at least five months, showing an unchanged slope of the calibration curve and also maintaining the same linear range as at the beginning of measurements. In addition, they are simple and convenient to use and allow for quick measurements and results obtained.

Acknowledgments

The author (Karolina Pietrzak) special thanks to the Institute of Physics in Zagreb for the internship opportunity, nanoparticles synthesis, and possibility of participating in research.

References

[1] Pretsch E.: The new wave of ion-selective electrodes. *TrAC, Trends Anal. Chem.* **26** (2007), 46–51.
[2] Bobacka J., Ivaska A., Lewenstam A.: Potentiometric ion sensors. *Chem. Rev.* **108** (2008), 329–351.
[3] Parra E.J., Crespo G.A., Riu J., Ruiz A., Rius F.X.: Ion-selective electrodes using multi-walled carbon nanotubes as ion-to-electron transducers for the detection of perchlorate. *Analyst* **134** (2009), 1905–1910.
[4] Hassan S.S.M., Eldin A.G., Amr A.E.G.E., Al-Omar M.A., Kamel A.H., Khalifa N.M.: Improved solid-contact nitrate ion selective electrodes based on multi-walled carbon nanotubes (MWCNTs) as an Ion-to-electron transducer. *Sensors* **19** (2019), 3891.
[5] Li F., Ye J., Zhou M., Gan S., Zhang Q., Han D., Niu L.: All-solid-state potassium-selective electrode using graphene as the solid contact. *Analyst* **137** (2012), 618–623.
[6] Fouskaki M., Chaniotakis N.: Fullerene-based electrochemical buffer layer for ion-selective electrodes. *Analyst* **133** (2008), 1072–1075.
[7] Paczosa-Bator B.: All-solid-state selective electrodes using carbon black. *Talanta* **93** (2012), 424–427.
[8] Qi L., Jiang T., Liang R., Qin W.: Polymeric membrane ion-selective electrodes with anti-biofouling properties by surface modification of silver nanoparticles. *Sens. Actuators, B* **328** (2021), 129014.
[9] Jaworska E., Wójcik M., Kisiel A., Mieczkowski J., Michalska A.: Gold nanoparticles solid contact for ion-selective electrodes of highly stable potential readings. *Talanta* **85** (2011), 1986–1989.
[10] Paczosa-Bator B., Piech R., Wardak C., Cabaj L.: Application of graphene supporting platinum nanoparticles layer in electrochemical sensors with potentiometric and voltammetric detection. *Ionics* **24** (2018), 2455–2464.

Evaluation of the potential of Microwave Plasma–Atomic Emission Spectrometry for trace elements leaching assessment from the concrete matrix with sewage sludge ash additives

Alicja Saczuk[a,*], Paulina Augustyniak[a], Elżbieta Haustein[b], Bartłomiej Cieślik[a]

[a] *Gdańsk University of Technology, Faculty of Chemistry, Gabriela Narutowicza 11/12, 80-233 Gdańsk, Poland* ✉ *s171455@student.pg.edu.pl*
[b] *Gdańsk University of Technology, Faculty of Civil Engineering, Gabriela Narutowicza 11/12, 80-233 Gdańsk, Poland*

Keywords
concrete
heavy metals
leachability
microwave
plasma–atomic emission spectroscopy
sewage sludge ash

Abstract
The management of ash generated during the thermal utilization of sewage sludge is a significant environmental problem requiring an effective technological solution. One alternative way to dispose of sewage sludge is to bind it in concrete as a substitute for part of the aggregate. The properties of the C-S-H phase enable effective immobilization of harmful substances that sewage sludge contains. The amount of individual compounds and elements is variable and fully dependent on the characteristics of the wastewater flowing into the sewage sludge treatment plant. The research investigated the effect of the addition of sewage sludge as a replacement for part of the sand, on the fresh concrete mix and the characteristics of the hardened concrete. The behavior of heavy metals were subjected to observation using microwave plasma–atomic emission spectrometer in three environments, such as nitric acid (pH ≈ 3), artificial groundwater and seawater solutions. The validity of using advanced spectroscopic methods, such as mentioned microwave plasma–atomic emission spectrometer, for improving the assessment of the danger of using waste materials in modern building materials was considered.

1. Introduction

Evaluation of the degree of transition of heavy metal ions from the solid waste to the used medium under laboratory conditions makes it possible to predict the behaviour of a building material with an alternative waste material additives, in the environment. It creates a possibility to plan the life cycle of manufactured

construction material in terms of the risk it poses to the environment. The phenomenon of heavy metals leaching from the construction material always occurs during contact with the environmental media (soil, water, or other liquids), which becomes the main carrier of substances posing an environmental hazard, as shown by Król [1]. The leaching process of heavy metal ions can be enhanced by external factors, such as material working conditions, the ratio of liquid to the solid phase, the duration of exposure to the leaching medium, temperature, or mechanical influences (freeze/thaw cycles, abrasion, erosion). Internal factors such as porosity, thermal conductivity, shape, expansion area, size, susceptibility to carbonation or alkalinity, and age of the product can also influence the leaching rate, as shown by Giergiczny and Król [2].

2. Experimental

All following studies were carried out using samples made of concrete with the addition of ash from the process of thermal utilization of sewage sludge from the wastewater treatment plants Gdańsk "East" and Gdynia Dębogórze. Described studies were divided into two phases. The first phase was focussed on leaching studies which were performed only in nitric acid solution, in pH ≈ 3. It made it possible to assess the behaviour of building materials in an aggressive environment and to draw conclusions about further steps. The second phase was focused on lowering the limit of quantification and detection for elements such as cadmium and cobalt. It was achieved using optimization techniques using microwave plasma–atomic emission spectrometer. Leaching tests were carried out, in this case, using different mediums: artificial solutions of groundwater and seawater.

2.1 Reagents and chemicals

Ash for the purposes of these studies was collected in 2020. Six types of tests were carried out with 2.5%, 7.5%, 12.11% content of ash from Gdansk "East" and 10%, 15%, and 20% content of ash from Gdynia Dębogórze as a substitute for aggregate in the form of sand. Solid samples made within this research were subjected to the test of heavy metals leachability according to the modified industry standard PN-EN 12457-2:2006 [3]. Concrete with the alternative additive (grain diameter <0. 20 μm) was mixed with the selected solvent in the solid:liquid ratio 1:10, the solvents used were nitric acid (pH≈3), groundwater, and seawater; the solvent compositions are shown in Table 1. The mixtures thus prepared were subjected to shaking using a shaker.

2.2 Instrumentation

Samples for testing were agitated for 120 h with 120 rpm in pH ≈ 3 (nitric acid). In case, when groundwater and seawater environments were used, the agitating

Table 1
Compositions of leaching solutions.

Ingredient	Weight / g	
	Groundwater	Seawater
$MgSO_4$	0.636	28.29
$CaCl_2$	1.85	2.49
$NaHCO_3$	1.35	3.52
Na_2SO_4	1.14	1.14
KCl	–	0.83
Distilled water	1 L	1 L

Table 2
Calibration procedure details.

c / mg L^{-1}	Intensity			
	Co (345.351 nm)	Co (340.512 nm)	Cd (228.802 nm)	Cd (226.502 nm)
0.00	0.02	–0.03	–20	0.02
0.03	255.91	180.32	455.31	51.22
0.05	554.98	391.76	726.05	23.68
0.09	801.72	582.21	1340.95	311.67
0.10	934.65	675.37	1648.74	572.78
0.50	4349.39	3171.72	7933.54	854.03
0.70	6886.88	4741.21	11995.9	1676.04
0.90	8583.88	5898.24	14531.65	2112.69
1.00	9941.77	6879.26	16662.11	2470.3
Correlation	0.99866	0.99927	0.99924	0.99649

conditions were the same; however, the processing time was extended to 408 h. Then each sample was filtered using a filter with a pore diameter of 45 μm. The samples prepared were analysed with the use of microwave plasma–atomic emission spectrometer 4210 supplied by Agilent. The results of the determinations were prepared using MA 3000 software supplied by NIC and MS Expert software supplied by Agilent.

3. Results and discussion

Under the conditions created by nitric acid (i.e., pH ≈ 3), none of the elements tested (Co, Cr, Mn, Cu, Zn, Cd, Al, Fe) could be determined; except for phosphorus, all concentrations were below the detection limit. Therefore, in the case of tests with the artificial ground and seawater solutions, the focus was on exploiting the potential of the apparatus used and by means of optimisation methods trying to achieve the lowest possible limit of detection and quantification for cobalt and cadmium. For this purpose, instrument parameters such as plasma viewing point and nebulizer flow were adjusted for selected wavelengths for cobalt 340.512 nm and 345.351 nm and for cadmium 226.502 nm and 228.802 nm, as well as careful

Table 3
The summary of limit of detection (*LOD*) and limit of quantitation (*LOQ*) for cobalt (340.512 nm) and cadmium (228.802 nm).

Element	Parameter	Before optimization (nitric acid, pH ≈ 3)	After optimization (groundwater, seawater)
Co	*LOD* / mg kg^{-1}	1.7	0.11
	LOQ / mg kg^{-1}	5.7	0.32
Cd	*LOD* / mg kg^{-1}	0.91	0.53
	LOQ / mg kg^{-1}	3	1.6

Table 4
Results for groundwater [mg kg^{-1}], values in brackets are the wavelengths chosen for the determination of the metals concerned: SSA1 – ash from wastewater treatment station Gdynia Dębogórze, SSA2 – ash from wastewater treatment station Gdańsk "East".

Sample	Chromium (425.433 nm)	Phosphorus (213.618 nm)	Cobalt (340.512 nm)
2.5% SSA2	7.471±0.70	403.7±4.3	1.373±0.082
7.5% SSA2	13.91±0.10	409.3±4.6	1.53±0.11
12.11% SSA2	17.964±0.052	107.1±4.7	0.524±0.026
10% SSA1	9.693±0.057	234.4±8.3	0.834±0.020
15% SSA1	14.512±0.082	376.9±9.2	1.243±0.028
20% SSA1	8.293±0.049	394±11	1.364±0.080

Table 5
Results for seawater [mg kg^{-1}], values in brackets are the wavelengths chosen for the determi-nation of the metals concerned: SSA1 – ash from wastewater treatment station Gdynia Dębogórze, SSA2 – ash from wastewater treatment station Gdańsk "East".

Sample	Chromium (425.433 nm)	Phosphorus (213.618 nm)	Cobalt (340.512 nm)
2.5% SSA2	18.093±0.023	<*LOQ*	0.694±0.074
7.5% SSA2	17.16±0.11	<*LOQ*	0.773±0.064
12.11% SSA2	17.65±0.78	<*LOQ*	0.42±0.11
10% SSA1	17.001±0.025	<*LOQ*	0.943±0.022
15% SSA1	13.312±0.064	<*LOQ*	0.973±0.034
20% SSA1	18.087±0.036	<*LOQ*	0.666±0.087

calibration of these elements in the low concentration range. The wavelength with the highest intensity of emission was chosen, which at the same time was not overlapped by emission wavelengths of other elements, which were determined in the solid materials. The data obtained from the calibrations are shown in Table 2. The summary of limit of detection and limit of quantitation before and after optimization is shown in Table 3. The results of the determinations made in one measurement are shown in Tables 4 and 5. The concentration of cadmium in the determined samples was below the detection limit despite the application of optimization.

4. Conclusions

Microwave plasma–atomic emission spectrometer system is a device with enormous analytical capabilities. Very low and high concentrations for a wide range of elements can be determined simultaneously in a single measurement. The optimization measures used, allow to achieve very low detection levels for cobalt and cadmium. Mentioned elements, as heavy metals, accumulates in the tissues of plants and animals, causing irreversible changes in the ecosystem. Therefore, accurate analysis in terms of the release of heavy metals into the environment is of utmost importance. Testing of alternative construction materials with such adapted equipment allows to assess, the possible risk for the environment and to determine the life cycle for the concrete made with recycled wastes additives.

References

[1] Król A.: *Uwalnianie metali ciężkich z kompozytów mineralnych z uwzględnieniem oddziaływania środowiska.* Opole, Politechnika Opolska 2012. (In Polish.)

[2] Giergiczny Z., Król A.: Immobilization of heavy metals (Pb, Cu, Cr, Zn, Cd, Mn) in the mineral additions containing concrete composites. *J. Hazard. Mater.* **160** (2008), 247–255.

[3] PN-EN 12457-4:2006 *Charakteryzowanie odpadów – Wymywanie – Badanie zgodności w odniesieniu do wymywania ziarnistych materiałów odpadowych i osadów – Część 4: Jednostopniowe badanie porcjowe przy stosunku cieczy do fazy stałej 10 l/kg w przypadku materiałów o wielkości cząstek poniżej 10 mm (bez redukcji lub z redukcją wielkości)*. (In Polish.).

Validation of capillary electrophoresis method for determination of monosaccharides found in glycopeptides

Alice Šimonová*, Tomáš Křížek, Petr Kozlík

Charles University, Faculty of Science, Department of Analytical Chemistry, Hlavova 8/2030, 128 43 Prague 2, Czech Republic ✉ *simonovaa@natur.cuni.cz*

Keywords
capillary electrophoresis
contactless conductivity detection
monosaccharides

Abstract
In this study, we optimized a method for the determination of monosaccharides in glycoproteins. Capillary electrophoresis with contactless conductivity detection was used for the separation of eight monosaccharides commonly found in glycoproteins in alkaline background electrolyte. The limits of detection were between 5–7 mg L^{-1} and the limits of quantification were between 16–22 mg L^{-1}.

1. Introduction

Saccharide profile in glycolipids and glycoproteins affects their conformations, biological activity and their metabolism, therefore there is an increased interest in their analysis. Glycoproteins are important for intercellular communication, ionic transport, and immunity. Glycosylation affects physicochemical properties of the protein. The profile of saccharides released from glycoprotein by enzymatic or acidic hydrolysis provide information useful in biomedical research and during detection of disease biomarkers; change of glycosylation may occur as a result of autoimmune disease, cancer or immunodeficiency [1–3].

Analysis of free monosaccharides released from protein can provide information on the relative proportions of individual monosaccharide units in the glycoprotein. The release of saccharide units from glycoprotein can be achieved by enzymatic or chemical hydrolysis and the chemical hydrolysis can be acidic or basic [2]. Monosaccharides commonly found in glycoproteins include glucose, galactose, mannose, fucose, *N*-acetylgalactosamine, *N*-acetylglucosamine, *N*-acetylneuraminic acid, and xylose [4]. Most commonly used methods for the separation and determination of saccharides are liquid chromatography, capillary electrophoresis (CE), and gas chromatography. Saccharides are problematic analytes and each of these methods has its advantages and disadvantages [5].

Capillary electrophoretic separation of neutral saccharides is hindered by their lack of charge. One possibility to overcome this problem is to use a borate-based background electrolyte. Borate creates negatively charged complexes with saccharides that can be separated [6]. Other option is to use a highly basic background electrolyte causing dissociation of hydroxyl groups of saccharides which provides them with a negative electric charge. Detection of saccharides is also problematic as most of them exhibit only weak UV absorption. Indirect UV detection, fluorescence detection of derivatized saccharides, or mass spectrometry can be used [7]. In combination with strongly alkaline background electrolytes, contactless conductivity detection proved to be a simple, economic, and user-friendly option. Conductivity of the analyte zone is significantly lower than that of the highly conductive background electrolyte. On the electropherogram saccharides thus appear as negative peaks [5]. With growing pH of background electrolyte, conductivity of the solution increases and with it increases the current during the separation. This may result in the solution overheating inside the capillary. One way to decrease the current is to use capillaries with small inner diameter that also have higher surface-to-volume ratio and thus allow for more efficient heat dissipation.

Although several authors report on the CE separation of various mono- and oligosaccharides in highly alkaline background electrolytes using contactless conductivity detection, there are no reports on CE separation of all eight monosaccharides commonly found in glycoproteins. Carvalho et al. [8] used CE with contactless conductivity detection for separation of fructose, glucose, galactose and sucrose in highly alkalic buffer containing sodium hydroxide, disodium phosphate and cetyltrimethylammonium bromide (CTAB). We used this background electrolyte and optimized its composition and the method for separation of monosaccharides.

2. Experimental

2.1 Reagents and chemicals

All chemicals were of p.a. or better grade. Each monosaccharide standard and lithium hydroxide were purchased from Sigma-Aldrich (USA). Sodium and potassium hydroxide were purchased from Penta (Czech Republic). 4-(2-hydroxy-ethyl)-1-piperazinethansulfonic acid was purchased from Carl-Roth (Germany). Disodium phosphate and hexadecyltrimethyl-ammonium bromide were purcha-sed from Merck (Germany). Samples and background electrolytes were prepared using deionized water produced by Milli-Q system from Millipore (USA).

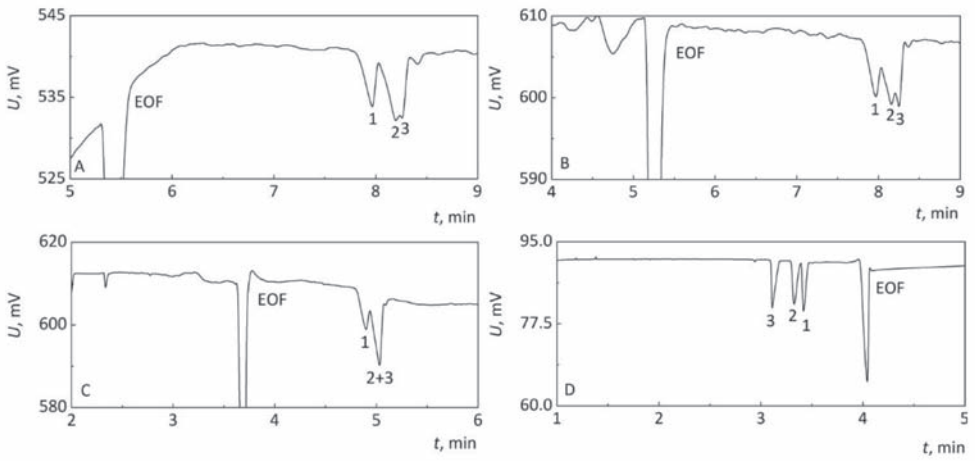

Fig. 1 Separation of monosaccharide standards at a concentration of 0.2 mg mL^{-1} in different background electrolytes: (A) 75 mM LiOH, (B) 75 mM NaOH, (C) 75 mM KOH, and (D) 10 mM NaOH + 4.5 mM Na_2HPO_4 + 0.2 mM CTAB. Peaks: (1) galactose, (2) glucose, (3) *N*-acetylglucosamine. Conditions: 20 µm ID, injection 5 kPa × 20 s, capillary length 50/35 cm, voltage 15 kV (A, B, C) or −25 kV (D).

2.2 Instrumentation

All capillary electrophoresis with contactless conductivity detection experiments were performed on a 7100 CE instrument from Agilent Technologies (Germany) with attached nitrogen cylinder for pressurizing the CE system. A fused-silica capillary was purchased from Polymicro Technologies (Phoenix, USA). For measurement of pH, 3540 pH/conductivity meter from Jenway (UK) was used.

The inner diameter of the fused-silica capillary was 10 µm, outer diameter was 375 µm, total length was 50.0 cm and 35.0 cm to detector. Before every set of measurements, capillary was flushed for 2 minutes with 1 mol L^{-1} NaOH and for 2 minutes with deionized water using a pressure of 1 MPa. Before each run, capillary was flushed for 3 minutes with the background electrolyte using a pressure of 1 MPa. Samples were injected hydrodynamically by a pressure of 5 kPa for 70 s. A separation voltage of −30 kV was then applied, inducted electric current was approximately 4 µA in 50 mM sodium hydroxide, 22.5 mM disodium phosphate and 0.2 mM cetyltrimethylammonium bromide as background electrolyte.

3. Results and discussion

3.1 Preliminary experiments

The initial screening of background electrolyte suitable for CE contactless conductivity detection measurements was performed with *N*-acetylglucosamine, glucose, and galactose as analytes. Three strongly basic background electrolytes

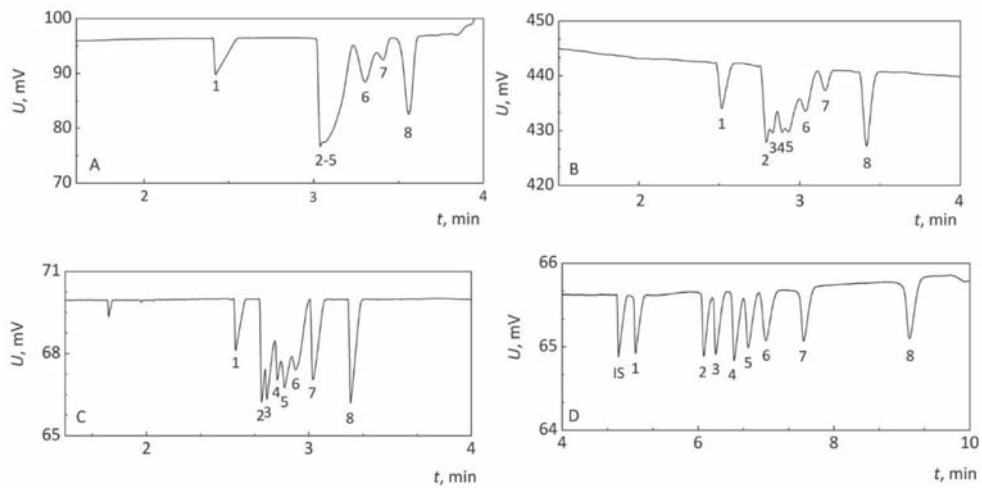

Fig. 2 Optimization of separation of 8 monosaccharides at a concentration of 0.2 mg mL^{-1} (HEPES as internal standard at the same concentration): (A) original conditions: background electrolyte 10 mM NaOH + 4.5 mM Na_2HPO_4 + 0.2 mM CTAB, 20 μm ID, injection 5 kPa × 20 s; (B) increased ionic strength: background electrolyte: 50 mM NaOH + 22.5 mM Na_2HPO_4 + 0.2 mM CTAB, 20 μm ID, injection: 5 kPa × 20 s; (C) smaller inner diameter: background electrolyte: 50 mM NaOH + 22.5 mM Na_2HPO_4 + 0.2 mM CTAB, 10 μm ID, injection: 5 kPa × 70 s; (D) counter directional pressure during the separation: background electrolyte: 50 mM NaOH + 22.5 mM Na_2HPO_4 + 0.2 mM CTAB, 10 μm ID, injection: 5 kPa × 70 s, –270 kPa. Peaks: (1) *N*-acetylneuraminic acid, (2) xylose, (3) mannose, (4) *N*-acetylglucosamine, (5) *N*-acetylgalactosamine, (6) glucose, (7) galactose, (8) fucose, (IS) HEPES. Capillary length 50/35 cm, voltage –30 kV.

were tested - lithium, sodium and potassium hydroxide solutions [9] and solution containing sodium hydroxide, sodium hydrogen phosphate and CTAB. This background electrolyte was chosen as the most suitable for monosaccharide analysis, because as you can see in Fig. 1, all three analytes were separated, their peaks were most symmetric and when compared with NaOH solution, as the most commonly used background electrolyte for monosaccharide analysis, total time was reduced to one half.

3.2 Method optimization

Background electrolyte containing 10 mM sodium hydroxide, 4.5 mM disodium phosphate and 0.2 mM CTAB did not provide baseline separation of all eight monosaccharides (Fig. 2A). The concentration of NaOH and Na_2HPO_4 was then increased 5 times, thus the ionic strength of the background electrolyte increased while the pH remained the same (Fig. 2B), the resolution of most peaks increased just slightly but separation of most saccharides was still insufficient. Another parameter that can increase separation efficiency and consequently resolution of analytes is inner diameter of the capillary, as shown in Fig. 2C using a 10-μm ID instead of 20-μm ID capillary increased separation efficiency although just three analytes were baseline separated. Thus longer time had to be given for the

Table 1
Parameters of the calibration curves for all monosaccharides (R^2 – coefficient of determination, *LOD* – limit of detection, *LOQ* – limit of quantification, $RSD_{A(rel)}$ – relative standard deviation of relative peak area, $RSD_{t(rel)}$ – relative standard deviation of relative migration time).

	Slope /mV s mg^{-1} mL	Intercept /mV s^{-1}	R^2	*LOD* / mg L^{-1}	*LOQ* / mg L^{-1}	$RSD_{A(rel)}$ /%	$RSD_{t(rel)}$ /%
N-acetylneuraminic acid	8.14	–0.20	0.9992	5	16	3.18	0.21
Xylose	5.56	+0.01	0.9997	5	17	1.33	0.74
Mannose	5.87	+0.01	0.9997	5	18	1.33	0.67
N-acetylglucos-amine	5.63	+0.05	0.9995	5	17	1.98	0.65
N-acetylgalactos-amine	6.48	–0.08	0.9995	6	21	2.98	0.75
Glucose	6.24	+0.04	0.9993	7	22	0.72	0.88
Galactose	7.59	–0.04	0.9994	5	18	3.53	1.04
Fucose	8.49	+0.00	0.9995	5	18	1.99	1.39

baseline separation of all eight monosaccharides. This can be achieved with increasing the capillary length or by applying counter directional pressure during the separation. While working with a 10-μm ID capillary, increasing capillary length can bring difficulties due to the increasing hydrodynamic resistance that causes problems with flushing and sample injection. Application of counter directional pressure was thus chosen for further experiments. The value of this pressure was optimized and a pressure of –270 kPa led to a baseline separation within 10 minutes (Fig. 2D), higher pressure caused tailing of peaks due to more significant parabolic flow profile inside the capillary and lower pressure did not yield baseline separation. To increase repeatability of the measurement and eliminate the effect of fluctuations in experimental conditions and/or during sample injection, 4-(2-hydroxyethyl)-1-piperazinethansulfonic acid (HEPES) was added to the sample as an internal standard. HEPES was chosen based on its similar properties with monosaccharides, especially its mobility (calculated using the PeakMaster program [10]), and the fact that its peak is separated from other peaks.

3.3 Method validation

The developed method was evaluated based on measuring calibration curves for all monosaccharides in the range from 0.03 to 0.5 mg mL^{-1} with 0.2 mg mL^{-1} HEPES as an internal standard. Linear regression parameters using the least-squares method were calculated and the obtained data are shown in Table 1. Coefficients of determination for all analytes were higher than 0.9990, which points to good linearity of the calibration dependences. Limits of detection and limits of quantifi-cation were calculated from peak-height calibration curves as a concentration corresponding to the threefold and tenfold standard error of noise.

Limits of detection were between 5 and 7 mg L^{-1} and limits of quantification were between 15 and 22 mg L^{-1}. The repeatability of peak areas and migration times was investigated by 10 repeated measurements of all analytes in a concentration of 0.2 mg mL^{-1} with 0.2 mg mL^{-1} HEPES as an internal standard. Relative standard deviations of peak areas related to internal standard were lower than 4% and relative standard deviation of migration times related to internal standard were lower than 2%. The method thus showed good repeatability of both, qualitative and quantitative analytical parameters.

4. Conclusions

A capillary electrophoresis method with contactless conductivity detection for separation and determination of eight monosaccharides commonly found in glycoproteins was developed. The developed method was validated and limit of detections were lower than 7 mg L^{-1}, limit of quantification were lower than 22 mg L^{-1} and relative standard deviation s of peak areas and migration times related to HEPES were lower than 4%.

Acknowledgments

This work has been supported by the Czech Science Foundation, Grant No 19-18005Y and by Specific University Research (SVV260560).

References

[1] Rauter A.P., Christensen B., Somsak L., Adamo R., Kosma P.: *Recent Trends in Carbohydrate Chemistry: Biomedical and Material Science Applications*. Elsevier 2020.
[2] *Český lékopis 2017.* Praha, Grada 2017. (In Czech.)
[3] Vajaria B.N., Patel P.S.: Glycosylation: a hallmark of cancer? *Glycoconj. J.* **34** (2017), 147–156.
[4] Rodwell V.W., Bender D.A., Botham K.M., Kennelly P.J., Weil P.A.: *Harper's Illustrated Biochemistry*. McGraw-Hill 2016.
[5] Volpi N. *Capillary Electrophoresis of Carbohydrates: From Monosaccharides to Complex Polysaccharides.* Springer 2010.
[6] Hoffstetter-Kuhn S., Paulus A., Grassmann E., Widmer H.M.: Influence of borate complexation on the electrophoretic behavior of carbohydrates in CE. *Anal. Chem.* **63** (1991), 1541–1547.
[7] Solá R.J., Griebenow K.: Effects of glycosylation on the stability of protein pharmaceuticals. *J. Pharm. Sci.* **98** (2009), 1223–1245.
[8] Carvalho A.Z., da Silva J.A.F., do Lago C.L.: Determination of mono- and disaccharides by capillary electrophoresis with contactless conductivity detection. *Electrophoresis* **24** (2003), 2138–2143.
[9] Rovio S., Yli-Kauhaluoma J., Sirén H.: Determination of neutral carbohydrates by CZE with direct UV detection. *Electrophoresis* **28** (2007), 3129–3135.
[10] https://web.natur.cuni.cz/gas/peakmaster.html (accessed March. 22, 2020)

Potential of novel atomic emission techniques as a tool for investigation of the possibilities of using industrial waste as additives in construction materials

Aleksandra Anna Liczbińska*, Bartłomiej Michał Cieślik

Gdańsk University of Technology, Department of Analytical Chemistry, Faculty of Chemistry, Gabriela Narutowicza Str. 11/12, 80-233 Gdańsk, Poland ✉ *aleksandra.liczba@wp.pl*

Keywords
cold vapour – atomic absorption spectrometry
construction materials
filter ash
hearth ash
industrial waste
microwave plasma – atomic emission spectrometry

Abstract
Nowadays, due to the global ecological crisis and ways to prevent a climate disaster, more and more attention is paid to green technologies and green Chemistry, which are part of the so-called "The Green Deal." The main assumption is the optimization of the processes of producing necessary goods and the implementation of methods of managing postproduction waste in the least environmentally harmful manner. In the presented research, the alternative bricks were made in "Brickyard Plecewice" from clay with 20% addition of wastes (by mass). As additive mineral wool from "Isoroc," cellulose from "Manufacturing Pulp and Paper" in Kwidzyn, filter ash, and hearth ash from "Brickyard Plecewice" were used. During the experimental work, the leachability of heavy metals, sodium, and calcium salts was evaluated. To perform the analysis, microwave plasma atomic emission spectrometry (MP-AES) and cold vapour atomic absorption spectrometry (CV-AAS) were used. Based on the obtained results, the possibility of using bricks doped with the above-mentioned wastes in the construction sector without negative influence on the environment was evaluated.

1. Introduction

In recent years, the topics of environmental protection, sustainable development, and recycling have become increasingly popular. The maximization of using raw materials in production and minimizing the production of post-process waste is currently the most important goal of producers in every field of industry and agriculture. Increasing focus is stressed on waste from construction industry management as it is the source of the most hazardous ones. It can be a result of the development of global economies, but also construction infrastructure. One of the most hazardous wastes is ash from the incineration of various types of materials

Table 1
Summary of data on dust-slag compounds and fly ash. Own study based on Główny Urząd Statystyczny data in 2015–2020.

Year	Waste generated during the year						
	Type of waste	Total / milion t	Recovered by producer / %	Disposed / %		Transferred to other recipient / %	Waste landfilled up to now (by the end of the year / million t
				Total	Of which landfilled		
2015	Dust-slag compounds from furnace waste	12.0	0.2	87.0	87.0	11.1	285.9
	Coal fly ash	*no data*	*no data*	*no data*	*no data*	*no data*	*no data*
2016	Dust-slag compounds from furnace waste	12.0	0.6	87.4	87.4	10.8	294.1
	Coal fly ash	3.3	3.3	6.6	0.1	89.3	26.3
2017	Dust-slag compounds from furnace waste	11.4	0.9	85.9	85.9	12.2	303.6
	Coal fly ash	3.3	1.1	6.1	0.0	90.8	26.0
2018	Dust-slag compounds from furnace waste	8.2	0.1	79.1	79.1	19.8	309.6
	Coal fly ash	3.4	0.9	2.7	0.0	94.8	25.3
2019	Dust-slag compounds from furnace waste	10.6	0.2	83.4	83.4	15.3	317.3
	Coal fly ash	*no data*	*no data*	*no data*	*no data*	*no data*	*no data*
2020	Dust-slag compounds from furnace waste	9.0	0.1	82.5	82.5	14.6	338.1
	Coal fly ash	*no data*	*no data*	*no data*	*no data*	*no data*	*no data*

for energy purposes, waste mineral wool (insulation wool), and cellulose residues from chemical paper production.

The possibility of using ash as additives to ceramic products has been known for years. Fly ash is used in the production of bricks and concrete due to its beneficial properties, such as improving mechanical properties (compressive strength), reducing the amount of energy needed to produce cement, and reducing CO2 emissions to the atmosphere [1]. Industrial ash, which properties and toxicity depend on the type of charge on the furnace, and other parameters of the process can be also involved. Table 1 presents data on ash and slag mixtures from furnace waste and coal fly ash in the years 2015–2020.

The most problematic waste tested in the research is mineral wool, for which the possibilities of processing, utilization, or recycling are very limited. It is widely used in construction as an insulating material. Due to the considerable scale of production (no need for recovery), postconsumer mineral wool usually ends up in landfills, where its fibers can pose a threat to human health, life, and the environment. It is difficult to find specific information on the amount of this waste stored [2]. Due to its fire resistance, water resistance, ability to absorb sounds, and resistance to chemical and weather factors, mineral wool seems to be an excellent component for the production of bricks and other building materials.

In the case of paper pulp, which is a waste from chemical paper production, you can expect additional chemicals in the waste, for example, sodium sulfate and sodium hydroxide (Kraft process) [3]. Therefore, its use as an additive to building materials can be cumbersome or even potentially hazardous.

According to statistical data conducted in Poland by the Central Statistical Office (Główny Urząd Statystyczny), the amount of hazardous waste is increasing year by year. However, no statistics are kept on the most important issue, which is the production and landfilling of the mentioned mineral wool and cellulose. One of the main problems concerning using wastes in production building materials is heavy metals concentration, which can have a negative effect on the health of people living in buildings made of these materials. Analytical chemistry is considered a powerful tool for the investigation of problems mentioned above. Therefore, the aim of this study was to estimate the concentration of heavy metals in bricks made with the use of the above-mentioned wastes and discussing possible reduction possibilities. Microwave plasma atomic emission spectrometry (MP-AES) is considered a suitable analytical method for such evaluation. Limits of detection, which are lower than popularly used atomic absorption and emission spectrometry (AAS and AES), seem to be enough to provide the necessary data. Moreover, the possibility of using nitrogen and the lack of expensive argon as a plasma gas significantly decrease the final costs of the analysis making the decision-making process economically and ecologically justified [4].

2. Experimental

Cold vapour atomic absorption spectrometry and MP-AES were used as a tool to study the heavy metal content of the brick samples. The bricks were hand-made in the Brickyard Plecewice. Basic materials used for their production were the same like those used in the company to produce building materials. In addition to the basic version of the ceramic product, modifications were made with 20% (by mass) addition of ground mineral wool, paper pulp, filter ash, and hearth ash. The base for the bricks production (clay, sand, and water) was mixed with a stirrer. Modifications were made to the finished mass in separate signed vessels and the samples were homogenized with a mechanical stirrer. Each of the masses (clay base and four samples modified with additives: clay (I–IV), mineral wool (I–IV), paper pulp (I–IV), filter ash (I–IV), and heart ash (I–IV)) were poured into four forms each. Using the above-described method, 20 samples were obtained, which were dried at 100 °C for 12 hours and then fired at 850 °C. Before the analysis, the bricks were ground to dust with a mortar.

2.1 Samples preparation for CV-AAS

For CV-AAS analysis, weighed the ground samples in the amount of approximately 0.3 g into the measuring cuvette and started the analysis. This procedure was

made to determine the theoretical ranges of mercury concentrations in the tested samples. Then appropriate calibration curves were prepared using the stock solution and the data were used to calculate limit of detection and limit of quantitation. The Hg concentration in the manufactured bricks was measured again with at least 3–8 repetitions.

2.2 Samples preparation for MP-AES

To determine heavy metals with MP-AES, namely Cd, Co, Cr, Cu, Fe, Mo, Mn, Ni, Se, Sr, and Zn, 0.3g of samples was weighed and subjected to mineralization. The mineralizing solution was prepared with 2 mL of HNO_3 and 6 mL of HCl. In the case of samples containing mineral wool, it was necessary to optimize the procedure by adding 2 mL of perhydrol to the mentioned solution. The pre-mineralization was carried out for 10 minutes at 120 °C, while the main stage was performed for 45 minutes at 200 °C. In the case of mineral wool, the optimization of the process was as follows: the pre-mineralization was carried for 20 minutes and the main stage for one hour.

As with the MP-AES analysis, preliminary analysis of the samples was performed to determine the approximate concentrations of heavy metals and the most optimal wavelengths for elements. Then, calibration solutions of the above-mentioned metals were made and calibration was performed. Fourfold and hundredfold dilutions of the samples were also performed. The concentrations of heavy metals in the manufactured bricks were measured again and the most optimal wavelengths were selected.

3. Results and discussion

After processing the results of the CV-AAS analysis, it was necessary to repeat some tests, especially those containing an admixture of filter ash and furnace ash. To determine the mercury in these samples weighed smaller amounts of ground brick.

In the case of MP-ASE analysis, for optimization purposes, it was necessary to perform four-fold and one-hundred-fold dilutions of the samples due to a large amount of iron and the selection of the appropriate wavelength so that it would not interfere with the determination of other elements.

In other cases, for some components, it was necessary to lower the limit of quantification due to very low concentrations. For this purpose, new calibration solutions with lower concentrations were prepared, but it turned out that it was impossible to determine arsenic and selenium at such low concentration levels, and in most cases also cadmium and molybdenum. In a few samples (wool I, wool II, wool IV, wool) the concentration of lead was below the quantification limit. Detailed data on the calibration parameters are presented in Table 2. The results of the determinations are presented in Fig. 1 and 2. Samples from individual batches were averaged.

Table 2
Summary of microwave plasma atomic emission spectrometry calibration, where *x* is concentration [mg L^{-1}] and *y* is intensity.

Element	λ /nm	Calibration equation	*R*	*LOD* / mg kg^{-1}	*LOQ* / mg kg^{-1}
As	234.984	Unable to determine for such low concentrations			
Cd	228.802	$y = 17615.746\,x - 18.099$	0.99997	0.540	1.799
Co	345.351	$y = 10083.885\,x + 335.486$	0.99836	3.381	11.187
Cr	425.433	$y = 18822.049\,x + 150.732$	0.99948	3.777	12.410
Cu	578.213	$y = 282.031\,x + 0.981$	0.99635	0.791	2.626
Fe	371.993	$y = 5936.797\,x - 563.664$	0.99973	3.058	10.072
Mn	403.076	$y = 29189.802\,x - 424.658$	0.99912	0.169	1.094
Mo	379.825	$y = 14866.931\,x - 57.253$	0.99992	0.353	1.158
Ni	361.939	$y = 5863.986\,x + 1401.584$	0.99993	0.410	1.367
Pb	405.781	$y = 1795.594\,x + 72.314$	0.99605	5.576	18.381
Se	196.026	Unable to determine for such low concentrations			
Sr	407.771	$y = 174292.817\,x + 3962.363$	0.99979	1.007	3.237
Zn	213.857	$y = 10521.931\,x + 886.355$	0.99754	0.791	2.626

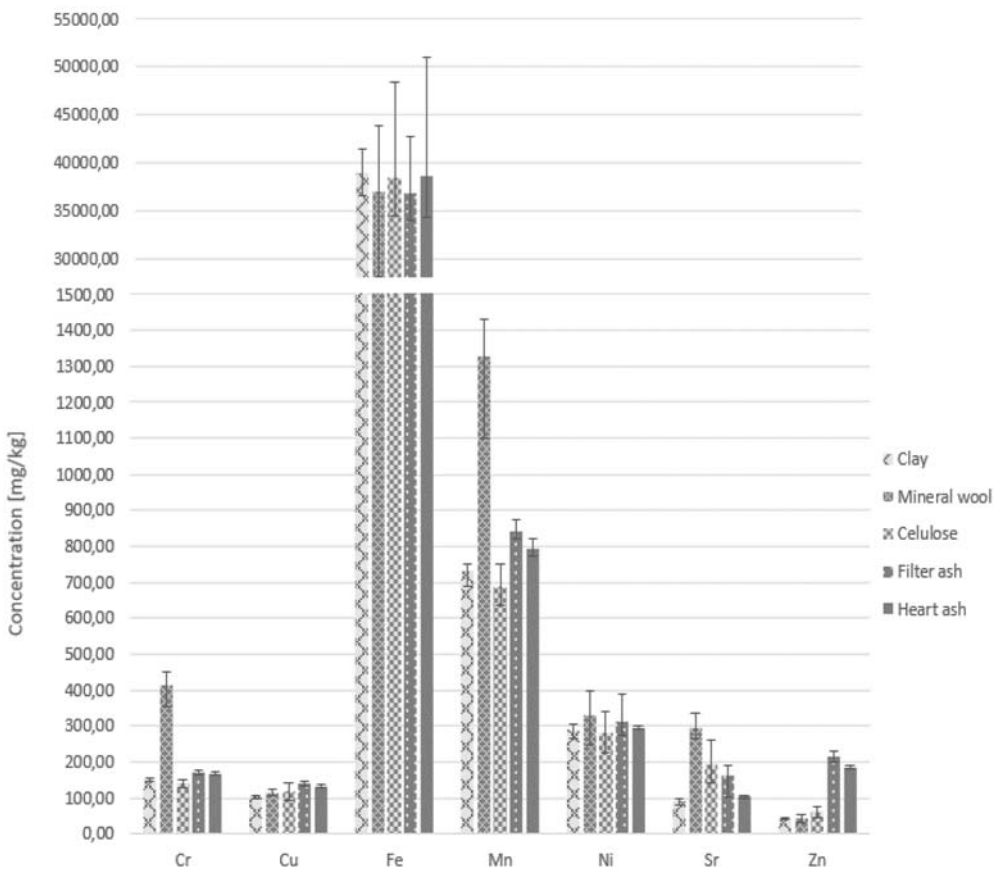

Fig. 1 Obtained results of concentrations of heavy metals for high values.

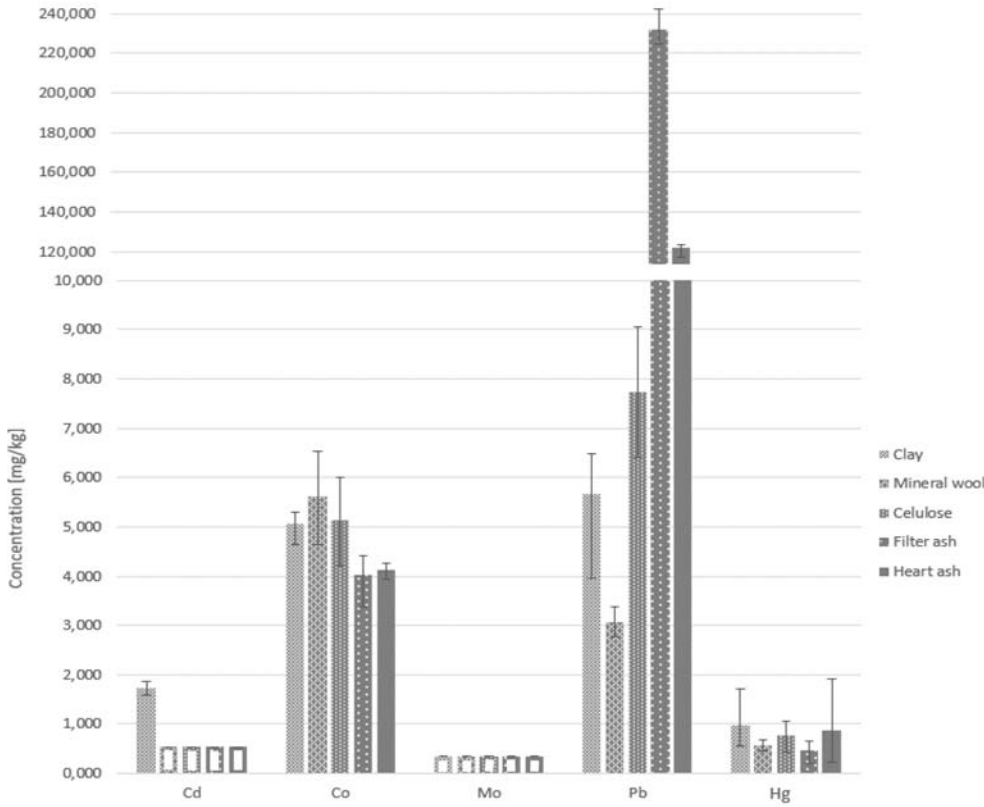

Fig. 2 Obtained results of concentrations of heavy metals for low values. Unfilled bars (Cd and Mo) show the concentration values below the limit of detection.

4. Conclusions

New atomic emission techniques are suitable tools to investigate the feasibility of using industrial waste as additives to building materials. On the basis of the obtained results, it was found that both CV-AAS and MP-AES can be used for the analysis of both very low and very high concentrations of heavy metals or other elements. Appropriate optimization was carried out, starting from the appropriate mineralizing solution and the conditions of the mineralization, by selecting the appropriate wavelength for the given elements depending on the theoretical content of metals in the sample to the parameters of the analysis. The detection limit and the quantification limit were lowered for a more precise analysis of heavy metals. Most of them were at very low concentration levels or were so low that they could not be determined. It is especially important because of the harmful influence of heavy metals on the health and life of living organisms. The use of construction or industrial waste as components of bricks may be a new way

of management and recycling without negative environmental impact, which can be proven with the use of modern analytical chemistry.

References

[1] Rutkowska G., Wichowski P., Franus M., Mendryk M., Fronczyk J.: Modification of ordinary concrete using fly ash from combustion of municipal sewage sludge. *Materials* **13** (2020), 487.

[2] Nowak D., Jasiewicz C., Szczerbińska-Byrska M.: Środowiskowe aspekty użytkowania, zagospodarowania i unieszkodliwiania wełny mineralnej w kontekście retardacji zanieczyszczania zasobów środowiska przez odpady. *Inżynieria ekologiczna* **34** (2013), 198–205. (In Polish.)

[3] Ahmad E., Pant K.K.: Lignin conversion: a key to the concept of lignocellulosic biomass-based integrated biorefinery. In: *Waste Biorefinery: Potential and Perspectives.* T. Bhaskar, A. Pandey, S.V. Mohan, D.J. Lee, S.K. Khanal (eds.). Elsevier 2008, p. 409–444.

[4] Balarm V.: Microwave plasma atomic emission spectrometry (MP-AES) and its applications: A critical review. *Microchem. J.* **159** (2020), 105483.

Solid-phase microextraction – a new green trend for analysis of psychotropic drugs

Magdalena Świądro[a,*], Weronika Wojciechowska[a], Klaudia Ordon[a], Dominika Dudek [b], Renata Wietecha-Posłuszny[a]

[a] *Jagiellonian University in Krakow, Faculty of Chemistry, Department of Analytical Chemistry, Gronostajowa 2, 30-387 Krakow, Poland* ✉ *magda.swiadro@doctoral.uj.edu.pl*
[b] *Jagiellonian University Medical College in Krakow, Department of Affective Disorders, Kopernika 21A, 31-501 Krakow, Poland*

Keywords
mood disorder
psychotropic drugs
solid-phase microextraction
UHPLC-MS

Abstract
The aim of this study was to verify a novel and quite popular nowadays technique called solid-phase microextraction for the isolation of psychotropic drugs from human blood. In the research, drugs from the selective serotonin reuptake inhibitor group such as citalopram, fluoxetine, fluvoxamine, paroxetine, and sertraline were used. In the first stage, the possibility of isolating drugs from blood was checked. Subse-quently, the proposed method was used for qualitative analysis of selected samples of patients with mood disorders treated with applied drugs. Each obtained extract was analyzed using ultra-efficient liquid chromatography with mass spectrometry. The conducted research indicated that solid-phase microextraction is a very promising technique enabling the reliable determination of psychotropic drugs for clinical purposes.

1. Introduction

Solid-phase microextraction (SPME) is one of the most popular extraction methods, developed in 1990 by Arthur and Pawliszyn [1]. It enables the extraction of xenobiotics from various biological materials and is a greener alternative to traditional methods of their isolation. Stationary phase microextraction involves the use of a thin glass or quartz fiber covered with a stationary phase, capable of extracting various types of analytes, which may be in the solid, liquid, and gas phases. The extraction process is based on the adsorption of analytes from the matrix and their subsequent desorption [1, 2].

The most frequently emphasized advantages of the SPME method are its simplified procedure, short extraction time of analytes, and the availability of fibers of different polarities. What is more, the SPME method significantly reduces, and in some cases even completely eliminates the need to use organic solvents. For this reason, the SPME method is classified as environmentally

friendly. Moreover, the miniaturization of the extraction kit has also reduced the amount of sample required for the analysis. Moreover, the proposed extraction technique enables the analysis of materials occurring in various states of aggregation: both liquid samples, normally subjected to extraction, as well as gaseous and solid samples [3, 4].

Another advantage of the SPME method is the possibility of combining it with instrumental techniques, including gas or liquid chromatography. Selective extraction of analytes from a complex matrix allows for the introduction of small amounts of sample into the chromatography column, which reduces the likelihood of clogging, and also facilitates the subsequent analysis of the results [4, 5]. Taking into account all the advantages of this method, the purpose of this research was to check the effectiveness of using the SPME procedure for the qualitative analysis of antidepressants such as citalopram, fluoxetine, fluvoxamine, paroxetine, sertraline in a group of patients with a mood disorder. These are drugs from the group selective serotonin reuptake inhibitors applied as first-line antidepressants in treatment [6].

2. Experimental

2.1 Reagents and chemicals

Drug standard solutions in the concentration of 1 mg mL^{-1}: citalopram, fluoxetine, fluvoxamine, paroxetine, sertraline, and their deuterated analogues: fluoxetine-d_6 and paroxetine-d_6 in the concentration 1 mg mL^{-1}, were purchased from Lipomed AG (Switzerland). Each solution was stored in methyl alcohol in the freezer at –20 °C. The whole blood applied in research was provided by the local blood bank (Krakow, Poland). Blood samples from patients who were taking one of the analysed drugs were provided by the Department of Adult Psychiatry at the Jagiellonian University Medical College (in accordance with Bioethical Commission Approval no. 1072.6120.302.2018). The whole blood samples were collected from patients treated with selective serotonin reuptake inhibitors drugs. The patients (case #I, case #III–case#V, and case #IX and case #X) were treated with drugs containing 50 mg sertraline. Case #II and case #VII were treated with drugs including 10 mg fluoxetine. For citalopram it was only in case #IV (10 mg), and paroxetine in case #VIII (20 mg). Each patient suffered from a mood disorder: bipolar disorder or depression.

The other chemicals used throughout the experiments: acetic acid, ethyl acetate, and sodium hydroxide, were purchased from Sigma-Aldrich (USA). Acetonitrile and methyl alcohol were supplied by Fluka Analytical (Germany), and also analytical grade formic acid was purchased from Merck (Germany). Ultrapure water (18.2 MΩ cm, < 3 ppb TOC) used to prepare all aqueous solutions was generated with the Milli-Q system by Merck-Millipore (Germany).

2.2 Instrumentation

The SPME experiment was conducted using commercially available C-18 SPME-LC silica fibers (Supelco), coating thickness: 45 μm and length of the fiber coverage: 1.3 mm, supplied by Merck (Germany). The following devices from VWR (Randor, USA) were also utilized: HPLC vials (1.5 mL), inserts (200 μL), Thermal Shake Touch, and Digital Vortex Mixer. Concentrator plus was purchased from Eppendorf AG (Germany). Adjustable manual pipettes were supplied by Sartorius AG (Germany).

The measurements were carried out using UltiMate 3000 RS liquid chromatography system (Dionex, USA) coupled to a mass spectrometer MicrOTOF-Q II with a time of flight mass analyzer (Bruker, Germany). The mobile phase consisted of 0.1% formic acid (A) and acetonitrile (B). The following gradient programme (B) at the flow rate of 0.3 mL min^{-1} was used: 0 min – 15%; 4 min – 40%; 7 min – 40%; 10 min – 70%, 12.5 min – 15%; 17 min – 15%. Separation was carried out in a Hypersil Gold Phenyl column (50×2.1 mm I.D., particles 1.9 μm, injection: 5 μL, Dionex) at 35 °C. The ESI ion source conditions were as follows: nebulizer pressure: 2.5 bar, dry gas: 5.5 L min^{-1} heated to 200 °C. Identification of particular substances was performed on the basis of the intensity of the received signals in the range covering the $[M+H]^+$ values of target analytes (ca. 237–337 *m/z*) and their retention times. Cluster mass calibration was performed using a mixture of 10 mM sodium formate and isopropanol before each run.

2.3 Sample preparation

The solid-phase microextraction (SPME) procedure consists of two main steps: adsorption and desorption. Before proceeding to the proper part of the process, it is necessary to perform fiber conditioning. For this, special C18 SPME LC fiber was used, which was conditioned according to the manufacturer's suggestion, using a mixture of methanol:water (1:1, *v/v*). The fibers were placed in vials containing 1.5 mL of said conditioning solution, and then the whole was shaken at 2200 rpm, at room temperature for 45 minutes. In the next step, fibers were transferred to 1.5 mL vials with inserts containing 200 μL of biological material (in this case, it was whole blood). Adsorption was carried out at room temperature for 60 min with a stirring speed of 2200 rpm. After the absorption process, the fibers were wiped with dust-free wipes and then washed with ultrapure water for 5 seconds using a Vortex shaker. Thus, matrix elements embedded on the surface of the fiber were removed. Next, the fibers thus cleaned were subjected to a desorption process. They were placed in 1.5 mL vials containing inserts with 200 μL acetonitrile: methanol: 0.1% formic acid solution (2:2:1, *v/v/v*) and shaken at 2200 rpm. at room temperature for 30 min. The solutions obtained in this way were evaporated by means of a vacuum evaporator for 50 min at a temperature of 45 °C. Prior to LC-MS analysis, 50 μL of mobile phase (0.1% formic acid solution) was added.

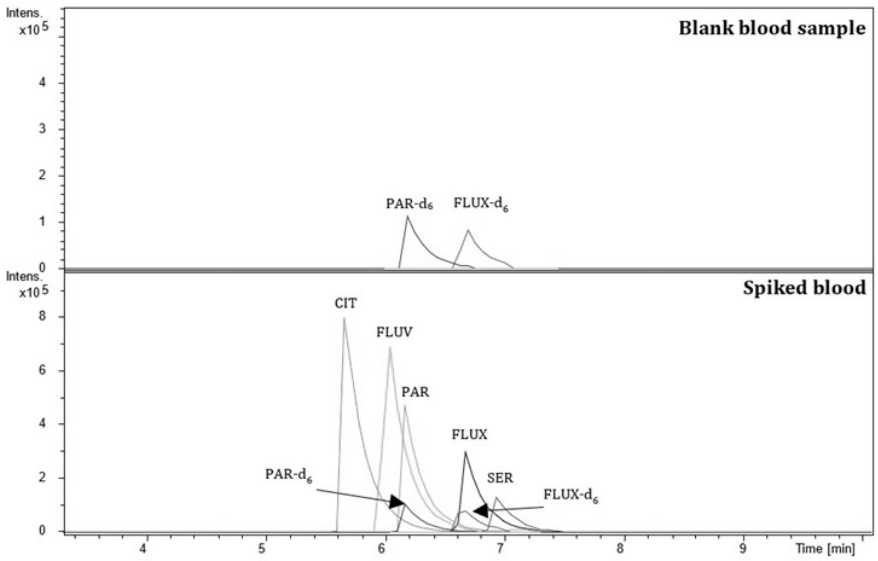

Fig. 1 Chromatogram for a blank blood sample and for mixture contained citalopram (CIT), fluoxetine (FLUX), fluvoxamine (FLUV), paroxetine (PAR), sertraline (SER), and their deuterated analogues paroxetine-d_6 (PAR-d_6) and fluoxetine-d6 (FLUX-d_6). Each drug has a concentration of 250 ng mL^{-1}.

Table 1
Masses $[M+H]^+$ of tested analytes and assigned deuterated standards alongside retention times (t_R) obtained as a result of separation.

Drug	$[M+H]^+$	t_R /min	Deuterated analogue	$[M+H]^+$	t_R /min
Citalopram	325.1722 ± 0.01	5.68 ± 0.02	Paroxetine-d_6	336.1877 ± 0.01	6.16 ± 0.02
Fluoxetine	310.1413 ± 0.01	6.67 ± 0.02	Fluoxetine-d_6	316.1789 ± 0.01	6.65 ± 0.02
Fluvoxamine	319.1621 ± 0.01	6.04 ± 0.02	Fluoxetine-d_6	316.1789 ± 0.01	6.65 ± 0.02
Paroxetine	330.1494 ± 0.01	6.18 ± 0.03	Paroxetine-d_6	336.1877 ± 0.01	6.16 ± 0.02
Sertraline	306.0807 ± 0.01	6.93 ± 0.02	Fluoxetine-d_6	316.1789 ± 0.01	6.65 ± 0.02

3. Results and discussion

The research was divided into two parts. In the first step, the mixture of internal standards and drug standards solution was subjected to the SPME extraction procedure in order to evaluate the effectiveness of the proposed methodology. As can be seen in Fig. 1. And Table 1, it is possible to identify all analysed drugs based on differences in their retention times. All compounds are separated from each other. They are also characterized by well shape and symmetry which is important from the qualitative analysis point of view. For this reason, in the second step, the proposed SPME technique was used to analyze the qualitative analysis of

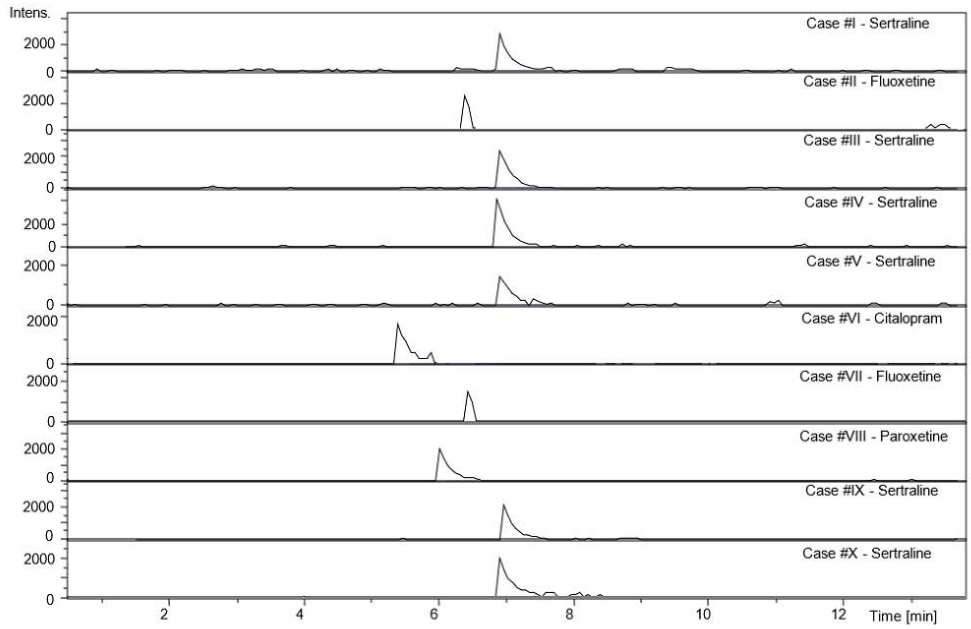

Fig. 2 Chromatogram obtained for analysed case#I–case#X samples.

intravenous blood collected from ten patients with mood disorders. It can be observed (Fig. 2). In each of these cases, it is drugs that actual patients use during therapy that have been identified. Therefore, the obtained results confirm the effectiveness of using SPME extraction as a necessary and very promising element of sample preparation in therapeutic drug monitoring.

4. Conclusions

The solid-phase microextraction is an easy and fast technique for isolating antidepressants from whole blood. Moreover, it is an excellent methodology for the qualitative analysis of drugs such as citalopram, fluoxetine, fluvoxamine, sertraline, and paroxetine. in the blood from patients with mood disorders. The proposed research is a good preliminary experiment and it may prove to be a useful contribution to therapeutic drug monitoring or in forensic and toxicology analysis. In the future, it could be modified for isolation and identification of all antidepressants used to treat mood disorders.

Acknowledgments

Magdalena Świądro acknowledges the support of InterDokMed project no. POWR.03.02.00-00-I013/16. The research was carried out with equipment purchased thanks to the financial support of the European Regional Development Fund within the framework of the Polish Innovation Economy Operational Program (contract no. POIG.02.01.00-12-023/08).

References

[1] Arthur C.L., Pawliszyn J.: Solid phase microextraction with thermal desorption using fused silica optical fibers. *Anal. Chem.* **62** (1990), 2145–2148.
[2] Boyaci E., Rodríguez-Lafuente Á., Gorynski K., Mirnaghi F., Souza-Silva É.A., Hein D., Pawliszyn J.: Sample preparation with solid phase microextraction and exhaustive extraction approaches: Comparison for challenging cases. *Anal. Chim. Acta* **873** (2015), 14–30.
[3] Majda A., Mrochem K., Wietecha-Posłuszny R., Zapotoczny Sz., Zawadzki M.: Fast and efficient analyses of the post-mortem human blood and bone marrow using DI-SPME/LC-TOFMS method for forensic medicine purposes. *Talanta* **209** (2020), 120533.
[4] Lord H., Bojko B.: Drug analysis by SPME. In: *Handbook of Solid Phase Microextraction*. J. Pawliszyn (ed.). Springer 2012, p. 335–382.
[5] Spietelun A., Marcinkowski Ł., de la Guardia M., Namieśnik J.: Recent developments and future trends in solid phase microextraction techniques towards green analytical chemistry. *J. Chromatogr. A* **321** (2013), 1–13.
[6] Świądro M., Wietecha-Posłuszny R., Dudek D.: Effective extraction methodology for the isolation of antidepressants from human blood. *Monatsh. Chem.* **151** (2020), 1225–1230.

FTIR/ATR technique in the analysis of divinylbenzene-silica composite

Alicja Bosacka[a,*], Anna Deryło-Marczewska[a], Beata Podkoscielna[b]

[a] *Maria Curie-Sklodowska University, Institute of Chemical Sciences, Department of Physical Chemistry, Maria Curie-Sklodowska Sq. 3, 20-031 Lublin, Poland*
✉ *alicja.bosacka@poczta.umcs.lublin.pl*
[b] *Maria Curie-Sklodowska University, Institute of Chemical Sciences, Department of Polymer Chemistry, Gliniana Street 33, 20-614 Lublin*

Keywords
ATR
FTIR
polymer, silica
SBA-15

Abstract
This work is focused on the Fourier transform infrared-attenuated total reflection (FTIR-ATR) spectroscopy, which could be a valuable tool for studying complex materials. In the introduction, the general characteristic of FTIR-ATR spectroscopy is presented with an indication of the applicability of this technique in the study of materials with a complex structure. In the following, material preparation is described and the FTIR-ATR results are presented and discussed. The main aim of the FTIR-ATR investigations was to assess the phases binding effectiveness of the divinylbenzene-silica material (DVB-SBA-15).

1. Introduction

The presented work is focused on a particular type of IR spectroscopy: Fourier-transform infrared spectroscopy (FTIR) combined with attenuated total reflectance (ATR) attachment. The infrared spectroscopy is a vibrational technique used to characterize the material at the molecular level where electrical dipole moments of vibrating functional groups undertake transition due to the absorption of infrared light. The spectral range of IR radiation is from 760 nm to 0.5 mm. The electromagnetic radiation is absorbed by molecules in the IR region, therefore, the IR spectrum shows characteristic bands in terms of intensity and position from individual groups and it is possible to identify the compound. The IR spectrum identification can be performed by comparing the experimental spectrum with the spectrum library or by assigning functional groups using correlation tables [1–3].

Fourier transform infrared spectroscopy (FTIR) is a technique widely used to identify the structure of chemical compounds from the infrared spectrum and using a mathematical operation: the Fourier transform. The FTIR spectrometer equipped with a polychromatic light source collects high-resolution spectral data

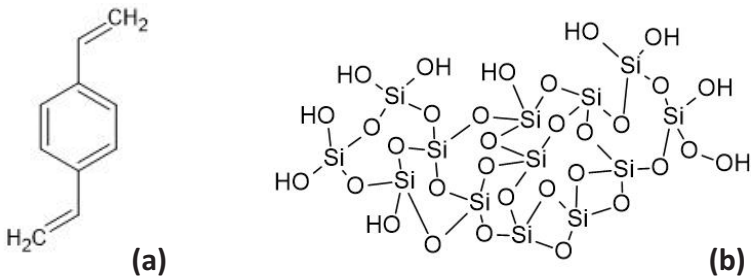

Fig. 1 The structures of organic-inorganic material components: (a) 1,4-divinylbenzene, and (b) silica.

over a wide spectral range at the same time in comparison to other monochromatic spectrometers in which spectrum is recorded in a narrow spectral range [4–5].

The attenuated total reflection (ATR) technique is commonly used in conjunction with FTIR. The total internal reflection is a physical phenomenon that occurs for waves and existing at the boundary of media with different refractive indexes. In the ATR technique the infrared beam is directed at an optically dense crystal with a high refractive index (zinc selenide, zinc sulfide, germanium, silicon, or diamond). In the regions of the infrared spectrum where the sample absorbs energy, the decaying wave is weakened or changed. The attenuated energy from each vanishing wave is transferred back to the infrared beam, which then comes out from the opposite end of the crystal and is moved to the detector. In this way, the system generates an infrared spectrum [6–7].

The FTIR-ATR technique can be applied to solids and liquids. It is a non-destructive technique and often no sample preparation is even required. In the FTIR-ATR technique, it is possible to register the spectrum in a greater frequency range than in classical transmission spectroscopy due to the lack of restrictions resulting from the absorption of the cuvette walls. The limitations of the FTIR-ATR technique include a small penetration depth into the sample (<5 μm), which depends on various factors: the wavelength of the light, the angle of incidence, or the refractive indexes of the ATR crystal and the tested medium. Moreover, the sample should adhere closely to the crystal and correction is necessary to avoid deformation of the bands [6]. Despite some restrictions of FTIR-ATR spectroscopy, a precisely conducted measurement allows obtaining the data on the structure of even the compounds with complex structures (polymers, proteins, pharmaceuticals, or multiphase materials) in a short time. The FTIR-ATR analysis can be used to evaluate the synthesis effectiveness of multi-component materials [8–10].

In this work, the polymeric-silica material (DVB-SBA-15) was obtained in the suspension polymerization reaction. The structure of divinylbenzene (DVB) and silica used as components are presented in Fig. 1. The SBA-15, DVB-SBA-15

material, and DVB-SBA-15 material after etching was subjected to FTIR-ATR studies to assess the effectiveness of polymer and silica phases bonding of DVB-SBA-15 material.

2. Experimental

2.1 Reagents, chemicals

Pluronic P123 (triblock copolymer: poly(ethylene oxide)-poly(propylene oxide)-poly(ethylene oxide), $EO_{20}PO_{70}EO_{20}$, M_r = 5800) and tetraethyl orthosilicate ($Si(OC_2H_5)_4$, TEOS, 98%) were purchased from Merck (Germany). Hydrochloric acid (35–38%) and sodium hydroxide (powder) were acquired from Chempur (Poland). Divinylbenzene (DVB) (62.2% of 1,4-divinylbenzene, 0.2% of 1,2-divinylbenzene and ethylvinylbenzene) and α,α^t-azoiso-bis-butyronitrile (AIBN) initiatior were bought from Merck (Germany). Pore forming diluents: decan-1-ol and poly(vinyl alcohol) (PVA) were purchased from Fluka AG (Switzerland). Acetone and toluene were acquired from Avantor Performance Materials Poland S.A. (Gliwice, Poland). Solutions were prepared with the usage of deionized water.

2.2 Materials preparation

Ordered mesoporous silica material (SBA-15) was obtained based on the procedure proposed by Zhao et al. [11]. Pluronic P123 (triblock copolymer) with a mass of 12 g was dissolved in a solution of 360 mL of HCl (2 mol L^{-1}) with 90 mL of deionized water was placed in the system consisting of 200 mL Erlenmeyer flask, stirrer (220 rpm), and thermostat (35 °C). In the second step, 27.4 mL of TEOS was added dropwise, and the mixture was constantly stirred (220 rpm, 35 °C) for 24 hours. In the third stage, the solution with precipitate was transferred to an autoclave and heated at 85 °C for 48 hours. After that, the precipitate was filtered, washed with deionized water, dried under vacuum, and calcined at 550 °C for 4 hours in a muffle furnace.

Divinylbenzene-silica (DVB-SBA-15) material was synthesized by a suspension polymerization reaction. For this purpose, 1 g of poly(vinyl alcohol) was dissolved in 75 mL of deionized water and transferred to the reaction vessel equipped with three-necked flask connected with a mechanical stirrer, thermometer, and air cooler. The solution of PVA was stirred for one hour at 80 °C. Then, the SBA-15 material, AIBN initiator (1 wt%), and the toluene and 1-decanol mixture taken in proportions 1/1 (*v/v*) were added to the reaction vessel. The molar phase ratio of DVB and SBA-15 was 1/1. The content of the reaction vessel was stirred at for 12 hours at 85 °C (210 rpm). The obtained materials were washed with at least 2 L of deionized water, filtered, dried, and extracted in a Soxhlet apparatus with boiling acetone for 3 hours.

For the removal of the etching method was used. For this target, the mixture of 5 g DVB-SBA-15 material with 25 mL acetone was placed in a 250 mL two-necked

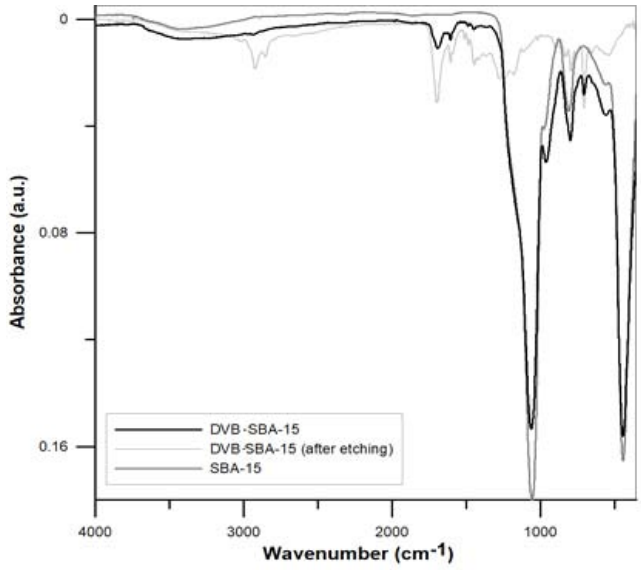

Fig. 2 FTIR-ATR spectra of SBA-15, DVB-SBA-15 and DVB-SBA-15 after etching.

bottom flask connected with a magnetic stirrer and thermometer. The mixture was stirred for 2 h at 25 °C. After 2 hours of stirring, the acetone was removed and 150 mL of 0.9 mol L^{-1} NaOH aqueous solution was added. The content of the reaction vessel was stirred for 1 h at 25 °C and next for 4 h at 100 °C and again for 15 h at 25 °C. Next, the material was filtered off and moved to a 500 mL glass beaker and 1.5 mol L^{-1} HCl aqueous solution was added. Finally, the mixture was filtered and dried [12].

2.3 Instrumentation

Fourier transformed infrared-attenuated total reflection (FTIR-ATR) analysis was carried out on IR spectrometer TENSOR 27 (Brucker, Germany) equipped with a diamond crystal. The spectra were recorded in the mid-infrared spectral range (400–4000 cm^{-1}). Prior to measurement, previously dried at 90 °C for 3 hours, the solid sample was placed in the sample stand.

3. Results and discussion

In order to evaluate the efficiency of the synthesized organic-inorganic material, the FTIR-ATR spectra of SBA-15 material, DVB-SBA-15 material, and DVB residue after SBA-15 etching are compared in Fig. 2. The FTIR-ATR positions of characteristic bands of studied materials are presented in Table 1. The bands at ~1060, 810, and 450 cm^{-1} correspond to the stretching and bending vibrations of Si-O-Si group and are observed for both SBA-15, and DVB-SBA-15 materials. Moreover,

Table 1
The peak positions of characteristic bands of the studied samples.

Sample name	Peak position (wavenumber) / cm^{-1}							
	Si-O-H		Si-O-Si			C-H		C=C
SBA-15	3416	966	1063	810	447	–	–	–
DVB-SBA-15	3413	964	1061	808	446	2935	700	1696
DVB-SBA-15 (after etching)	–	–	–	–	–	2928	695	1701

for SBA-15 and DVB-SBA-15 samples, the bands in the range of 3800–2900 cm^{-1} and at ~970 cm^{-1} indicate the occurrence of Si-OH vibrations. All these bands are not visible on the DVB residual spectrum.

For the residue of DVB after SBA-15 etching, as well as for DVB-SBA-15 material, the bands visible in the range of 2900–2800 cm^{-1} and 700 cm^{-1} are related to stretching and bending vibrations of the C-H groups. In both samples, the peak at ~1690 cm^{-1} is associated with the stretching vibration of vinyl group. The bands from the C–H and C=C groups are not present on the SBA-15 spectrum.
In general, characteristic bands of DVB and SBA-15 phases are indicated in DVB-SBA-15 material. The introduction of the silica component to the divinylbenzene weakens the intensity of bands particularly the CH (2928 cm^{-1}) and also other groups of DVB phase. It confirms the high efficiency of DVB and SBA-15 phases bonding. The FTIR-ATR investigations confirm the successful incorporation of the silica into the polymeric body.

4. Conclusions

In this work, the Fourier-transform infrared-attenuated total reflection (FTIR-ATR) spectroscopy was used to assess the dispersion efficiency of phases of the synthesized polymeric-silica material. Generally, the high efficiency of binding of SBA-15 and DVB phases in SBA-15-DVB material was confirmed. Beyond, the characteristic bands of the studied samples visible in the spectra were assigned. The presented results confirmed that FTIR-ATR is a valuable technique in the study of organic-inorganic materials. Using the FTIR-ATR technique, it is possible to evaluate the phase-bonding effectiveness of multi-component materials.

References

[1] Guerrero-Pérez M.O., Patience G.S.: Experimental methods in chemical engineering: Fourier transform infrared spectroscopy—FTIR. *Can. J. Chem. Eng.* **98** (2020), 25–33.
[2] Wendi B., Droschl H., Kern W.A.: A comparative study of polymerization lamps to determine the degree of cure of composites using infrared spectroscopy. *Eur. J. Orthod.* **26** (2004), 545–551.
[3] Lee L.C., Liong C.Y., Jemain A.A.: A contemporary review on Data Preprocessing (DP) practice strategy in ATR-FTIR spectrum. *Chemom. Intell. Lab. Syst.* **163** (2017), 64–75.

[4] Petit T., Puskar L.: A FTIR spectroscopy of nanodiamonds: Methods and interpretation. *Diam. Relat. Mater.* **89** (2018), 52–66.
[5] Herres W., Gronholtz J.: Understanding FT-IR data processing. Part 1: Data acquisition and Fourier transformation. *Comput. Appl. Lab.* **2** (1984), 1–23.
[6] Hind A.R., Bhargava S.K., McKinnon A.: At the solid/liquid interface: FTIR/ATR - The tool of choice. *Adv. Colloid Interface. Sci.* **93** (2001), 91–114.
[7] Tinti A., Tugnoli V., Bonora S., Francioso O.: Recent applications of vibrational mid-infrared (IR) spectroscopy for studying soil components. A review. *J. Cent. Eur. Agric.* **16** (2015), 1–22.
[8] Kar S., Kaur T., Thirugnanam A.: Microwave-assisted synthesis of porous chitosan-modified montmorillonite-hydroxyapatite composite scaffolds. *Int. J. Biol. Macromol.* **82** (2016), 628–636.
[9] Raut I., Calin M., Vuluga Z.: Comparative study on the behavior of virgin and recycled polyolefins–cellulose composites in natural environmental conditions. *J. Compos. Sci.* **3** (2019), 60.
[10] Varlec A., Eršte A., Bobnar V., Remškar M.: Influence of preparation conditions on structural and dielectric properties of PVDF–MoS2 nanotubes composite films. *J. Polym. Res.* **23** (2016), 1–7.
[11] Zhao D., Feng J., Huo Q.: Triblock copolymer syntheses of mesoporous silica with periodic 50 to 300 angstrom pores. *Science* **279** (1998), 548–552.
[12] Podkościelna B., Sobiesiak M.: Synthesis and characterization of organic–inorganic hybrid microspheres. *Adsorption* **22** (2016), 631–638.

New effective method of extraction of "date-rape drugs" from blood samples

Paweł Stelmaszczyk*, Ewa Gacek, Renata Wietecha-Posłuszny

Jagiellonian University, Faculty of Chemistry, Department of Analytical Chemistry, Gronostajowa 2, 30-387 Cracow, Poland ✉ pawel.stelmaszczyk@doctoral.uj.edu.pl

Keywords
date rape drugs
dried blood spots
microwave assisted extraction

Abstract
The dry blood spot method allows the sampling of a small volume of blood in a simple and micro-invasive way and ensures the stability of the analytes in the sample placed on dry blood spot cards. The analysis of blood samples collected on dry blood spot cards requires the development of an effective extraction process of analytes from the sample matrix. The technique that could be very useful to increase the extraction efficiency of a wide range of substances is microwave assisted extraction technique. Optimization of the parameters of the microwave assisted extraction, such as microwave power, extraction time and temperature enable the development of a process of simultaneous isolation of substances with different structures and properties. The aim of the research was to develop a method of extracting selected substances from the "date-rape drugs" group from whole blood samples collected using the dry blood spot method based on the microwave assisted extraction technique.

1. Introduction

The group of "date-rape drugs" includes chemicals that are used by perpetrators of drug-facilitated sexual assault crimes. The typical action of most of these substances is to reduce the activity of the central nervous system and lead to loss of consciousness and memory. Substances with such an action are γ-hydroxybutanoic acid, ketamine, and flunitrazepam. These three substances are reported in the literature as typical examples of substances present in so-called "rape pills". In addition, these substances exhibit properties desired by the perpetrators: they do not have a specific taste and smell, are easily soluble in alcohol (which facilitates their secret administration e.g., in a drink) and they are quickly absorbed after oral administration and quickly cleared from the body. Other substances classified as "date-rape drugs" are other benzodiazepine derivatives, barbiturates, antidepressants. Mentioned substances reduce the activity of the central nervous system but also substances which stimulate the central nervous system are used by perpetrators, e.g., amphetamine-type stimulants (amphe-

tamine, methamphetamine, 3,4-methylenedioxymethamphetamine, mephedrone), cocaine [1].

The dry blood spot method allows the sampling of a small volume of blood in a simple and micro-invasive way from the fingertip or heel (in the case of newborns). The finger is lanced and then a drop of blood with a volume of up to 50 µL is applied to special dry blood spot cards. The surface of dry blood spot cards can be modified depending on the needs of the analysis. The application of blood to the card can be done by directly putting drops on the card or by using an appropriate capillary pipette. The dry blood spot method has many advantages such as: 1) easy to collect a blood sample, even without much training as in the case of traditional blood sampling, 2) a drop of blood properly dried ensures the stability of many substances at room temperature, 3) the storage of such collected samples is much easier because the sample does not require storage at low temperatures [2]. Due to the mentioned advantages, this method could be used to quickly secure a blood sample of a rape victim at the scene. The small amount of sample requires the development of effective methods of extracting analytes from dried dry blood spot cards. Microwave assisted extraction is an extraction that enables the isolation of many substances with a high extraction efficiency [3, 4].

2. Experimental

2.1 Reagents and chemicals

Drug standards of ketamine, flunitrazepam, diazepam, temazepam, nitrazepam, lorazepam, cocaine, norcocaine, cocatylene, and their deuterated analogues (flunitrazepam-d_3, diazepam-d_5, temazepam-d_5, nitrazepam-d_5, lorazepam-d_4) at a concentration of 1 mg mL^{-1} were used (Lipomed AG, Switzerland). Standard drug stock solutions (500 ng mL^{-1}) prepared in methanol were stored in a freezer at −20 °C. During the experiments the following reagents were used: ethyl acetate, 30% sodium hydroxide water solution (Merck, Germany), *n*-hexane, methanol, acetonitrile, trihydroxyaminomethane, formic acid, sodium hydrogen phosphate, sodium dihydrogen phosphate, sodium tetraborate, chloride ammonium, 28–30% ammonium water solution (Sigma-Aldrich, USA), 35–38% hydrochloric acid (POCH, Poland), isoamyl alcohol (Chempur, Poland), technical nitrogen with 90–99% purity (Air Products, Poland), and ultrapure water (18.2 MΩ cm, less than 3 ppb TOC) generated with the Milli-Q system by Merck-Millipore (Germany), which was used to prepare all aqueous solutions. Whatman FTA DMPK C cards (not chemically impregnated) were used and 6-mm discs were cut out using a Harris Uni-Core puncher (Sigma-Aldrich, USA). Whole human blood (drug-free) was provided by a local blood bank (Cracow, Poland).

2.2 Instrumentation

The chromatographic analyses were carried out using the UltiMate 3000 RS liquid chromatography system (Dionex, USA) equipped with a Hypersil Gold Phenyl column (50×2.1 mm I.D., particles 1.9 μm; Thermo Scientific, Germany). Mass spectrometer equipped with electrospray ionization source and MicroTOF-Q II time of flight analyzer (Bruker, Germany) was used to detect analytes based on signal integration with positive ion mode. The data acquisition and processing were performed using Chromeleon 6.8 (Dionex), HyStar 3.2, MicrTOFcontrol and Compass DataAnalysis software (Bruker). The extraction process was carried out using a MARS 5 microwave-assisted sample preparation system (CEMMatthews NC, USA), equipped with 24 Xpress® PFA vessels (40 mL).

2.3 Sample preparation

The spiked blood samples contain each analyte (ketamine, flunitrazepam, diazepam, temazepam, nitrazepam, lorazepam, cocaine, norcocaine, cocatylene) at a concentration of 250 ng mL^{-1} were applied on dry blood spot cards in a volume of 25 μL for one drop one day before analysis. Next, from each drop 6-mm disc were cut out. Two discs for each sample were transferred to microwave assisted extraction vessel. To vessels 1 mL of a buffer with a known pH value and 3 mL of extractant were added. The vessels were then placed in a microwave rotor and extraction was performed under the selected conditions. After extraction, the contents of the vessels were transferred to 15 mL plastic tubes and centrifuged (4000 rpm, 4 °C, 10 min). Then 2.5 mL of extractant was withdrawn and transferred to a 5 mL Eppendorf vials. At this stage, 26 μL of standard solution of deuterated analogues (internal standards) at a concentration of 100 ng mL^{-1} was added to each vial. The contents were evaporated under a stream of nitrogen at 40 °C. Next, 500 μL of extractant was added to the evaporation residue and vortexed for 10 seconds. The samples were centrifuged again (10,000 rpm, 4 °C, 10 min). Then, 450 μL of the solution was withdrawn into a 1.5 mL Eppendorf vials and evaporated again at 40 °C. To the evaporation residue, 50 μL of the phase was added and vials were vortexed for 10 seconds. Next, 40 μL of the sample was taken into an insert placed in a glass vial and analysed by LC-MS.

3. Results and discussion

Optimization of microwave assisted extraction was started with the selection of the best extraction mixture for selected drugs. To optimize the best extraction mixture (extractant and extraction medium with a known pH value) for selected drugs, the nineteen different mixtures were tested. All experiments were performed at the same temperature and during the same time. From among the tested extraction mixture, the one that allows the identification of as many analytes as

possible while maintaining the optimal extraction efficiency of each of the tested substances was selected.

To score the extraction mixtures, an evaluation function *F'* was developed

$$F' = \frac{k^2 \sum_{n=1}^{k} \frac{E_n}{SD_n} + l \sum_{n=1}^{l} \frac{E_n}{SD_n}}{8} \quad (1)$$

Function *F'* differentiated the analytes into two groups: one for which the extraction efficiency (E_n) of the analyte was above 60% (k) and the other for which the extraction efficiency was below 60% (l). The function also considers different values of the standard deviation (SD_n) of the obtained extraction efficiency values.

The tested mixtures contained among others methanol, acetonitrile, *n*-hexane, ethyl acetate as extractant. For some mixtures, buffers of known pH values were also used. For a mixture of ethyl acetate with the buffer of pH = 9 contained sodium tetraborate and hydrochloric acid it was possible to isolate all analytes from the sample and for this mixture obtained *F'* value was the highest.

For the selected extraction mixture the parameters such as temperature and time of extraction were optimized using simplex method optimization. In the first step, the parameters of the initial simplex were determined (experiments A, B, C), for which the value of *F'* function was calculated. In the next steps, appropriate mathematical transformations were made to determine the parameters of the next experiments (D–H experiments). According to the *F'* values for experiments A–H the best parameters for extraction of selected substances seem to be extraction carried out at 50˚C for 15 minutes. For the process performed in these parameters the extraction efficiencies for all analytes are below 60%.

4. Conclusions

The aim of this research was to the development of the microwave assisted extraction method of "date-rape drugs" from blood samples collected on dry blood spot cards. The best extraction system for selected analytes was extraction with ethyl acetate with a buffer medium with pH = 9 (which contained sodium tetraborate and hydrochloric acid). For the selected system, the temperature and time of the extraction process were optimized by using simplex method optimization. The optimal extraction efficiency for selected "date-rape drugs" substances was obtained for the process carried out at 50 °C in 15 minutes. Under these conditions, extraction efficiencies above 60% were obtained for all tested analytes. In future studies, the developed procedure will be validated to determine its suitability for use in the toxicological analysis of blood samples collected in-vivo and post-mortem.

Acknowledgments

Authors gratefully acknowledge the Ministry of Science and Higher Education, National Science Centre, Poland for financial support (R. Wietecha-Posłuszny, Preludium Bis 1, no. 2019/35/O/ST4/-00978).

References

[1] Grela A., Gautam L., Cole M.D.: A multifactorial critical appraisal of substances found in drug facilitated sexual assault cases. *Forensic Sci. Int.* **292** (2018), 50–60.

[2] Amsterdam P.V., Waldrop C.: The application of dried blood spot sampling in global clinical trials. *Bioanalysis* **2** (2010), 1783–1786.

[3] Świądro M., Stelmaszczyk P., Wietecha-Posłuszny R., Dudek D.: Development of a new method for drug detection based on a combination of the dried blood spot method and capillary electrophoresis. *J. Chromatogr. B* **1157** (2020), 122339.

[4] Woźniakiewicz A., Wietecha-Posłuszny R., Woźniakiewicz M., Bryczek E., Kościelniak P.: A quick method for determination of psychoactive agents in serum and hair by using capillary electrophoresis and mass spectrometry. *J. Pharm. Biomed. Anal.* **111** (2015), 177–185.

On the optimization of critical parameters for flow modulated comprehensive two-dimensional gas chromatography in the analysis of chiral compounds in wine samples

Nemanja Koljančić*, Olga Vyviurska, Marek Leder, Ivan Špánik

Slovak University of Technology in Bratislava, Faculty of Chemical and Food Technology, Institute of Analytical Chemistry, Radlinského 9, 812 37 Bratislava, Slovak Republic
✉ *nemanja.koljancic@stuba.sk*

Keywords
carrier gas flow rates
flow-modulated comprehensive gas chromatography
modulation period
stationary phase selection

Abstract
Comprehensive two-dimensional gas chromatography (GC×GC) enables high performances in the analysis of trace compounds. In this study, the optimization of the flow-modulated comprehensive GC×GC method in the analysis of chiral compounds in wine samples was conducted. For optimization, five columns in the second dimension were used of which HP-5ms (5 m × 0.25 mm × 0.15 μm) showed the best performances in terms of reduced peak tailing and separation space occupation. Further optimization was focused on the determination of modulation period and flow rate in the second dimension column. Based on the obtained results of the analysis of enantiomers of ethyl lactate and linalool oxide, the optimal flow rate in the secondary column was determined to be 25 mL min^{-1} with the modulation period of 4 s. The new method was applied in the analysis of a test wine sample.

1. Introduction

Comprehensive two-dimensional gas chromatography is today a useful method for the qualitative and quantitative analysis of trace compounds [1, 2]. In flow-modulated GC×GC, the analyte is separated in the first column and afterward collected in the modulator during the modulation period (P_M). The analyte is then focused and reinjected into the second column in the form of periodic distinctive pulses during the injection period (t_{Inj}). Upon exiting the modulator, rapid separation takes place in the secondary column. However, connecting two columns with a modulator leads to the introduction of certain complexities in this method. Parameters such as the flow rate in the primary ($^1D_{Flow}$), and secondary column

($^1D_{Flow}$), P_M, the injection time into the second dimension as well as the operating temperature program of the columns and detector must be selected to achieve optimal analysis results [1]. Most optimization methods are based on simple experiments and the intuition of analysts, but it has been shown that the application of mathematical models in order to obtain a clearer picture of the results is almost inevitable [1, 3–5]. So far, several papers have been published in which the approaches of parameter optimization in the flow-modulated GC×GC method are considered [1, 3–5]. These methods are mainly based on the percentage of separation space used, chromatographic response functions, information on synentropy, entropy, and solvation parameters.

The application of the enantioselective GC×GC method for the analysis of compounds in wine samples provides a comprehensive distribution of enantiomers, better sample information, selectivity, sensitivity, resolution as well as lower values of *LOD* and *LOQ* compared to the classical one-dimensional GC method. It has been shown that a ratio of enantiomers of individual chiral compounds in wines can serve to determine their authenticity and the mode of production [1, 6]. In this study, the modulator parameters, as well as $^2D_{Flow}$, were optimized and secondary column stationary phase was selected for the purpose of determining chiral compounds by the enantioselective GC×GC-MS/FID method. In addition, the experiment was performed with five different column setups in the second dimension in order to provide the best method compatibility. The optimal values of parameters were determined based on the application of the method of analysis of wine-specific compound standards. The optimized method was applied for non-target analysis of the test wine sample.

2. Experimental

2.1 Reagents and chemicals

The standard chemicals used for the identification of volatile organic compounds were obtained from Sigma Aldrich (USA). LiChrolut EN resins (200 mg with a volume of 3 mL) were purchased from Merck (Germany). Ethanol was supplied from Mikrochem (Slovakia), *n*-hexane was supplied from Merck (Germany) while dichloromethane and methanol were obtained from VWR Chemicals BDH® (Poland).

2.2 Sample and standards preparation

Before the extraction, cartridges with the sorbent were rinsed with 4 mL of dichloromethane, 4 mL of methanol, and, finally, with 4 mL of a water–ethanol mixture (12%, *v/v*). Fifty milliliters of wine samples were passed through the SPE cartridge at around 2 mL min^{-1}. After this, the sorbent was dried by letting air pass through it (20.6 bar, 10 min). Analytes were recovered by elution with 1.3 mL of

dichloromethane [7]. After extraction, the samples were analyzed with flow modulated GC×GC-MS/FID method. A standard mixture of the R and S isomers of ethyl lactate and cis and trans isomers of linalol oxide in n-hexane was prepared at a concentration of 1 μL mL^{-1}.

2.3 Instrumentation

Flow modulated GC×GC-MS/FID experiments were performed on an Agilent 7890A GC (Agilent Technologies, USA) equipped with a reverse fill/flush (RFF) modulator (Agilent G3486A CFT Modulator, USA). The GC×GC column setup contains 30 m × 0.25 mm × 0.25 μm Rt-ßDEXse (Restek, USA) in the first dimension while in the second dimension 5 different column setups were used in order to determine the best combination:

- 5 m × 0.25 mm × 0.15 μm HP-5 ms (Agilent Technologies, USA),
- 3 m × 0.25 mm × 0.15 μm HP-5 ms (Agilent Technologies, USA),
- 5 m × 0.25 mm × 0.15 μm HP-INNOWax (Agilent Technologies, USA),
- 5 m × 0.25 mm × 0.25 μm BPX-50 (SGE, Australia & Pacific Region),
- 5 m × 250 m × 0.2 μm SLB-IL59 (Supelco, USA).

A supplementary restrictor (5 m × 250 μm ID) facilitates a switch of the carrier gas direction in the modulator between loading and injection mode. After leaving the secondary column, the analyte is directed from the splitter to the FID and MS detector. A 0.5 m × 100 μm ID restrictor and a 1.2 m × 250 μm ID restrictor were connected to MS and FID, respectively. The $^{1}D_{Flow}$ was kept constant at 0.7 mL min^{-1}. For optimization purposes, the $^{2}D_{Flow}$ was changed with values of 21, 23, 25, 27, and 30 mL min^{-1} with different P_M ranging from 2 to 6 s (2, 3, 4, 5, and 6 s). The initial temperature in the GC oven was 40 °C with hold up time of 10 min. The temperature was then raised to a maximum of 220 °C with hold up time of 15 min. The method duration is 115 min. 1 μL of the sample was injected in splitless mode at 230 °C with helium (99.9999%) as a carrier gas, in a constant flow rate. Flow rates in the restrictors to MS and FID were 2.60 mL min^{-1} and 30.77 mL min^{-1}, respectively. The FID was operated at a temperature of 250 °C with flow rates of hydrogen, air and nitrogen of 50 mL min^{-1}, 400 mL min^{-1}, and 25 mL min^{-1}, respectively. A data acquisition rate of 100 Hz was used for the FID detector. Transfer of the analyte to the MS detector was performed at a constant temperature of 250 °C. The MS quad and MS source temperatures were 180 °C and 300 °C, respectively. The acquisition rate for MS was 21.43 spectra s^{-1} (40–400 *m/z* range). All obtained results were processed with GC Image software (Zoex Corporation, USA), and MSD ChemStation software (version F.01.01.2317, Agilent Technologies, USA) with NIST14, FFNSC2, MPW2007, and W9N11 databases.

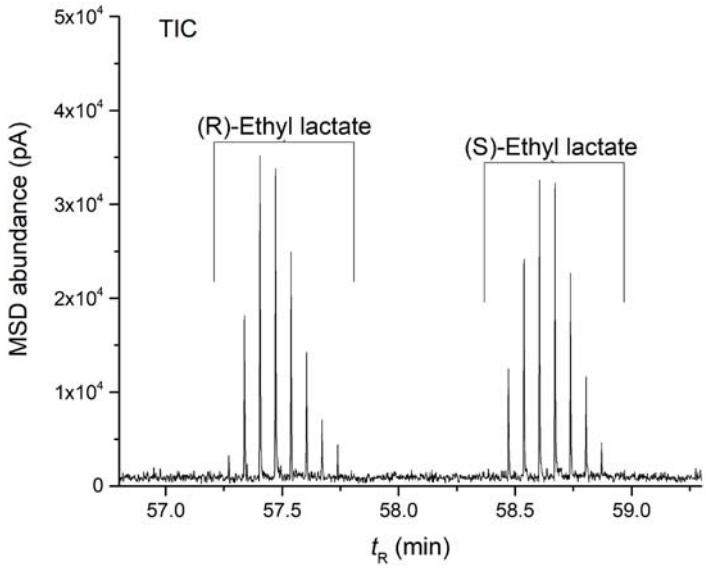

Fig. 1 Part of the total ion chromatogram (TIC) of MSD showing the peaks of the standard mixture of *R* and *S* isomers of ethyl lactate. The figure depicts a clear Gaussian distribution of the modulated peaks of both enantiomers without tailing effects. The analysis was performed with selected stationary phase, 5m HP-5ms, $^{2}D_{Flow}$ = 25 mL min^{-1}, and modulation period 4 s.

3. Results and discussion

The enhancement of the shape and intensity of the 2D peak depends on different critical parameters such as modulation time, flow rates in the first and secondary columns as well as on the type of stationary phase in both dimensions [1, 3]. The best separation performances in the second dimension were conducted with the nonpolar stationary phase 5 m × 0.25 mm × 0.15 µm HP-5ms. Given the polarity of the stationary phase, the separation space is more occupied and the peaks are better separated compared to other stationary phases. In addition, the lowest tailing peaks were observed using the HP-5ms column. Further optimization of the modulation and flow parameters in the secondary column, was continued on the HP-5ms secondary column. Figure 1 shows the part of the total ion chromatogram of MSD obtained by analyzing a mixture of standards of linalool oxide and ethyl lactate *R* and *S* enantiomers with HP-5ms stationary phase in the second dimension. Using different modulation times, the optimal shape was determined by Gaussian distribution using the Origin program. Among different P_M with values of 2, 3, 4, 5, and 6 s, it was determined that the optimal peak shape was obtained at a value of 4s. At the stated P_M, the volume of analyte collected in the modulator, V_F, was calculated to be 45.3833 µL. The dimensions of the RFF plate of the CFT modulator are 19.6 cm length × 0.535 mm i.d. which corresponds to an internal volume of 44 µL. The additional volume of analyte that enters the modulator is not reinjected into the secondary column rather it is directed into the

Table 1
Mean and standard deviation of peak widths at different modulation period (P_M) and volume of analyte collected in the modulator (V_F) values, different flow rate in the secondary column ($^2D_{Flow}$) and injected volume (V_{Inj}), resp., for both enantiomers of ethyl lactate and linalool oxide ($^1D_{Flow}$ = 0.7 mL min^{-1}, t_{Inj} = 11 s).

$^2D_{Flow}$ /mL min^{-1}	P_M/s	V_F/µl	V_{Inj}/µl	(*R*)-Ethyl lactate		(*S*)-Ethyl lactate		*cis*-Linalool oxide		*trans*-Linalool oxide	
				$\overline{W}$/ms	$\sigma(W)$/ms	$\overline{W}$/ms	$\sigma(W)$/ms	$\overline{W}$/ms	$\sigma(W)$/ms	$\overline{W}$/ms	$\sigma(W)$/ms
23	6	68.7167	42.1667	200	0	200	0	200	0	200	0
23	5	57.0500	42.1667	200	0	200	0	200	0	200	0
23	4	45.3833	42.1667	200	0	200	0	200	0	212	33.1
23	3	33.7167	42.1667	186	35	200	0	226	60.6	225	43.3
23	2	22.0500	42.1667	156	52.7	190	30.7	200	0	200	0
21	4	45.3833	38.5000	200	0	200	0	208	27.6	221	41
23	4	45.3833	45.8333	200	0	200	0	200	0	200	0
25	4	45.3833	42.1667	200	0	200	0	208	26.6	213	34.2
27	4	45.3833	49.5000	200	0	209	28.7	200	0	219	39
30	4	45.3833	55.0000	175	43.3	200	0	200	0	218	51.3

restrictor. Table 1 shows the values for V_F ranging from 22.05–68.72 uL for different P_M at a constant gas flow rate in the primary column. The volume of the analyte which enters the modulator is calculated as the ratio of the flow rate in the primary column and the flushing time of the modulator. Other examined modulation periods exhibit the property of incomplete flushing of the modulator,

Table 2
Chiral compounds obtained by wine analysis with optimized enantioselective flow-modulated GC×GC-MS/FID method.

Number	^1t_R / min	^2t_R / min	Compound	Formula	CASRN
1	44.021	1.02	Ethyl lactate	$C_5H_{10}O_3$	97-64-3
2	44.688	1.02	Ethyl lactate	$C_5H_{10}O_3$	97-64-3
3	56.821	1.726	Linalool oxide	$C_{10}H_{18}O_2$	5989-33-3
4	58.021	1.648	Linalool oxide	$C_{10}H_{18}O_2$	5989-33-3
5	60.555	1.491	Linalool formate	$C_{11}H_{18}O_2$	115-99-1
6	60.888	1.491	Linalool formate	$C_{11}H_{18}O_2$	115-99-1
7	61.421	1.883	Nerol oxide	$C_{10}H_{16}O$	1786-08-9
8	61.688	1.883	Nerol oxide	$C_{10}H_{16}O$	1786-08-9
9	70.088	1.726	Hotrienol	$C_{10}H_{16}O$	20053-88-7
10	71.888	1.334	Hotrienol	$C_{10}H_{16}O$	20053-88-7
11	71.955	1.805	*trans*-2-Pinanol	$C_{10}H_{18}O_2$	4948-29-2
12	76.555	1.334	Diethyl malate	$C_8H_{14}O_5$	626-11-9
13	78.288	1.334	8-Hydroxylinalool	$C_{10}H_{18}O_2$	64142-78-5
14	79.288	1.334	Whiskey lactone	$C_9H_{16}O_2$	39212-23-2
15	80.288	1.491	1-Terpinenol	$C_{10}H_{18}O_2$	586-82-3
16	81.821	1.412	Whiskey lactone	$C_9H_{16}O_2$	39212-23-2
17	82.355	1.412	Ethyl linalool	$C_{12}H_{22}O$	72845-33-1
18	83.421	1.334	8-Hydroxylinalool	$C_{10}H_{18}O_2$	64142-78-5
19	90.955	1.491	γ-Decalactone	$C_{10}H_{18}O_2$	706-14-9
20	84.488	1.334	α-Limonene diepoxide	$C_{10}H_{16}O_2$	96-08-2
21	92.155	1.491	Massoilactone	$C_{10}H_{16}O_2$	54814-64-1
22	94.488	2.119	Aristolene	$C_{15}H_{24}$	17334-55-3

which appears in the form of tailing peaks. On the other hand, when the P_M is too long, fronting peaks occur. However, the occurrence of fronting or tailing peaks also depends on other factors, such as the type of stationary phase as well as the $^1D_{Flow}$ and $^2D_{Flow}$ [1]. In order to determine the optimal P_M and $^1D_{Flow}$, mean peak width values ($\overline{W}$), and standard deviation σ(W), were calculated for the enantiomers of ethyl lactate and linalool oxide (Table 1). Determination of peak widths was performed using the ChemStation software integrator. The peak widths ranged from 156 to 225 ms, for different values of P_M and V_F which is in accordance with the general requirements of the GC×GC method (Table 1) [1, 8]. After determining the optimal value of the P_M, the compatible $^2D_{Flow}$ was determined. In general, when using a flow modulator, the $^2D_{Flow}$ must be approximately 30 times larger compared to the $^1D_{Flow}$ so as to achieve rapid separation in accordance with the P_M. The performance of the method was examined with respect to the flow rates in the secondary column of 21, 23, 25, 27, and 30 mL min^{-1}. The lowest tailing was shown to occur using a $^2D_{Flow}$ of 25 mL min^{-1}, while the highest peak area values for the analyzed standard were recorded with the same flow rate. Peak widths ranged from 175 to 221 ms for different $^2D_{Flow}$ and V_{Inj} values at a constant P_M of 4 s (Table 1). The volume of injected analyte into the secondary column, V_{Inj}, at a flow rate of 25 mL min^{-1} is

45.3833 μL, which is almost identical to the V_F at a P_M of 4 s. With such parameters, 2D modulated peaks for enantiomers of linalool oxide and ethyl lactate were obtained that corresponds to the Gaussian curve and do not have tailing effects. Table 1 shows the values of injected analyte volumes at different flow rate values in the secondary column.

With the optimized parameters of the FM-GC×GC method, a non-target analysis of the test wine sample was performed. A number of 22 chiral compounds from the group of lactones and terpenes were identified, of which 7 in both enantiomeric forms and together with retention data (^1t_R – first dimension retention time and ^2t_R – second dimension retention time) showed in Table 2.

4. Conclusions

Optimization of the comprehensive GC×GC method is based on finding appropriate values of critical parameters that allow high sensitivity, selectivity, low limit of detection, limit of quantitation, good resolution, peak shape, and peak capacity. The enantioselective flow modulated comprehensive GC×GC method with RFF modulator was optimized with respect to critical parameters such as stationary phase type, $^2D_{Flow}$ and P_M. HP-5ms with a length of 5 m and a carrier gas flow rate of 25 mL min^{-1} was determined as the optimal stationary phase in the secondary dimension. A modulation period of 4 s proved to be compatible for enantioselective analysis of wine samples. A non-target analysis of the test wine sample was performed with optimized FM-GC×GC-MS/FID parameters and 22 chiral compounds were identified.

Acknowledgments

The authors would like to thank for financial support from Grant Agency of Ministry of Education of Slovak Republic for contract VEGA 1/0521/19.

References

[1] Krupčík J., Gorovenko R., Špánik I., Sandra P., Giardina M.: Comparison of the performance of forward fill/flush and reverse fill/flush flow modulation in comprehensive two-dimensional gas chromatography. *J. Chromatogr. A* **1466** (2016), 113–128.

[2] Furdíková K., Khvalbota L., Machyňáková A., Špánik I.: Volatile composition and enantioselective analysis of chiral terpenoids in Tokaj varietal wines. *J. Chromatogr. B* **1167** (2021), 122565.

[3] Májek P., Krupčík J., Gorovenko R., Špánik I., Sandra P., Armstrong D.W.: Computerized optimization of flows and temperature gradient in flow modulated comprehensive two-dimensional gas chromatography. *J. Chromatogr. A* **1349** (2014), 135–138.

[4] Magagna F., Liberto E., Reichenbach S.E., Tao Q., Carretta A., Cobelli L., Giardina M., Bicchi C., Cordero, C.: Advanced fingerprinting of high-quality cocoa: Challenges in transferring methods from thermal to differential-flow modulated comprehensive two-dimensional gas chromatography. *J. Chromatogr. A* **1536** (2018), 122–136.

[5] Stilo F., Gabetti E., Bicchi C., Carretta A., Peroni D., Reichenbach S.E., Cordero C., Curry J.M.: A step forward in the equivalence between thermal and differential-flow modulated comprehensive two-dimensional gas chromatography methods. *J. Chromatogr. A* **1627** (2020), 461396.

[6] Gomes A.A., Khvalbota L., Machyňáková A., Furdíková K., Zini C.A., Špánik I.: Slovak Tokaj wines classification with respect to geographical origin by means of one class approaches. *Spectrochim. Acta. A* **257** (2021), 119770.
[7] López R., Aznar M., Cacho J., Ferreira V.: Determination of minor and trace volatile compounds in wine by solid-phase extraction and gas chromatography with mass spectrometric detection. *J. Chromatogr. A* **966** (2002),167–177.
[8] Marriott P., Shellie R.: Principles and applications of comprehensive two-dimensional gas chromatography. *TrAC Trends Anal. Chem.* **21** (2002), 573–583.

Chemical vapor generation of cadmium: detector comparison

Linda Sagapova[a, b, *], Barbora Štádlerová[a, b], Milan Svoboda[a], Jan Kratzer[a], Stanislav Musil[a]

[a] *Institute of Analytical Chemistry of the Czech Academy of Sciences, Veveří 97, 602 00 Brno, Czech Republic* ✉ *sagapova@iach.cz*

[b] *Charles University, Faculty of Science, Department of Analytical Chemistry, Hlavova 8/2030, 128 43 Prague 2, Czech Republic*

Keywords
atomic absorption spectrometry
atomic fluorescence spectrometry
cadmium
chemical vapor generation

Abstract
Chemical vapor generation of cadmium was optimized in the presence of various additives using atomization in an externally heated quartz tube atomizer and atomic absorption spectrometry. Employing Cr^{3+}/KCN modifiers in a four channel chemical vapor generation system was found to provide the most robust conditions, the highest overall chemical vapor generation efficiency and the lowest limit of detection of 60 pg mL^{-1} Cd. The vapor generation system was subsequently connected to an in-house assembled atomic fluorescence spectrometer equipped with a miniature diffusion flame atomizer in order to achieve substantially better sensitivity. The optical path of the spectrometer was optimized as well as the feeding current of an electrodeless discharge lamp used for excitation of atomic fluorescence. A preliminary evaluation of analytical performance (limit of detection of 3 pg mL^{-1}) revealed that the significant contribution to the measured noise comes from serious contamination from reagents used for chemical vapor generation. Nevertheless, these results promise extremely high sensitivity that is substantially better than that achieved with atomic absorption spectrometry.

1. Introduction

Cadmium compounds are among the most dangerous toxic pollutants in the environment [1]. Its widespread industrial use leads to increased environmental pollution. It is one of the most serious carcinogens with a biological half-life of 10–30 years, it accumulates in humans through the food chain. For this reason, there is a great interest in an accurate rapid analytical method for monitoring Cd in environmental and food samples at (ultra) trace levels. An appropriate method is chemical vapor generation (CVG) with atomic absorption spectrometry (AAS) or atomic fluorescence spectrometry (AFS) detection. Conversion to a volatile species results in enhanced analyte introduction efficiency into the detector, which can be reflected in better limits of detection (*LOD*). In this work, we present

the optimization of conditions of CVG with AAS detection and atomization in a quartz tube atomizer. The most robust conditions were chosen and subsequently, the generator was coupled to AFS to achieve substantially better sensitivity. A non-dispersive atomic fluorescence spectrometer developed at our laboratory and hitherto applied only to the sensitive determination of arsenic and bismuth was adjusted [2–4]. After optimization of the optical path of the AFS spectrometer, the *LOD* was evaluated and compared to that obtained with AAS.

2. Experimental

2.1 Reagents and chemicals

Deionized water (< 0.1 μS cm^{-1}, Ultrapur, Watrex, USA) was boiled, deaerated by Ar bubbling through for 30 min and used to prepare all solutions. Working Cd standards were prepared by a serial dilution from 1000 μg mL^{-1} Cd stock solution Astasol (Analytika, Czech Republic) in 0.2 mol L^{-1} HCl. HCl (37%, p.a.) was sourced from Merck (Germany). Solid reductant $NaBH_4$ (≥ 97%, Sigma-Aldrich, Germany) was used to prepare a solution of 5% (*m/v*) $NaBH_4$ in deionized water that was stabilized in 0.4% (*m/v*) KOH (p.a., Merck, Germany). Solutions of modifier Cr^{3+} (0.04 mol L^{-1} and 0.001 mol L^{-1} Cr^{3+}) were prepared from $Cr(NO_3)_3$ $9H_2O$ (≥ 99.99% trace metal basis, Sigma-Aldrich, Germany). Solution of 0.1 mol L^{-1} KCN (≥ 97.0%, Fluka, Switzerland) was used as a second modifier. A mixture 3:7 (*v/v*) of HF (38%, Spolchemie, Czech Republic) and HNO_3 (65%, Lach-Ner, Czech Republic) was used to clean the quartz tube atomizer when needed.

2.2 Instrumentation

2.2.1 Chemical vapor generation system

A four channel chemical vapor generation system in a flow injection mode was employed (Fig. 1). The flow rates of HCl and $NaBH_4$ were both 1 mL min^{-1} while the flow rates of modifier I (0.001 mol L^{-1}) Cr^{3+} and modifier II (0.1 mol L^{-1} KCN) were 0.5 mL min^{-1}. The volume of the sample loop was 0.15 mL. A carrier gas flow rate of 75 mL min^{-1} Ar was controlled by a mass flow controller (Cole-Parmer, USA). The gas phase leaving the gas-liquid separator was transported via a PTFE tube (1 mm i.d., 10 cm long) either directly to a quartz tube atomizer for AAS detection or to a miniature diffusion flame for AFS detection, which necessitated supply of additional gases, i.e., Ar flame and H_2 flame (displayed in Fig. 1). Liquid phase from the gas-liquid separator was pumped into the waste by the second peristaltic pump. At the beginning of the measurement, the CVG system was pre-conditioned by 0.04 mol L^{-1} Cr^{3+} aspired into modifier I channel during the first 5 replicates.

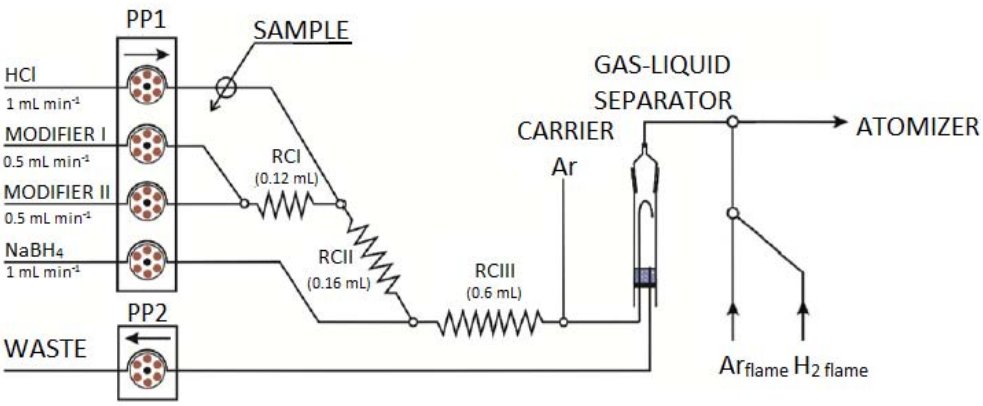

Fig. 1 Four channel chemical vapor generator.: (PP) peristaltic pump, (RC) reaction coil. Modifier I Cr^{3+}, modifier II KCN.

2.2.1 Atomic absorption spectrometry

Shimadzu model AA-7000 (Japan) atomic absorption spectrometer was employed without background correction. A Cd hollow cathode lamp (Photron, Australia) operated at 12 mA and the analytical line at 228.8 nm was used in the measurements with 0.7 nm as the spectral bandwidth. The T-shaped multiatomizer was employed as an atomizer and was heated to 900 °C by an in-house made furnace controlled by the REX-C100 controller (Syscon, USA) with the K-type thermocouple sensor (Omega Engineering, USA).

2.2.2 Atomic fluorescence spectrometry

An in-house assembled non-dispersive atomic fluorescence spectrometer was used as a detector. This spectrometer of a design depicted in Fig. 2 consists of three major components: source of radiation, atomizer, and photomultiplier tube. A Cd electrodeless discharge lamp (PerkinElmer, System 2) was used as the radiation source with feeding current square-wave modulated at frequency of 40 Hz and with 52% duty cycle (13 ms lamp on, 12 ms lamp off) [4]. Feeding current of the electrodeless discharge lamp was 230 mA. A beam of radiation from the lamp was focused using two UV fused silica lenses. A planoconvex lens (d = 25 mm, 40 mm focal length) was inserted into the exit orifice of the cavity including the bulb and a doubleconvex lens (d = 22 mm, 45 mm focal length) was attached, in a lens holder, to the rim of the electrodeless discharge lamp. The photomultiplier was placed perpendicularly to the lamp to collect the produced fluorescence radiation. A combination of two positive meniscus UV fused silica lenses (d = 17 and 22 mm; 21 mm focal length) was used to focus the produced radiation onto the interference filter, which was used for wavelength selection. A broadband interference filter 228 nm (Melles Griot, full width at half maximum 10 nm and peak transmittance around 17%) was used to cover the most intense Cd fluorescence

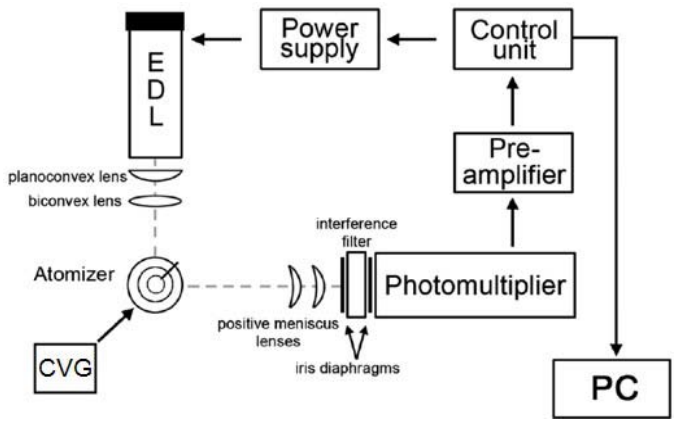

Fig. 2 A block scheme of the non-dispersive atomic fluorescence spectrometer [4].

line at 228.8 nm [5]. A solar-blind photomultiplier (MH 1922, 165–320 nm, PerkinElmer Optoelectronics, Germany) supplied with negative voltage was used as a detector.

In-house assembled AFS instrument was placed inside a fume hood. The glass door was covered with a black curtain during all the measurements to prevent any parasitic radiation from the laboratory environment from contributing to the measured signal.

The detector output provided signals in μV. Peak area (in μV s) corrected to baseline and a signal to noise ratio were the parameters used to evaluate the data. Noise was calculated as an average standard deviation of three blank replicates (each measured for 10 s representing 400 values). Signal to noise ratio was determined by dividing the peak height (corrected to baseline) by an average standard deviation of blank.

3. Results and discussion

Experimental conditions for CVG were optimized with AAS detection employing the externally heated quartz tube atomizer in our recent paper [6]. To sum the results, very good robustness and the highest sensitivity in AAS measurements were obtained with the four channel system in the presence of Cr^{3+}/KCN and Ti^{4+}/KCN as modifiers used for CVG. The *LOD* for Cr^{3+}/KCN was 0.06 ng mL^{-1} while *LOD* for Ti^{4+}/KCN was 0.12 ng mL^{-1}. Much worse results were typical of the same system employing Co^{2+}/ascorbic acid/thiourea as the additive or when no modifiers were employed. The overall CVG efficiency was determined by two different approaches, i.e., by means of ^{115m}Cd radioactive indicator and sensitivity comparison of liquid nebulization and CVG, both coupled to inductively coupled plasma mass spectrometry. The highest efficiency, between 60 and 70%, was reached in the presence of Cr^{3+}/KCN and Ti^{4+}/KCN as modifiers reflecting reliably the results obtained with AAS [6].

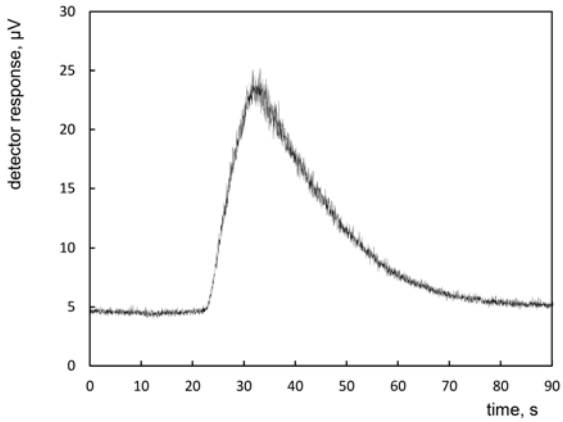

Fig. 3 Typical CVG transient signal from 250 pg mL^{-1} of Cd, photomultiplier voltage 1300 V.

In order to improve *LOD*, the four channel system (Fig. 1) was coupled to AFS. The miniature diffusion flame was employed as the atomizer and the optimal conditions found for atomization of bismuthane, i.e., 500 mL min^{-1} total Ar, 100 mL min^{-1} total H_2 and observation height 7 mm [4], were taken as default for initial studies. A typical signal of 250 pg mL^{-1} of Cd obtained with the AFS is displayed in Fig. 3.

Firstly, the optical path of the AFS spectrometer was optimized so as to achieve the highest sensitivity and signal to noise ratio. This covered tuning of mutual positions of the lamp, atomizer and detector with respect to the highest peak area sensitivity and signal to noise ratio. Secondly, the feeding current of the electrodeless discharge lamp was optimized. Finally, the limit of detection of a current setup was estimated by measuring a peak area sensitivity (using 250 pg mL^{-1} Cd standard) and 10 peak areas of blank and it equaled 3 pg mL^{-1}. Similarly, the instrumental *LOD* was evaluated when blanks were measured but CVG was switched off. During these measurements the background fluorescence intensity significantly dropped and that is why the instrumental *LOD* reached only 0.1 pg L^{-1}.

This suggests very high contribution of Cd contamination in the reagents used for CVG to the measured background, which impairs the real *LOD*. Despite contamination, the *LOD* with AFS was still by more than one order of magnitude lower than that with AAS detection (60 pg L^{-1}). Taking into account very low instrumental *LOD* this methodology based on AFS seems to be highly promising for ultrasensitive determination of Cd in various environmental matrices.

4. Conclusions

The initial experiments with CVG-AFS suggest very high sensitivity for Cd determination and are promising for further work. Contamination in the reagents used for CVG seems to be a big issue and its elimination will be the future subject of

our research. Future experiments will also focus on optimization of conditions of atomization in the miniature diffusion flame. Once the best *LOD* is achieved, the methodology will be verified by the determination of Cd in various certified reference materials and in real environmental samples (e.g., water, seawater, rice). Also the potential of CVG step coupling with ICP-MS detection will be explored in future experiments allowing thus to assess analytical performance of AAS, AFS and ICP-MS detectors for Cd determination after CVG.

Acknowledgments

This research was supported by the Czech Science Foundation under contract 19-17604Y, by the Institute of Analytical Chemistry of the Czech Academy of Sciences (Institutional Research Plan RVO 68081715), and Charles University (Project SVV260560 and GAUK 377321).

References

[1] Cornelis R., Caruso J., Crews H., Heumann K.: *Handbook of Elemental Speciation II.* Chichester, Wiley 2005.

[2] Musil S., Matoušek T., Currier J.M., Stýblo M., Dědina J.: Speciation analysis of arsenic by selective hydride generation-cryotrapping-atomic fluorescence spectrometry with flame-in-gas-shield atomizer: achieving extremely low detection limits with inexpensive instrumentation. *Anal. Chem.* **86** (2014), 10422–10428.

[3] Marschner K., Musil S., Dědina J.: Flame-in-gas-shield and miniature diffusion flame hydride atomizers for atomic fluorescence spectrometry: optimization and comparison. *Spectrochim. Acta B* **109** (2015), 16–23.

[4] Štádlerová B., Kolrosová M., Dědina J., Musil S.: Atomic fluorescence spectrometry for ultrasensitive determination of bismuth based on hydride generation – the role of excitation source, interference filter and flame atomizers. *J. Anal. At. Spectrom.* **35** (2020), 993–1002.

[5] Sychra V., Svoboda V., Rubeška I.: *Atomic Fluorescence Spectroscopy*. London, Van Nostrand Reinhold 1975.

[6] Sagapova L., Musil S., Kodríková B., Svoboda M., Kratzer J.: Effect of additives on cadmium chemical vapor generation and reliable quantification of generation efficiency. *Anal. Chim. Acta* **1168** (2021), 338601.

Optimization of photochemical vapor generation of tellurium for analytical atomic spectrometry

Eva Jeníková[a, b, *], Stanislav Musil[b], Jakub Hraníček[a]

[a] *Charles University, Faculty of Science, Department of Analytical Chemistry, Hlavova 8/2030, 128 43 Prague 2, Czech Republic* ✉ *jenikoev@natur.cuni.cz*
[b] *Czech Academy of Sciences, Institute of Analytical Chemistry, Veveří 97, 602 00, Brno, Czech Republic*

Keywords
atomic absorption spectrometry
photochemical vapor generation
tellurium

Abstract
Photochemical vapor generation of tellurium was accomplished in a simple reactor consisted of a polytetrafluorethylene reaction coil wrapped around a low-pressure mercury bench lamp. The volatile species were generated using a flow-injection system. The composition of a reaction medium, the influence of irradiation time' and the effect of sensitizers and interferents were investigated using a miniature diffusion flame atomizer and high-resolution continuum source atomic absorption spectrometry. Combination of 5 mol L^{-1} acetic acid and 3.5 mol L^{-1} formic acid in the reaction medium, the addition of 15 mg L^{-1} Fe^{2+} and 250 mg L^{-1} Mn^{2+} as sensitizers in a sample and a flow rate of 4 mL min^{-1} (corresponding to an irradiation time of 28 s) were found optimal for photochemical vapor generation. A limit of detection of 3.2 µg L^{-1} and repeatability of 2.4% at 500 µg L^{-1} were achieved. Photochemical vapor generation efficiency of 50±2% was determined from a relative comparison of sensitivities obtained with photochemical vapor generation and liquid nebulization, both coupled to inductively coupled plasma mass spectrometry.

1. Introduction

Photochemical vapor generation (PVG) is a relatively new vapor generation technique, an alternative to well established hydride generation. The mechanism of PVG is based on photodecomposition of low molecular weight organic acids by UV radiation and formation of radicals such as $H^{\bullet}$, $R^{\bullet}$ and $COO^{-\bullet}$ and hydrated electrons (e^{-}(aq)) [1]. These radical species interact with elements of interest to form volatile compounds, e.g., hydrides, carbonyl or alkyl compounds. Generated volatile compounds are efficiently separated from the sample matrix and transported with high efficiency to any atomic spectrometry detector. Recently, some transition metal ions, mainly Cd^{2+}, Co^{2+}, Cu^{2+}, $Fe^{2+/3+}$, have been employed as

sensitizers to substantially enhance PVG of several elements, such as As, Bi, Cd, Co, Mo, Ni, Pb, Te, W and Cl [2–9].

Tellurium has been considered as a technology-critical element and its use has rapidly increased in new applications [10, 11]. Exposition of organisms to Te negatively affects kidneys, nervous system, lungs and gastrointestinal tract [12].

In this work, we optimized conditions of PVG of Te by means high-resolution continuum source atomic absorption spectrometer (HR-CS-AAS) with atomization in a miniature diffusion flame and investigated an effect of various metal sensitizers to enhance efficiency of PVG. Finally, the analytical characteristics as well as photochemical vapor generation efficiency were determined.

2. Experimental

2.1 Reagents and chemicals

Deionized water (< 0.2 μS cm^{-1}, Ultrapur, Watrex, USA) was used for preparation of all solutions. A stock solution of 1000 mg L^{-1} of Te^{4+} was sourced from Astasol (Czech Republic). Acetic acid (≥99,5%, Sigma-Aldrich, USA) and formic acid (≥98%, Merck, Germany) were used for preparation of the reaction media ions and these solutions were prepared fresh daily. Stock solutions of sensitizers of various concentrations were prepared from following compounds: bismuth(III) acetate (p.a., Sigma-Aldrich, USA), cadmium(II) acetate tetrahydrate (p.a., Lach-Ner, Czech Republic), cobalt(II) acetate tetrahydrate (p.a., Lach-Ner, Czech Republic), copper(II) acetate monohydrate (p.a., Merck, Germany), iron(II) acetate (p.a., Sigma-Aldrich, USA), manganese(II) acetate tetrahydrate (p.a., Sigma-Aldrich, USA), nickel(II) acetate tetrahydrate (p.a., Sigma-Aldrich, USA), sodium selenite(IV) (p.a., Merck, Germany), sodium tungstate(VI) dihydrate (p.a., Merck, Germany). Other chemicals used for interference studies were: nitric acid (65%, Sigma-Aldrich, USA); hydrochloric acid (37%, Merck, Germany); sulfuric acid (98%, p.a.) from Lach-Ner (Czech Republic).

2.2 Instrumentation

The measurements were performed with ContrAA 300 HR-CS-AAS (Analytik Jena AG, Germany) at 214.3 nm. Three pixels of the detector were taken for evaluation of peak area. A commercial flame sample introduction system and a burner were replaced with an in-house made PVG system and with a miniature diffusion flame atomizer (Fig. 1). Almost all tubing was made of PTFE (1 mm i.d.) except for tubes used in peristaltic pumps equipped with Tygon tubing (1.42 mm i.d., Ismatec, Germany). The photoreactor was made of a low-pressure mercury UV bench lamp (20 W, dimensions 610×35 mm, Ushio, Japan) placed in a power supply with mirror walls covered with aluminium foil to protect the operator from UV radiation. This tube lamp was tightly wrapped with 480 cm long PTFE tube of

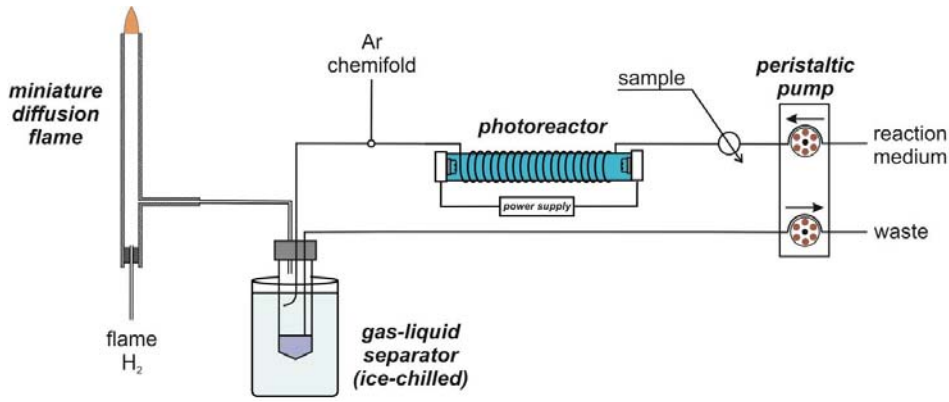

Fig. 1 Schematic diagram of a photochemical vapor generation system with a miniature diffusion flame atomizer.

1 mm i.d. where PVG was carried out. A steady flow of the reaction medium was supplied by a peristaltic pump (Masterflex, Cole-Parmer, USA). Sample/standard solution was introduced into a stream of reaction medium using an injection valve (V-451, INDEX Health and Science, USA; sample loop volume 0.5 mL). The outflow from the photoreactor was mixed with a flow of argon (250 mL min^{-1}) controlled by a mass-flow controller (Cole-Palmer, USA) and carried to a gas-liquid separator (modified polypropylene centrifuge vial with inner volume of 15 mL), where the volatile species were separated from the liquid phase. The gas-liquid separator was connected to the miniature diffusion flame atomizer by means of PTFE tubing (2 mm i.d.). This atomizer consisted of a vertical quartz tube with 6 mm i.d. and was supplied at the lower end with a flow of hydrogen (100 mL min^{-1}) that served as a fuel.

3. Results and discussion

The PVG conditions were optimized using the miniature diffusion flame atomizer and HR-CS-AAS. The first optimized parameter was composition of the reaction medium. A synergistic effect of formic and acetic acid on PVG of Te^{4+} was identified when only a combination of both acids led to efficient PVG while almost no signal was obtained in the absence of formic or acetic acid in the reaction media. As shown in Fig. 2, the optimal composition of the reaction medium was 3.5 mol L^{-1} formic acid and 5 mol L^{-1} acetic acid that provided the highest sensitivity. Higher concentration of both acids than optimum led to rapid signal decrease.

The influence of irradiation time was examined by altering the flow rate of the reaction medium. The highest peak area was observed for 4 ml min^{-1}, which corresponds to an irradiation time of approximately 28 s.

The effect of sensitizers was investigated by addition of various concentrations of various metal ions (Bi^{3+}, Cd^{2+}, Co^{2+}, Cu^{2+}, Fe^{2+}, Mn^{2+}, Ni^{2+}, Se^{4+}, and W^{6+}). These metals were added in the form of acetate or in the form other than nitrate or

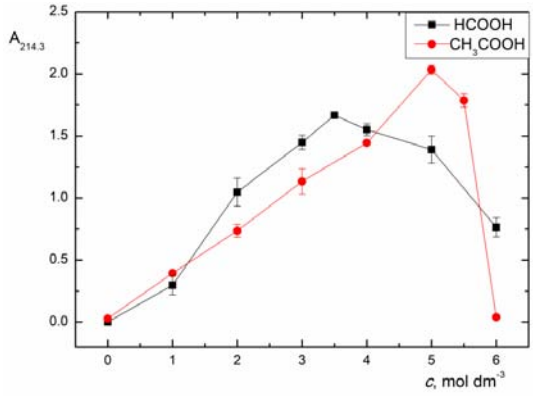

Fig. 2 Effect of the composition of reaction media on peak area: ■ – effect of formic acid, experimental conditions: 1 mg L^{-1} Te^{4+}, 4 mol L^{-1} acetic acid, sample flow rate 4 mL min^{-1}, ● – effect of acetic acid, experimental conditions: 1 mg L^{-1} Te^{4+}, 3.5 mol L^{-1} formic acid, sample flow rate 4 mL min^{-1}.

chloride as these anions can cause serious interference during PVG (see below). While the majority of elements was found to interfere at concentrations of 1 or 10 mg L^{-1}, the use of Fe^{2+} and Mn^{2+} led to a significant enhancement of the signal. Similarly as for organic acid, a synergistic effect of both ions was observed wherein maximum sensitivity was achieved with addition of 15 mg L^{-1} Fe^{2+} and 250 mg L^{-1} Mn^{2+}, reaching around 3-fold enhancement.

Interferences caused by inorganic anions (NO_3^-, SO_4^{2-}, Cl^-) were also investigated. The NO_3^- anions were found to be the most serious interferent even at concentrations as low as 25 mmol L^{-1}. Cl^- and SO_4^{2-} anions started interfering at much higher concentrations (around 500 mmol L^{-1}).

Generation efficiency was determined from a comparison between sensitivities obtained with PVG and conventional solution nebulization, both simultaneously coupled with inductively coupled plasma mass spectrometry. Nebulization efficiency was determined as 3.85±0.01% using a modified waste collection method [4-6] and PVG efficiency of 50±2% was derived from sensitivity enhancement between PVG and nebulization.

At optimal conditions of PVG (5 mol L^{-1} acetic acid; 3.5 mol L^{-1} formic acid, and irradiation time of 28 s) a calibration curve was measured by means of 0, 50, 100, 250, 500 and 1000 μg L^{-1} Te^{4+} standards spiked with 15 mg L^{-1} Fe^{2+}; 250 mg L^{-1} Mn^{2+} as sensitizers. The calibration was linear in the whole range of concentrations (R^2 = 0.9994). The limit of detection was established as 3σ where σ is the standard of peak area of 10 blank measurements and reached 3.2 μg L^{-1}. Repeatability of 10 consecutive measurements of 500 μg L^{-1} was 2.4%.

4. Conclusions

The conditions for PVG of Te^{4+} were optimized. Mn^{2+} and Fe^{2+} ions were identified as sensitizers increasing the PVG efficiency about 3-fold. To our best knowledge,

this is a first report when Mn^{2+} was used as the sensitizer in PVG. Nevertheless, severe interferences from inorganic anions were observed. The next step will be a coupling PVG with inductively coupled plasma mass spectrometry to reach much better sensitivity and validate this technique for ultrasensitive Te determination and speciation analysis of Te^{4+} and Te^{6+} in environmental samples.

Acknowledgments

The authors thank Charles University for financial support. This research was carried out within the framework of Specific University Research (Project SVV 260560) and with a support of the Grant Agency of Charles University (Project GA UK 516119) and of Czech Academy of Sciences (Institutional support RVO: 68081715).

References

[1] Sturgeon R.E.: Photochemical vapor generation: a radical approach to analyte introduction for atomic spectrometry. *J. Anal. At. Spectrom.* **32** (2017), 2319–2340.

[2] Zhou J., Deng D., Su Y., Lv Y.: Determination of total inorganic arsenic in water samples by cadmium ion assisted photochemical vapor generation-atomic fluorescence spectrometry. *Microchem. J.* **146** (2019), 359–365.

[3] Wang Y., Lin L., Liu J., Mao X., Wang J., Qin D.: Ferric ion induced enhancement of ultraviolet vapour generation coupled with atomic fluorescence spectrometry for the determination of ultratrace inorganic arsenic in surface water. *Analyst* **141** (2016), 1530–1536.

[4] Vyhnanovský J. Yildiz D., Štádlerová B., Musil S.: Efficient photochemical vapor generation of bismuth using a coiled Teflon reactor: Effect of metal sensitizers and analytical performance with flame-in-gas-shield atomizer and atomic fluorescence spectrometry. *Microchem. J.* **164** (2021), 105997.

[5] Vyhnanovský J., Sturgeon R.E., Musil S.: Cadmium Assisted Photochemical Vapor Generation of Tungsten for Detection by Inductively Coupled Plasma Mass Spectrometry. *Anal. Chem.* **91** (2019) 13306–13312.

[6] Nováková E., Horová K., Červený V., Hraníček J., Musil S.: UV photochemical vapor generation of Cd from a formic acid based medium: optimization, efficiency and interferences. *J. Anal. At. Spectrom.* **35** (2020), 1380–1388.

[7] Hu J., Sturgeon, R.E., Nadeau K., Hou X., Zheng C., Yang L.: Copper ion assisted photochemical vapor generation of chlorine for its sensitive determination by sector field inductively coupled plasma mass spectrometry. *Anal. Chem.* **90** (2018), 4112–4118.

[8] Zeng W., Hu J., Chen H.J., Zou Z.R., Hou X.D., Jiang X.D.: Cobalt ion-enhanced photochemical vapor generation in a mixed acid medium for sensitive detection of tellurium(IV) by atomic fluorescence spectrometry. *J. Anal. At. Spectrom.* **35** (2020), 1405–1411.

[9] Gao Y., Xu M., Sturgeon R.E., Yang L.: Metal ion-assisted photochemical vapor generation for the determination of lead in environmental samples by multicollector-ICPMS. *Anal. Chem.* **87** (2015), 4495–4502.

[10] Tan Q., Pan Y., Liu L., Shu S., Liu Y.: Determination of ultratrace tellurium in water by hydride generation atomic absorption spectrometry using online separation and pre-concentration with nano-TiO_2 microcolumn. *Microchem. J.* **144** (2019), 495–499.

[11] Filella M., Reimann C., Biver M., Rodushkin I., Rodushkina K.: Tellurium in the environment: Current knowledge and identification of gaps. *Environ. Chem.* **16** (2019) 215–228.

[12] Ba L.A., Mandy D., Jamier V., Jacob C.: Tellurium: an element with great biological potency and potential. *Org. Biomol. Chem.* **8** (2010), 4203–4216

Construction and application of the amperometric uric acid biosensors based on the covalent immobilization of uricase by different strategies

Sofiia Tvorynska[a, b, *], Jiří Barek[a], Bohdan Josypčuk[b]

[a] *Charles University, Faculty of Science, Department of Analytical Chemistry, UNESCO Laboratory of Environmental Electrochemistry, Hlavova 2030/8, 128 43 Prague 2, Czech Republic*
[b] *J. Heyrovský Institute of Physical Chemistry of the Czech Academy of Sciences, Dolejškova 3, 182 23 Prague 8, Czech Republic* ✉ *sofiia.tvorynska@jh-inst.cas.cz*

Keywords
amalgam electrode
amperometric biosensor
enzymatic mini-reactor
uric acid
uricase

Abstract
In this work, a promising combination of a biosensor based on the enzymatic mini-reactor with the detection principle of four-electron reduction of the consumed oxygen at highly negative potential has been developed for uric acid determination using flow injection analysis. The construction of the biosensor provides a spatial segregation of the biorecognition (uricase-based mini-reactor) and detection (tubular detector of silver solid amalgam (TD-p-AgSA)) parts. To find out the most appropriate enzyme immobilization protocol, three different strategies of the covalent attachment for uricase from *Bacillus fastidiosus* have been compared. It was found that the biosensor with the mini-reactor based on the covalent attachment of uricase via glutaraldehyde to $-NH_2$ functionalized mesoporous silica powder MCM–41 showed extremely high stability (>1 year) and reusability (at least 600 measurements) The biosensor's practical applicability was confirmed by successful determination of uric acid in human urine.

1. Introduction

Uric acid is an important metabolic product of purine. The normal concentration range of uric acid is 240–520 μmol L^{-1} in serum and 1.4–4.4 mmol L^{-1} in urinary excretion. An abnormal uric acid level is related to many disorders [1]. Thus, simple, rapid, and reliable methods for the determination of uric acid in human physiological fluids are indispensable for diagnosing these diseases.

The use of uricase-based biosensors enhances the selectivity of uric acid determination in the biological matrices. Uricase catalyses the oxidation of uric acid to form allantoin, CO_2, and H_2O_2. Most of the previously reported uric acid

biosensors are based on the uricase attachment at the working electrode surface through additional supports with the amperometric monitoring of the enzymatically generated H_2O_2 [1]. However, such biosensors frequently suffer from i) the short lifetime, and ii) interference effect.

The aim of this work is the development of the uric acid biosensor with a uricase-based mini-reactor coupled with the amperometric monitoring of the oxygen consumption, which would help to overcome both above-mentioned limitations. The special attention is focused on the critical comparison of three different strategies for the covalent uricase immobilization.

2. Experimental

2.1 Reagents

All chemicals were of p. a. or better grade. Uricase from *Bacillus fastidiosus* (uricase, ~9 U mg^{-1}), uric acid (≥99.0%), glutaraldehyde (GA, grade II, 25% aqueous solution), *N*-(3-dimethylaminopropyl)-*N*'-ethylcarbodiimide hydrochloride (EDC, ≥98.0%), *N*-hydroxysuccinimide (NHS, ≥97.0%), (3-aminopropyl)triethoxysilane (APTES), (3-glycidyloxypropyl)trimethoxysilane (GOPTMS), mesoporous silica powder SBA−15 (surface area ≈ 600 m^2g^{-1}), mesoporous silica powder MCM−41 (surface area ≈ 1000 m^2g^{-1}) were purchased from Sigma Aldrich.

2.2 Instrumentation

Amperometric measurements were carried out at 25±0.5 °C using computer-controlled electrochemical stand (Polaro-Sensors, Czech Republic) with Multi-Elchem v. 3.1 software (J. Heyrovský Institute of Physical Chemistry of the CAS). Flow injection analysis (FIA) with the three-electrode laboratory-made flow-through cell was used: working electrode − tubular detector of polished silver solid amalgam [2] (TD-p-AgSA, laboratory-made, inner diameter (ID) 0.5 mm, the amalgam tube length 6.0 mm), reference electrode − a miniaturized saturated calomel electrode based on silver paste amalgam [3] (laboratory-made, it has the same potential as a saturated calomel electrode – SCE), auxiliary electrode − platinum wire (diameter 1.0 mm, length 10 mm). The system for FIA with electrochemical detection comprised of a linear syringe pump, a 2-position 6-port sample injector valve, an injection loop laboratory-made of Teflon® (PTFE) tubing (100 μL), a solenoid operated micro-pump, an enzymatic mini-reactor, and a flow-through cell.

2.3 Preparation of powders for uricase-based mini-reactors by different strategies

- Strategy A: uricase coupling by its $-NH_2$ groups through GA to $-NH_2$ functionalized SBA–15 or MCM–41 forming stable secondary amine bonds (uricase–$SBA15_{(GA)}$, uricase–$MCM41_{(GA)}$).
- Strategy B: uricase immobilization by its –COOH groups via EDC/NHS to SBA15–NH_2 forming stable amide bonds (uricase–$SBA15_{(EDC/NHS)}$).
- Strategy C: uricase attachment by its $-NH_2$ groups directly to SBA15–epoxy forming stable secondary amine bonds (uricase–$SPA15_{(epoxy)}$).

The detailed procedures of the enzymatic powders preparation are described in [4]. Each enzymatic powder has been placed into Plexiglas® tube (ID 4 mm, height of the enzymatic powder column ≥5.0 mm) forming the enzymatic mini-reactor.

3. Results and discussion

3.1 Principle of uric acid detection with the proposed biosensor

The detection of uric acid is based on the amperometric monitoring of oxygen dissolved in the carrier solution, the concentration of which decreases as the result of the enzymatic reaction. Oxygen dissolved in carrier solution can be determined via its reduction using four-electron pathway at potential more negative than –1000 mV on mercury and silver solid amalgam electrodes (AgSAE)

$$O_2 + 2\,H_2O + 4\,e^- \rightarrow 4\,OH^- \qquad (1)$$

that leads to higher sensitivity of measurements [5]. The highly negative potential of hydrogen evolution on AgSAE enables its successful application up to –1900 mV in aqueous medium.

3.2 Influence of the different strategies and powders for the covalent uricase immobilization

The biosensor response strongly depends on the enzyme attachment strategy and the microenvironment generated around the enzyme [6]. Therefore, three strategies for the covalent uricase immobilization at mesoporous silica powder SBA–15, which differ in the functional groups anchored to SBA–15, coupling reagents, and the enzymatic groups involved in the binding, have been compared (Fig. 1(A)).

The strategies used for uricase covalent coupling have the major effect and the uric acid biosensor responses decrease in the order strategy A → strategy B → strategy C (Fig. 1(B)).The difference between the peak currents obtained with uricase–$SBA15_{(GA)}$ (strategy A) and uricase–$SBA15_{(EDC/NHS)}$ (strategy B)

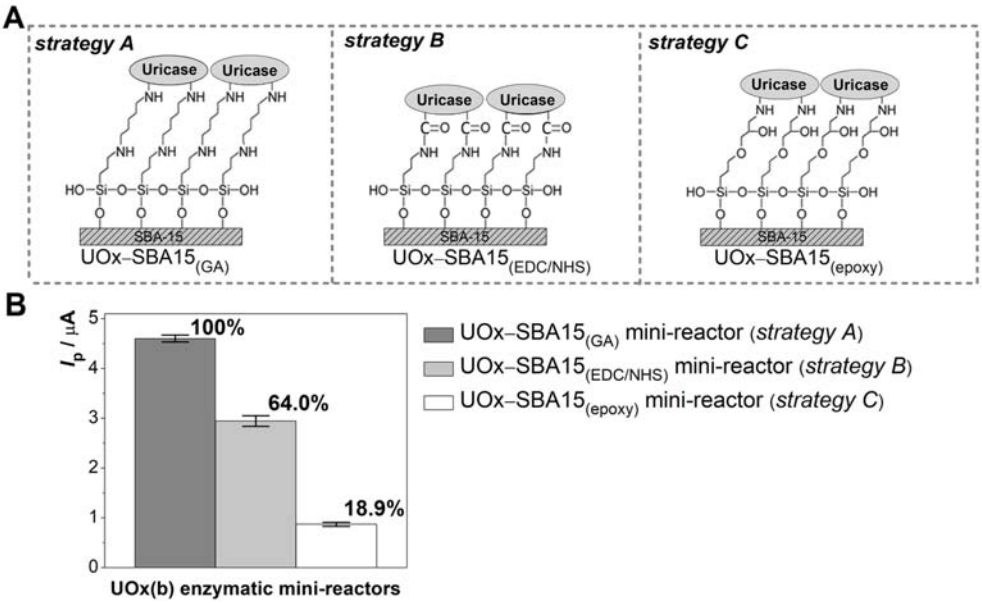

Fig. 1 (A) Scheme of the covalent uricase immobilization at SBA–15 using three different strategies. (B) Comparison of the current responses of the biosensors with various enzymatic mini-reactors based on the covalently immobilized of uricase (UOx) at SBA–15 by three different strategies. Experimental conditions: c(uric acid) = 0.5 mmol L^{-1}, E_{det} = −1100 mV, v_{flow} = 0.1 mL min^{-1}, V(uric acid) = 40 µL, carrier solution: 0.1 mol L^{-1} borate buffer, pH = 9.1.

mini-reactor s could be attributed to i) difference in the reactivity of the activation agents and ii) difference in their geometry effect and molecular spacer, affecting the enzyme loading [4, 7]. The lowest peak current of the biosensor with uricase–$SBA15_{(epoxy)}$ mini-reactor could be explained by the fact that amount of epoxy groups introduce to the surface of 1 g SBA–15 is 6.1 times lower than $–NH_2$ groups. Evidently, the decrease of the support functional group content might decrease the ability to bind enzyme.

The covalent attachment of uricase at two different mesoporous silica powders (SBA–15 and MCM–41) has been compared using the most suitable strategy A. The biosensor with uricase–$MCM41_{(GA)}$ mini-reactor to 0.5 mmol L^{-1} uric acid showed the slightly higher peak current compared to the biosensor with uricase–$SBA15_{(GA)}$ one. These data are in a good agreement with the contents of $–NH_2$ groups introduced on the support surfaces. Next, it was found that 1 mL of uricase solution with the activity of 13.4 U mL^{-1} is sufficient to reach a complete enzyme coverage of the surface of 50 mg MCM41–NH_2 powder.

3.2 Optimization of the biosensor response

The influence of the key parameters, included the detection potential (E_{det}), pH and composition of carrier solution, the flow rate of carrier solution, (v_{flow}), and

Table 1
The optimal parameters for uric acid determination with the developed flow amperometric biosensor consisting of uricase–MCM41$_{(GA)}$ mini-reactor and TD-p-AgSA.

Parameter	Studied range	Optimal value
E_{det} / mV	(–200)–(–1500)	–1100
v_{flow} / mL min^{-1}	0.05–0.3	0.1
V(uric acid) / µL	20–180	40
pH and composition of carrier solution	7.0–8.5 (0.1 mol L^{-1} phosphate buffer) 8.0–10.0 (0.1 mol L^{-1} borate buffer) 9.0–10.5 (0.1 mol L^{-1} carbonate buffer)	9.1 (0.1 mol L^{-1} borate buffer)

Table 2
The analytical performances of the developed flow uric acid biosensor.

Parameter	Value(s)
Linear range / µmol L^{-1}	50–800
LOD / µmol L^{-1}	18.5
LOQ / µmol L^{-1}	56.5
Repeatability ($RSD_{n=11}$) / %	2.8
Reproducibility ($RSD_{n=9}$) / %	3.9
Storage stability / %	90.5% / 365 days
Operational stability / %	98.5% / 600 measurements / 50 days

the injected volume of the substrate (V(uric acid)) on the response of the biosensor with uricase–MCM41$_{(GA)}$ mini-reactor was optimized (Table1).

3.3 Analytical performances of the developed flow uric acid biosensor

Under the optimized conditions, the analytical characteristics of uric acid biosensor consisting of TD-p-AgSA with uricase–MCM41$_{(GA)}$ mini-reactor have been evaluated (Table 2). It could be summarized that the newly developed biosensor provided good results in terms of sensitivity, repeatability, and reproducibility for uric acid determination. The reached extremely high storage and operational stability of the developed biosensor would help to significantly reduce the cost of uric acid biosensing.

The proposed flow uric acid biosensor with uricase–MCM41$_{(GA)}$ mini-reactor was tested for uric acid determination in human urine using the standard addition method (Fig. 2). The concentration of uric acid in the urine sample was found to be 2.98±0.04 mmol L^{-1}, which is in the normal range for the healthy people.

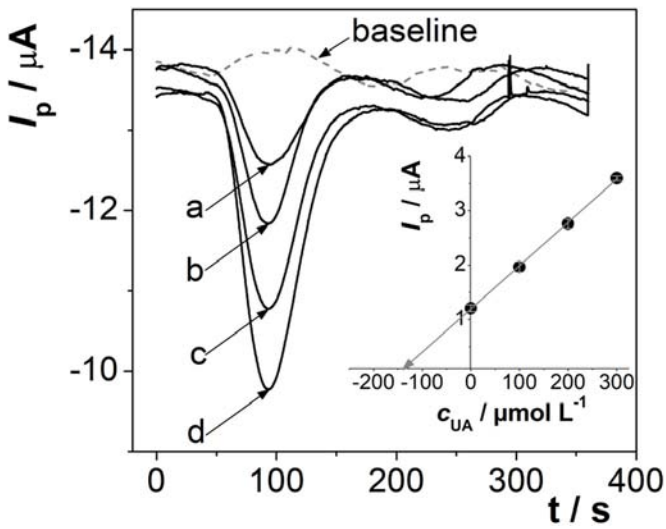

Fig. 2 Amperograms of FIA of the urine sample with the developed flow biosensor based on uricase–MCM41(GA) mini-reactor and TD-p-AgSA using a method of the standard addition: (a) 0.1 mL of urine sample + 1.9 mL of 0.1 mol L^{-1} borate buffer, pH = 9.0, (b) 0.1 mL of urine sample + 1.7 mL of 0.1 mol L^{-1} borate buffer, pH = 9.0 + 0.2 mL of 1.0 mmol L^{-1} uric acid, (c) 0.1 mL of urine sample + 1.5 mL of 0.1 mol L^{-1} borate buffer, pH = 9.0 + 0.4 mL of 1.0 mmol L^{-1} uric acid, (d) 0.1 mL of urine sample + 1.3 mL of 0.1 mol L^{-1} borate buffer, pH = 9.0 + 0.6 mL of 1.0 mmol L^{-1} uric acid. Inset: the quantification of uric acid.

4. Conclusions

A significant achievement of this work is the clarification of the optimal technique for uricase immobilization and the development of the perspective type of the flow amperometric biosensor based on the spatially separated enzymatic (uricase–$MCM41_{(GA)}$ mini-reactor) and detection (TD-p-AgSA) parts. The biosensor advantage of the extremely high storage and operational stability accompanied by the benefits of FIA like the high sample throughput indicated the proposal of a perspective platform for uric acid biosensing in the biological matrix.

Acknowledgments

This research was performed within the framework of Specific Charles University Research (SVV 260560). Financial support provided by the Grant Agency of Charles University (Project 1356120) and by the Grant Agency of the Czech Republic (Project 20-01589S) is gratefully acknowledged.

References

[1] Erden P.E., Kilic E.: A review of enzymatic uric acid biosensors based on amperometric detection. *Talanta* **107** (2013), 312–323.

[2] Yosypchuk O., Barel J., Yosypchyk B.: Tubular detector of silver solid amalgam for electrochemical measurements in flow systems. *Electroanalysis* **24** (2012), 2230–2234.

[3] Yosypchuk B., Barek J., Yosypchuk O.: Preparation and properties of reference electrodes based on silver paste amalgam. *Electroanalysis* **23** (2011), 2226–2231.
[4] Tvorynska S., Barek J., Josypčuk B.: Flow amperometric uric acid biosensors based on different enzymatic mini-reactors: A comparative study of uricase immobilization. *Sens. Actuators B* **344** (2021), 130252.
[5] Tvorynska S., Barek J., Josypčuk B.: Acetylcholinesterase-choline oxidase-based mini-reactors coupled with silver solid amalgam electrode for amperometric detection of acetylcholine in flow injection analysis. *J. Electroanal. Chem.* **860** (2020), 113883.
[6] Zucca P., Sanjust E.: Inorganic materials as supports for covalent enzyme immobilization: methods and mechanisms. *Molecules* **19** (2014), 14139–14194.
[7] Wang Y., Hasebe Y.: Carbon felt-based biocatalytic enzymatic flow-through detectors: Chemical modification of tyrosinase onto amino-functionalized carbon felt using various coupling reagents. *Talanta* **79** (2009), 1135–1141.

Comparison of radiation sources for atomic fluorescence spectrometry

Barbora Štádlerová[a, b, *], Jiří Dědina[a], Stanislav Musil[a]

[a] *Institute of Analytical Chemistry of the Czech Academy of Sciences, Veveří 97, 602 00 Brno, Czech Republic* ✉ *stadlerova@iach.cz*
[b] *Charles University, Faculty of Science, Department of Analytical Chemistry, Hlavova 8/2030, 128 43 Prague 2, Czech Republic*

Keywords
atomic fluorescence spectrometry
bismuth
hydride generation
radiation source

Abstract
The performance of two radiation sources – an electrodeless discharge lamp and a boosted-discharge hollow cathode lamp – in the atomic fluorescence spectrometry was studied for bismuth as a model analyte at 222.8 nm line. An in-house assembled nondispersive atomic fluorescence spectrometer was modified to operate with both radiation sources. Hydride generation was employed for sample introduction and a miniature diffusion flame for atomization. Limits of detection of 1.8 and 11 ng L^{-1} for the electrodeless discharge lamp and the boost-discharge hollow cathode lamp, respectively, were achieved at optimal operational parameters. Around 5 times higher sensitivity obtained with the electrodeless discharge lamp suggests significantly higher emission intensity of the electrodeless discharge lamp at 222.8 nm line.

1. Introduction

Atomic fluorescence spectrometry (AFS) coupled with hydride generation (HG) is a sensitive method used for ultra-trace analysis of several elements from the Groups IVA–VIA of the periodic table. Among its advantages are, e.g., low purchase and operational costs and the possibility of reaching extremely low limits of detection (*LOD*s). An atomic fluorescence spectrometer can be also constructed in a laboratory. The choice of a radiation source is crucial as the intensity of fluorescence radiation detected is proportional to the intensity of the excitation radiation [1–3]. The most common radiation source in commercial AFS instruments is a boosted-discharge hollow cathode lamp (BD-HCL) [4] while an electrodeless discharge lamp (EDL) has gained a particular importance in laboratory assembled instruments [1, 2, 5, 6].

EDLs consist of the element, or its salt, sealed in a quartz bulb filled with inert gas at low pressure. When a radiofrequency field is applied, the inert gas is ionized, the element is vaporized and the atoms are excited, which results in the emission of a characteristic spectrum [7]. BD-HCLs consist of an anode,

a cylindrical cathode (between which the normal sputtering discharge operates) and a second "hot" cathode (providing a secondary discharge). The secondary discharge improves excitation efficiency of the atoms sputtered in the discharge plasma [8]. The BD-HCLs are available on the market for a broad range of analytes while the EDLs are limited mainly to hydride forming elements, mercury, cadmium, zinc and a few others. The crucial question arises with comparison of emission intensity for both sources that has a direct impact on sensitivity in AFS. To our best knowledge, a comparison of the EDL and BD-HCL with the use of the same detector has never been reported for AFS.

The main aim of this study was to draw a comparison between these two radiation sources using bismuth as a model analyte. Following our previous studies with Bi EDL [2], the performance of the BD-HCL was optimized using a nondispersive atomic fluorescence spectrometer and a miniature diffusion flame atomizer for atomization of bismuthane.

2. Experimental

2.1 Reagents and chemicals

Deionized water was used for preparation of all solutions. A 0.5% (*m/v*) $NaBH_4$ in 0.4% (*m/v*) KOH was used as a reducing agent. A stock solution of 1 mol L^{-1} HCl (Merck, Germany) was used as a carrier and blank. Working Bi solutions were prepared fresh daily by serial dilution of a 1000 mg L^{-1} Bi standard (Sigma-Aldrich, Germany).

2.2 Atomic fluorescence spectrometer

A nondispersive atomic fluorescence spectrometer constructed in our laboratory, described in detail in [1], was employed. It consists of three main components: radiation source, atomizer and photomultiplier tube (Fig.1). A Bi EDL (Perkin-Elmer, System 2) was used with feeding power square-wave modulated at frequency of 40 Hz. The operating current for the EDL was 400 mA. A Bi BD-HCL (Photron, Australia) was the second radiation source employed. The photomultiplier tube was placed perpendicularly to the lamp to collect the fluorescence radiation emitted from the atomizer. The fluorescence radiation passed through an interference filter (222.63 nm, FWHM 10 nm, Melles Griot), covering the Bi fluorescence line at 222.8 nm, and was then focused into a solar-blind photomultiplier tube (MH 1922, 165–320 nm, Perkin-Elmer Optoelectronics, USA), which was employed as the detector. The preamplifier, control unit and a dedicated software were designed by DIRAM company (Prague, Czech Republic).

A miniature fibre optics UV-vis spectrometer BLACK-Comet C (StellarNet, USA) was employed to acquire the emission spectra of the lamps.

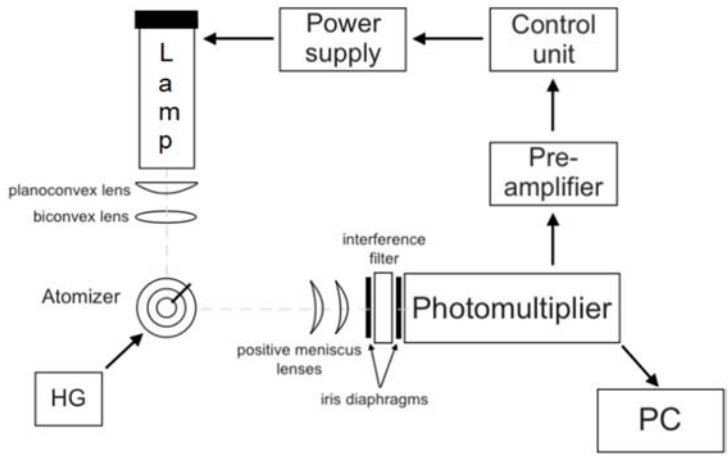

Fig. 1 Experimental setup of the atomic fluorescence spectrometer.

2.3 Hydride generator and atomizers

A flow injection hydride generator (HG) was employed [2]. The reducing agent (1.2 mL min^{-1}) and carrier (4 mL min^{-1}) were pumped by a peristaltic pump Reglo Digital (Ismatec, Switzerland). The manifold was constructed from PTFE tubing (1 mm i.d.). The sample was injected through a 1 mL sample loop into the flow of a carrier and subsequently merged with the reductant. A glass gas-liquid separator (5 mL) with a forced waste removal was employed in order to separate the gas phase containing bismuthane employing carrier argon (80 mL min^{-1}). The gas phase exiting the gas-liquid separator was supplied with an additional flow of argon and hydrogen to maintain a stable flame of the atomizer. The miniature diffusion flame consisted of a vertical quartz support tube (≈ 6 mm i.d.) and the optimal parameters for atomization were as follows: total argon flow rate 500 mL min^{-1}, total hydrogen flow rate 100 mL min^{-1} and observation height 7 mm [2]. All gas flow rates were controlled by mass flow controllers (Omega engineering or Cole-Parmer, USA).

2.4 Procedure and data evaluation

A 1 or 10 μg L^{-1} Bi standard solution was used. The standard was injected 5 s after the signal recording had started (60 s recording in total). The detector output provided signals in μV. Peak area (in μV s) corrected to baseline, or rather sensitivity (in μV s L $μg^{-1}$), and a signal to noise ratio (*SNR*) were the parameters used to evaluate the data. Noise was calculated as an average standard deviation of three blank replicates (each measured for 10 s representing 400 values). *SNR* was determined by dividing the peak height by an average standard deviation of blank.

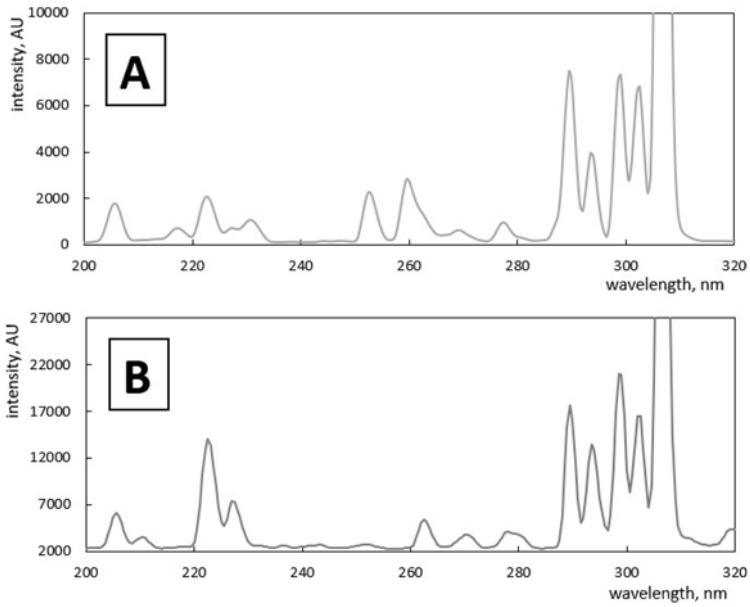

Fig. 2 Emission spectra of (A) electrodeless discharge lamp, and (B) hollow cathode lamp of Bi.

3. Results and discussion

The optical path of the spectrometer was optimized to reach the highest sensitivity and *SNR*. That includes, e.g., the selection of a suitable lens used to focus the radiation beam from the radiation source onto the volume of the flame. Moreover, the mutual distances of the lamp, the atomizer and the detector influence the resulting sensitivity. The geometry and construction of the EDLs and the BD-HCLs is different, so different lenses have to be used in order to reach the best focusing of the radiation. In the case of the EDL, a combination of two UV fused silica lenses was found optimal to focus the emitted radiation onto the atomizer. A planoconvex lens (d = 25 mm, 40 mm focal length) was inserted into the exit orifice of the cavity containing the bulb and a biconvex lens (d = 22 mm, 45 mm focal length) was attached to the rim of the lamp using a lens holder. The radiation beam from the BD-HCL was focused using a planoconvex UV fused silica lens (d = 25 mm; 40 mm focal length). The radius of the beam, when focused onto the flame, corresponded to ≈ 5 and 2 mm, for the EDL and BD-HCL, respectively.

The emission spectra of both lamps were recorded using an optical fibre spectrometer (Fig. 2). More emission lines are present in the spectrum of the EDL (Fig. 2 B). The reason behind this is that the EDL contains a certain amount of impurities, in this case antimony (with emission lines at 207, 218, 229, 231, 253, 260 and 261 nm) and mercury (254 nm), discussed in detail in [2]. This has to be taken into account when Bi is determined in real samples that could possibly contain antimony or mercury and a suitable detection wavelength has to be selected in order to avoid interferences. It should be noted that the intensity on

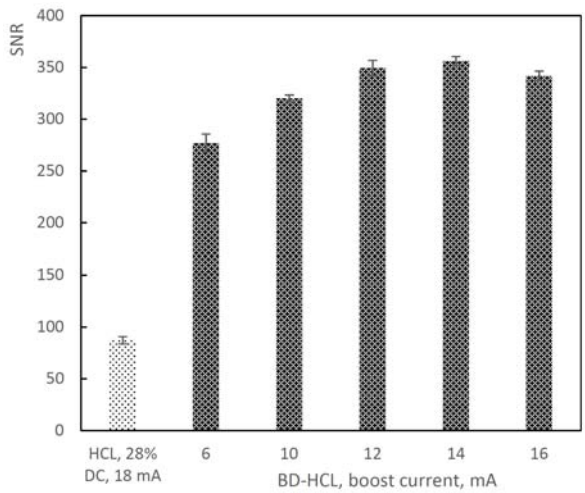

Fig. 3 Comparison of *SNR* for HCL (light) at optimum conditions (28% duty cycle, 18 mA anode current) and BD-HCL (dark) for various boost currents; 10 μg L^{-1} Bi.

y-axes in Fig. 2 does not reflect the true intensity of emitted Bi lines as the spectra were not collected with the same geometry.

The performance of the EDL was carefully optimized in our previous work [2]. This work mainly focused on the optimization of the parameters for the BD-HCL and a subsequent comparison of both.

The main parameters to be optimized were: the anode current, the boost current and the duty cycle (the fraction of one period during which the lamp is on). First, the lamp was operated as HCL (without the boost discharge) and the anode current and the duty cycle were optimized. The optimum conditions for HCL were 18 mA anode current and 28% duty cycle. That means that during a 25 ms period, the lamp is powered only for 7 ms. These conditions were taken as the default conditions for the boost current optimization. The boost current was optimized from 6 to 16 mA (Fig. 3). Not just the highest sensitivity or *SNR* but also the lifespan of the lamp needs to be considered when choosing the optimum conditions. Similar *SNR* values were obtained at 12 and 14 mA of boost current, so 12 mA was selected as optimal. The sensitivity and *SNR* achieved with the BD-HCL at optimum conditions is 7 and 4-fold higher, respectively, than with the HCL.

For comparison of the analytical performance, the calibration curves (0.4–1 and 1–10 μg L^{-1} for EDL and BD-HCL, respectively) were measured and *LOD*s evaluated under the optimum conditions for both radiation sources. The modulation frequency was kept at 40 Hz (25 ms period) while the duty cycle was 52% for the EDL and 28% for the BD-HCL. The *LOD* achieved with the EDL was 8 times lower than with the BD-HCL (Table 1). The sensitivity with the EDL was ca. 5 times higher than with the BD-HCL.

Table 1
Analytical characteristics of bismuth determination by HG-AFS with the EDL and the BD-HCL.

	sensitivity / μV s L μg^{-1}	*LOD* / ng L^{-1}
EDL	122[a]	1.8
BD-HCL	26[a]	11

[a] *SD* < 0.5 μV s L μg^{-1}

4. Conclusion

The most important outcome of this work lies in a direct comparison of two different radiation sources for excitation of atomic fluorescence of Bi using the laboratory-made atomic fluorescence spectrometer. The sensitivity and *SNR* achieved with the EDL are overall better, which undoubtedly reflects the higher emission intensity of the EDL. Nonetheless, the possibility of using BD-HCL is important as it spans the applicability of this instrumentation to more analytes for which the EDL is not commercially available.

Acknowledgments

The support of the Czech Science Foundation (19-17604Y), Czech Academy of Sciences (Institutional support RVO: 68081715) and Charles University (Project SVV260560 and Project GAUK 1048120) is gratefully acknowledged.

References

[1] Musil S., Matoušek T., Currier J. M., Stýblo M., Dědina J.: Speciation analysis of arsenic by selective hydride generation-cryotrapping-atomic fluorescence spectrometry with flame-in-gas-shield atomizer: achieving extremely low detection limits with inexpensive instrumentation. *Anal. Chem.* **86** (2014), 10422–10428.
[2] Štádlerová B., Kolrosová M., Dědina J., Musil S.: Atomic fluorescence spectrometry for ultrasensitive determination of bismuth based on hydride generation – the role of excitation source, interference filter and flame atomizers. *J. Anal. At. Spectrom.* **35** (2020), 993–1002.
[3] Winefordner J. D., Elser R. C.: Atomic fluorescence spectrometry. *Anal. Chem.* ***43*** (1971), 24–42.
[4] Corns W. T., Stockwell P. B., Ebdon L., Hill S. J.: Development of an atomic fluorescence spectrometer for the hydride-forming elements. *J. Anal. At. Spectrom.* **8** (1993), 71–77.
[5] Vyhnanovský J., Yildiz D., Štádlerová B., Musil S.: Efficient photochemical vapor generation of bismuth using a coiled Teflon reactor: Effect of metal sensitizers and analytical performance with flame-in-gas-shield atomizer and atomic fluorescence spectrometry. *Microchem. J.* **164** (2021), 105997.
[6] Chen Y. W., D'Ulivo A.: The determination of bismuth by hydride generation and non-dispersive atomic fluorescence detection. *Anal. Lett.* **22** (1989), 1609–1622.
[7] www.perkinelmer.com/category/electrodeless-discharge-lamps (accessed 11.6.2021)
[8] www.photronlamp.com/collections/super-lamps (accessed 11.6.2021)

Quantum dot luminescent probe for caspase-3/7 imaging inside cells

Markéta Procházková[a, b, *], Michael Killinger[a, b], Karel Klepárník[a]

[a] *Institute of Analytical Chemistry, v.v.i., Czech Academy of Sciences, Veveří 967/97, 602 00 Brno, Czech Republic* ✉ *prochazkova@iach.cz*
[b] *Faculty of Science, Masaryk University, Kotlářská 267/2, 611 37 Brno, Czech Republic*

Keywords
capillary electrophoresis
caspase
fluorescence
ligand-exchange
quantum dot

Abstract
Nowadays luminescent semiconductor quantum dots are widely applied in different areas due to their unique optical properties. Quantum dots can be used as photoluminescent labels with excellent possibilities for high-throughput detection and diagnostics. For most of such applications quantum dots must be coupled to biomolecules, which often represents a fundamental challenge. In this work synthesis and testing of novel quantum dot luminescent probe is presented in this work. The probe enables long-time luminescent imaging of active caspases under microscope.

1. Introduction

Maturation (differentiation) and programmed cell dead (apoptosis) are essential processes for the maintenance of organism homeostasis. With respect of this, caspases play major role as a mediators of cell death via apoptosis, and thus a reasonable scientific effort has been associated with the investigation of their corresponding biological roles. Deregulations of the mediators in apoptotic pathways are linked to a wide range of pathological conditions such as cancer, autoimmune or neurodegenerative diseases, and viral infections. Since the down-regulation and decreased activity of caspase-3/7 is a prognostic indicator of different tumors, an improvement in screening of this enzyme in individual cells proved to be of a diagnostic importance [1–3].

Recent progress of bioanalytical techniques has accelerated the deep understanding of cellular states and development of novel drugs as well as medical diagnosis. To analyze the biological events in single cells, technologies related to fluorescence and luminescence imaging advanced rapidly in the past two decades. Three prominent types of fluorescent molecules have been used for bioimaging: fluorescent proteins, artificially synthesized organic dyes, and fluorescent nanoparticles [4–7].

During the past two decades, quantum dot (QD) nanoparticles have become frequent components of highly luminescent tags, probes, and sensors with a

broad application in bioanalytical chemistry [8, 9]. Compared with traditional luminescent organic dyes, QDs exhibit excellent photophysical properties, for example, high photostability, broad excitation, and narrow symmetric emission bands. The emission wavelengths of QDs, dependent on their sizes, are tunable by particle synthesis. Moreover, their high extinction coefficients make them ideal for absorption and transfer of relatively large amounts of energy [10]. Water-dispersed QD particles are usually charged. Therefore, capillary electrophoresis with laser induced fluorescence (CE-LIF) is a method of choice for analyses of the QD surface modifications including determination of particle effective charge [11, 12]. Bioanalytical applications of QDs include luminescent labeling and bioconjugation of biological macromolecules, in vivo animal imaging, cell tracking, or pathogen and toxin detection [13]. Recently luminescent semi-conductor QDs are widely applied in different areas due to their unique optical properties. QDs can be used as photoluminescent labels with excellent possibilities for high-throughput detection and diagnostics. Although QDs have a lot of advantages over organic dyes, most of the techniques that have been developed for QD functionalization and bioconjugation, are more complicated than the corresponding techniques for organic fluorescent dyes [14].

2. Experimental

2.1 Reagents and chemicals

The following chemicals were used for synthesis CdTe core-type quantum dots (COOH functionalized; Sigma-Aldrich, USA), specific peptide composed of GTADEVDTSC sequence of amino acids with purity 95.44% (ProteoGenix, France) and quencher BHQ-2 Succinimidyl Ester (Biosearch Technologies, USA). Human recombinant caspase-3 protein (Abcam, UK) was used as a standard for model measurements. Coumarin 334 (Sigma-Aldrich, USA) was used as a marker of electro-osmotic flow (EOF) in CE-LIF. Tris(hydroxymethyl)aminomethane (TRIS) and 3-(*N*-morpholino)propanesulfonic acid (MOPS) (Sigma-Aldrich, USA) were used as a background electrolyte (BGE, 50 mM, pH = 9) for CE-LIF. DMSO (Penta, CR) and acetonitrile (MeCN), (VWR, CR) were used as solvents in synthesis of the fluorescent probe. Sodium carbonate, sodium bicarbonate (Lachema, CR) were used as a buffering solution in DMSO for the second step of synthesis of the luminescent probe.

2.2 Instrumentation

The QDs and their conjugates were analyzed by a laboratory built CE-LIF system. A laser diode, RLTMLL-405 Series (Roithner Lasertechnik, Austria) with 405/10 nm laser cleanup filter (MaxDiodeTM; Shamrock, USA) was used as the excitation source. The luminiscence emission was collected by a microscope

objective (40×0.65 NA, Oriel) positioned perpendicularly to the separation capillary and to the excitation laser beam. A PMT detector (R647; Hamamatsu, Japan) was used for the monitoring of luminescence emission at 607±35 nm selected by a system of two optical filters including a 405 nm long pass edge filter (EdgeBasic™) and a 607±35 nm band-pass filter (BrightLine®). The detector signal was recorded at a sampling rate of 25 Hz by the data acquisition and evaluation system CSW 1.6 (Data Apex, Czech Republic). The CE separation was driven by Spellman CE 1000R high voltage power supply. Before each analysis, the bare fused-silica capillary of 75 μm id and 375 μm od (Polymicro Technologies, USA) was rinsed successively with 0.1 M NaOH, water, and finally with the running buffer. The samples were introduced electrokinetically at a voltage of +5 kV. At this high positive voltage, a strong electroosmotic flow (EOF) carried the sample, including the quantum dots and their conjugate with peptide, toward the detector located at the grounded end of the separation capillary. The velocity of the EOF was determined using coumarin, a neutral fluorescent marker.

Luminescence excitation and emission spectra of the probe were recorded by spectrofluorometer FP-8500 (Jasco) at 25°C in 3 mm quartz cuvette. Luminescence emission spectra were recorded in the range from 550 to 650 nm with excitation at 405 nm.

3. Results and discussion

3.1 Luminescent probe conjugation – two step synthesis

The luminescent probe is synthesized in two steps. In the first step of the synthesis, water-soluble QDs were conjugated with a specifically designed peptide using a ligand-exchange approach, where the SH- group of cysteine at the end of the peptide substitutes the mercaptosuccinic acid at the QD surface by forming covalent bond with the Cd atom in nanoparticle crystal lattice (Fig. 1). In the second step the opposite terminal amino group of the peptide reacts with the BHQ-2 quencher via succinimidyl group (Fig. 2). In more detail, the peptide was dissolved at concentration 1 mg mL^{-1} in a solution of ultrapure water and acetonitrile at a ratio: 1:3. QDs with diameter of 3.5 nm and the molecular weight of 79 kDa were dissolved in ultrapure water at a concentration of 1 mg mL^{-1}. The conjugation of QDs and the peptide was carried out in a 1.5 mL Eppendorf tube at a molar ratio of QD: peptide 1:100 in darkness with constant shaking overnight. The excess of the unreacted peptide was then removed by centrifugal filtration (14,000 rpm, for 15 min) by a membrane with 30 kDa cut-off of centrifugal filter units (AMICON, Merck). The filtrate was then washed twice with ultrapure water. The product of the first step synthesis was analyzed by CE-LIF. After the control analysis, the product was washed twice with DMSO and finally eluted using carbonate buffer solution in DMSO to get an approximate concentration of 1 mg mL^{-1} of the solution.

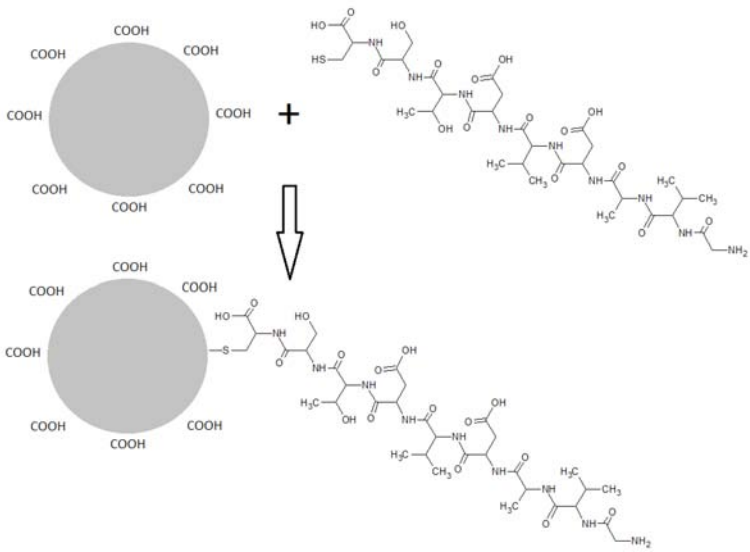

Fig. 1 Reaction scheme of the ligand-exchange part of synthesis.

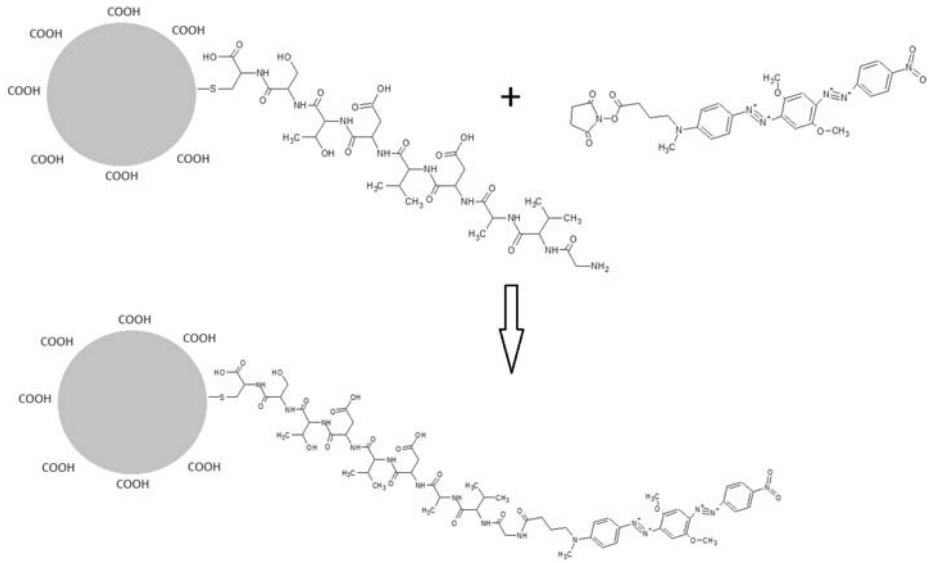

Fig. 2 Reaction scheme of the second part of synthesis with the final product.

In the second step, the BHQ-2 quencher was dissolved at concentration of 1 mg mL^{-1} in DMSO. Immediately after the first step of the synthesis, the QD-peptide conjugate was mixed with solution of the quencher BHQ-2 at a molar ratio QDs peptide conjugate: BHQ-2, 1:10 in darkness with constant shaking overnight. The excess of the quencher was again removed using centrifugal filter units (AMICON, Merck) as in the first step. The final product was washed twice with

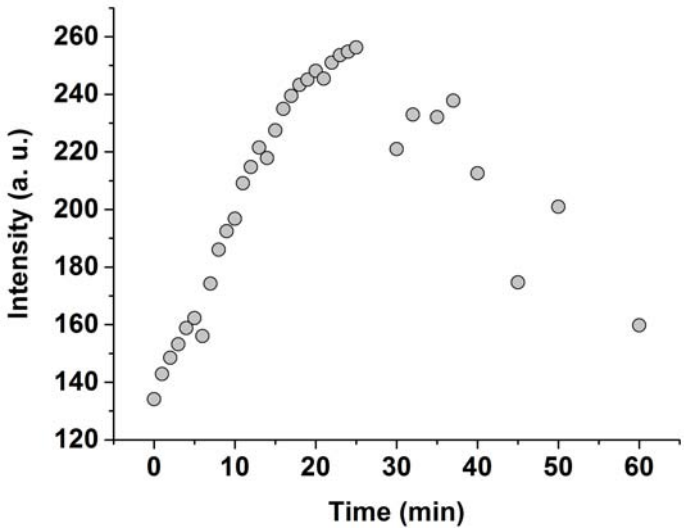

Fig. 3 Reaction of the luminescent probe (c = 1 mg mL^{-1}) with Recombinant caspase-3 protein (m = 1.5 pg).

DMSO and finally eluted in DMSO in an approximate concentration of 1 mg mL^{-1} and stored at 4 °C. All the reactions were performed at room temperature.

3.2 Luminescent probe for imaging of active caspase enzyme

A model reaction of the synthetized luminescent probe with active human recombinant caspase-3 protein was monitored in quartz cuvette of fluorimeter. The caspase enzyme reaction is based on the specific cleavage of the DEVD peptide sequence. Thus, the BHQ-2 quencher is released, and consequently the red light luminescence of the quantum dot emitted. Luminescence emission spectra of the reaction were recorded in the range from 550 to 650 nm with excitation at 405 nm in time (Fig. 3). The synthetized luminescent probe proved to enable much longer imaging of active caspases than commercially available probes.

4. Conclusions

Two step synthesis of luminescent probe based on ligand-exchange in the first step and the specific reaction of amino group in the second step was optimized. The luminescence properties of the final product were checked by time course of active recombinant caspase protein reaction under the model conditions in fluorimeter. The novel luminescent probe enables long-time imaging of active caspases in living cells or tissues.

Acknowledgments

The paper was founded by Czech Foundation Agency, grant number 20-00726s.

References

[1] Cohen G. M.: Caspases: The executioners of apoptosis. *Biochem. J.* **326** (1997), 1–16.
[2] Broz P.: Caspase target drives pyroptosis. Nature, news & views. *Imunology* **526** (2015), 642–643.
[3] Minor L. K.: *Handbook of Assay Development in Drug Discovery.* New York, Taylor & Francis 2006.
[4] Ozawa T., Yoshimura H., Kim S. B.: Advances in fluorescence and bioluminescence imaging. *Anal. Chem.* **85** (2013), 590–609.
[5] Cheng J., Tian L., Ma J., Gong Y., Zhang Z., Chen Z., Xu B., Xiong H., Li C., Huang Q.: Dying tumor cells stimulate proliferation of living tumor cells via caspase-dependent protein kinase Cδ activation in pancreatic ductal adenocarcinoma. *Mol. Oncol.* **9** (2015), 105–114.
[6] Shaulov-Rotem Y., Merquiol E., Weiss-Sadan T., Moshel O., Salpeter S., Shabat D., Kaschani F., Kaiser M., Blum G.: A novel quenched fluorescent activity-based probe reveals caspase-3 activity in the endoplasmic reticulum during apoptosis. *Chem. Sci.* **7** (2016), 1322–1337.
[7] Ostapchenko V.G., Snir J., Suchy M., Fan J., Cobb M.R., Chronik B.A., Kovacs M., Prado V.F., Hudson R.H.E., Pasternak S.H., Prado M.A.M., Bartha R.: Detection of active caspase-3 in mouse models of stroke and Alzheimer's disease with a novel dual positron emission tomography/fluorescent tracer [^{68}Ga]Ga-TC3-OGDOTA. *Contrast Media Mol. Imaging* 2019, https://doi.org/10.1155/2019/6403274
[8] Blanco-Canosa J.B., Wu M., Susumu K., Petryayeva E., Jennings T.L., Dawson P.E., Algar W.R., Medintz I.L.: Recent progress in the bioconjugation of quantum dots. *Coordin. Chem. Rev.* **263** (2014), 101–137.
[9] Petryayeva E., Algar W.R., Medintz I.L.: Quantum dots in bioanalysis: a review of applications across various platforms for fluorescence spectroscopy and imaging. *Appl. Spectrosc.* **67** (2013), 215–252.
[10] Klostranec J.M., Chan W.C.W.: Quantum dots in biological and biomedical research: recent progress and present challenges. *Adv. Mater.* **18** (2006), 1953–1964.
[11] Sang F.M., Huang X.Y., Ren J.C.: Characterization and separation of semiconductor quantum dots and their conjugates by capillary electrophoresis. *Electrophoresis* **35** (2014), 793–803.
[12] Liskova M., Voracova I., Kleparnik K., Hezinova V., Prikryl J., Foret F.: Conjugation reactions in the preparations of quantum dotbased immunoluminescent probes for analysis of proteins by capillary electrophoresis. *Anal. Bioanal. Chem.* **400** (2011), 369–379.
[13] Jamieson T., Bakhshi R., Petrova D., Pocock R., Imani M., Seifalian A.M.: Biological applications of quantum dots. *Biomaterials* **28** (2007), 4717–4732.
[14] Foubert A., Beloglazova N.V., Rajkovic A., Sas B., Madder A., Goryacheva I.Y., Saeger S.D.: Bioconjugation of quantum dots: Review & impact on future application. *TrAC – Trend. Anal. Chem.* **83** (2016), 31–48.

Development of approaches for obtaining the chromatographic profiles of phenolics and amino acids of biotechnological *Iris sibirica* L. raw plant material

Dmitry Karpitsky[a,*], Elena Bessonova[a], Lyudmila Kartsova[a], Lyudmila Tikhomirova[b]

[a] *Saint-Petersburg State University, Institute of Chemistry, Department of Organic Chemistry, Universitetskiy pr. 26, 198504 Saint-Petersburg, Russian Federation* ✉ *karpitskyda@mail.ru*
[b] *Altai State University, Institute of Chemistry, Department of Organic Chemistry, Krasnoarmeysky pr. 90, 656099 Barnaul, Russian Federation*

Keywords
amino acids
design of experiment
flavonoids
HPLC-DAD-MS
Iris sibirica L.

Abstract
Biotechnological *Iris sibirica* L. raw plant material is perspective in medicine. One of the key moments is the regulation of plant metabolism with phytohormones. In this study, the conditions for selective separation of phenolic compounds and amino acids in the leaves of *Iris sibirica* L. by HPLC coupled with diode-array detection and electrospray ionization tandem mass spectrometry were optimized. The schemes for effective extraction of analytes from raw plant materials for HPLC analysis were developed using fractional factorial experimental design. The main factors that affected the extraction efficiency were obtained. Using the developed technique, chromatographic profiles of extracts of *Iris sibirica* L. grown on nutrient media with different phytohormones concentrations were obtained. It was shown the effect of different concentrations of hormones in nutrient media on plant metabolism and provoked plant stress. So, this method can be used for controlling the biotechnology of *Iris sibirica* L.

1. Introduction

Medicinal plants of the genus *Iris* are widely known for their valuable properties. Their extracts have antioxidant, antibacterial, antiviral, anti-inflammatory properties due to the accumulation of flavones and isoflavones, flavonoids, xanthones, isoprenoids steroids, and others [1]. Widely distributed in Russia *Iris sibirica* L. is promising from a medicinal point of view [2], but its phytochemical composition has not been studied in detail yet, which makes it a promising subject for research. Moreover, the amino acid composition of the *Iris genus* has been insufficiently studied, but it can give more information about plant stress and metabolism [3].

Biologically active compounds are traditionally obtained from wild-growing plants. However, despite the wide disturbance of *Iris sibirica* L. in Russia, this approach threatens biological diversity. Biotechnologies such as micropropagation and hydroponics are new and perspective solutions for the industrial use of medicinal plants.

At Altai State University biotechnological approaches for *Iris sibirica* L. are being developed [4]. However, it is still unclear which growing conditions are optimal and how to effectively control such production. Moreover, there is a lack of suitable methods for qualitative and quantitative analysis of bioactive compounds in plants. So, the aims of this study were to establish chromatographic determination of phenolic compounds and amino acids in leaves of *Iris sibirica L.* and to obtain chromatographic profiles of these characteristic metabolites in biotechnological Iris *sibirica L.* grown on various nutrient media.

2. Experimental

2.1 Reagents and chemicals

Deionized water was prepared from distilled water using Aquilon D-301 (Russia). All chemicals and reagents (the highest commercially available purity) were purchased from Reachim, Fluka, Baker, Acros Organics, and Sigma Aldrich.

2.2 Instrumentation

HPLC analysis was carried out using an HPLC LC-20 Prominence (Shimadzu) diode array detector and LC-DAD-ESI/MS (Shimadzu LC-30 Nexera) with Q-TOF MS Maxis (Bruker). Separation of flavonoids was carried out on Luna C18 column (150×2.0 mm, 5 μm; Phenomenex, USA), for amino acids was used C18 column (150×2.1 mm, 2,6 μm; Kinetex, USA). Experimental plans were made with Minitab 19 software.

2.3 Conditions for HPLC-DAD-ESI/MS determination of flavonoids and amino acids

HPLC-DAD-ESI/MS conditions for the separation of polyphenols and amino acids: (A) 0.1% formic acid in water, (B) 0.1% formic acid in acetonitrile gradient mode; ESI: capillary voltage –3.5 kV, nebulizer gas flow rate: 3 L min^{-1}, drying gas flow rate 10 L min^{-1}, and 180 °C.

2.4 Raw plant material

Microclonally propagated regenerating plants and aeroponic plants were grown in the Department of Plant Biotechnology of the Altai State University.

2.5 Extraction method

The dried powdered raw plant leaves (0.1000 g) were extracted with 5.0 mL of the extractant by heating using a water bath according to the experiment plan for flavonoids. For extraction of amino acids, powdered plant leaves of Iris were mixed with concentrated muriatic acid (10–100 μL) and were extracted with 5 mL extractant by heating. Extracts were transferred to a 10 mL volumetric flask and diluted to 10 mL, then were filtered through a 0.45 μm Nylon syringe filter (Whatman). The resulting solution was analyzed by HPLC-DAD and HPLC-MS.

2.6 Experimental plan for flavonoids and amino acids

The fractional factorial experimental plan for flavonoids included three replicas of the central points for the experiment, in which a middle value was taken for each factor. The degree of extraction was controlled by the sum of the peak areas for the interval from 14 to 28 min, which has a characteristic absorption spectrum for flavonoids. The same procedure was done for amino acids. The degree of extraction was controlled by the peak area on extracted ion chromatogram.

2.7 Derivatization of amino acids

Before analysis, the dansyl derivatives of amino acids were obtained under the following conditions: 45 μL of the extract was mixed with 280 μL of borate buffer solution (pH = 9.5) and 100 μL of dansyl chloride (7 μg mL^{-1} in acetonitrile), kept for 15 min in a thermostat at 75 °C, then 20 μL of acetic acid was added and centrifuged for 10 min. The upper layer (250 μL) was transferred to vials for analysis.

3. Results and discussion

3.1 Developing of extraction procedure

Separations of phenolics are generally performed using RP HPLC due to their hydrophobicity. Amino acids are polar compounds and many of them do not contain chromophore groups. So, for their determination, we used derivatization with dansyl chloride. The natural extracts of raw plant materials have complex compositions, therefore conditions for selective separation of analytes by RP HPLC coupled with DAD and ESI-MS/MS method were optimized using real samples.

On the chromatogram in the region of 14–28 min, the detected components correspond to phenolic derivatives, since they have characteristic absorption bands at 220 nm, 270–280 nm, and 330–350 nm.

Based on the literature [5–8], the most significant factors affecting the extraction of phenolic compounds and their range of variation were selected: temperature (50–80 °C), time (15–60 min), and methanol content (50–100%). To minimize the number of experiments, a fractional factorial experimental plan with resolution 1/2 was used. Three factors varied at two levels.

The construction of the mathematical model for phenolics extraction and its subsequent analysis showed that the best result is achieved when considering the interactions of the selected factors (R^2 = 64.49%, R^2(adj) = 37.87%, R^2(pred) = = 20.79%). The low R^2 values are explained by too wide range values of factors, but the indicators have acceptable values for building an indicative model. According to the Pareto graph, the interaction of time and the heating temperature has the greatest influence. Finally, for the heating temperature, the maximum is observed near 68°C, which corresponds to the boiling point of methanol. Increasing in flavonoids content is observed with an increase in the methanol content in the extractant and a decrease in the heating time.

The effect of ultrasound (15, 30, 45 and, 60 min) on the extraction of phenolic compounds was analyzed outside the experimental plan. It was obtained no significant effect of ultrasound treatment on extraction efficiency of polyphenols, so sonication was not included in sample preparation. So, the selected conditions for polyphenols extraction were the following: extraction at 65 °C for 15 min with 100% methanol.

The same experimental scheme for effective extraction of amino acids from *Iris sibirica* L. was done. In fractional factorial experimental for amino acids methanol content in extractant (0–50%), time (20–60 min), the temperature of the process (70–100 °C), and a hydrochloric acid aliquot (10–100 μL) were chosen as the most significant factors. The plotting of the mathematical models and its analysis showed that the best result is achieved when taking into account the interactions of the selected factors, as for polyphenols. It was established that the dependences of different amino acids extraction on chosen factors were similar. The main factors that have the greatest influence were methanol content and heating temperature. So, optimal conditions for extraction of amino acids were extraction at 50 °C for 20 minutes with 50% methanol.

3.2 Analysis of raw plant materials

Using the developed conditions, chromatographic profiles of polyphenols and amino acids of extracts of *Iris sibirica L.* grown on nutrient media with phytohormonal additives 6-benzeneaminopurine and α-naphthaleneacetic acid at different concentrations (provided by the Altai State University) were obtained. Chromatograms for phenolic compounds are shown in Fig. 1.

After comparison, it was clear that some peaks and peak groups significantly changed with phytohormone concentration increasing, for example on 27–29 minutes. Auxin-like hormone additive increased non-polar phenolic content, eluted

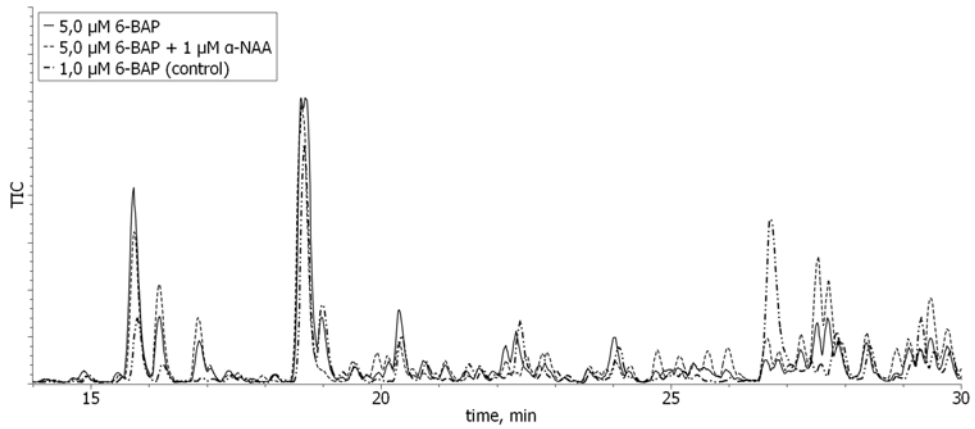

Fig. 1 Effect of phytohormonal additives on chromatographic profiles of polyphenols in extracts of *Iris sibirica L.* raw plant materials: 6-benzeneaminopurine (6-BAP) and α-naphthaleneacetic acid (α-NAA).

on 25–30 minutes, and decreased the content of polar phenolics, but the variation of cytokine caused individual changes for studied peaks through all analysis.

Polar extracts were analyzed on 19 amino acids content. The domain analytes in extracts of leaves of *Iris sibirica* L. were Ala, Pro, His, Ser, Glu, Val, Phe, Leu, and Ile. As for phenolics, 6-BAP acted for every amino acid individually, but α-naphthaleneacetic acid significantly increased the content of 15 amino acids.

4. Conclusions

Selective separation conditions for phenolic compounds and amino acids in the leaves of *Iris sibirica* L. by HPLC-DAD-ESI-MS/MS were optimized. The schemes for effective extraction of analytes from raw plant materials for HPLC analysis were developed using fractional factorial design of experiment. The main factors that affected the extraction efficiency were obtained: time and heating temperature for phenolic compounds, methanol content in extractant, and heating temperature for amino acids. Using the developed technique, chromatographic profiles of extracts of I. sibirica grown on nutrient media with different phytohormone concentrations (provided by the Altai State University) were obtained. It was shown that different concentrations of hormones in nutrient media influenced plant metabolism and provoked plant stress.

Acknowledgments

This work was supported by the RSF (project No 19-13-00370). Research group expresses gratitude to the Resource Centers "Methods of Substance Composition Analysis" and "Development of Molecular and Cell Technologies" of the St. Petersburg State University Science Park for the equipment provided.

References

[1] Kukula-Koch W., Sienwanska E., Widelski J., Urjin O., Głowniak P., Skalicka-Woźniak K.: Major secondary metabolites of *Iris* spp. *Phytochem. Rev.* **14** (2015), 51–80.

[2] Тихомирова Л.И., Базарнова Н.Г., Микушина И.В., Долганова З.В.: Фармакологобиохимическое обоснование практического использования некоторых представителей рода *Iris* L. (обзор). *Химия растительного сырья* **3** (2015), 25–34. (In Russian.)

[3] Li L., Li T., Jiang Y. Yang Y., Zhang L., Jiang Z., Wei C., Wan X., Yang H.: Alteration of local and systemic amino acids metabolism for the inducible defense in tea plant (*Camellia sinensis*) in response to leaf herbivory by *Ectropis oblique. Arch. Biochem. Biophys.* **683** (2020), 108301.

[4] Тихомирова Л.И., Базарнова Н.Г., Ильичева Т.Н., Мартиросян Ю.Ц., Афанасенкова И.В.: Получение растительного сырья ириса сибирского (*Iris sibirica* L.) методами биотехнологии. *Химия растительного сырья* 4 (2018), 235–245. (In Russian.)

[5] Zhao L., Liu L., Li J.: Qualitative and quantitative analysis of five bioactive flavonoids in *Salix bordensis* Turcz. by HPLC-DAD and HPLC-ESI-MS. *Am. J. Anal. Chem* **5** (2014), 851–860.

[6] Khuluk, R.H.; Yunita, A.; Rohaeti, E.; Syafitri, U.D.; Linda, R.; Lim, L.W.; Takeuchi, T.; Rafi, M. An HPLC-DAD method to quantify flavonoids in *Sonchus arvensis* and able to classify the plant parts and their geographical area through principal component analysis. *Separations* **8** (2021), 12.

[7] Kagisha V., Frederich M., Ledoux A., Olivia Jansen O., Nyirimigabo A., Muganga R., Djang'eing'a R.M.: HPLC-UV method for standardization of *Neorautanenia mitis*, an African plant used in an anti-scabies ointment. *Rev. Bras. Farmacogn.* **30** (2020), 582–587.

[8] Zhuo Z., Xu D., Li Y., Pu B., Yed M.: Fingerprint analysis of *Zanthoxylum armatum* DC. by HPLC. *J. Food Compos. Anal.* **96** (2021), 103736

Epitachophoretic preconcentration of proteins

Helena Hrušková[a, b, *], Ivona Voráčová[a], František Foret[a, c]

[a] *Institute of Analytical Chemistry of the Czech Academy of Sciences, Department of Bioanalytical Instrumentation, Veveří 967, 602 00 Brno, Czech Republic* ✉ *HelenaHruskova@email.cz*
[b] *Masaryk University, Faculty of Science, Department of Chemistry, Kotlářská 2, 611 37 Brno, Czech Republic*
[c] *CEITEC, Masaryk University, 601 77 Brno, Czech Republic*

Keywords
cleaning
epitachophoresis
isotachophoresis
preparative concentration

Abstract
This project is focused on the epitachophoretic preconcentration of proteins from biological fluids. In this paper, the method for preparative concentration of three standards of proteins, cytochrome c, myoglobin, and hemoglobin, was developed and described. Concentration conditions, such as concentration and pH of leading and trailing electrolytes, gel composition, and time of concentration, were optimized. The recovery of each protein was at least 70% and concentration factor 50.

1. Introduction

The study of proteins and other biological compounds as DNA, RNA is one of the most important scientific fields and plays a key role in diagnostics and molecular biology. By studying these compounds, we can describe the current and long-term state of the organism. However, the way to obtain serious data is complicated in terms of the number of compounds and processes that take place in the organism. Therefore, the demands on the extraction of these compounds from biological fluids are also increasing. For further analyses, it is essential to obtain samples of sufficient concentration and purity [1].

In 2019 a new separation technique able to concentrate and collect samples from large volumes was introduced by our group in collaboration with Roche, Inc. It was named epitachophoresis [2]. This brand-new technique is based on the discontinuous electrophoresis principle with a unique circular design (Fig. 1). It can concentrate analytes, e.g. DNA, from large sample volumes (15 ml) into µl volumes. The concentration of analytes is fast, efficient, provides high recovery (80% and more), and is easy to perform. It is possible to focus long and short DNA fragments in one zone or focus only on selected sizes (combination with sieving media and selected buffer system for a precise range of electrophoretic mobilities). Besides the presented negative polarity mode for focusing DNA fragments,

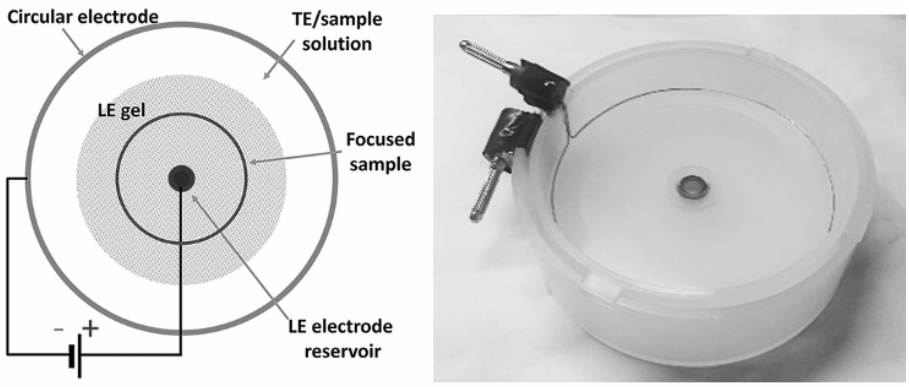

Fig. 1 Architecture and design of the epitachophoretic device: (LE) leading, and (TE) trailing electrolytes (according [2]).

this technique is also able to concentrate cations in positive mode. This greatly expands the field of application of the device. Thus, it can be used for the preconcentration of small proteins, carbohydrates, bacteria, viruses, quantum dots, and others.

Proteins can play an important role as biomarkers of a wide range of diseases. Cytochrome c is a protein with more functions and it is a part of the electron transport chain. This protein transports electrons from the bc1 complex to cytochrome c oxidase to start type II apoptosis [3]. It can serve as a biomarker of diseases and for monitoring the current state of the organism (for example drug-induced liver injury) [4]. Myoglobin and hemoglobin are carriers of oxygen and therefore they are important for the physiological function of the heart and muscles [5, 6]. Myoglobin can serve as a biomarker for acute myocardial infarction [7, 8].

2. Experimental

2.1 Reagents and chemicals

All chemicals mentioned below were analytical grade: acetic acid (LachNer, Czech Republic), ammonium acetate (LachNer, Czech Republic), hemoglobin human heart (Sigma Aldrich, USA), cytochrome c bovine heart (Sigma Aldrich, USA), myoglobin horse heart (Sigma Aldrich, USA), agarose NEEO (Carl Roth, Germany), acrylamide/bisacrylamide 30% Rotiphorese Gel (37.5:1) (Carl Roth, Germany), cetyltrimethylammonium bromide (Lachema, Czech Republic)

2.2 Instrumentation

The epitachophoretic device (Fig. 1) is composed of two parts: an inner vessel with a 10 cm diameter with a central hole for placing a collection cup and an outer

Table 1
Optimisation of pH of leading electrolyte, evaluated parameters were the total analysis time, the shape of the zone, and the highest temperature at the center of the device.

pH (leading electrolyte)	Analysis time / min	Shape of the zone	The highest temperature at the center of the device / °C
4	34	narrow zone	62
5	58	narrow zone	82
6	58	narrow zone	76
7	56	narrow zone	78
8	65	narrow zone	86

vessel with a diameter of 11 cm. The platinum ring electrode (or conductive graphite tape) was placed on the edge of the circular separation inner vessel. The second platinum wire electrode was placed in the outer part of the device. At the center of the inner vessel, a collection well with a dialysis membrane 9 mm in diameter was placed. The sealing between the collection cup and inner vessel was secured by a rubber O-ring. Before the experiment, the inner vessel was put in the outer part filled with leading electrolyte. 100 mL of ammonium acetate solution of a given pH and concentration was used as the leading electrolyte. The circular gel was prepared from the leading electrolyte and 0.5% agarose gel (diameter 7.5 cm) or 6% polyacrylamide gel (diameter 7.5 or 3.5 cm). The gel was placed into the center of the inner vessel. In the next step, 10 or 20 mL of trailing electrolyte of a given concentration mixed with 1 mg the sample was poured around the gel. The electrodes were connected to the power supply using banana plugs. For each experiment electric power of 5 W was used. Experiments were recorded and pictures were taken using a mobile phone camera (Samsung Galaxy S4). The recoveries were determined by fluorimeter Qubit (Invitrogen, USA) using a Protein Qubit Quantification Assay Kit.

3. Results and discussion

For the optimization process, cytochrome c was chosen as a model protein because of its high solubility, color, and small size. Firstly, suitable electrolytes were chosen for the preconcentration of analytes. The concentration of leading electrolyte, trailing electrolyte, and pH of leading electrolyte were optimized. The example of obtained results for the pH optimization of leading electrolyte is shown in Table 1. The observed parameters were the total time of the experiment, temperature at the center of the device, and the shape of the zone. In Table 1, average values and observations from two experiments are shown.

The optimum experimental conditions obtained after the optimization are 40 mM ammonium acetate pH = 4 as the leading electrolyte, 20 mM acetic acid as the trailing electrolyte. Using this buffer system decreased the total time of the experiment to 35 minutes. A narrow zone of the analyte was formed (Fig. 2) and

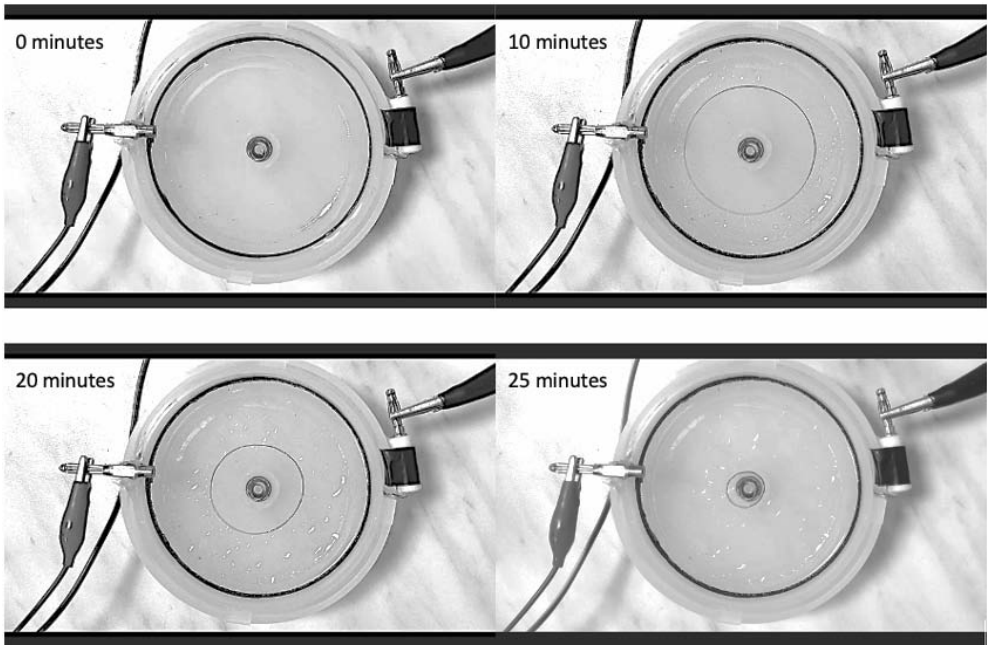

Fig. 2 Preconcentration of cytochrome c after optimization in 0.5% agarose gel. 40 mM ammonium acetate pH = 4 was used as the leading electrolyte, and 20 mM acetic acid was used as the terminating electrolyte. Sample preparation: 1 mg of cytochrome c was dissolved in 10 mL of the trailing electrolyte. Pictures were captured in minute 0, 10, 20, and 25 after switching on the electric power (5 W).

the maximum temperature at the center of the device was approximately 60 °C (this temperature can be further decreased by using lower electric power at the end of the experiment).

3.1 Preconcentration of myoglobin and hemoglobin

The epitachophoretic preconcentration of other proteins (hemoglobin and myoglobin) in agarose gel was problematic. The proteins were adsorbed at the edge of the gel. Using a strong cationic detergent (CTAB) improved adsorption, but CTAB is incompatible with many analytical techniques, so it isn't suitable for our purposes. The use of the different gel as polyacrylamide solved the problem with adsorption, but even with a very low (6%) concentration of polyacrylamide the separation was slow (it took about 2 hours) and the temperature at the center of the device was high (over 80 °C). To avoid this problem, the diameter of the polyacrylamide gel was decreased (from 7.5 cm to 3.5 cm). So, the total time of the experiment was approximately 30 minutes and the temperature was not higher than 60 °C using electric power 5 W.

Table 2
The recoveries determined for cytochrome c, myoglobin, hemoglobin using Qubit Fluorimetric Quantification.

Protein	Recovery (n = 2) / %
Cytochrome c	74
Myoglobin	77
Hemoglobin	71

3.2 Determination of recovery and preconcentration

The recoveries were determined using Qubit Fluorimetric Quantification. The experiments provided overall recoveries higher than 70 % for all three proteins (Table 2). The highest concentration achieved was fiftyfold (from 20 mL to approximately 0.4 mL), but this value is variable and depends on the way of collecting the sample.

4. Conclusions

In this work, we present a developed method for preconcentration of standards of proteins cytochrome c, myoglobin, and hemoglobin. Firstly, the electrolyte system was selected and optimized to provide low analysis time, narrow shape of the protein zone, and eliminate overheating at the center of the device. In the next step, the developed method was tested on the preconcentration of proteins: cytochrome c, myoglobin, and hemoglobin. After several adjustments myoglobin and hemoglobin were also successfully preconcentrated. After evaluation of pilot results, this technique provides up to fiftyfold preconcentration and recovery of over 70 % for each protein. The next plan is to preconcentrate proteins from complex biological matrices such as urine or blood plasma.

Acknowledgments

This work was supported by the European Regional Development Fund-Project "SINGING 521 PLANT" (No. CZ.02.1.01/0.0/0.0/16_026/0008446). Additional support was provided by Roche Sequencing Solutions (Pleasanton, USA), and by RVO 68081715 of the Institute of Analytical Chemistry, Czech Academy of Sciences in Brno.

References

[1] Thatcher S.A.: DNA/RNA preparation for molecular detection. *Clin. Chem.* **61**(2015), 89–99.
[2] Foret F., Datinská V., Voráčová I., Novotný J., Gheibi P., Berka J., Astier Y.: Macrofluidic device for preparative concentration based on epitachophoresis. *Anal. Chem.* **91**(2019), 7047–7053.
[3] Wan J., Kalpage H.A., Vaishnav A., Liu J., Lee I., Mahapatra G., Turner A.A., Zurek M.P., Ji Q., Moraes C.T., Recanati M.A., Grossman L.I., Salomon A.R., Edwards B.F.P., Hüttemann M.: Regulation of respiration and apoptosis by cytochrome c threonine 58 phosphorylation. *Sci. Rep.* **9** (2019), 15815.
[4] Miller T.J., Knapton A., Adeyemo O., Noory L., Weaver J., Hanig J.P.: Cytochrome c: a non-invasive biomarker of drug-induced liver injury. *J. Appl. Toxicol.* **28** (2008), 815–828.

[5] Gros G., Wittenberg B.A., Jue T.: Myoglobin's old and new clothes: from molecular structure to function in living cells. *J. Exp. Biol.* **213** (2010), 2713–2725.
[6] White J.C., Beaven G.H.: A review of the varieties of human haemoglobin in health and disease. *J. Clin. Pathol.* **7** (1954), 175–200.
[7] El-Said W.A., Fouad D.M., El-Safty S.A.: Ultrasensitive label-free detection of cardiac biomarker myoglobin based on surface-enhanced Raman spectroscopy. *Sens. Actuators B Chem.* **228** (2016), 401–409.
[8] Pur M.R.K., Hosseini M., Faridbod F., Ganjali M.R.: Highly sensitive label-free electrochemiluminescence aptasensor for early detection of myoglobin, a biomarker for myocardial infarction. *Microchim Acta* **184** (2017), 3529–3537.

Spectroscopic techniques for the analysis of biological forensic samples

Anna Wójtowicz[a,*], Marcin Reciak[a], Aneta Blat[b], Kamilla Małek[b], Renata Wietecha-Posłuszny[a]

[a] *Jagiellonian University, Faculty of Chemistry, Department of Analytical Chemistry, Laboratory for Forensic Chemistry, Gronostajowa 2, 30-387 Kraków, Poland*
✉ *anna.wojtowicz@doctoral.uj.edu.pl*
[b] *Jagiellonian University, Faculty of Chemistry, Raman Imaging Group, Gronostajowa 2, 30-387 Krakow, Poland*

Keywords
ATR FTIR
forensic
PCA
post-mortem analysis
vitreous humor

Abstract
Vitreous humor is an alternative matrix often used in forensic chemistry. Its most important application is the identification of the time since death based on biochemical changes in its composition. A simple and rapid technique of Attenuated Total Reflectance Fourier Transform Infrared (ATR FTIR) spectroscopy was used for the detection of time-related changes in vitreous humor composition over one month. The influence of three storage temperatures of –20, 4, and 20 °C was studied. Changes in the intensity of the bands assigned to amino acids, polysaccharides, and fatty acids were detected after 18 days for temperatures of 20 and 4 °C and on the 30th day for –20 °C. This preliminary study demonstrates the great potential of the ATR FTIR technique in detecting changes in vitreous humor structure over time and its further forensic applications.

1. Introduction

Vitreous humor is a transparent gelatinous tissue composed almost entirely of water (98–99%) with trace amounts of hyaluronic acid, glucose, anions, cations, ions, and collagen, located in the posterior chambers of the eyes [1]. Vitreous humor is commonly used in toxicological and forensic analyses as an alternative to classical matrices such as blood or urine, mainly due to its high resistance to degradation in post-mortem processes, and thus longer available for analysis. Currently, the most important forensic application of vitreous humor is the identification of the time elapsed since death based on biochemical changes in its composition [2, 3]. Thus, techniques are needed that can effectively detect and identify changes in this biological matrix. An additional benefit for the analysis of forensic-relevant samples would be the use of simple, fast, minimally destructive, and relatively portable techniques. These requirements can be met with

Attenuated Total Reflectance Fourier Transform Infrared (ATR FTIR) spectroscopy, which has already proven its potential to detect biochemical changes over time in post-mortem vitreous humor samples [4] and other biological tissues and organs such as liver or kidneys [5].

The aim of this study was to investigate the changes occurring in vitreous humor samples during 30 days of storage at three temperatures of –20, 4, and 20 °C.

2. Experimental

2.1 Reagents and chemicals

Bovine vitreous humor samples supplied by a meat establishment (Laskopol, Poland) were used. The samples were deposited on microscope slides and, after 24 hours of drying at room temperature, scraped with a scalpel, and measured.

2.2 Instrumentation

ATR FTIR measurements were performed using an Agilent 670-IR spectrometer equipped with a diamond crystal (Agilent, USA) by co-adding 64 scans in the range of 400–4000 cm^{-1} with a 4 cm^{-1} resolution. Samples were measured in triplicates. The background was measured before each sample (128 scans) and the crystal was washed with 96% ethyl alcohol. ATR correction was performed on the spectra and crystal bands were removed in OPUS 7.0 (Bruker Optics, USA). ATR FTIR spectra were baseline corrected, smoothed (Savitzky-Golay (SG), 13 pts), normalized by sum, and plotted in OriginPro 2021 (OriginLab Corporation, USA). Further data processing included second derivatives generation (from the original spectra), smoothing (SG, 17 pts), and vector normalization in OPUS 7.0. Statistical analyses were performed using R (R-4.0.4 for Windows) equipped with the ChemoSpec 5.3.2 package.

3. Results and discussion

The ATR FTIR spectra collected were analysed only in the fingerprint region between 900 and 1800 cm^{-1}. An averaged vitreous humor spectrum obtained after pre-processing is shown in Fig. 1. It was noticed that the storage time did not affect the presence of individual bands in the spectra, but only their intensity.

The bands' assignments were made based on the literature [4, 6–7]. In the range of 900–1200 cm^{-1}, the bands related to CO-O-C symmetric vibrations of polysaccharides (1041 cm^{-1}) and CO vibrations of glucose (1078 cm^{-1}), lactates and polysaccharides (1122 cm^{-1}) were present. In the range of 1300–1500 cm^{-1}, the bands located at 1313, 1414, and 1456 cm^{-1} were observed and assigned respectively to the amide III band of proteins, symmetric stretching vibrations of

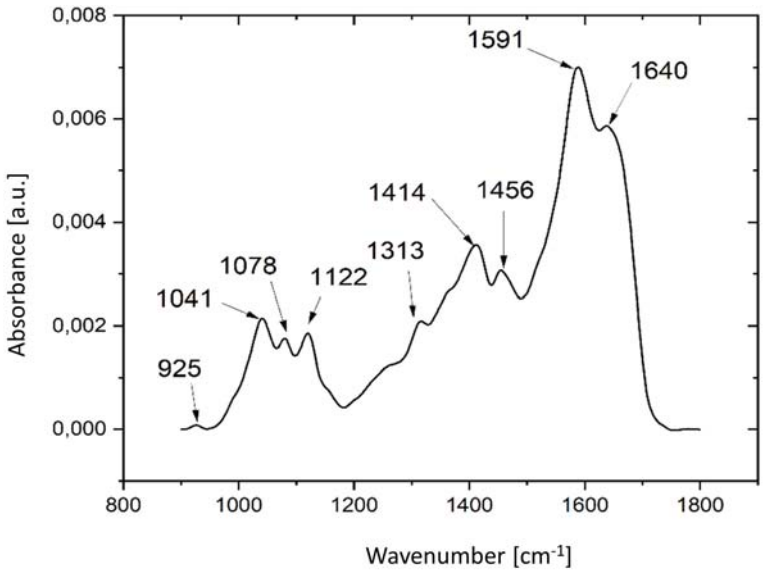

Fig. 1 Averaged ATR FTIR spectrum of vitreous humor in the range 900–1800 cm^{-1} after ATR correction, baseline correction, normalization by sum and smoothing (SG 13 points). The positions of the main bands are indicated by arrows and their numerical values of wavenumbers are given.

COO^- groups of amino acids and fatty acids, and bending vibrations of $–CH_2–$ and $–CH_3$ groups of lipids and proteins. Finally, in the range from 1500 to 1700 cm^{-1}, two bands at 1591 and 1640 cm^{-1} were visible. The first band was assigned to the antisymmetric stretching vibrations of COO^- groups of fatty acids and amino acids. However, the assignment of the band at 1640 cm^{-1} was not clear. It could be assigned to the vibrations of the amide I band of proteins, as discussed in our previous paper [8], but due to the high water content of vitreous humor samples [1], it is also justified to assign this band to the water –OH bending vibrations.

The effect of 30-days storage on vitreous humor samples was statistically analyzed using principal component analysis (PCA). The PCA analysis was performed on the second derivatives of the spectra, which allowed to avoid the influence of background changes and appropriate baseline adjustments on the PCA results, as well as taking into account the changes for the bands not visible in the original spectra. The PCA score plots supported by the respective loading plots obtained for a given group of samples stored at 20, 4, and –20 °C are shown in Fig. 2.

For vitreous humor samples stored at 20 °C, PCA allowed for a clear separation of the results obtained on days 18, 24, and 30 from those on days 0–12 (Fig. 2.1A). The analysis focused on the results obtained for the first two components: PC1 and PC2. PC1 had the lowest score for the 0–12-days group and then increased from day 18 to day 30. At the same time, no changes that could be clearly correlated with time were observed along PC2. Based on the analysis of the loading plot obtained for the samples stored at 20 °C (Fig. 2.1B), it can be

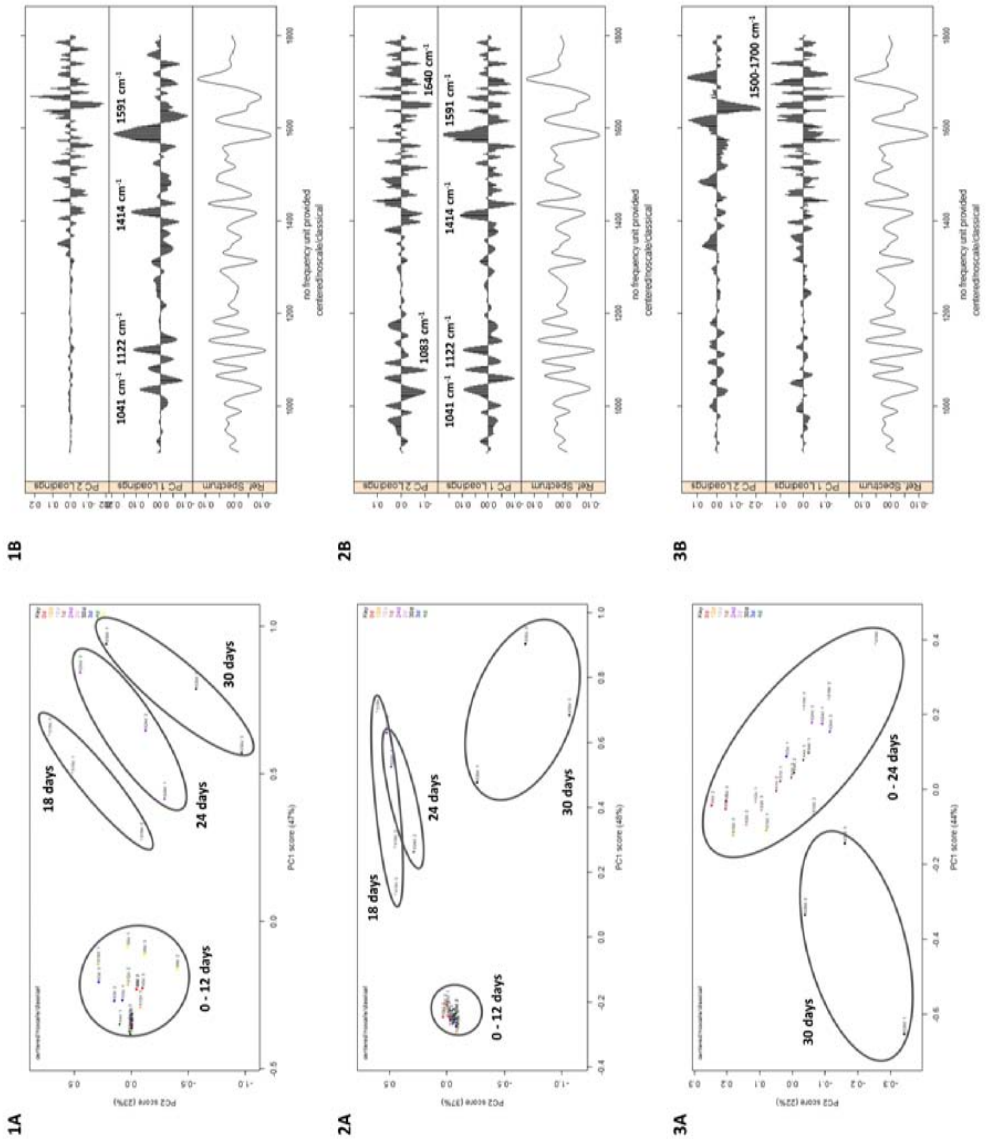

Fig. 2 (A) PCA score plots, and (B) the corresponding loading plots, along PC1 and PC2 together with the second derivatives of the spectra obtained for vitreous humor samples stored for 30 days at (1) 20 °C, (2) 4 °C, and (3) –20 °C. The groups of spectra defined by PCA score plots are outlined and labelled with the storage day; the numerical values of wavenumbers are given for the bands indicated by the loading plots.

concluded that the bands located at 1078, 1122, 1414, and 1591 cm^{-1} had the greatest influence on the separation along PC1. The assignments of these bands were previously made and include vibrations of the functional groups of glucose, lactates, polysaccharides, amino acids, and fatty acids. Since the value of PC1 increased over the period of 0–30 days, and the indicated bands responsible for the separation are negative in the second derivatives plots, it can be concluded that the intensity of these bands decreased over time. This may indicate a decrease in the concentration of these vitreous humor components, possibly due to progressive decomposition at 20 °C.

The analysis of the PCA results (Fig. 2.2A, B) obtained for vitreous humor samples stored at 4 °C also indicated the separation of the last three storage days: 18, 24, and 30 days. Along PC1, there was a clear separation of days 0–12 from the last three days, while along PC2, additionally, the division of day 30 from 18 and 24 was observed. The division along PC1 was most influenced by the bands located at 1041, 1122, 1414, and 1591 cm^{-1} which decreased with time, so the same as for PC1 at 20 °C, however, the results obtained for days 18-30 were better separated for the temperature of 20 than 4 °C. This may demonstrate the rate of potential decomposition processes in the structure of lactates, polysaccharides, amino acids, and fatty acids occurring for these samples after day 18, significantly greater at 20 °C. On the other hand, the bands which had the greatest impact on the distribution along PC2 were additionally located at 1083 and 1640 cm^{-1}, as described earlier, assigned respectively to glucose and amide I / water vibrations. The changes observed for these bands were clearly different on day 30 when the PC2 score dropped significantly. To confirm whether this change on the 30th day was a result of a random error or indicated the onset of changes of a different nature, it is necessary to study samples stored longer than 30 days.

For the temperature of –20°C, the PCA analysis along PC1 allowed for the separation of only the 30th day of storage, while no separation was observed for the remaining days (Fig. 2.3A). This confirms that such storage conditions were clearly more favorable than 4 and 20 °C but still did not ensure storage stability for the entire time of the study, i.e., one month. The separation along PC1 was influenced by changes in the intensity of the bands in the range of 1500–1700 cm^{-1}, but as can be seen in the loading plot (Fig. 2.3B), these changes were less distinct than for other temperatures.

4. Conclusions

The ATR FTIR spectroscopy technique was successfully used for the determination of time changes in the vitreous humor composition. Over time, biochemical changes were detected mainly in the structure of amino acids, lactates, polysaccharides, and fatty acids. Moreover, the rate of these potential decomposition processes increased with the storage temperature. For vitreous humor samples stored at 4 and 20 °C, detectable changes were visible after 18 days, and at

–20°C only for day 30. The temperature of –20°C did not ensure storage stability for the entire time of the study, i.e., one month. The main conclusion that can be drawn from this study is that ATR FTIR spectroscopy is able to detect biochemical changes occurring in the vitreous humor matrix over time, making it a promising application for identifying post-mortem changes in tissues and correlating them with the post-mortem interval.

Acknowledgments

The authors gratefully acknowledge the Ministry of Science and Higher Education, National Science Centre, Poland for financial support (R. Wietecha-Posłuszny, Opus 19, no. 2020/37/B/ST4/01364).

References

[1] Scott K.S., Oliver J.S.: The use of vitreous humor as an alternative to whole blood for the analysis of benzodiazepines. *J. Forensic Sci.* **46** (2001), 694–697.

[2] Wójtowicz A., Wietecha-Posłuszny R., Snamina M.: Contemporary trends in drug analysis of vitreous humor: A critical review. *TrAC Trends Anal. Chem.* **129** (2020), 115935.

[3] Pigaiani N., Bertaso A., De Palo E.F., Bortolotti F., Tagliaro F.: Vitreous humor endogenous compounds analysis for post-mortem forensic investigation. *Forensic Sci. Int.* **310** (2020), 110235.

[4] Zhang J., Wei X., Huang J., Lin H., Deng K., Li Z., Shao Y., Zou D., Chen Y., Huang P., Wang Z.: Attenuated total reflectance Fourier transform infrared (ATR-FTIR) spectral prediction of postmortem interval from vitreous humor samples. *Anal. Bioanal. Chem.* **410** (2018), 7611–7620.

[5] Zhang K., Wang Q., Liu R., Wei X., Li Z., Fan S., Wang Z.: Evaluating the effects of causes of death on postmortem interval estimation by ATR-FTIR spectroscopy. *Int. J. Legal. Med.* **134** (2020), 565–574.

[6] Zhang Z., Lin H., Li Z., Luo Y., Wang L., Chen L., Huang P.: Identification of fatal hypothermia via attenuated total reflection Fourier transform infrared spectroscopy of rabbit vitreous humour. *Austr. J. Forensic Sci.* **53** (2021), 27–39.

[7] Staniszewska E., Małek K., Barańska M.: Rapid approach to analyze biochemical variation in rat organs by ATR FTIR spectroscopy. *Spectrochim. Acta A* **118** (2014), 981–986.

[8] Wójtowicz A., Mitura A., Kurczab R., Zawadzki M., Wietecha-Posłuszny R.: Spectroscopy as a useful tool for the identification of changes with time in post-mortem vitreous humor for forensic toxicology purposes. *Monatsh. Chem.* (2021). DOI: 10.1007/s00706-021-02786-8.

Selenium enrichment in broccoli sprouts as an initial step in the preparation of Certified Reference Material

Chintankumar Padariya*, Małgorzata Rutkowska, Piotr Konieczka

Gdańsk University of Technology, Faculty of Chemistry, Department of Analytical Chemistry, 11/12 G. Narutowicza Street, 80-233 Gdańsk, Poland ✉ chipadar@student.pg.edu.pl

Keywords
micronutrient
reference material
selenium
selenium speciation
trace analysis

Abstract
Selenium is considered one of the essential elements in animals and humans. The main source of selenium intake for humans is the diet. Selenium deficiency has one of the most concerning issues worldwide. Broccoli sprouts are five-to-six-day old broccoli plants, and they may exhibit stronger chemoprotective effects. Thus, the enrichment of selenium in broccoli sprouts can enhance anticancer properties. As a result of conducted study, four batches of selenium-enriched sprouts have been produced in order to verify the efficiency of selenium uptake by broccoli sprouts under commercial conditions. Sodium selenite solution (10 mg L^{-1}) was used to prepare selenium-enriched broccoli sprouts. Sodium selenite is available for biological uptake by plants. The results might be different while the addition of sodium selenite in each step of the germination process could enhance the concentration of selenium in broccoli sprouts. Therefore, it could be potentially selected as a candidate for certified reference materials.

1. Introduction

The healthy development and growth of life functional organisms depend on acquired nutrients that one of which is called micronutrients. A semi-metal, selenium is among one of the essential micronutrients. Selenium exists with distinct chemical forms in soils such as metal selenides (Se^{2-}), elemental selenium (Se^0) microelement forms (SeO_4^{2-}, SeO_3^{2-}), and organic selenium compounds [1]. The major source of selenium uptake is via diet for humans which includes seafood, vegetables, and meats [2]. The uptake of selenium should be limited in human as it is poisonous when exceeds a minimum requirement of intake [3]. The selenium content of food may have varied based on its geological conditions, such as soil conditions, climate conditions, protein content, and food processing [4]. As implications of selenium deficiency on human health have become understood, interest in the dietary amount of this mineral has grown [5]. Thus, agronomic

selenium biofortification is an interesting research topic, mainly applied by the use of fertilizers enriched with selenium to soils and crops [6–8]. The presented study handles the hydroponic system applied to broccoli sprouts with the addition of sodium selenite mixture.

The study is implemented to evaluate the changes in selenium content in four differently prepared spouts sets which are: i) control sprouts (natural content of selenium); ii) soaking seeds in sodium selenite solution; iii) Se-enriched sprouts (everyday watering with sodium selenite solution); iv) Se-enriched sprouts (everyday watering with sodium selenite solution and soaking seeds in sodium selenite solution). It is also important to be notified that the nutritional bioavailability of selenium from plants is mostly determined by selenium compounds. These palatable sprouts are usually served in a variety of diets, which is beneficial for human health, including anti-cancer protection [9]. Therefore efforts were made to examine the potential certified reference material (CRM) with the use of Se-enriched sprouts for the aim of a study of total selenium content in four different conditioned batches. This investigation was conducted utilizing selenium enhanced sprouts to produce reference materials for the complete analysis of selenium. This is a beginning attempt and its good outcome will allow the development of analytical methods for selenium determination as well as extend the information about the organic form of selenium's beneficial influences on living creatures.

2. Experimental

2.1 Reagents and chemicals

Chemicals and reagents used were in the analytical grade. Deionize water from the Milli-Q water purification system unit (Merck Millipore, Germany) was used in preparations of solutions in case of total Se determination. Germination solutions were developed using sodium selenite dissolution in tap water (Sigma Aldrich, Germany). Sprout seeds were purchased from Hurtownia PRIMA (Piła, Poland). The samples were digested with HNO_3 (Suprapur, 65%, Merck, Darmstadt, Germany). Samples were diluted in deionized water from a Milli-Q for total Se measurement.

2.2 Processing of sprouts

Seed germination was done using tap water and with a solution containing 10 mg L^{-1} of Na_2SeO_3 (as a controlled growing media). The seeds were steeped in the appropriate solutions (250 mL) for 6 hours before germination. The seed had been put in commercial germination bowls for sprouting. Germination was performed at room temperature (20–24 °C) and during the day and night, under the prevalent light and dark conditions during the time of day and night. The entire germination time was around 178 hours, which includes also the time for

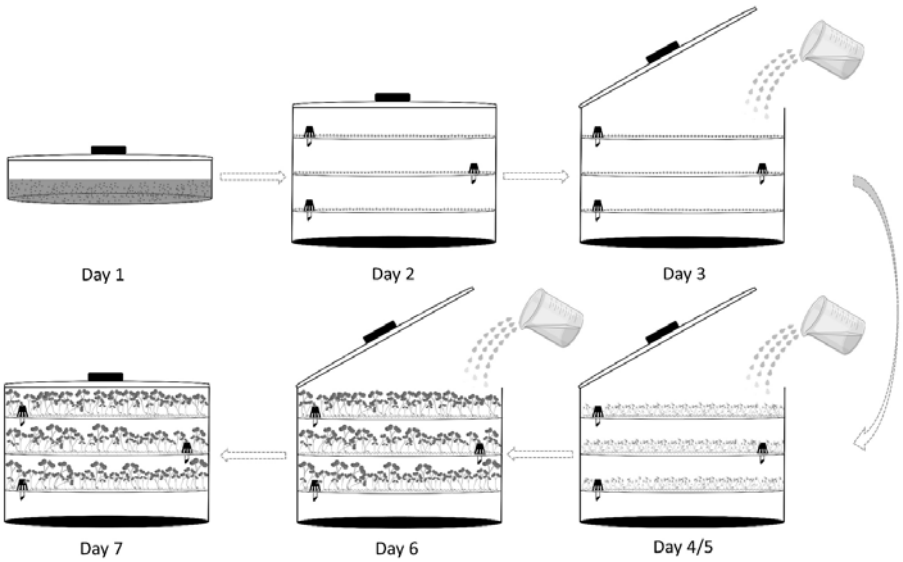

Fig. 1 Preparation steps of broccoli sprouts.

Table 1
The preparation of broccoli sprouts with applicable conditions is discussed.

Time period	Conditions
Day 1	10 g of seeds soaked in solution[a]; stored in dark place
Day 2	Watering twice a day[a]; stored in dark place
Day 3	Watering twice a day[a]; stored in dark place
Day 4/5	Watering twice a day[a]; exposed to indirect sunlight
Day 6	Watering twice a day[a]; exposed to indirect sunlight
Day 7	Cultivation of sprouts

[a] 250ml of corresponding solution.

soaking the seeds in water. The sprouts had been washed twice a day with 250 mL of the appropriate solutions throughout the germination process. All sprouts were rinsed after harvesting with deionized water (2×500 mL) to prevent contamination by the culture solution of the sprout surface. The sprouts were then placed in PE screenable bags and kept in a freezer at –20 °C. All samples were freeze-dried. The dry samples were then ground into a blender purchased from First Austria, transferred into screenable bags, and stored in a freezer at –20 °C. Around 5 g of sample was obtained for broccoli sprouts. The germination process is graphically described in Table 1 and Fig. 1.

Four batches have been generated of Se-enriched sprouts that includes: i) control sprouts; ii) sprouts seeds with the solution addition of 10 mg L^{-1} Na_2SeO_3 into (while soaking seeds) iii) watering the sprouts (with 10 mg L^{-1} Na_2SeO_3); iv) combination of point ii) and iii).

2.3 Instrumentation

For germination commercial germination bowls (E-TRADE, Pruszków, Poland), equipped with a drain and a plastic lattice at the bottom of the bowl to keep the seeds at constant moisture without overwatering them, were used. The blank was utilized as the sample matrix with target element level beneath the detection limit by microwave plasma atomic emission spectroscopy (MP-AES) analysis. Lyophilization was performed in a Labconoco FreeZone 6 system (USA). For total selenium analysis, samples were digested in a microwave digestion system Muliwave GO (Anton Paar, Austria). The mineralization process was performed in 8 mL of suprapur grade 65% HNO_3 solution (purchased from Merck). The masses of the mineralized samples were around 1 g. Each mineralization process was performed in two cycles to prevent rapid pressure increase. Total selenium determination was performed under MP-AES supplied by Agilent.

Calibration solutions used were prepared with 20% concentrated nitric acid of ICP grade. The wavelength used was 196.026 nm. The standard addition method was performed in means to find out the matrix influence of the material.

3. Results and discussion

All sprout samples were evaluated by the measurement of total selenium content (Table 2). The substantial rise in the total selenium content in samples has been achieved via watering the sprouts with a 10 mg L^{-1} sodium selenite solution. It is worth noting that irrigation with the 10 mg L^{-1} sodium selenite solution should not have negative consequences during sprouts development, such as rotting, molding, and growth suppression.

A preliminary study suggests that matrix highly influences the results of the measurement of selenium in sprouts. Therefore, the standard addition method was used to evaluate the effect of the matrix on the results. The method of standard addition is widely used when the aim is to obtain accurate quantitative results. As an initiative step, calibration solutions were prepared with 20% HNO_3 and deionized water to meet this requirement. The comparison of calibration curves (with the used of 20% HNO_3 and with use of deionized water) is depicted in Fig. 2. Two measurements (sample sprouts, sample sprouts and addition of known standard with concentration of 4 ppm of selenium) were taken of four replicates for each of the batches. The selenium standard was added prior to the mineralization process.

Table 2 shows the selenium concentration in the samples with obtained solution concentration and intensity obtained under MP-AES. It was found that batches iii) and iv) are overaged the concentration as observed in obtained calibration curve in Fig. 2B. It would be notified that CRM (ERM e BC210a, wheat flour, certified total selenium content of 17.23± 0.91 mg kg^{-1} dry weight) was also analyzed for total selenium, and that was digested in the same way as samples. It

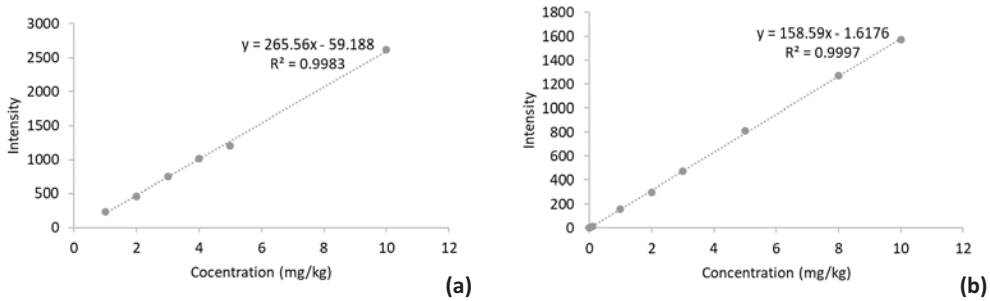

Fig. 2 (a) Calibration standards made from of deionized water. (b) Calibration standards made from addition of 20 % HNO_3 and deionized water.

Table 2
Obtained results under MP-AES with used of standard-addition method.

Batch	Sample	*c*(Se) / ppm	Intensity	Linear regression
i)	Normal sprouts	1.26	199.17	$Y = 133.79\,X + 199.17$
	Normal sprouts + added 4 ppm concentrated Se standard	4.62	734.32	
ii)	Soaked seeds (with 10 mg L^{-1} Na_2SeO_3 before germination)	0.74	116.15	$Y = 175.40\,X + 116.15$
	Soaked seeds (with 10 mg L^{-1} Na_2SeO_3 before germination) + added 4 ppm concentrated Se standard	5.15	817.75	
iii)	Watering the sprouts (with 10 mg L^{-1} Na_2SeO_3)	11.61	1846.86	$Y = 233.62\,X + 1846.9$
	Watering the sprouts (with 10 mg L^{-1} Na_2SeO_3) + added 4 ppm concentrated Se standard	17.49	2781.35	
iv)	Combination of batch ii) and iii)	12.94	2058.47	$Y = 126.28\,X + 2058.5$
	Combination of batch ii) and iii) + added 4 ppm concentrated Se standard	16.12	2563.57	
CRM	ERM-BC210a wheat flour (selenium)	2.76	438.14	$Y = 325.43\,X + 438.14$
	ERM-BC210a wheat flour (selenium) + added 4 ppm concentrated Se standard	10.94	1739.85	

could be notified in Table 2 that this CRM has a huge difference in obtained solution concentration. The availability of CRMs for it is total selenium content is very less in the market.

4. Conclusions

A preliminary effort was made to evaluate CRMs for the total selenium analysis by MP-AES. The needs are required of CRMs certified for their total selenium content in the matrix form of plant materials. The used standard addition method could be helpful to evaluate the particular type of matrix effect. The matrix effect has a major impact on the obtained results of the samples. The standard addition method allows detecting the mistake in a quality controlled analytical run. An instrumental sensitivity would possibly influence the value of the elemental concentration. To minimize or eliminate the matrix effect, the sample preparation step would be optimized so that samples can be removed from interfering compounds, changing the MP-AES parameters. It would be helpful to solve the problem to obtain reliable results for total selenium content in the samples in the future. It is important to notify that once a kind of CRM will be produced, which would play important role in quality assurance and quality control (QA/QC) elements.

References

[1] Saha U.: Selenium in the Soil-Plant Environment: A Review. *Int. J. Appl. Agric. Sci.* **3** (2017), 1–18.

[2] Choi Y., Kim J., Lee H.S., Kim C., Hwang I.K., Park H.K., Oh C.H.: Selenium content in representative Korean foods. *J. Food Compos. Anal.* **22** (2009), 117–122.

[3] Hartikainen H.: Biogeochemistry of selenium and its impact on food chain quality and human health. *J. Trace Elem. Med. Biol.* **18** (2005), 309–318.

[4] Navarro-Alarcon M., Cabrera-Vique C.: Selenium in food and the human body: A review. *Sci. Total Environ.* **400** (2008), 115–141.

[5] Funes-Collado V., Morell-Garcia A., Rubio R., López-Sánchez J. F.: Study of selenocompounds from selenium-enriched culture of edible sprouts. *Food Chem.* **141** (2013), 3738–3743.

[6] Muleya M., Young S. D., Reina S. V., Ligowe I. S., Broadley M. R., Joy E. J. M., Choper P., Bailey E.H.: Selenium speciation and bioaccessibility in Se-fertilised crops of dietary importance in Malawi. *J. Food Compos. Anal*. **98** (2021), 103841.

[7] Radawiec A., Szulc W., Rutkowska B.: Selenium biofortification of wheat as a strategy to improve human nutrition. *Agriculture* **11** (2021), 144.

[8] Ramkissoon C., Degryse F., da Silva R. C., Baird R., Young S. D., Bailey E. H., McLaughlin M.J.: Improving the efficacy of selenium fertilizers for wheat biofortification. *Sci. Rep.* **9** (2019), 19520.

[9] Bodnar M., Konieczka P.: Evaluation of candidate reference material obtained from selenium-enriched sprouts for the purpose of selenium speciation analysis. *LWT* **70** (2016), 286–295.

PTR-MS and electronic nose application for volatile fraction analysis of cigar tobacco

Paweł Jacek Hać*, Julia Dobosz, Łukasz Kołodziejski, Bartłomiej Michał Cieślik, Piotr Konieczka

Gdańsk University of Technology, Faculty of Chemistry, Department of Analytical Chemistry, 11/12 Gabriela Narutowicza Street, 80-233 Gdańsk, Poland ✉ *pawel.hac@pg.edu.pl*

Keywords
cigar analysis
electronic nose
proton transfer reaction–mass spectrometry
volatile organic compounds

Abstract
Cigar consumers attach great importance to the quality of these products. At the same time, cigars are often expensive, so destructive analytical methods of quality control are not being desired. However, it has been found that there are many volatile organic compounds in their headspace. Because of that, proton transfer reaction–mass spectrometry and electronic nose were used to analyse it. The obtained results were used to distinguish between cigars of different quality.

1. Introduction

Combustible tobacco products constitute a special type of consumer exposure to toxic substances due to their sensitive route of intake and addictive nature. The consumer becomes, in a sense, a slave of the poisoning addiction by losing control over drug-taking behaviour [1, 2].

There are many combustible tobacco products, among which we can mention: cigarettes, pipe tobacco, roll-your-own tobacco, and cigars. The latter is rarely the subject of scientific publications. Meanwhile, their popularity has been growing since the Cigar Aficionado magazine appeared [3].

Another problem is the nomenclature because three different products are usually referred to as "cigar": "large cigars", "little cigars", and "cigarillos". For consumers, these are three completely different products and should not be equated with each other. Large cigars are cylindrical products traditionally made from fermented and aged tobacco, wrapped in a leaf of tobacco. Cigarillos are smaller than these, while little cigars are usually about the size of a cigarette and contain a wrapper made of paper that contains tobacco [4].

In addition, large cigars can be divided into hand-made and machine-made ones. Cigarillos and little cigars are almost always machine-made. The way it is made affects the price of a cigar, in general, it can be said that large cigars which are hand-made are more expensive. As you can see, it is hard to disagree with the title

of the paper [3] entitled: "*Sometimes a cigar [magazine] is more than just a cigar [magazine]*", because sometimes much more work, time, and attention are devoted to valued, large cigars than to other products generally classified as "cigars". Consumers expect authenticity when buying an expensive handmade cigar.

However, the popularization of cigars creates a tempting possibility of committing counterfeits, especially in the area of cheap and medium-cheap products. A simple example of a counterfeit is to sell a machine-made cigar as a hand-made cigar. Their distinction with analytical techniques is the aim of this study.

Many volatile organic compounds occurring in the subsurface phase cigar are known [6]. These compounds are emitted without the need to interfere with the structure of the cigar, therefore the proposed method is based on their analysis.

2. Experimental

2.1 Samples

The cigars used for the research were purchased from online stores. Products from four countries (Kuba, Mexico, the Dominican Republic, and Nicaragua) were selected. Among them, both types were ordered: hand- and machine-made.

2.2 Reagents and chemicals

The advantage of the proposed approach is no necessity of using any solvents, reagents, or other chemicals.

2.3 Instrumentation

In response to the need for the development of novel, effortless, time-saving, and possibly minimally polluting analytical methods, the PTR TOF1000 ultra proton transfer reaction mass spectrometer (Ionicon, Austria) was used. This technique has already found an application in food analysis [5]. PTR-MS enables the identification and determination of volatile organic compounds. It was used to analyse the gas fraction of the cigar headspace to search for potential differentiator compounds. An electronic nose as a non-targeted method was also used.About 0.5 g of each tested cigar was closed in a headspace vial. To increase the emission of volatile organic compounds, the samples were heated to 60 °C.

3. Results and discussion

One of the observed compounds that occurred in a mass spectrum at a value around m/z = 107.1 is a potential differentiator of hand-made cigars. Judging by its

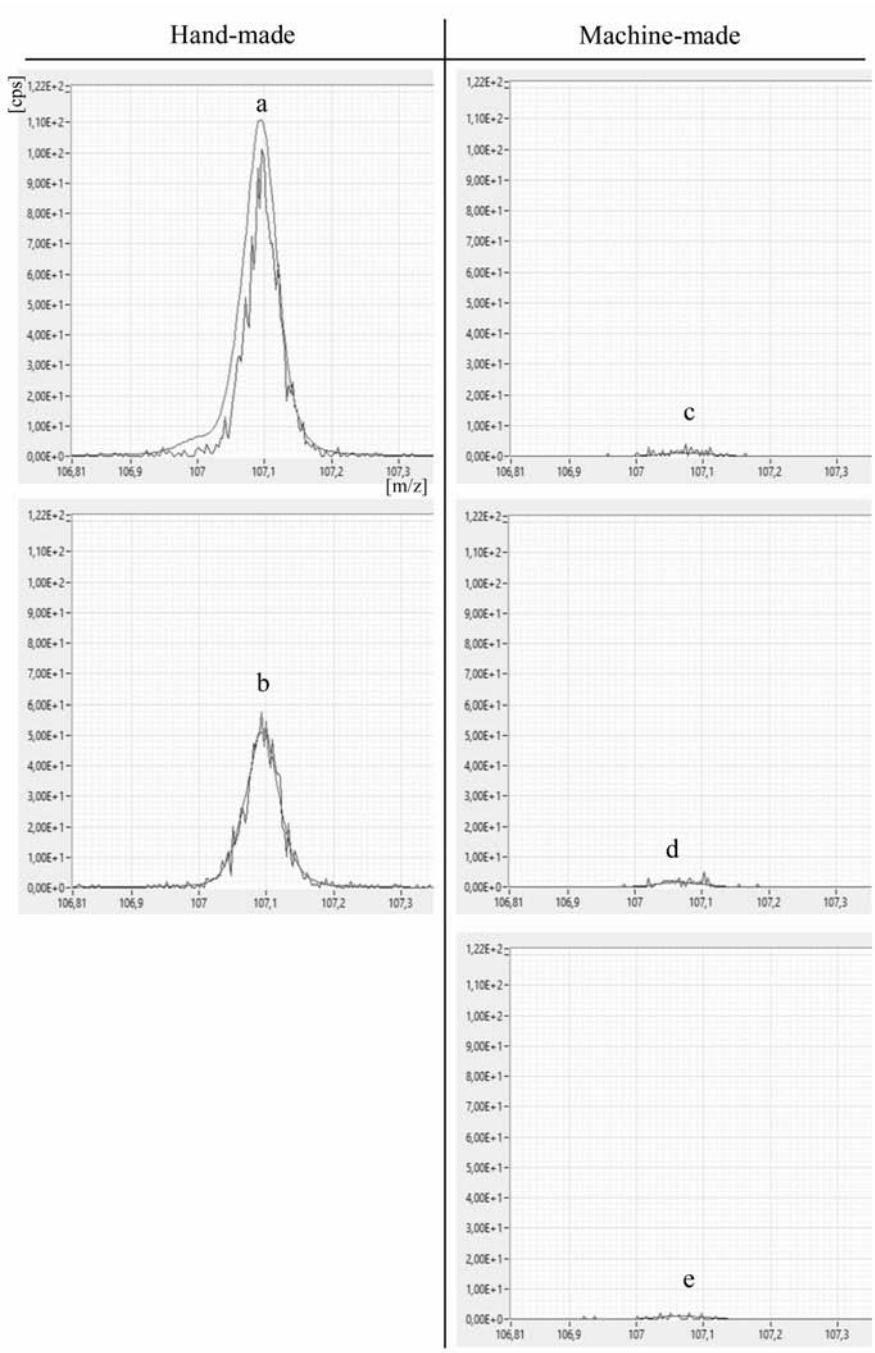

Fig. 1 Fragment of the mass spectrum for the compound at about m/z = 107.1. Values on the vertical axis are in counts per second [cps]: (a) *Oliva Serie V Lancero* (Nicaragua), (b) *Arturo Fuente Magnum R No.54* (The Dominican Republic), (c) *Oliva Serie G Cigarillo* (Nicaragua), (d) *La Prueba No. 2* (Mexico), and (e) *Guantanamera Puritos* (Cuba).

mass and data found in the literature, this is tentatively identified as xylenes. Spectra fragments for some of the tested cigars are presented in Fig. 1. It can be seen that in the case of machine-made cigars intensities of the signals are much lower than in the case of hand-made cigars.

Cigars are however produced from different types of tobacco. The chosen method of leaves processing has a large impact on the aroma of a final product. Therefore, the quantity of volatile organic compounds in the headspace may be determined not by the method of cigar production, but by the quality of the leaves used. Because machine-made cigars are generally cheaper than hand-made, it is expected that manufacturers use cheaper leaves to their production and reduces the costs by choosing inappropriate storage methods. Nevertheless, the observed differences in the composition of volatile organic compounds in the headspace would testify to the difference in product quality, so the approach would still be appropriate, but the aim would slightly change.

In addition to a targeted cigar analysis, there is a wide field to use of untargeted analysis approaches, like electronic nose, but also data mining and chemometric methods. This could be the basis for the incorporation of the mechanic learning protocols.

Moreover, it is possible that some products are „mixed variant". Manual production does not necessarily preclude the usage of low-quality leaves. It is hard to predict the results in those cases.

4. Conclusions

Analysis of volatile organic compounds in cigar headspace provides valuable information which can be used to estimate the quality of the products. The results range from 50 ppb to even 5 ppm correspond to the hand-made cigars. Lower results correspond to the machine-made. For technical reasons, only a slice of the cigar was used for testing, but the approach can be applied to the whole product without its destruction. It is a big advantage of the proposed method.

Acknowledgments

We are very grateful to Dr Tomasz Majchrzak and Dr Wojciech Wojnowski for their time, support, and advice.

References

[1] Benowitz N.L.: Cigarette smoking and nicotine addiction. *Med. Clin. North Am.* **76** (1992), 415–437.

[2] Benowitz N.L., Hukkanen J., Jacob P.: Nicotine chemistry, metabolism, kinetics and biomarkers. In: *Nicotine Psychopharmacology (Handbook of Experimental Pharmacology, vol. 192)*. Henningfield J.E., London E.D., Pogun S. (eds.). Springer, Berlin 2009, p. 29–60.

[3] DeSantis A.D., Morgan S.E.: Sometimes a cigar [magazine] is more than just a cigar [magazine]: Pro-smoking arguments in Cigar Aficionado, 1992–2000. *Health Commun.* **15** (2003), 457–480.

[4] Kong G., Creamer M.L.R., Simon P., Cavallo D.A., Ross J. C., Hinds J. T., Fishbein H., Gutierrez K.: Systematic review of cigars, cigarillos, and little cigars among adolescents: Setting research agenda to inform tobacco control policy. *Addict. Behav.* **96** (2019), 192–197.
[5] Majchrzak T., Wojnowski W., Głowacz-Różyńska A., Wasik A.: On-line assessment of oil quality during deep frying using an electronic nose and proton transfer reaction mass spectrometry. *Food Control.* **121** (2021), 107659.
[6] Wahlberg I., Karlsson K., Austin D.J., Junker N., Roeraade J., Enzell C.R., Johnson W.H.: Effects of flue-curing and ageing on the volatile, neutral and acidic constituents of Virginia tobacco, *Phytochemistry* **16** (1977), 1217–1231.

A new method for double bond characterization in lipids by ultraviolet photodissociation mass spectrometry

Barbora Rumlová[a, b, *], Timotej Strmeň[b], Josef Cvačka[a, b]

[a] *Institute of Organic Chemistry and Biochemistry of the Czech Academy of Sciences, Flemingovo náměstí 542/2, 160 00 Prague 6, Czech Republic* ✉ *barbora.rumlova@uochb.cas.cz*
[b] *Charles University, Faculty of Science, Department of Analytical Chemistry, Hlavova 8/2030, 128 43 Prague 2, Czech Republic*

Keywords
double bond
lipids
mass spectrometry
ultraviolet photodissociation

Abstract
Lipids are structurally diverse biomolecules with vital functions in biological systems. Some of these functions are closely associated with the specific location of the carbon-carbon double bond in the lipid acyl chains. The chain length and the number of unsaturated carbon-carbon bonds can be determined using conventional MS/MS-based structural elucidation methods employing low or higher energy collision-induced dissociation. However, these dissociation techniques do not provide more subtle structural details, for example, the position of unsaturated bonds. Another type of activation method – ultraviolet photodissociation can be used for this purpose. In this study, a new method for characterization of double bond location in lipids acyl chain was developed using 193 nm ultraviolet photodissociation implemented on Orbitrap Fusion Lumos mass spectrometer. This approach is based on the derivatization of the double bond with bis-(5-iodo-[2]pyridyl)-disulfide; subsequent specific cleavages provide a unique diagnostic pair bearing information about the double bond position.

1. Introduction

Mass spectrometry is an analytical tool used for the structural characterization of analytes based on their mass spectra [1]. Activation techniques are used to obtain structural information on biomolecules. Nowadays, the most commonly used activation technique is based on collisions [2]. A collision between an accelerated precursor ion and neutral gas leads to increased ion's internal energy, resulting in bond cleavages [3]. Recently, interest in UV photodissociation has grown. This technique has been commercially available only since a few years ago in the form of a UV laser implemented in the Orbitrap Fusion Tribrid mass spectrometer. UVPD energizes ions by absorption of high-energy photons. UV photoabsorption brings ions to excited electronic states, thus accessing higher-energy dissociation

pathways not typically observed upon low-energy collisional activation [4]. Since many biomolecules exhibit some degree of photoabsorptivity, there have been many applications for their characterization.

Lipids are one of the four major classes of biological molecules. They are very structurally diverse, which corresponds with their multiple functions in the human body. They can serve as energy depots, act as building blocks for cellular structures, and participate in signal transduction [5]. Alternations in lipid composition can result in pathological processes and play critical roles in the emergence of severe conditions, including Alzheimer's disease, Parkinson's disease, cardiovascular diseases, and cancer. Hence, lipid characterization is vital for understanding the pathways involved in cellular metabolism [6, 7]. UV photodissociation has already been utilized for many lipid classes and made it possible to elucidate their structural features [8]. One of the essential features of lipids is the double bond position. Many double bond positional isomers exist, and their determination remains a long-standing challenge in lipidomics [9]. Some methods for selective fragmentation of double bonds have been developed. An example is an ozone-induced dissociation (OzID)-MS/MS that produces a diagnostic pair of product ions differing by 16 Da [10]. Charge-switch derivatization of the carboxylic group of fatty acids has been utilized to generate characteristic ions for double bond localization [11]. Direct identification of double bonds in various classes of lipids position can also be achieved by Paternò–Büchi reaction combined with MS/MS ultraviolet photodissociation. It has been firstly reported in contrast to higher energy collisional dissociation in the structural characterization of phosphatidylcholine. This method allowed localization of double bonds in the acyl chains based on the formation of product ion pairs differing by 24 Da. With the UVPD commercialization, efforts to characterize lipids using UVPD at 213 nm accelerated [8].

2. Experimental

2.1 Chemicals

2-Chloro-5-iodopyridine (97%), sodium hydrosulfide hydrate (≥60%), lithium formate monohydrate (BioUltra, ≥99%) were purchased from Sigma-Aldrich (Germany). Sodium carbonate anhydrous (analytical grade) and sodium thiosulfate (analytical grade) were obtained from Erba Lachema (Czech Republic). Methanol (LC/MS grade) was purchased from Fisher Chemical (USA), 2-propanol (Chromaslov LC/MS), and chloroform (Chromasolv Plus, for HPLC) were obtained from Honeywell/Riedel de Haen (Germany). Standards of lipids were purchased from Nu-Chek-Prep (Minnesota, USA).

2.2 Sample preparation

Bis-(5-iodo-[2]pyridyl)-disulfide was synthesized by suspending 5 mg of 2-chloro-5-iodopyridine in 600 µL of chloroform and methanol mixture (1:2, *v:v*) followed by the addition of 6 mg of sodium hydrosulfide hydrate. A sealed glass ampoule with the reaction mixture was incubated at 95 °C for 24 hours. After opening the ampoule, the reaction mixture was neutralized by adding sodium carbonate aqueous solution, and the organic phase was separated from the aqueous phase. Investigated lipid standard (about 1 mg) was added to 100 µl of solution bis-(5-iodo-[2]pyridyl)-disulfide and 30 µL of I_2 dissolved in toluene to concentration 60 mg mL^{-1}. Excess iodine was removed by an aqueous solution of sodium thiosulfate. All samples were diluted to the final concentration of 0.01 mg mL^{-1}.

For lithium adduct experiments, lipids were dissolved in isopropanol:methanol:chloroform (4:2:1, *v:v:v*) containing lithium formate (2mM) at a concentration of 0.01 mg mL^{-1}.

2.3 Mass spectrometry

Mass spectra were collected with the Orbitrap Fusion Lumos Tribrid (Thermo Fisher Scientific, USA) equipped with a Class 213 nm laser system with a 2.5 kHz repetition rate delivering > 1.2 µJ per pulse. Inlet capillary temperature was set at 275 °C. The samples were delivered to the mass spectrometer using an Advion Triversa Nanomate ionization source (Advion, USA). The spray voltage was set at 1.4 kV, and a gas pressure of 0.3 psi was used. The isolation window ± 0.5 *m/z* for selection of precursor ion was used. Data were manually interpreted in Xcalibur Qual Browser.

3. Result and discussion

A new derivatization reagent for localizing double bond position in lipids was designed and prepared [12]. The structure of the derivatization agent is based on our previous work, where 2,2′-dipyridyl disulfide was used for the derivatization of the double bonds in unsaturated compounds [13]. When collisionally activated, the derivatized lipids provide diagnostic peaks for the determination of double bond positions. The current derivatization agent contains a photolabile aryl

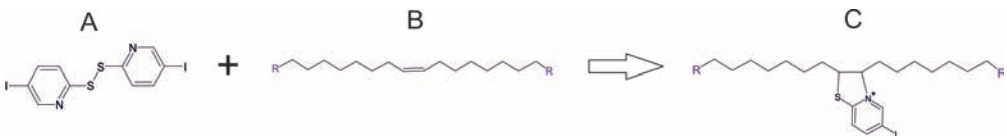

Fig. 1 Scheme of derivatization reaction: (A) bis-(5-iodo-[2]pyridyl)-disulfide, (B) lipid with double bond, and (C) derivatized lipid, the reaction product.

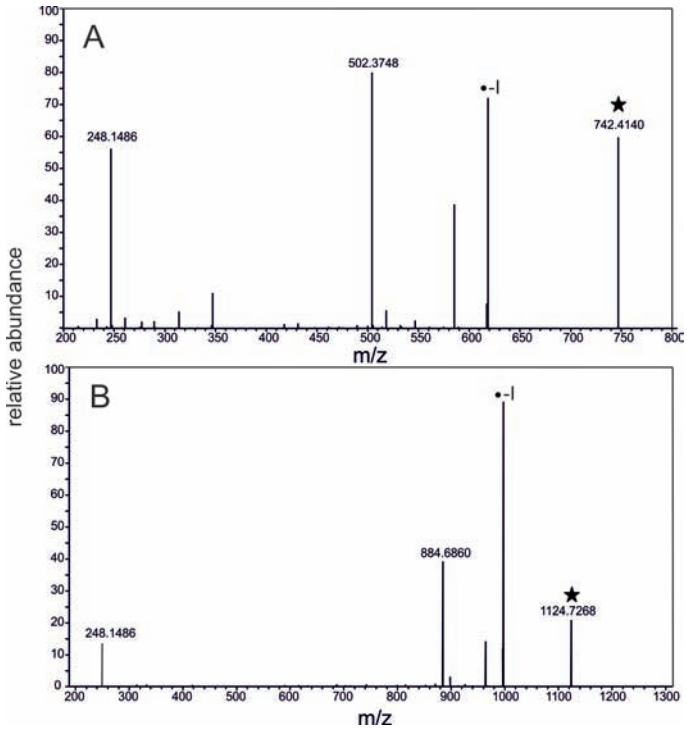

Fig. 2 UV photodissociation MS/MS spectra of (A) palmityl oleate, and (B) 1-palmitoyl-2-oleyl-3-arachidonyl-glycerol. The activation time was 150 ms.

iodine motif, which can be selectively activated by the UV laser implemented in Orbitrap mass spectrometer [14, 15]. The activation gives rise to diagnostic product ions that enable the assignment of double bond positions. Figure 1 shows the reaction scheme with the proposed structure of the product. Lipids with different double bond positions were used in this study.

3.1 Monounsaturated lipids

The UV photodissociation MS/MS spectrum of the precursor ion M^+ *m/z* 742.4140 (marked with asterisks), the derivative of palmityl oleate, is shown in Fig. 2A. A pair of unique product ions *m/z* 502.3748 and *m/z* 248.1486, which provided information about the original double bond at the *n-9* position, was observed in the spectrum. The cleavages occurred in the carbon-carbon bonds adjacent to the double bond. Figure 2B shows photodissociation of the precursor ion of 1-palmitoyl-2-oleyl-3-arachidonyl-glycerol *m/z* 1124.7268. The abundant ion *m/z* 884.6860 and a minor peak *m/z* 248.1486 are two diagnostic fragments for the double bond at the *n-9* position in the oleyl chain of the triacylglycerol. Loss of iodine is an important fragmentation channel in the UVPD of the derivatives (Fig. 2).

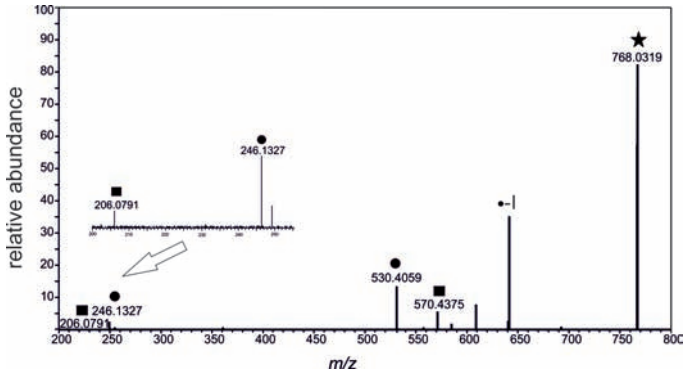

Fig. 3 UV photodissociation MS/MS spectra of stearyl linoleate. The activation time was 150 ms.

3.2 Polyunsaturated lipids

Two or three pairs of the diagnostic fragments were observed in the spectra of lipids with two or three double bonds. Stearyl linoleate was successfully derivatized, and the location of methylene-interrupted double bonds was determined from two sets of diagnostic fragment ions (Fig. 3). The first set of diagnostic pairs, marked with the circles, *m/z* 206.0791 and 570.4374, correspond to an *n-6* double bond position. The second set *m/z* 246.1327 and 530.4058, marked with squares, indicates the *n-9* double bond position. As can be seen in Fig. 3, only monosubstituted derivatives were observed.

3.3 Laser activation time

In the next step, the effect of laser activation time on the formation of diagnostic product ions was investigated. UV photodissociation MS/MS spectra of myristyl oleate derivative were collected at various activation times and used to assess the effect of laser activation time on the diagnostic fragment intensities. The presented method was compared with another approach to determine double bonds based on UV photodissociation of lithium adducts [16]. UV dissociation MS/MS spectra of myristyl oleate lithium adduct $[M+Li]^+$ (*m/z* 485.4906) resulted in a pair of unique product ions with a mass difference of 24.0000 Da, which provided information about the position of the double bond. These ions *m/z* 347.3496 and *m/z* 371.3496 are generated by 1,2-elimination at the carbon-carbon bonds adjacent to the double bond (Fig. 4A1) [16]. Their intensities were also collected at various laser activation times. In the lithium adduct method, the intensities of the diagnostic fragments linearly increased with the laser activation time (Fig. 4A2). A spectrum of the precursor M^+ *m/z* 714.3822 using the novel derivatization agent is shown in Fig. 4. A pair of unique product ions *m/z* 248.1485 and *m/z* 474.3432, which provided information about the original double bond at the *n-9* position, were recognized in the spectrum (Fig. 4B1). The signal intensities

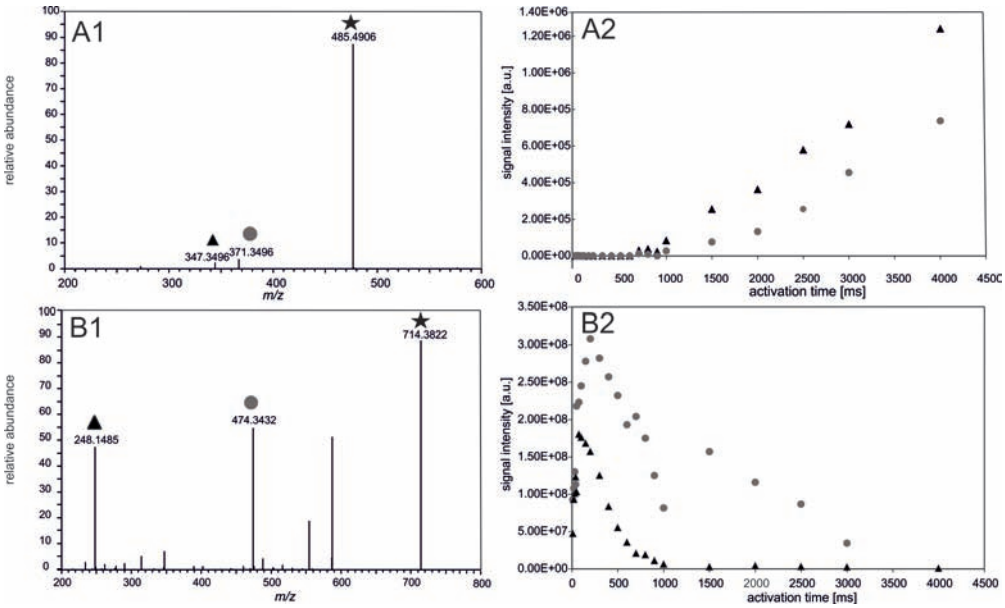

Fig. 1 (A1) UV photodissociation MS/MS spectra of myristyl oleate using lithium adduct method. (A2) Signal intensities of the diagnostic product ions from UVPD-MS/MS of lithiated myristyl oleate as a function of laser activation time. (B1) UV photodissociation MS/MS spectra of derivatized myristyl oleate using the new method. (B2) Signal intensities of the diagnostic product ions from UVPD-MS/MS of derivatize myristyl oleate as a function of laser activation time.

of this pair of product ions were plotted as a function of laser activation time. On the contrary, the highest signals of product ions appeared at low activation times (150 ms), which renders this method much faster than the lithium adducts approach (Fig. 4B). Such short activation times make it possible to use UVPD for HPLC/MS experiments. Moreover, higher diagnostic pair intensities were observed for the derivatization method.

4. Conclusion

A new method for double bond localization in lipids based on specific derivatization on double bond with bis-(5-iodo-[2]pyridyl)-disulfide and ultraviolet photodissociation mass spectrometry was developed. The reaction introduced a permanent charge into the molecule and incorporated a photolabile aryl-iodine motif to generate structurally diagnostic ions. Furthermore, ultraviolet activation-induced cleavage between one of the carbon-carbon bonds adjacent to the double bond resulted in diagnostic fragment pairs. This approach shows the utility of UVPD for the structural characterization of double bonds in lipids, even with methylene-interrupted bonds. Moreover, intensities of diagnostic pairs for the presented method and lithium adduct were compared. The proposed method provides significantly better intensities of diagnostic pair fragments using the same activation times.

Acknowledgments

The research was supported by Specific University Research (SVV 260560) and the Charles University Grant Agency (GAUK 650520).

References

[1] Buchanan M.V., Hettich R.L.: Fourier transform mass spectrometry of high-mass biomolecules. *Anal. Chem.* **65** (1993), 245A–259A.
[2] McLuckey S.A.: Principles of collisional activation in analytical mass spectrometry. *J. Am. Soc. Mass Spectrom.* **6** (1992), 599–614.
[3] Levsen K.: *Fundamental Aspects in Organic Mass Spectrometry.* 2nd ed. New York, Wiley 1978.
[4] Ryan E., Nguyen C.Q.N., Shiea C., Reid G.E.: Detailed structural characterization of sphingolipids via 193 nm ultraviolet photodissociation and ultra high resolution tandem mass spectrometry. *J. Am. Soc. Mass Spectrom.* **28** (2017), 1406–1419.
[5] Vance J.E., Vance D.E.: *Biochemistry of Lipids, Lipoproteins and Membranes.* 4th ed. Elsevier 2008.
[6] Harayama T., Riezman H.: Understanding the diversity of membrane lipid composition. *Nat. Rev. Mol. Cell Biol.* **20** (2018), 281–296.
[7] Wenk M.R.: The emerging field of lipidomics. *Nat. Rev. Drug Discov.* **4** (2005), 594–610.
[8] Brodbelt J.S., Morrison L.J., Santos I.: Ultraviolet photodissociation mass spectrometry for analysis of biological molecules. *Chem Rev.* **7** (2020), 3328–3380.
[9] Wei F., Lamichhane S., Orešič M., Hyötyläinen T.: Lipidomes in health and disease: Analytical strategies and considerations. *TrAC – Trends Anal. Chem.* **120** (2019), 115664.
[10] Poad L.J.B., Pham H.T., Thomas M.C., Nealon J.R., Campbell J.L., Mitchell T.W., Blanksby S.J.: Ozone-induced dissociation on a modified tandem linear ion-trap: Observations of different reactivity for isomeric lipids. *J. Am. Soc. Mass Spectrom.* **21** (2010), 1989–1999.
[11] Klein D.R., Blevins M.S., Macias L.A., Douglass M.V., Stephen Trent M.S., Brodbelt J.S.: Localization of double bonds in bacterial glycerophospholipids using 193 nm ultraviolet photodissociation in the negative mode. *Anal. Chem.* **92** (2020), 5986–5993.
[12] Räth C., Binz A.: Mercaptane und Sulfosäuren des Pyridins. XII. Mitteilung über Derivate des Pyridins. *Justus Liebigs Ann. Chem.* **487** (1993), 105–119.
[13] Strmeň T., Cvačka J.: Aldrithiol-2 as a new derivatization agent for double bond localization in unsaturated compounds by mass spectrometry. In: *Proceedings of the 15th ISC Modern Analytical Chemistry.* K. Nesměrák (ed.). Prague, Faculty of Science, Charles University 2019, p. 117–117.
[14] Narreddula V.R., Boase N.R., Ailuri R., Marshall D.L., Poad B.L.J., Kelso M.J., Trevitt A. J., Mitchell T.W., Blanksby S.J.: Introduction of a fixed-charge, photolabile derivative for enhanced structural elucidation of fatty acids. *Anal. Chem.* **15** (2019), 9901–9909.
[15] Narreddula V.R., McKinnon B.I., Marlton S.J.P., Marshall D.L., Boase N.R.B., Poad B.L.J., Trevitt A.J., Mitchell T.W., Blanksby S.J.: Next-generation derivatization reagents optimized for enhanced product ion formation in photodissociation-mass spectrometry of fatty acids. *The Analyst* **146** (2021), 156–169.
[16] Ryan E., Nguyen C.Q., Shiea C., Reid G.E.: Detailed structural characterization of sphingolipids via 193 nm ultraviolet photodissociation and ultra high resolution tandem mass spectrometry. *J. Am. Soc. Mass Spectrom.* **28** (2017), 1406–1419.

Novel photochemical vapor generation of rhenium for its ultratrace determination

Jaromír Vyhnanovský[a, b, *], Karolína Hašlová[a, b], Stanislav Musil[a]

[a] *Institute of Analytical Chemistry of the Czech Academy of Sciences, Department of Trace Element Analysis, Veveří 97, 602 00 Brno, Czech Republic* ✉ *jaromir.vyhnanovsky@gmail.com*
[b] *Charles University, Faculty of Science, Department of Analytical Chemistry, Hlavova 8/2030, 128 43 Prague 2, Czech Republic*

Keywords
inductively coupled plasma mass spectrometry
photochemical vapor generation
rhenium

Abstract
Volatile species of rhenium were generated using a 19 W thin film flow-through UV photoreactor from 6 mol L^{-1} formic acid. The addition of 1000 mg L^{-1} Cd^{2+} and 10 mg L^{-1} Fe^{2+} as sensitizers was found to be critical for achieving analytically useful photochemical vapor generation efficiency. Wrapping the UV photoreactor in aluminum foil also had a positive effect on the photochemical vapor generation efficiency and the optimal carrier flow rate was found to be 1.6 mL min^{-1}. Using these optimal conditions, the limit of detection and repeatability (at 100 ng L^{-1} Re) were determined to be 0.2 ng L^{-1} and 4.8% (n = 10), respectively.

1. Introduction

Sample introduction is the Achilles' heel of atomic spectrometry methods. Photochemical vapor generation is nowadays an emerging alternative sample introduction technique. It employs a source of UV-radiation that irradiates a low molecular weight organic acid containing medium (most commonly formic acid, acetic acid, or their combinations) with an analyte. Highly reducing radicals and aquated electrons are produced and convert the analyte into a volatile species which is then transported into a detector [1]. So far, the use of photochemical vapor generation has been described for some 30 elements spanning hydride-forming elements [1–3], transition metals [1, 4–8] and even non-metals [1, 9–10].

The photochemical vapor generation of rhenium was described only very recently in a review article by Zhen et al. [11] who performed a basic optimization and described a positive effect of sensitizers and their combinations. With their optimal conditions the authors were able to achieve a limit of detection of 1 ng L^{-1}, which was not sufficient for analysis of rhenium in real samples. Other parameters, such as the repeatability or photochemical vapor generation efficiency are not discussed in the article.

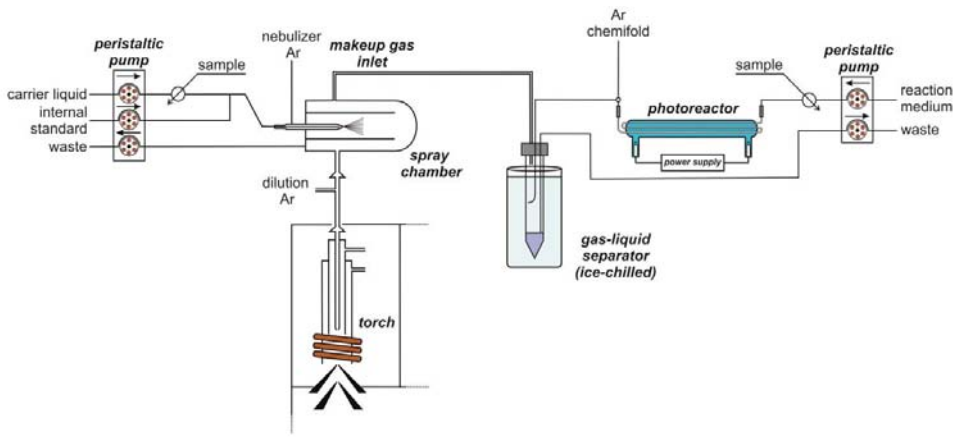

Fig. 1 Schematic diagram of a photochemical vapor generation coupled to ICP-MS.

The main aim of this work was to optimize the conditions of photochemical vapor generation of Re with inductively coupled plasma mass spectrometry (ICP-MS) detection, examine the effect of various metal sensitizers to achieve the highest generation efficiency possible and reach a low limit of detection which would enable the determination of rhenium in real environmental samples that typically contain extremely low concentrations.

2. Experimental

2.1 Reagents and chemicals

Deionized water (< 0.2 μS cm^{-1}, Ultrapur, Watrex, USA) was used for preparation of all solutions. Formic acid (98%, p.a., Lach-Ner, Czech Republic) was used for preparation of the reaction medium. A 1000 mg L^{-1} Re stock solution was sourced from Sigma-Aldrich (USA). The following compounds were investigated as potential metal sensitizers: cadmium(II) acetate dihydrate (p.a., Lach-Ner, Czech Republic), iron(II) acetate (99.99% trace metal basis, Sigma-Aldrich, USA), copper(II) acetate monohydrate (p.a., Merck, Germany), cobalt(II) acetate tetrahydrate (p.a., Sigma-Aldrich, USA) and manganese(II) acetate tetrahydrate (99.99% trace metal basis, Sigma-Aldrich, USA).

2.2 Instrumentation

A schematic diagram of the photochemical vapor generation system coupled to the ICP-MS is shown in Fig. 1 (detailed description can be found in reference [6]). Briefly, a single quadrupole ICP-MS Agilent 7700x (Agilent Technologies, USA) was used as the detector. Deionized water was mixed with a 10 μg L^{-1} Rh internal standard solution in 2% HNO_3 and was subsequently nebulized by a MicroMist

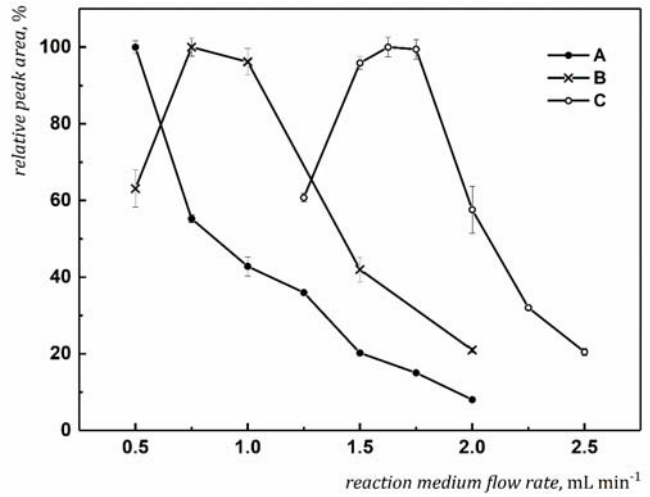

Fig. 2 The influence of reaction medium flow rate on the relative peak area (normalized for the highest value of a given curve): (A) 6 mol L^{-1} formic acid, (B) 6 mol L^{-1} formic acid, 1000 mL min^{-1} Cd^{2+} and 10 mL min^{-1} Fe^{2+}, and (C) 6 mol L^{-1} formic acid, 1000 mL min^{-1} Cd^{2+} and 10 mL min^{-1} Fe^{2+}, photoreactor wrapped in aluminum foil.

nebulizer during photochemical vapor generation. Isotopes of ^{185}Re, ^{187}Re, and ^{103}Rh were monitored, no gas mode in the reaction/collision cell and time resolved analysis mode (peak area evaluated) were employed for all measurements. All tubing used was made from PTFE except for tygon tubing in the peristaltic pump (Reglo ICC, Ismatec, Switzerland). The high-efficiency flow-through photoreactor was a 19 W low-pressure mercury discharge lamp (Beijing Titan Instruments, China) with a quartz central channel (≈720 μL internal volume). Sample solutions were introduced into a stream of the reaction medium using an injection valve (V-451, IDEX Health and Science, USA; sample loop volume 0.5 mL). An effluent from the photoreactor was carried by a flow of argon into the gas-liquid separator (internal volume 15 mL), where the volatile species were separated from the liquid waste and carried to the inlet of a Scott-type spray chamber (originally the inlet for makeup argon) of the ICP-MS.

3. Results and discussion

Preliminary experiments demonstrated that volatile species of rhenium (most probably dirhenium decacarbonyl) can be generated from a formic acid based medium. First, the optimization of generation conditions was done without any sensitizers and the optimal conditions were chosen as: formic acid concentration 6 mol L^{-1} at a reaction medium flow rate of 1 mL min^{-1} (corresponding to irradiation time of ≈ 44 s) and 600 mL min^{-1} argon gas flow rate. It is important to note that at the reaction medium flow rate of 1 mL min^{-1} the highest sensitivity was not reached, and the sensitivity further increased at flow rates lower than 1 mL min^{-1} (longer irradiation time) (Fig. 2) but at such flow rates analysis time per one

sample injection was significantly prolonged. Hence, 1 mL min^{-1} was chosen for further experiments as a compromise between sensitivity and analysis time.

Using the above-mentioned optimal conditions, the use of various metal sensitizers was investigated in order to enhance the photochemical vapor generation efficiency. Possible sensitizers were chosen with respect to their significant enhancement effect described for other analytes [1–3, 6, 8, 11]. Enhancement of the signal was observed when Cd^{2+}, Fe^{2+}, and Co^{2+} were added, Cd^{2+} being the most effective, enhancing the sensitivity some 25-fold when 3000 mg L^{-1} of Cd^{2+} were added to the sample. In the case of Fe^{2+} and Co^{2+}, the enhancement factor and the optimal concentrations were 4-fold at 20 mg L^{-1} of Fe^{2+} and 3-fold at 10 mg L^{-1} of Co^{2+}, respectively. The addition of Mn^{2+} did not exhibit any positive or negative effect across the tested range (1 to 100 mg L^{-1}), and the addition of Cu^{2+} caused a severe interference at concentrations higher than 10 mg L^{-1}. Possible combinations of multiple modifiers were investigated to further increase the photochemical vapor generation efficiency and the optimal combination (and concentration) of sensitizers was finally found to be 1000 mg L^{-1} Cd^{2+} and 10 mg L^{-1} Fe^{2+}, with the final enhancement of the signal of around 40-fold. Mixing 1000 mg L^{-1} Cd^{2+} with Co^{2+} led to a drop in sensitivity for all tested concentrations of Co^{2+} (5, 10, and 20 mg L^{-1}).

With the optimal combination of sensitizers, concentration of formic acid and the reaction medium flow rate (irradiation time) were re-optimized. The latter parameter exhibited a different effect on sensitivity than in the absence of metal sensitizers because a distinct optimal value was identified (Fig. 2); a maximum of sensitivity was found at 0.75 mL min^{-1} (i.e., irradiation time of ≈ 51 s). This shift suggests that lower dose of UV radiation is needed to form the volatile species when sensitizers are used.

Lastly, the effect of aluminum foil wrapped around the photoreactor was examined. This resulted in an additional 2-fold increase in sensitivity. Similarly, the optimal value of the reaction medium flow rate was further shifted to 1.6 mL min^{-1} (i.e., irradiation time of ≈ 32 s; Fig. 2), probably due to more efficient irradiation of the sample caused by the reflection of the UV light by the aluminum foil and/or due to the increased temperature inside the photoreactor.

To summarize, the optimal conditions for the photochemical vapor generation of rhenium were 6 mol L^{-1} formic acid at a reaction medium flow rate of 1.6 mL min^{-1}, 1000 mg L^{-1} of Cd^{2+} and 10 mg L^{-1} of Fe^{2+} added to the sample as sensitizers, photoreactor wrapped with aluminum foil, and 600 mL min^{-1} argon flow rate.

At these conditions, a calibration curve was measured and evaluated (Re concentrations 0, 5, 25, 100, 500, and 2000 ng L^{-1}). The calibration was linear in the whole range of concentrations (R^2 = 0.9999). The limit of detection was determined as 3 times the standard deviation of peak area of 10 blank measurements and was calculated as 0.2 ng L^{-1}. The repeatability of 10 consecutive measurements of 100 ng L^{-1} Re standard was 4.7%.

4. Conclusions

The conditions of photochemical vapor generation of rhenium were optimized using ICP-MS as the detector and the resulting conditions are in main aspects in good agreement with the very recent work [11]. Namely, long irradiation times and the use of sensitizers were found to be essential in both works, but the individual optimal conditions do not match, which may be in part caused by different approaches and conventions used during optimization (e.g., stop-flow vs. continuous flow irradiation of the sample). Further efforts will be made to increase the photochemical vapor generation efficiency as well as to decrease the limit of detection to sub 0.1 ng L^{-1} levels. This should enable determination of rhenium in certified reference materials as well as in environmental samples such as drinking, ground, river and seawater. Simultaneously, possible interferences will be examined as they can pose a big challenge during the analysis of such real samples.

Acknowledgments

The support of The Czech Science Foundation (Project No. 19-17604Y), Czech Academy of Sciences (Institutional support RVO: 68081715), and Charles University (project SVV260560 and project GAUK 60120) is gratefully acknowledged.

References

[1] Sturgeon R.E.: Photochemical vapor generation: a radical approach to analyte introduction for atomic spectrometry. *J. Anal. At. Spectrom.* **32** (2017), 2319–2340.
[2] Vyhnanovský J., Yildiz D., Štádlerová B., Musil S.: Efficient photochemical vapor generation of bismuth using a coiled Teflon reactor: Effect of metal sensitizers and analytical performance with flame-in-gas-shield atomizer and atomic fluorescence spectrometry. *Microchem. J.* **164** (2021) 105997.
[3] Xu T., Hu J., Chen H.J.: Transition metal ion Co(II)-assisted photochemical vapor generation of thallium for its sensitive determination by inductively coupled plasma mass spectrometry. *Microchem. J.* **149** (2019) 103972.
[4] Šoukal J., Sturgeon R.E., Musil S.: Efficient photochemical vapor generation of molybdenum for ICPMS detection. *Anal. Chem.* **90** (2018), 11688–11695.
[5] de Oliveira R.M., Borges D.L.G.: UV photochemical vapor generation of noble metals (Au, Ir, Pd, Pt and Rh): a feasibility study using inductively coupled plasma mass spectrometry and seawater as a test matrix. *J. Anal. At. Spectrom.* **33** (2018), 1700–1706.
[6] Vyhnanovský, R.E. Sturgeon, S. Musil: Cadmium assisted photochemical vapor generation of tungsten for ICPMS detection. *Anal. Chem.* **91** (2019), 13306–13312.
[7] Guo X., Sturgeon R.E., Mester Z., Gardner G.J.: Vapor generation by UV irradiation for sample introduction with atomic spectrometry. *Anal. Chem.* **76** (2004), 2401–2405.
[8] Nováková E., Horová K., Červený V., Hraníček J., Musil S.: UV photochemical vapor generation of Cd from a formic acid based medium: optimization, efficiency and interferences. *J. Anal. At. Spectrom.* **35** (2020), 1380–1388.
[9] Hu J., Sturgeon R.E., Nadeau K., Hou X., Zheng C., Yang L.: Copper ion assisted photochemical vapor generation of chlorine for its sensitive determination by sector field inductively coupled plasma mass spectrometry. *Anal. Chem.* **90** (2018), 4112–4118.
[10] Sturgeon R.E., Pagliano E.: Evidence for photochemical synthesis of fluoromethane. *J. Anal. Atom. Spectrom.* **35** (2020), 1720–1726.
[11] Zhen Y., Chen H., Zhang M., Hu J., Hou X.: Cadmium and cobalt ions enhanced-photochemical vapor generation for determination of trace rhenium by ICP-MS. *Appl. Spectrom. Rev.* (2021). DOI: 10.1080/05704928.2021.1878368

Synthetized membranes for ultrasound-assisted solvent extraction of porous membrane packed solid samples

Martyna Jurczyk*, Emilia Gontarek-Castro, Justyna Płotka-Wasylka

Gdańsk University of Technology, Faculty of Chemistry, Department of Analytical Chemistry, 11/12 Narutowicza Street, 80-233 Gdańsk, Poland ✉ *juswasyl@pg.edu.pl*

Keywords
diapers
extraction
membranes
phthalates
PVDF

Abstract
Membranes are becoming more and more popular in analytical chemistry, which is why they are used, among others, in extraction processes. Therefore, this work focuses on the process of synthesizing polyvinylidene fluoride membranes and their optimization. The obtained membranes were used as bags for phthalate extraction in disposable diapers for babies. Extraction was accomplished by method ultrasound-assisted solvent extraction of porous polyvinylidene fluoride membrane packed solid samples. As a result of the research, it was found that the most optimal temperature for the synthesis of membranes was 40 °C. The phthalates were extracted in this process. However, the reproducibility was insufficient.

1. Introduction

Nowadays, a key role in analytical chemistry is the extraction of analytes from samples of complex matrix composition. Unfortunately, analytical methods involving the extraction of components from such samples usually require their dilution or dissolution in a solvent. In order to avoid analytes loss, a new method for direct extraction into a suitable solvent from solid analytes was invented. An interesting and relatively simple method of analyzing different kinds of samples, including solid samples, can be the micro-solid extraction phase protected by a porous membrane (μ-SPE). It consists of packing the sorbent containing the adsorbed analyte in bags equipped with membranes. Unfortunately, in this case, the samples are also diluted or dissolved. An alternative that can solve the problem may be the aforementioned ultrasound-assisted solvent extraction of porous membrane packed solid samples (UA-SEPMPS), in which instead of packing the sorbent, the solid sample is directly packed into a membrane bag and immersed in a suitable solvent. The membrane used for such a process may be a membrane made of polyvinylidene fluoride (PVDF). Polyvinylidene fluoride is a thermoplastic fluoropolymer having a relatively high degree of crystallization. It

has good mechanical, electrical, and thermal properties, and is additionally characterized by high chemical resistance and hydrophobicity. For this reason, it is often used for the production of membranes, e.g., for microfiltration or ultrafiltration. These membranes can be obtained, inter alia, by the method of inversion of the dry and wet phase, in which it is possible to change the temperature parameter. This paper presents the process of obtaining membranes made of polyvinylidene fluoride and the optimization of the parameters of their preparation. The results of properties such as contact angle, thickness, brittleness, and porosity as a function of the membrane preparation temperature are also presented. In addition, the synthesized membranes were applied for the microextraction process of phthalates in disposable baby diapers [1, 2].

2. Experimental

2.1 Reagents and chemicals

To synthesize membranes purity chemical reagents were used. The polymer used for the synthesis was polyvinylidene fluoride, PVDF Solef® (type 6020 Solvay company). 1-Methyl-2-pyrrolidine about purity 99% (Sigma-Adrich) was a solvent, in which polymer was dissolved. For rising membranes isopropanol was used. Kerosene (Thermo-Fisher Scientific) was applied for measuring the porosity of membranes.

2.2 Samples

Commercially available disposable baby diapers of the common brand were used. The bag of diapers was opened prior to analysis.

2.3 Instrumentation

The resistance to wetting with pure water was investigated by measuring the contact angle value (OCA 15 apparatus, Dataphysics). Fourier transform infrared spectroscopy (FTIR) was used to collect spectra of the membranes in the scan range of 400–4000 cm^{-1} in ATR mode with a resolution of 16 cm^{-1} using a Nicolet iS10 FTIR spectrometer (Thermo Scientific Instrument). The thickness of the membrane was measured using an electronic micrometer (Schut).

2.4 Synthesis and optimization procedure

Synthesis membranes were performed by the dry-wet phase inversion method. The general scheme of the synthesis is shown in Fig. 1. The first had to be measured out 12% polymer solution in 1-methyl-2-pyrrolidinone. In this way, 6 grams of polymer polyvinylidene fluoride powder for 50 grams of a solution was

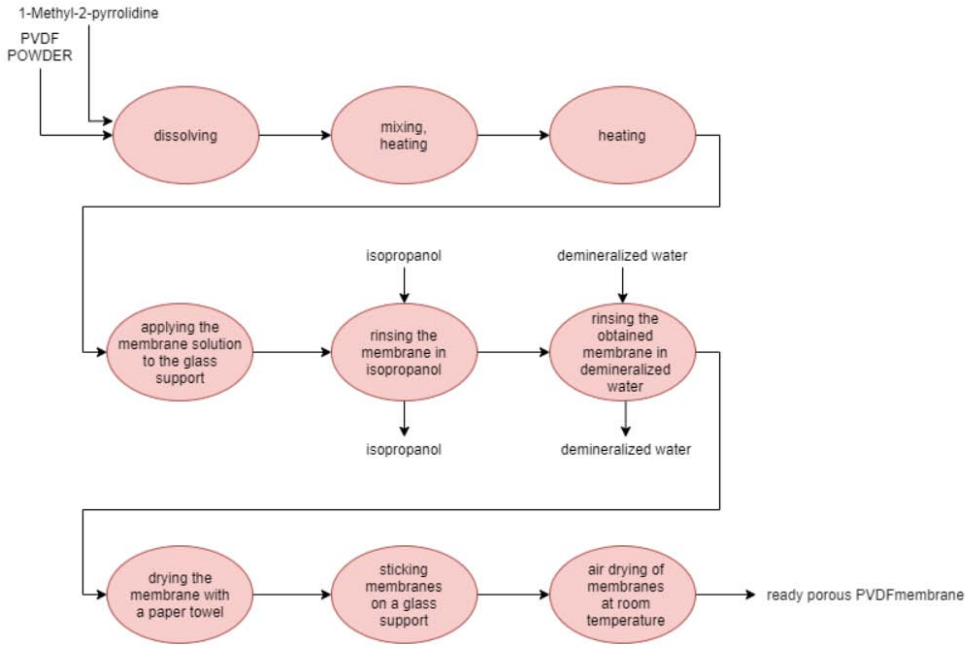

Fig. 1 General scheme for the synthesis of polyvinylidene fluoride (PVDF) membranes by dry-wet phase inversion method.

weighted out. Next, the solution prepared in this way was placed on a mechanical stirrer and mixed and heated to set temperature for about 24 hours. After that time, mixing was stopped to avoid excessive bubbles but heating was held. It was for the next 24 hours. When the solution was homogenized, the polymeric solution was spread onto glass using a special membrane knife set in width 250 µm. After poured, glass with membrane was immersed in isopropanol for 10 minutes in order to promote solid-liquid demixing and next, in demineralized water for 24 hours for thorough rinsing. The next action was drying membranes. Rinsed membranes were pre-drained by paper towel and then, glued to the glass by adhesive tape. It was drying by the air at room temperature, after which it was removed from the glass. The optimization process was based on the temperature changing during mixing and synthesis. The temperature used was 20, 40, and 70 °C. Each membrane was examined in terms of mechanical properties, contact angle, infrared spectrum, thickness, and porosity [3].

3. Results and discussion

The possibility of using membranes for ultrasound-assisted solvent extraction of porous membrane packed solid samples for determination of selected analytes from solid samples directly, shows innovation, however, poses a challenge to

Table 1
Porosity and the contact angle of the obtained polyvinylidene fluoride membranes synthesized at various temperatures.

Temperature of synthesis / °C	Porosity	Contact angle / °
20	0.65±0.04	134.5±1.0
40	0.85±0.02	144.4±3.8
70	0.83±0.02	143.4±1.8

select the appropriate membranes that can be used in the process. In this work, polyvinylidene fluoride membranes were synthesized and applied for extraction for the first time. The membranes were obtained at 20, 40, and 70 °C, each with different properties. Already upon receipt, differences in brittleness and properties of the membranes could be noticed. Membrane synthesized at a temperature of 20 °C, the polymer solution was unevenly solution and in some places differed in density, which was noticeable when pouring the membrane. Thus, the resulting membranes differed in thickness over the entire surface.

After drying, the membranes obtained at 40 °C exhibited the best mechanical properties. They detached easily from the glass, did not tear, showed a uniform thickness, and were not brittle. On the other hand, the membranes obtained at 70 °C dissolved evenly, but after drying they were characterized by high brittleness and were torn already when they were removed from the glass.

The thicknesses of the obtained membranes also varied. The average membrane thickness was 0.041 μm for 20 °C, 0.102 for 40 °C, and 0.094 for 70 °C. So after drying, the thickest membrane turned out to be the one obtained at 40 °C, which could involve showing the best mechanical properties. The thinnest ones turned out to be those obtained at 20 °C, but the thickness varied across the surface. All membranes were applied to the glass with the use of the "Knife for membranes" applicator with a set thickness of 250 μm in each case. The analysis of the IR spectra showed almost identical spectra for all tested membranes, which means that homogeneous products were obtained in all synthesized membranes. The results of the porosity of the obtained membranes are presented in Table 1. The highest porosity was obtained for membranes synthesized at 40 °C and it was 0.85±0.02. The contact angle test showed high hydrophobicity for all membranes. The results of the test are presented in Table 1. The highest contact angle was recorded for membranes produced at 40 °C, it was 144.4°±3.8°, therefore these membranes showed the highest hydrophobicity. The drop size of water used in the test was 4 μL. All of the research carried out during optimization unambiguously allowed to state that the obtained membranes with the best properties were those synthesized at 40 °C, both in terms of mechanical and hydrophobic properties, porosity, and thickness. Therefore, these membranes were applied as a bag in ultrasound-assisted solvent extraction of porous membrane packed solid samples for the selected phthalates extraction from spiked disposable baby diapers.

Furthermore, the sample extract was analyzed by GC-MS. The selected analytes were extracted, however, the repeatability was insufficient.

4. Conclusions

The use of polyvinylidene fluoride polymer membranes to extract analytes from solid samples is an interesting issue. A modern technique ultrasound-assisted solvent extraction of solid samples packed in porous polyvinylidene fluoride membrane, which allows avoiding the dilution or dissolution of the test solids samples in order to perform the extraction seems to be a promising discovery. The results of the research on disposable diapers for babies with the used synthesized membranes after the optimization process showed the effectiveness in the extraction of phthalates. However, due to insufficient repeatability, they require refinement and a series of tests to improve a given method.

References

[1] http://www.plastem.pl/oferta/tworzywa-sztuczne/pvdf/ (accessed Jun. 25, 2021).
[2] Ji J., Liu F., Hashim N. A., Abed M. R. M., Li K.: Poly(vinylidene fluoride) (PVDF) membranes for fluid separation. *React. Funct. Polym.* **86** (2015), 134–153.
[3] Ahmad A. L., Ideris N., Ooi B. S., Low S. C., Ismail A.: Synthesis of polyvinylidene fluoride (PVDF) membranes for protein binding: Effect of casting thickness. *J. Appl. Polym. Sci.* **128** (2013), 3438–3445.

Application of deep eutectic solvents in analytical chemistry

Aleksandra Kramarz[a,*], Patrycja Makoś-Chełstowska[a], Justyna Płotka-Wasylka[b]

[a] *Gdansk University of Technology, Faculty of Chemistry, Department of Process Engineering and Chemical Technology, 11/12 G. Narutowicza Street, 80-233 Gdansk, Poland*
✉ *s183836@student.pg.edu.pl*
[b] *Gdansk University of Technology, Faculty of Chemistry, Department of Analytical Chemistry, 11/12 G. Narutowicza Street, 80-233 Gdansk, Poland*

Keywords
deep eutectic solvents
extraction
green solvents
microextraction

Abstract
Recent years have been associated with efforts to reduce the impact on the natural environment. A greener approach has been introduced in various areas of science, including analytical chemistry. One of the basic procedures for preparing a sample for analysis is its extraction. Traditional methods involve the use of large amounts of organic compounds, often toxic, with an unfavorable impact on the environment. A representative of the "green" approach to the problem of organic solvents are new materials: deep eutectic solvents. They are promising solvents with many advantages (low toxicity, biodegradability, low cost), which are increasingly used in many chemical and technological processes, including the extraction process.

1. Introduction

Sample preparation for chemical analysis is considered to be the most important step in the analytical procedures. During this stage, the sample undergoes many processes and modifications in order to purify, preconcentration, or adapts it to the appropriate analytical equipment. Sample preparation may focus on analyte extraction, matrix transformation, or both. All activities are to ensure a better analytical result [1–2].

Recent years have been associated with paying more attention to "green" analytical techniques, including replacing traditional extraction methods with new, "green" microextraction techniques. This trend in science began with the introduction of green chemistry and its principles. The main goal is to transform the existing analytical techniques in such a way that they would become more environmentally friendly. Most of the assumptions are focused on the elimination of toxic and volatile organic solvents, and reduction of the solvent volume. Another assumption involves the development of direct analytical techniques that do not use chemical reagents [1–4].

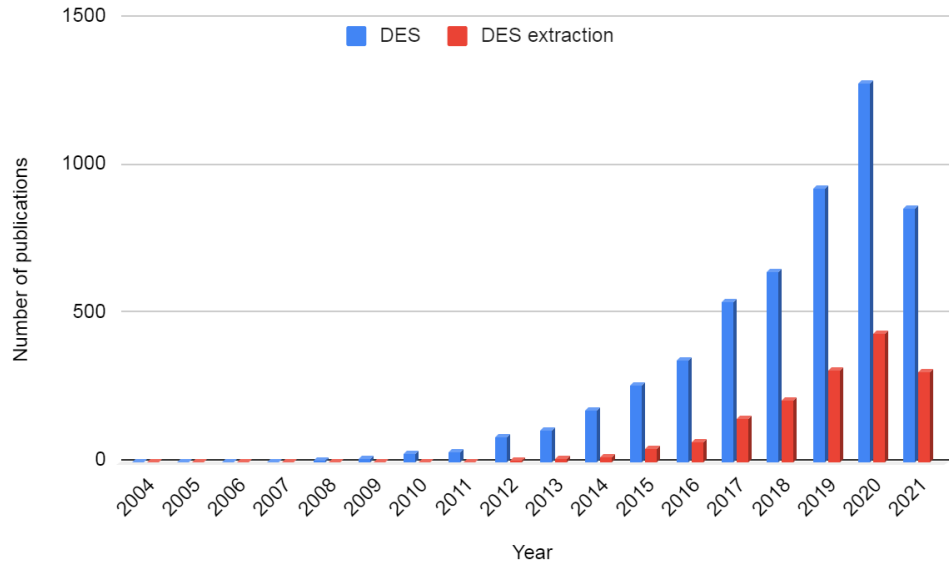

Fig. 1 Number of papers published during 2004–2021 on extraction with the deep eutectic solvents (DES) based on Scopus database (searched keywords: deep eutectic solvents and deep eutectic solvents extraction; accessed on 24.06.2021).

There are extraction techniques that do not require the use of toxic solvents, such as static headspace (SHS), or dynamic headspace (DHS), or solid phase microextraction (SPME). However, there are some limitations to these techniques, i.e., low sensitivity towards high-boiling compounds, time consumption, and expensive analytical equipment. Green extraction methods include also liquid phase microextraction (LPME) and its modification, i.e., dispersive liquid-liquid microextraction (DLLME), solidification of floating drop dispersive liquid-liquid microextraction (SFD), single drop microextraction (SDME), and hollow fiber-based liquid phase microextraction (HF-LPME) due to the application of very small amounts of solvents. However, these techniques still require the use of small amounts of toxic solvents. Therefore, in recent years, new green solvents that will be more environmentally friendly are searched [1–2, 4–6].

2. Deep eutectic solvents

Recently, deep eutectic solvents are gaining more and more attention as new generation green solvents. As shown in Fig. 1, interest in deep eutectic solvents began around 2004, and since then a continuous and intensive increase in publications on this subject has been observed. The use of deep eutectic solvents in the extraction process began a little later, in 2012, and a steady increase in research on this subject has been observed since then.

Deep eutectic solvents are created by mixing two or more components, which can form a new solvent with a melting point much lower than the individual

components. The components of deep eutectic solvents bind with each other through various interactions, including hydrogen bonding and electrostatic interaction. So, a hydrogen bond donor component and a hydrogen bond acceptor component can be distinguished. Chemical compounds forming deep eutectic solvents are natural, non-toxic, and biodegradable, as a result of which the resulting mixture is also safe for the natural environment. The formation of these solvents is also associated with economic advantages, as the ingredients are inexpensive, and the entire synthesis procedure is simple and cheap and does not require the use of expensive equipment. Deep eutectic solvents can be hydrophilic or hydrophobic, their nature will be determined by the substrates [7–8].

2.1 Deep eutectic solvents synthesis

There are two main deep eutectic solvents synthesis approaches, including the grinding and heating method. The grinding method involves mixing and grinding two or more ingredients in a mortar with a pestle at room temperature. The great advantage of this method is the lack of formation of unfavorable esters due to the process being carried out at room temperature. However, this method is very rarely used. The most common heating method is based on mixing two or more components and heating them simultaneously until a homogeneous mixture is obtained. Heating is carried out to about 100 °C. This method is faster and easier; however, it can cause the formation of impurities, i.e., hydrogen chloride and corresponding esters if quaternary ammonium salts with chlorine atoms are mixed with carboxylic acids.

Several types of deep eutectic solvents can be distinguished. By combining quaternary salts with hydrophilic hydrogen bond acceptor, the obtained deep eutectic solvents will have hydrophilic nature. The use of these deep eutectic solvents s has some disadvantages when working with the aquatic environment. Water modifies the connections between the ingredients, and this causes changes in structural properties. As the amount of water in deep eutectic solvents increases, the interactions between the components weaken. For this reason, research is conducted mainly on hydrophobic deep eutectic solvents, which will remain stable in the aquatic environment [1]. Hydrophobic deep eutectic solvents can be obtained by mixing a quaternary salt or terpenes (hydrogen bond acceptor) with an appropriate hydrogen bond donor compound. Some compounds can be both acceptor and hydrogen bond donors. Hydrogen bond acceptors based on long-chain ammonium salts are often used in the synthesis of hydrophobic and ionic deep eutectic solvents, as the longer hydrocarbon chain enhances the hydrophobic character. In addition in non-ionic hydrophobic deep eutectic solvents, components from a group of monoterpenes, i.e., camphor, eucalyptol can be used as hydrogen bond acceptor due to their high hydrophobic nature. Long-chain alcohols, acids, amino acids, polyphenols, and sugars are often used as hydrogen bond donor [2]. Examples of hydrogen bond acceptor and hydrogen bond donor are shown in Fig. 2.

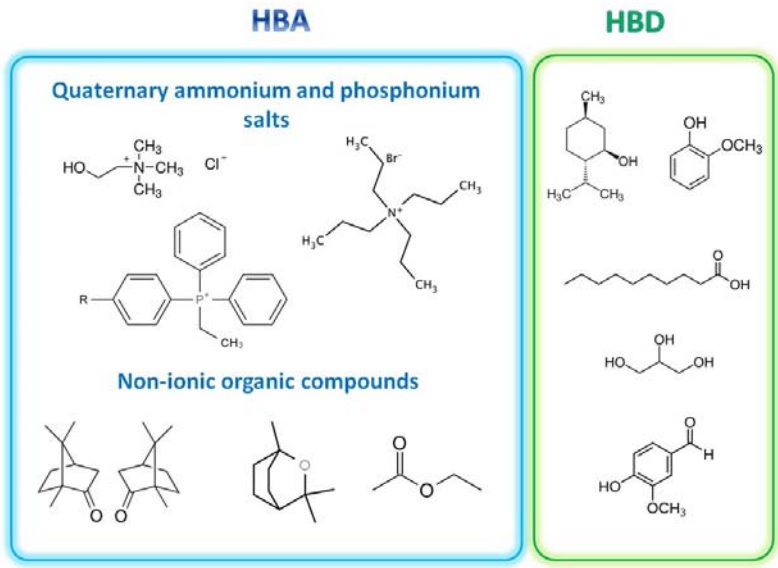

Fig. 2 Typical structures of deep eutectic solvents components: (HBA) hydrogen bond acceptor, and (HBD) hydrogen bond donor.

2.2 Physicochemical properties of deep eutectic solvents

Physicochemical properties such as viscosity, density, conductivity, acidity, surface tension, volatility, melting point, and boiling point depend on the type of deep eutectic solvents components, their molar ratio, and the type of bonds between them. Both these parameters, and biodegradability, toxicity, and thermal stability are taken into account when choosing the best solvent for analytical techniques.

The hydrophobicity is greater for deep eutectic solvents when both components are hydrophobic than when one compound is hydrophobic and the other is hydrophilic. As the chain length increases, the stability of deep eutectic solvents in the aquatic environment increases. Deep eutectic liquids by definition have a significantly lower melting point than pure ingredients. The stronger the interaction between the components, the lower the melting point. Melting points below 20 °C are particularly advantageous for utility purposes [2]. According to the twelve principles of green chemistry, solvents should be characterized by low vapor pressure. Due to the fact that the main deep eutectic solvents are composed of ionic compounds, they have non-volatile nature.

Density during the extraction process is one of the most important parameters. The most advantageous are large differences in deep eutectic solvents and water density (during extraction from an aqueous medium). The greater the difference in density, the easier the phases separate. Ionic deep eutectic solvents densities vary from 850 to 980 kg m^{-3} while non-ionic deep eutectic solvents in the range of 870 to 1091.8 kg m^{-3} at 25 °C.

The viscosity of deep eutectic solvents is another important parameter strongly affected on extraction. Most deep eutectic solvents are characterized by relatively high viscosities (>100 mPas) at room temperature. Viscosity increases as the tetra alkyl quaternary chain increases. Non-ionic deep eutectic solvents composed of monoterpenes have slightly lower viscosities. Their values are usually in the range from 1 to 20 mPas.

Surface tension also plays an important role in the extraction process. Deep eutectic solvents are characterized by high values of this parameter, which is very advantageous. The greater the surface tension force, the greater the efficiency of mass transfer between the phases [2].

3. Deep eutectic solvents in sample preparation

Due to its green nature, interest in deep eutectic solvents is constantly growing, and with it the number of possible applications. The traditional liquid-liquid extraction method uses large amounts of organic solvents that deep eutectic solvents can replace. So far, deep eutectic solvents were successfully applied in conventional liquid-liquid extraction (LLE) due to the possibility to structurally tune to facilitate the extraction of vide range of metals including Cr(VI), Cu(II), ^{111}In(III), and organic compounds, i.e., pesticides, organic acids, and alcohols from water samples [2].

However, most of the described applications of deep eutectic solvents are in microextraction processes, which are characterized by small amounts of solvents, at the level of microliters [1–2]. For example head space single drop micro-extraction was made using deep eutectic solvents composed of choline chloride and 4-chlorophenol to extract pesticides from vegetables and fruits [3]. Dispersive liquid–liquid microextraction was successfully made using tetrabutyl-ammonium bromide as a hydrogen bond acceptor and ethylene glycol, glycerol, acetic and formic acids as donors of hydrogen bond [6]. Another type of extraction is solid phase extraction. It can be conducted in a standard way, i.e., with solid sorbents. Solid sorbents can be modified with deep eutectic solvents [1–2].

4. Conclusion

Deep eutectic solvents are a very promising class of solvents that allows the replacement of organic solvents in analytical processes. Research on new materials and their application is constantly being carried out dynamically. They have many attractive functional features and are safe for the environment. They are thermally stable, stable in water, cheap, biodegradable, and less toxic than standard solvents. Moreover, the properties of deep eutectic solvents can be controlled by selecting the appropriate components, which makes them more attractive. According to the conducted research, deep eutectic solvents can be used very well in the preparation of samples for chemical analysis. Thanks to

them, it is possible to selectively separate an analyte from another phase using various extraction methods.

Acknowledgments

The research is funded by National Science Centre, Poland within the grant project (No.: 2020/37/B/ST4/02886).

References

[1] Plastiras O.E., Andreasidou E., Samanidou V.: Microextraction techniques with deep eutectic solvents. *Molecules* **25** (2020), 6026.

[2] Makoś P., Słupek E., Gębicki J.: Hydrophobic deep eutectic solvents in microextraction techniques: A review. *Microchem. J.* **152** (2019), 104384.

[3] Abolghasemi M.M., Piryaei M., Imani R.M.: Deep eutectic solvents as extraction phase in head-space single-drop microextraction for determination of pesticides in fruit juice and vegetable samples. *Microchem. J.* **158** (2020) 105041.

[4] Aydin F., Yilmaz E., Soylak M.: Vortex assisted deep eutectic solvent (DES)-emulsification liquid-liquid microextraction of trace curcumin in food and herbal tea samples. *Food Chem*. **243** (2018) 442– 447.

[5] Liu C., Liu D., Liu X., Jing X., Zong Z., Wang P., Zhou Z.: Deep eutectic solvent-based liquid phase microextraction for the determination of pharmaceuticals and personal care products in fish oil. *New J. Chem.* **41** (2017) 15105–15109.

[6] Shishov A., Volodina N., Nechaeva D., Gagarinova S., Bulatov A.: Deep eutectic solvents as a new kind of dispersive solvent for dispersive liquid-liquid microextraction. *RSC Adv.* **8** (2018), 38146–38149.

[7] Makoś P., Boczkaj G.: Deep eutectic solvents based highly efficient extractive desulfurization of fuels: Eco-friendly approach. *J. Mol. Liq.* **296** (2019), 111916.

[8] Paiva A., Matias A.A., Duarte A.R.C.: How do we drive deep eutectic systems towards an industrial reality? *Curr. Opin. Green Sustain. Chem.* **11** (2018) 81–85.

Challenges in the separation of neutral and hydrophobic compounds using the micellar electrokinetic capillary chromatography

Małgorzata Gołąb*, Iwona Biel, Mateusz Gromba, Aneta Woźniakiewicz, Michał Woźniakiewicz

Jagiellonian University, Faculty of Chemistry, Department of Analytical Chemistry, Gronostajowa 2, 30-387 Cracow, Poland ✉ *mgolab@doctoral.uj.edu.pl*

Keywords
CE-DAD
hydrophobic compounds
MEKC

Abstract
The development of a CE-based analytical method exploits differences in physicochemical properties of investigated compounds. Usually, the following considerations are taken into account: if the compound could be ionized, its size and hydrophobicity, and spectroscopic characteristics (UV-Vis, fluorescence). These differences supported with complex interactions with the separation media are commonly efficient enough to provide a separation of the analytes found in complex matrices. One of the particularly challenging groups of compounds is represented by hydrophobic, neutral entities, e.g., myristicin (a psychoactive compound present in nutmeg). Thus, the aim of the research was to develop a robust method for separation neutral and hydrophobic compounds found in nutmeg. Micellar electrokinetic capillary chromatography (MEKC) with spectrophotometric detection was applied, as it enables for separation of neutral species and is more cost-effective than for example liquid chromatography. During the experiments, some problems related to repeatability were observed and will be discussed in this contribution.

1. Introduction

During the development of the analytical method, it is important to choose the technique which enables exposing differences in compounds expected in the sample. For analysis of volatile, hydrophobic substances it is beneficial to use gas chromatography, for ionic species it might be capillary zone electrophoresis or liquid chromatography, where the affinity to one of the phases or migration velocity might be modified, e.g., by changing the pH value of the separation medium. However, if compounds of interest are neutral the situation becomes problematic as the separation is occurring basically just on the basis of the differences of the partition coefficient (hydrophobicity, log *P*). Thus, in the case of the capillary electrophoresis technique (which is noted as a rather less expensive

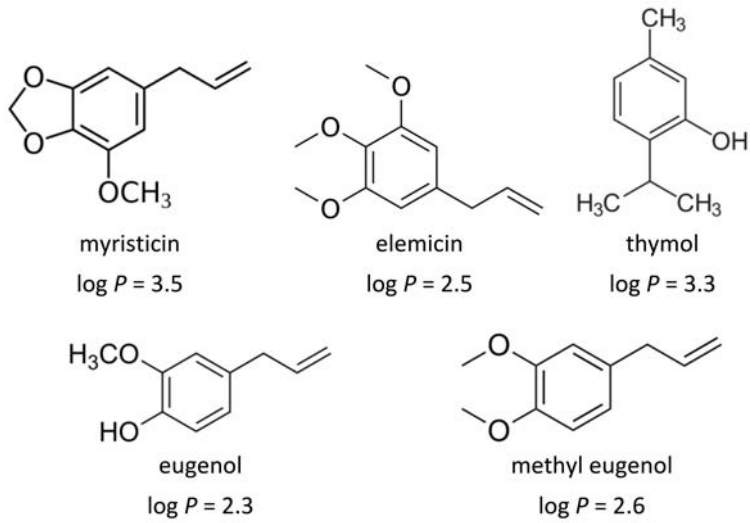

Fig. 1 Structures of the analytes and their values of the partition coefficient [2].

technique than liquid chromatography), there are two modes that might be applied for separation neutral compounds: micellar electrokinetic capillary chromatography (MEKC) and microemulsion electrokinetic capillary chromatography (MEEKC). Both of them require the addition of the surfactant to the background electrolyte (BGE), which will form a pseudo stationary phase [1].

The aim of the research was to develop a method for the analysis of neutral, hydrophobic compounds (Fig. 1.) found in nutmeg, a popular spice, which is also used for intoxication. Myristicin, which is the main psychoactive compound found in nutmeg causes disorientation, hallucinations, nausea. During the research, some challenges related to the analysis of hydrophobic compounds were encountered, which will be described in this report.

2. Experimental

2.1 Reagents and chemicals

All chemicals used were of analytical grade. Myristicin, methyl eugenol, eugenol, thymol, phenyl benzoate, urea, and sodium dodecyl sulfate (SDS) were purchased from Sigma-Aldrich (USA). Elemicin was bought from Toronto Research Chemicals (Canada). Methanol and acetonitrile were obtained from Honeywell (USA). Sodium hydroxide 30% solution was supplied by Avantor Performance Materials (Poland). Calcium chloride hydrate was bought from Chempur (Poland). Ultrapure water (18.2 MΩ·cm, 3 ppb total organic carbon) was generated in our laboratory in a Milli-Q system by Merck-Millipore (Germany).

Stock solutions of myristicin, elemicin, methyl eugenol (10 mg mL^{-1}); eugenol, and thymol (1 mg mL^{-1}) were prepared in methanol and stored in amber glass

vials in the freezer. A mixture of all the analytes (100 μg mL^{-1} each) was also prepared in methanol and kept at +4 °C. Solution of phenyl benzoate, which was used as an internal standard (IS), was also prepared in methanol and stored in an amber glass vial at +4 °C.

2.2 Instrumentation

Experiments were performed on the PA800 Plus Capillary Electrophoresis System (Beckman-Coulter, USA) equipped with a diode array detector. Signal acquisition was carried out at 210 nm. The uncoated bare fused-silica capillary was used. The capillary (ID 50 μm) was of 30.5 cm total length, 20.5 cm effective length. Before the first separation run at a working day the capillary was rinsed (137.90 kPa, 20 psi) with the sequence: methanol (3 min), 1 M NaOH (3 min), 0.1 M NaOH (10 min), water (5 min) and BGE (10 min). For the fresh capillary conditioning was the same. Between runs, the capillary was rinsed with BGE (0.5 min), ultrapure water (2 min), methanol (2 min), 1 M NaOH (2 min), water (2 min), and BGE (10min). Sample injection was conducted using forward pressure of 3.45 kPa (0.5 psi) for 4 s. The temperature of the cooling liquid was set at 25 °C. Each measurement was done in triplicate.

3. Results and discussion

At the beginning of the project conditions from the work of Huhn et al. [3] were set as the starting conditions. Background electrolyte consisted of 1.88 mM sodium tetraborate, 60 mM SDS, 20% (*v/v*) acetonitrile, 4 M urea, and 0.5 mM calcium chloride (BGE1); although most of the results in the cited publication were obtained using capillary of the 53.5 cm effective length (L_{tot} = 75 cm) and applied voltage of 30 kV, it was mentioned that it is also possible to use shorter capillary (L_{eff} = 20 cm, L_{tot} = 27 cm) and decreased voltage (10 kV), which will benefit in a shorter analysis time. Thus, the capillary of approximately 30 cm total length was used in the further experiments. It was stated that the addition of urea and calcium chloride modify retention factors, widening the migration time window, which might increase the resolution of the most closely migrating peaks. To investigate the effect of the urea and calcium chloride in the separation buffer for our case, apart from the BGE1, two buffers were prepared. The first one did not contain urea (BGE2) and the second was also without calcium chloride (BGE3). The preliminary research showed that for analysis of substances of particular interest the BGE3 provides the best results, e.g., a shorter analysis time (15 min for BGE1 vs. 9 min for BGE3) and is more robust due to the simple composition of the solution. Unfortunately, the critical evaluation of the precision revealed that the variability in migration times affects also the analytical signal (time-corrected peak area for analyte divided by the time-corrected peak area for IS, CV > 3% for thymol and myristicin). The observed changeability was not systematic and it could not be compensated by the use of the internal standard. As it is shown in Fig. 2 migration

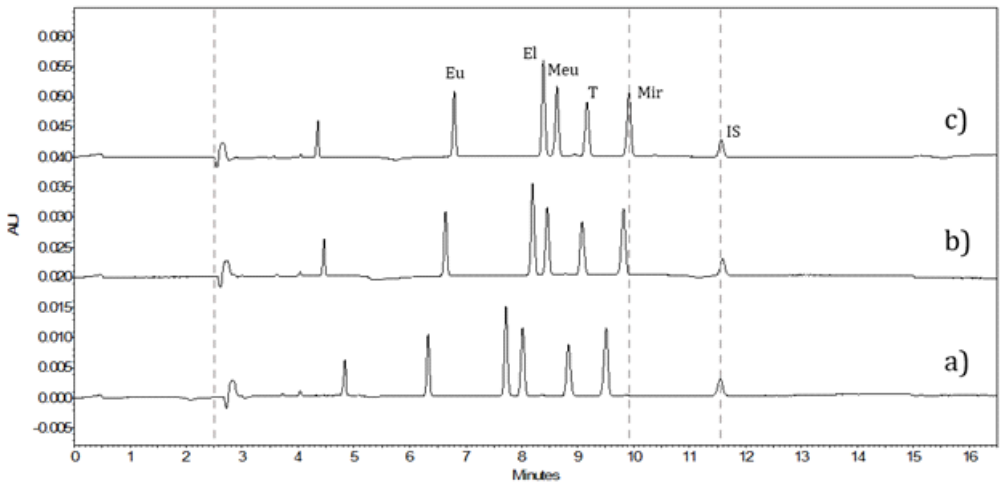

Fig. 2 Electropherograms of three injections a)–c) of the sample containing eugenol (Eu), elemicin (El), methyl eugenol (Meu), thymol (T), myristicin (Mir), each on concentration of 30 μg mL^{-1}, and 25 μg mL^{-1} of phenyl benzoate (IS). Conditions: separation buffer 1.88 mM sodium tetraborate, 60 mM SDS, 20% (*v*/*v*) acetonitrile; L_{eff} = 20.5 cm, L_{tot} = 30.5 cm; voltage: +10 kV.

time of the IS is stable in all repetitions of the same sample (three injections, *CV* = 0.18%), however, migration times of the analytes vary significantly (*CV* was 1.89–5.61%). Furthermore, it can be seen that these changes were not caused by the change of the electroosmotic flow, because even some changes are observed (first dotted line, signal from methanol included in the sample, which acts as an EOF marker) the behavior of the analytes is opposite: with the shorter migration time of the EOF marker (faster EOF; Fig. 2a and 2c), migration times for analytes are increasing.

It was hypothesized that the observed variation of migration times is due to the adsorption of the sample or BGE components to the capillary wall, so in the next step, a series of experiments aiming to find the optimal rinsing procedure were performed. The following rinsing procedures were taken under consideration: (I) electric enhanced rinsing by the introduction of 0.5 min applied voltage of 10 kV in the reversed polarity mode [4] , (ii) elimination of methanol from rinsing sequence, as short-chain alcohols may interfere with micellization process and (iii) simplifying the rinsing between the runs procedure to use only BGE rinse. None of them caused a significant improvement in terms of increasing of the repeatability of the migration times and corrected peak areas (*CV* ≤ 3%).

It was also hypothesized that the observed variability is related to the physico-chemical properties of the micelles, therefore in the research SDS was used as a surfactant, which forms negatively charged micelles. It was decided to check whether shortening the analysis time by changing the separation buffer to one at pH = 4 (the EOF is very weak) and using the negative polarity of the electrodes will be a solution in this case. Such an approach will reverse the migration order, e.g., anions will reach the detector first. As, in this case, analytes are hydrophobic,

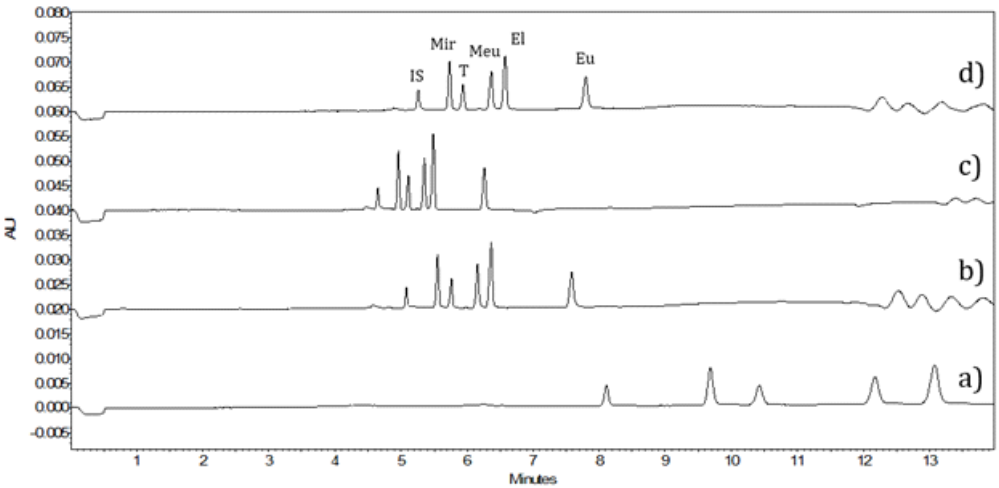

Fig. 3 Effect of SDS concentration on the separation. Acetate buffer modified with 20% (*v/v*) acetonitrile and (a) 50 mM SDS, (b) 60 mM SDS, (c) 70 mM SDS, and (d) 80 mM SDS. Conditions: L_{eff} = 20.5 cm, L_{tot} = 30.5 cm; voltage: –10 kV.

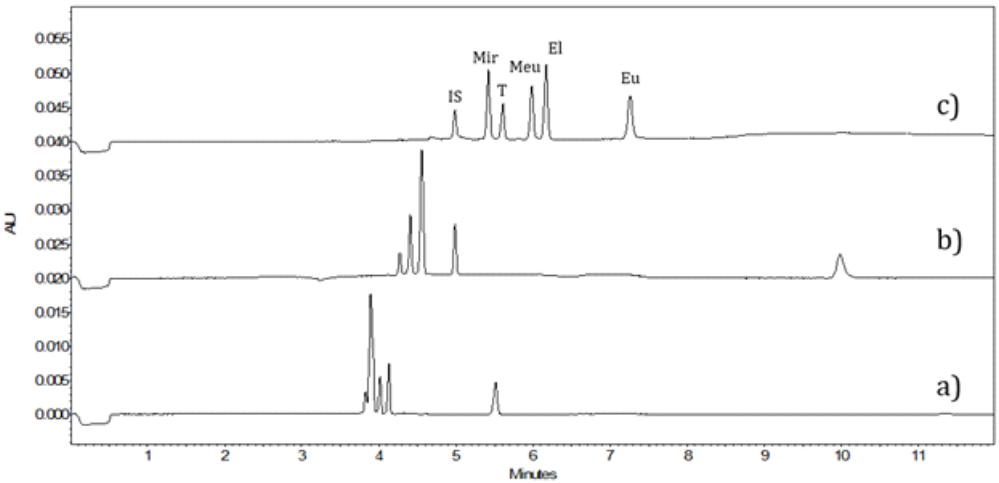

Fig. 4 Effect of acetonitrile concentration on the separation. Acetate buffer with 80 mM SDS modified to (a) 0% acetonitrile, (b) 10% (*v/v*) acetonitrile, (c) 20% (*v/v*) acetonitrile. Conditions: L_{eff} = 20.5 cm, L_{tot} = 30.5 cm; voltage: –10 kV.

neutral compounds they will interact with negatively charged SDS micelles and should migrate towards the detector. To verify that approach a series of acetate buffers (122 mM acetic acid, 25 mM sodium acetate) with different SDS (50–80 mM) and acetonitrile (0–20%, *v/v*) concentrations were prepared and tested. The results are presented in Fig. 3 and 4.

In most cases with increasing SDS concentration the migration times were decreasing, the exception was acetate buffer with 80 mM SDS and 20% (*v/v*)

acetonitrile. Thus, the effect of acetonitrile concentration (in the range 0–20% (*v/v*) acetonitrile) was tested using this buffer.

As it is shown in the Fig. 4 addition of acetonitrile in concentration at least 20% (*v/v*) is required to obtain separation of all analytes. In the case of lower concentration, some peak pairs (elemicin and methyl eugenol, thymol and myristicin) remain not separated. It was also observed that a concentration of 80 mM SDS causes crystallization of that BGE component on the vial's cap after few runs, which may lead to a high voltage leak or clogging the capillary. So, for the acetate buffers, one with 70 mM SDS and 20% (*v/v*) acetonitrile was chosen as an optimal, due to the shorter analysis time and lack of crystallization on the caps. Nevertheless, the test of repeatability of peak areas was below expectations, as the CV value for corrected peak areas (time-corrected peak area for analyte divided by the time-corrected peak area for IS) was up to 7.8% ($n = 4$).

4. Conclusions

The development of an analytical method is a challenge itself because the method should be characterized by high specificity for analytes and should be robust. This means that little changes in conditions should not affect the performance of the analysis. In the experiments, buffer ingredients commonly used in MEKC separation: sodium tetraborate, SDS, and acetonitrile were used providing separation of all analytes (despite their similar log *P* values). Although a similar group of compounds was analyzed by another research group [3], the repeatability found in this study was not satisfactory. The systematic research did not enable to identify the true source of variability as none of the applied modifications (composition of the BGE, addition of organic solvent, pH of the BGE, rinsing procedure) was pointed out as a golden solution for the analysis of such complex mixtures.

Acknowledgments

The work was the result of the research project No. 2019/03/X/ST4/01637 financed by The National Science Centre (NCN).

References

[1] Lauer H.H., Rozing G.P.: *High Performance Capillary Electrophoresis.* 2nd Ed. https://www.agilent.com/cs/library/primers/public/5990-3777EN.pdf

[2] https://pubchem.ncbi.nlm.nih.gov/ (accessed 25th June 2021)

[3] Huhn C., Pütz M., Holthausen I., Pyell U.: Separation of very hydrophobic analytes by micellar electrokinetic chromatography. I. Optimization of the composition of the sample solution for the determination of the aromatic ingredients of sassafras and other essential oils of forensic interest. *Electrophoresis* **29** (2008), 526–537.

[4] Gładysz M., Król M., Mystek K., Kościelniak P.: Application of micellar electrokinetic capillary chromatography to the discrimination of red lipstick samples. *Forensic Sci. Int.* **299** (2019), 49–58.

3D printed materials for the electrochemical determination of biologically active compounds

Marta Choińska[a, b, *], Tomáš Navrátil[b], Vojtěch Hrdlička[b]

[a] *Charles University, Faculty of Science, Department of Analytical Chemistry, Hlavova 8/2030, 128 43 Prague 2, Czech Republic*
[b] *J. Heyrovský Institute of Physical Chemistry of the Czech Academy of Sciences, Dolejškova 3, 182 23 Prague 8, Czech Republic* ✉ *marta.choinska@jh-inst.cas.cz*

Keywords
analgesics
antidepressants
3D printing materials
illicit drugs
voltammetric determination

Abstract
3D printing materials are relatively novel materials in electrochemistry, used for manufacturing of electrochemical cells, electrodes etc. They have been widely used mainly for tailored, fast, inexpensive, and easy preparation of various equipment for analyses of biologically active compounds. Various medicinal products and illicit drugs belong to this broad group of analytes which need to be monitored because of the possibility of (un)intentional overdose or recreational consumption, which can cause serious side effects or even death. Due to this risk, we decided to focus our research on the development of new, sensitive, selective, and easily customizable 3D printed sensors for the determination of some commonly used antidepressants, analgesics, and illicit drugs.

1. Introduction

In recent decades, 3D printing materials have started to play an important role in electrochemistry. Their advantages consist in the ability to design the desired shape of the electrode, cell, or reactor, as well as in affordable costs, and relatively short time of production. Moreover, such manufacturing is precise, repeatable, and the materials used are environmentally friendly [1, 2].

The non-conductive polymers can be used as substrates or connecting parts of printed equipment. These non-conductive polymers can be mixed in the proper ratio with conductive additives, e.g., carbon nanotubes, copper, and thus to form the electrodes [2, 3]. In addition, surfaces of these electrodes can be modified [4, 5].

Biologically active compounds are among the most relevant analytes worth monitoring from the environment or clinical point of view [6–12]. Antidepressants and painkillers belong to the most commonly used compounds of medicinal importance from this group, which should be under control. They can be abused,

cause adverse effects, or be overdosed, intentionally or accidentally [13, 14]. In addition, the massive excretion of these drugs and/or their metabolites into wastewaters (or even into drinking waters) may pose a danger for the environment [15].

Another biologically active compounds group is represented by illicit drugs. Many of them have been (ab)used for their relaxing, psychotic, or hallucinogenic effects [16] and their consumption is associated with daily routine and social interactions [17]. Unfortunately, the use of illicit drugs, especially unknown mixtures, as well as overdoses, can lead to health problems and even deaths [18].

Due to the global problems with the growing number of overdoses of biologically active compounds [14, 19], their identification and determination in various matrices are necessary for medical and forensic purposes. Our study aims to develop a fast, inexpensive, reliable, and selective method for the determination of selected biologically active compounds using 3D printed electrodes.

2. Experimental

2.1 Reagents and chemicals

The following biologically active compounds were selected for our experiments: antidepressants venlafaxine (Velaxin, Egis Pharmaceuticals PLC, Hungary), sertraline (Asentra, KRKA, Slovakia), and trazodone (Trittico, Angelini Pharma, Italy), fentanyl analgesic (Lipomed, Switzerland), and illicit drug lysergic acid diethylamide (LSD; Lipomed, Switzerland). Stock solutions of antidepressants were prepared by dissolving them in 0.1 M borate buffer (prepared from boric acid and sodium hydroxide (Lachema, Czech Republic)) of pH = 8. Stock solution of LSD was prepared by its dissolution in 0.1 mol dm^{-3} lithium perchlorate (Sigma Aldrich, USA). For all described measurements deionized water from Milli-Q-Gradient (Millipore, Czech Republic, conductivity <0.05 μS cm^{-1}) was used.

2.2 Instrumentation

Voltammetric measurements were performed using Eco-Tribo Polarograph (Polaro-Sensors, Czech Republic), controlled by the software MultiElChem 3.3 for Windows 10 (J. Heyrovský Institute of Physical Chemistry of the Czech Academy of Sciences, Czech Republic). Results recorded by two working electrodes were compared: glassy carbon electrode (GCE, laboratory made) and 3D printed carbon fiber PLA electrode (CF-PLAE, laboratory-made). For manufacturing of 3D printed electrode, the carbon PLA filament ProtoPasta (ProtoPlant, USA) was used. Ag|AgCl(3M KCl) was used as the reference and platinum wire as the auxiliary electrode (both Elektrochemické detektory, Czech Republic). Buffer pH was measured with pH-meter Jenway 3505 (Bibby Scientific Limited, UK).

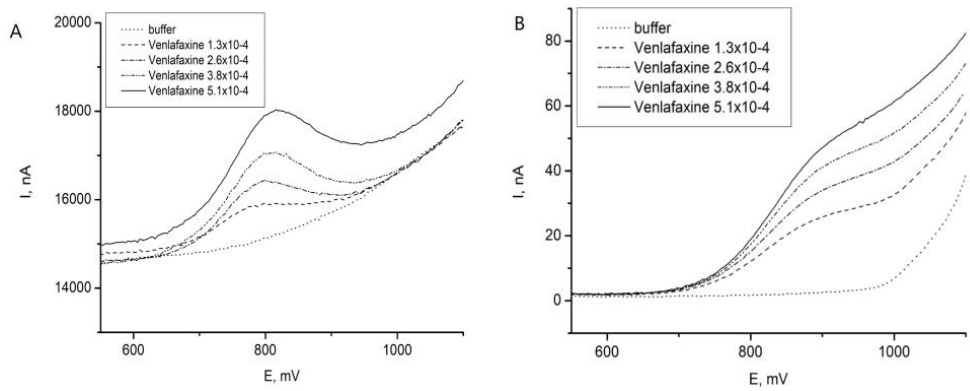

Fig. 1 Difference pulse voltammogram venlafaxine at (A) GCE, and (B) CF-PLAE. Venlafaxine concentrations: 1.3×10^{-4} mol dm^{-3}, 2.6×10^{-4} mol dm^{-3}, 3.8×10^{-4} mol dm^{-3}, and 5.1×10^{-4} mol dm^{-3}. Condtitions: supporting electrolyte boric buffer of pH = 8, scan rate 20 mV s^{-1}, initial potential +550 mV, final potential +1100 mV, pulse height +50 mV, pulse width 80 ms.

3. Results and discussion

Pilot experiments realized with LSD and venlafaxine were performed with GCE and CF-PLAE to obtain information on the possibility to determine selected analytes using cyclic voltammetry (CV) and differential pulse voltammetry (DPV).

Firstly, a suitable buffer and its pH value were optimized. Boric buffer of pH = 8 was chosen as the optimum electrolyte for the determination of venlafaxine at both GCE and CF-PLAE. CV and DPV were used for the determination of this drug with the following parameters: scan rate 20 mV s^{-1}, initial potential +550 mV, and final potential +1100 mV, pulse height +50 mV, pulse width 80 ms. Four concentration levels of venlafaxine were investigated: 1.3×10^{-4} mol dm^{-3}, 2.6×10^{-4} mol dm^{-3}, 3.8×10^{-4} mol dm^{-3}, and 5.1×10^{-4} mol dm^{-3}. Recorded signals at GCE and CF-PLAE proved to be comparable, the venlafaxine peaks were recorded at about +850 mV at both electrodes. At GCE, the signal was slightly better developed than at CF-PLAE (Fig. 1). Elimination voltammetry with linear scan (EVLS) [20–22] helped to reveal the reaction mechanisms.

In the following experiments, CV at the GCE was performed to investigate current signal dependence on the increasing concentration of LSD in the supporting electrolyte (lithium perchlorate, 0.1 mol dm^{-3}). Three concentration levels of this drug were analyzed: 1.0×10^{-6} mol dm^{-3}, 2.0×10^{-6} mol dm^{-3}, and 3.0×10^{-6} mol dm^{-3} using the following optimized parameters: scan rate 100 mV s^{-1}, initial potential –100 mV, and final potential +1300 mV. The recorded peaks at the potential of +900 mV raised with increasing LSD concentration (Fig. 2).

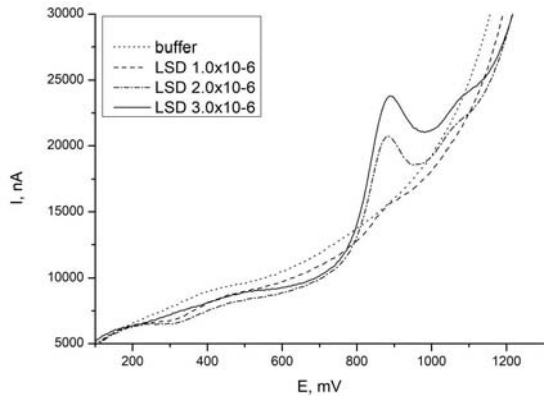

Fig. 2 Cyclic voltammogram (anodic scan) at GCE of lysergic acid diethylamide (concentrations: 1×10^{-4} mol dm^{-3}, 2×10^{-4} mol dm^{-3}, and 3×10^{-4} mol dm^{-3}) in 0.1 mol dm^{-3} lithium perchlorate. Conditions: scan rate 100 mV s^{-1}, initial potential –150 mV, final potential +1300 mV.

4. Conclusions

All achieved results are in good agreement with the literature sources [23, 24] and prove that CV and DPV at laboratory-made GCE as well as CF-PLAE can be successfully used for the determination of biologically active compounds. This pilot study represents the first step in the further development of new laboratory-made 3D printed sensors for analysis of the above-mentioned analytes.

Acknowledgments

The authors thank the project of Czech Science Foundation (GA ČR) No. 20-01589S, Specific University Research (SVV260560) (M.C.) and Grant Agency of the Charles University No. 373521 (M.C.) for financial support.

References

[1] Escobar J.G., Vaneckova E., Lachmanova S.N., Vivaldi F., Heyda J., Kubista J., Shestivska V., Spanel P., Schwarzova-Peckova K., Rathousky J., Sebechlebska T., Kolivoska V.: The development of a fully integrated 3D printed electrochemical platform and its application to investigate the chemical reaction between carbon dioxide and hydrazine. *Electrochim. Acta* **360** (2020), 136984.

[2] Hamzah H.H., Shafiee S.A., Abdalla A., Patel B.A.: 3D printable conductive materials for the fabrication of electrochemical sensors: A mini review. *Electrochem. Commun.* **96** (2018), 27–31.

[3] Choinska M., Hrdlicka V., Sestakova I., Navratil T.: Voltammetric determination of heavy metals in honey bee venom using hanging mercury drop electrode and PLA/carbon conductive filament for 3D printer. *Monatsh. Chem.* **152** (2021), 35-41.

[4] Vaneckova E., Bousa M., Lachmanova S.N., Rathousky J., Gal M., Sebechlebska T., Kolivoska V.: 3D printed polylactic acid/carbon black electrodes with nearly ideal electrochemical behaviour. *J. Electroanal. Chem.* **857** (2020), 113745

[5] Vaneckova E., Bousa M., Sokolova R., Moreno-Garcia P., Broekmann P., Shestivska V., Rathousky J., Gal M., Sebechlebska T., Kolivoska V.: Copper electroplating of 3D printed composite electrodes. *J. Electroanal. Chem.* **858** (2020), 113763

[6] Cabalkova D., Barek J., Fischer J., Navratil T., Peckova K., Yosypchuk B.: Voltametrické stanovení herbicidu bifenoxu na stříbrné pevé amalgamové elektrodě modifikované rtuťovým meniskem. *Chem. Listy* **103** (2009), 236–242. (In Czech.)
[7] Barek J., Cabalkova D., Fischer J., Navratil T., Peckova K., Yosypchuk B.: Voltammetric determination of the herbicide Bifenox in drinking and river water using a silver solid amalgam electrode. *Environ. Chem. Lett.* **9** (2011), 83–86.
[8] Sebkova S., Navratil T., Kopanica M.: Graphite composite electrode in voltammetry. *Anal. Lett.* **38** (2005), 1747–1758.
[9] Barek J., Dodova E., Navratil T., Yosypchuk B., Novotny L., Zima J.: Voltammetric determination of N,N-dimethyl-4-amine-carboxyazobenzene at a silver solid amalgam electrode. *Electroanalysis* **15** (2003), 1778–1781.
[10] Sebkova S., Navratil T., Kopanica M.: Comparison of different types of silver composite electrodes to varied amount of silver on example of determination of 2-nitronaphtalene. *Anal. Lett.* **36** (2003), 2767–2782.
[11] Navratil T., Kopanica M., Krista J.: Anodic stripping voltammetry for arsenic determination on composite gold electrode. *Chem. Anal. (Warsaw)* **48** (2003), 265–272.
[12] Sebkova S., Navratil T., Kopanica M.: Silver composite electrode for voltammetric determination of halogenides. *Anal. Lett.* **37** (2004), 603–628.
[13] Jones C.M., Guy G.P., Board A.: Comparing actual and forecasted numbers of unique patients dispensed select medications for opioid use disorder, opioid overdose reversal, and mental health, during the COVID-19 pandemic, United States, January 2019 to May 2020. *Drug Alcohol Depen.* **219** (2021), 108486.
[14] Weedn V.W., Zaney M.E., McCord B., Lurie I., Baker A.: Fentanyl-related substance scheduling as an effective drug control strategy. *J. Forensic. Sci.* (2021), DOI: 10.1111/1556-4029.14712.
[15] Tajik S., Beitollahi H., Dourandish Z., Zhang K.Q., Le Q.V., Nguyen T.P., Kim S.Y., Shokouhimehr M.: Recent advances in the electrochemical sensing of venlafaxine: an antidepressant drug and environmental contaminant. *Sensors* **20** (2020), 3675.
[16] Brandt S.D., Kavanagh P.V., Westphal F., Stratford A., Odland A.U., Klein A.K., Dowling G., Dempster N.M., Wallach J., Passie T., Halberstadt A.L.: Return of the lysergamides. Part VI: Analytical and behavioural characterization of 1-cyclopropanoyl-d-lysergic acid diethylamide (1CP-LSD). *Drug Test. Anal.* **12** (2020), 812–826.
[17] Manthey J., Kilian C., Carr S., Bartak M., Bloomfield K., Braddick F., Gual A., Neufeld M., O'Donnell A., Petruzelka B., Rogalewicz V., Rossow I., Schulte B., Rehm J.: Use of alcohol, tobacco, cannabis, and other substances during the first wave of the SARS-CoV-2 pandemic in Europe: a survey on 36,000 European substance users. *Subst. Abuse Treat. Prev. Policy* **16** (2021), 36.
[18] Pergolizzi J.V., Dahan A., LeQuang J.A., Raffa R.B.: Overdoses due to fentanyl and its analogues (F/FAs) push naloxone to the limit. *J. Clin. Pharm. Ther.* (2021), DOI: 0.1111/jcpt.13462.
[19] Niles J.K., Gudin J., Radcliff J., Kaufman H.W.: The opioid epidemic within the COVID-19 pandemic: Drug testing in 2020. *Popul. Health Manag.* **24** (2021), S43–S51.
[20] Skopalova J., Navratil T.: Application of elimination voltammetry to the study of electrochemical reduction and determination of the herbicide metribuzin. *Chem. Anal. (Warsaw)* **52** (2007), 961–977.
[21] Navratil T., Yosypchuk B., Barek J.: A multisensor for electrochemical sequential autonomous automatic measurements. *Chem. Anal. (Warsaw)* **54** (2009), 3–17.
[22] Navratil T., Senholdova Z., Shanmugam K., Barek J.: Voltammetric determination of phenylglyoxylic acid in urine using graphite composite electrode. *Electroanalysis* **18** (2006), 201–206.
[23] Merli D., Zamboni D., Protti S., Pesavento M., Profumo A.: Electrochemistry and analytical determination of lysergic acid diethylamide (LSD) via adsorptive stripping voltammetry. *Talanta* **130** (2014), 456–461.
[24] Beitollahi H., Jahani S., Tajik S., Ganjali M.R., Faridbod F., Alizadeh T.: Voltammetric determination of venlafaxine as an antidepressant drug employing Gd_2O_3 nanoparticles graphite screen printed electrode. *J. Rare Earth* **37** (2019), 322–328.

Application of advanced spectroscopic methods in the assessment of the leachability degree of hazardous elements from the matrix of cellular concrete

Paulina Augustyniak[a,*], Alicja Saczuk[a], Hubert Byliński[b], Bartłomiej Cieślik[a]

[a] *Gdańsk University of Technology, Faculty of Chemistry, Department of Analytical Chemistry, Narutowicza 11/12, 80-233 Gdańsk, Poland* ✉ *s171135@student.pg.edu.pl*
[b] *Gdańsk University of Technology, Faculty of Civil and Environmental Engineering, Department of Mechanics of Materials and Structures, Narutowicza 11/12, 80-233 Gdańsk, Poland*

Keywords
cellular concrete
construction materials
heavy metals
leachability
microwave plasma atomic emission spectroscopy (MP-AES)

Abstract
Due to its structure, autoclaved cellular concrete exhibits good insulating properties with relatively high compressive strength values. It is increasingly used in construction because of its economic attractiveness. Autoclaved cellular concrete is mainly used in interior structure layers, and therefore its potential exposure to heavy metal leaching from the matrix may be related to the presence of a high pH medium from other materials in the structure. The effectiveness of the immobilization of hazardous substances potentially occurring in the concrete structure depends on many factors, including the characteristics of the raw material input and the conditions of material maturation. This study investigated the immobilization level of potentially hazardous substances in cellular concrete available on the Polish market. The leaching of heavy metals from the aforementioned materials, using different media and environments for the exploitation of potential future building blocks was also discussed, as well as the possibility of using advanced spectroscopic techniques in this type of study.

1. Introduction

Autoclaved cellular concrete is an increasingly widely used material in the building industry, replacing conventional concrete in many constructions. It can be used for building foundations or walls, as an inner or outer layer. Since autoclaved cellular concrete is directly exposed to the environment, an environmental impact study is necessary. Because autoclaved cellular concretes are placed in the ground, there is a potential risk of exposing the vegetation living nearby to toxic elements such as Zn, Cd, Pb, Al, Fe or elevated concentrations of P.

Plants may take up the mentioned elements together with other macro- and microelements from the soil. The interaction of such potentially toxic elements with molecules used in cells as the structure of enzymes, such as proteins or polynucleotides, is a threat [1]. Metallic elements can be toxic to the environment depending on their concentration in a given matrix, ease of complexation, or degree of oxidation. An important role in the binding of metals is often assigned to the C-S-H phase formation (amorphous hydrated calcium silicate formed as a product of hydration of individual components of cellular concrete). The mentioned phenomenon provides the possibility to incorporate various ions into its structure [2, 3].

Investigating the content of potentially hazardous metals in cellular concrete is challenging due to the small but still hazardous content of above-mentioned elements. It is therefore necessary to choose the most suitable optimization method so that the limits of quantification/detection values are below the permissible environmental concentrations laid down in the standards.

2. Experimental

2.1 Reagents and chemicals

Commercially available cellular concrete was tested. Depending on the site and manufacturing conditions, different technological variants of autoclaved cellular concrete production are used. The main raw material set consists of:

- binders (cement, lime, gypsum),
- aggregates (sand, ash),
- blowing agent (aluminium powder, paste),
- water [4, 5].

Taking into account the above assumptions, without knowing the exact composition of the samples, large amounts of lime, sodium, iron and aluminium were expected (during the autoclaving of cellular concrete, the aluminium powder should evaporate, nevertheless aluminium content is expected from the aggregate and from the other components of autoclaved cellular concrete).

To determine the potential danger of using cellular concrete in the environment, leachability tests were performed. The agitation time was 1, 2, and 3 weeks (samples respectively described as: 1T, 2T, 3T), in a 10:1 liquid to solid ratio (20 mL of water, 2 g of sample ground to gradation <150 μm) according to the modified standard/norm PN-EN 12457-2 for the elements: Al, Fe, Pb, Zn, Cd, P [6].

The selected time interval was used to reflect the initial "lifetime" of an autoclaved cellular concrete located in a given environment where it is exposed to water/moisture. Three environments were used for the study: distilled water, artificial groundwater, and artificial seawater. The basis of artificial seawater and groundwater solutions was distilled water and appropriate chemical compounds included in natural waters. The compositions of the artificial solutions are shown in Table 1.

Table 1
Concentration of compounds constituting artificial solutions of groundwater and seawater.

Compound	Concentration / g L^{-1}	
	Groundwater	Seawater
$CaCl_2$	1.849	1.141
KCl	–	0.831
$MgCl_2$	–	2.489
$MgSO_4$	0.635	3.521
NaCl	–	28.292
$NaHCO_3$	1.352	–
Na_2SO_4	1.139	–

After a specified leaching time, the samples were filtered and subjected to determination of potentially hazardous elements using Microwave Plasma–Atomization Emission Spectrometry (MP-AES). For distilled water, the leachability of Ca, Na, Mg, K was additionally investigated. To assess the degree of immobilization, a ground cellular concrete sample was also tested by previously mineralizing it in a microwave-assisted mineralization system (Multiwave GO supplied by Anton Paar) for 2 hours. Approximately 0.1 g of areated concrete samples, ground to a gradation of <150 μm, were prepared (with an accuracy 0.0001 g), then 2 mL of HNO_3 and 6 mL of HCl were added. Digestion was performed in 200 °C. After digestion, the samples were transferred to 10 mL flasks filled with deionized and then filtered. All elements were determined without residual fraction (Si-bound).

2.2 Instrumentation

Selected elements determination were performed with the use of MP-AES 4210 supplied by Agilent. Agilent's MP Expert software was used to optimize the measurement Conditions. The following parameters were optimized: nebulizer flow and viewing point for sensitivity increase; wavelengths used for particular elements determination and selectivity; uptake time and stabilization time were determined to increase the sensitivity/precision of the measurement. With the software's "Conditions tab" and "read time"/"uptake time" functions were used to examine the time in which the signal for a given element will be stable for individual elements [7–9].

2.3 Calibration

In the case of calibration, a wide range of concentrations were used which allowed the determination of calcium, sodium, potassium and magnesium at high levels without the need for dilution of the primary samples, thus avoiding the introduction of further error, and obtaining results of higher accuracy.

The first of four repetitions of the calibration was rejected in several cases due to the error resulting from the delay in pumping the liquid. The rejection of results

Table 2
Basic calibration parameters of microwave plasma–atomization emission spectrometry (y = intensity, x = concentration / mg kg^{-1}).

Element	λ / nm	Nebulizer flow / L min^{-1}	Viewing position	Calibration equation	R^2
Ca	643.907	0.95	10	$y = 981.3057\,x - 438.8235$	0.9997
Na	615.423	0.30	–10	$y = 10.2144\,x + 8.7252$	0.9990
K	766.491	0.85	30	$y = 22285.1327\,x + 192440.2577$	0.9991
Al	394.401	0.90	10	$y = 8358.0806\,x - 266.5989$	0.9998
Fe	358.119	0.95	10	$y = 2405.9921\,x - 126.1822$	0.9990
Pb	405.781	0.95	20	$y = 1417.9422\,x + 242.2472$	0.9954
Mg	279.533	0.50	0	$y = 71198.1010\,x + 196269.3749$	0.9976
Zn	481.053	0.55	–40	$y = 130.4106\,x - 37.5798$	0.9987
Cd	228.802	0.50	0	$y = 13239.5452\,x - 28.5456$	0.9987
P	214.915	0.45	–20	$y = 159.8683\,x + 652.1473$	0.9988

Table 3
Limits of quantification and limits of detection for the determination of the content of potentially hazardous molecules in leachate and autoclaved cellular concrete matrix.

Element	*LOD* / mg kg^{-1}	*LOQ* / mg kg^{-1}
Ca	55.6	166.9
Na	141.1	423.1
K	29.3	88.0
Al	05.7	17.1
Fe	08.2	24.6
Pb	01.9	05.7
Mg	20.3	61.0
Zn	03.7	11.1
Cd	1.0	3.0
P	52.3	156.8

strongly deviating in intensity from the others allowed us to achieve better correlation coefficients for individual calibrations. It was than possible to estimate the optimal linear range for certain wavelength used for the determination of selected elements. The calibration plots for the best correlation coefficients are shown in Table 2.

The calibration curves show excellent linearity over the entire final calibration range. For the optimization, a double calibration was performed to separate the part of the wavelengths that gave lower intensities for the elements that were determined at low levels and to cut out the high intensities for the elements that were determined at high levels [10]. Good correlation coefficients were also obtained by discarding results that deviated significantly from linearity and often by discarding the first measurements of the four replicates due to the error that may have occurred when a new sample was aspirated through the nebulizer, which could mean that the uptake time or stabilization time should be increased

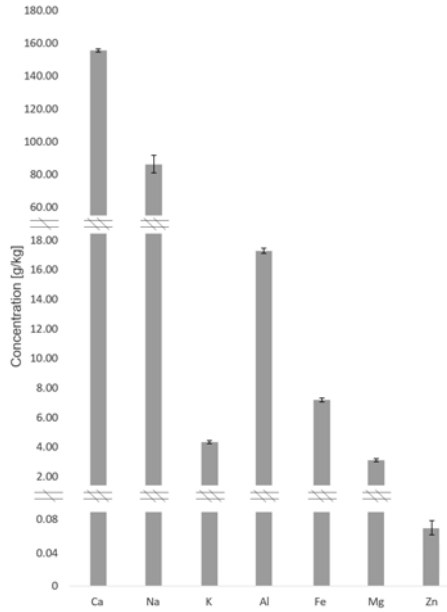

Fig. 1 Concentration of mainly occurring in the leachate after autoclaved cellular concrete leaching test (WD – distilled water; WG – artificial groundwater; 1T, 2T, 3T – one, two, three weeks of agitation; 1, 2 – repetition of sample).

by 1–3 sec. The obtained calibration parameters along with the optimization parameters are shown in Table 2.

The limits of detection (*LOD*) were estimated by the directional coefficient method, the limits of quantification (*LOQ*) were calculated as 3 times the *LOD*. The *LOQ* and *LOD* values are shown in Table 3.

3. Results and discussion

The study shows that this technique can be used to estimate the environmental hazard of trace element leaching (low *LOD* and *LOQ* values for Cd, Pb, Zn, Al, Fe) and the determination of very high concentrations of main elements in leachate and cellular concrete matrix such as Ca, Na, K, Mg (calibration solutions up to 1400 mg L^{-1}) in a single measurement. Figures 1 and 2 show the results obtained for the content of leached elements and the main components of the autoclaved cellular concrete matrix.

The greatest challenge was the determination of calcium and sodium at high concentration levels and decreasing the *LOD/LOQ* for the trace elements, namely, Cd, Zn, Pb, P. Despite reducing the limits of detection and quantification by performing additional optimization steps, the remaining elements could not be detected. It should be taken into account that commercially available autoclaved cellular concrete was tested, which means that the individual components for its production had to meet acceptable standards. In addition, a properly optimized

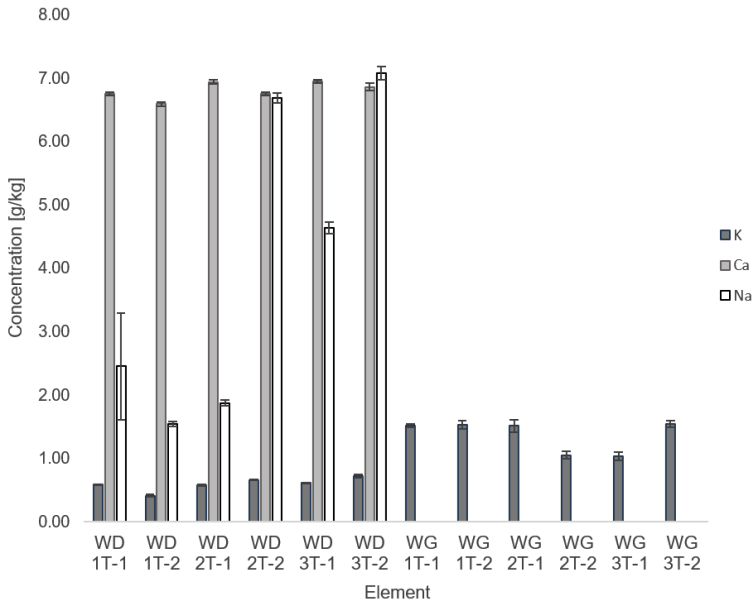

Fig. 2 Concentration of potentially toxic elements in autoclaved cellular concrete matrix.

autoclave maturation technology of autoclaved cellular concrete may have contributed to the incorporation of potentially hazardous elements into the structure during the phase formation process in cellular concrete [11]. Good correlation coefficients (R^2>0.999) were obtained for Fe, Al, K, and Ca at 358.119 nm, 394.401 nm, 766.491 nm, and 643.907 nm wavelengths respectively.

4. Conclusions

The Microwave Plasma–Atomic Emission Spectrometry technique allows us to determine the elemental toxicity of autoclaved cellular concretes by studying the leachability of potentially hazardous elements from the autoclaved cellular concrete matrix and determining their content in the leachate. The challenge, on the other hand, is to reach a limit of detection/quantification that allows determining whether the content of a given element does not exceed acceptable environmental standards or the limits of detection that are lower than the concentration limits defined by available standards.

As an extension of the study, it is planned to extend the leaching time to mimic the living conditions of the autoclaved cellular concrete, which will allow observing changes in leachability as the concrete is exposed to seawater and groundwater conditions. As a control, leaching in distilled water will be adopted as before, in order to check whether specific ions present in artificial solutions cause increased leaching over a longer period of time.

Acknowledgments

This study was funded by an internal Gdańsk University of Technology grant supporting young researchers at Faculty of Civil and Environmental, entitled "Toxicological characteristics of aearated concrete and its potential environmental impact assessment".

References

[1] Baranowska-Morek A.: Roślinne mechanizmy tolerancji na toksyczne działanie metali ciężkich. *Kosmos* **52** (2003), 283–298. (In Polish.)
[2] Owsiak Z., Sołtys A.: Autoclaved cellular concrete as an environmentally friendly construction material. *Structure and Environment* **5** (2013), 18–24.
[3] Kurdowski W.: Faza C-S-H – stan zagadnienia. Część 1. *Cement Wapno Beton* **4** (2008), 216–222. (In Polish.)
[4] Jatymowicz H., Siejko J., Zapotoczna-Sytek G.: *Technologia autoklawizowanego betonu komórkowego.* Warszawa, Arkady 1980. (In Polish.)
[5] https://www.solbet.pl/jak-powstaje-autoklawizowany-beton-komorkowy/ (accessed 26st June, 2021). (In Polish.)
[6] PN-EN 12457-2:2006. *Charakteryzowanie odpadów – Wymywanie – Badanie zgodności w odniesieniu do wymywania ziarnistych materiałów odpadowych i osadów – Część 2: Jednostopniowe badanie porcjowe przy stosunku cieczy do fazy stałej 10 l/kg.* (In Polish.)
[7] *Microwave Plasma Atomic Emission Spectroscopy (MP-AES) Application eHandbook*. https://www.agilent.com/cs/library/applications/5991-7282EN_MP-AES-eBook.pdf
[8] *Elemental Analysis that Runs on Air Agilent 4210 MP-AES.* https://www.agilent.com/cs/library/brochures/5991-7237EN.pdf
[9] Sungur Ş., Gülmez F.: Determination of metal contents of various fibers used in textile industry by MP-AES. *Journal of Spectroscopy* **2015** (2015), 640271.
[10] Balaram V.: Microwave plasma atomic emission spectrometry (MP-AES) and its applications: A critical review. *Microchem. J.* **159** (2020), 105483.
[11] Schreiner J., Jansen D., Ectors D., Goetz-Neunhoeffer F., Neubauer J., Volkmann S.: New analytical possibilities for monitoring the phase development during the production of autoclaved aerated concrete. *Cem. Concr. Res.* **107** (2018), 247–252.

The perspectives of Relative Response Factors tabulation while alcoholic products analysis with GC-MS

Anton Korban[a, b, *]

[a] *Charles University, Faculty of Science, Department of Analytical Chemistry, Hlavova 8, 128 43 Prague 2, Czech Republic* ✉ *karbonat7@gmail.com*
[b] *Belarusian State University, Faculty of Chemistry, Department of Analytical Chemistry, Leningradskaya 14, 220050 Minsk, Belarus*

Keywords
alcoholic products
calibration
GC-MS
internal standard method
relative response factors

Abstract
This work assesses the use of relative response factors (RRFs) for the quality control of alcoholic products by GC-MS, using two internal standard (IS) methods. A standard IS method using 1-pentanol was compared with an "Ethanol as IS" method. The stability of RRF values for both methods was tested using standard solutions based on 20, 40, and 96% ethanol-water matrices. Within these three matrices, solutions of the ten most abundant volatile compounds were analyzed at four different concentrations (250, 500, 1000, and 5000 mg L^{-1} absolute alcohol, AA). Each solution was measured four times by GC-MS in SIM mode under repeatability conditions. Our results showed that the relative standard deviations of RRFs for all concentrations were found to be 8% for the standard method and 40% for the ethanol method.

1. Introduction

Gas chromatography (GC) is one of the most powerful separation and identification techniques used for volatile and semi-volatile chemicals in many fields of chemistry. The quality of analytical results directly relates to the quality of instrument calibration. There are several common methods of quantitative calibration, for example: internal standard, external standard (absolute graduation) and the standard addition method. Quantification of compounds requires the measurement of peak area and the relation to analyte quantity, i.e., knowledge of the response factor. It is simpler to carry out relative internal standard (IS) measurements than absolute ones. Absolute measurements require a calculation of the exact amount of sample injected into the chromatogram and therefore introduces an additional source of error. For this reason, the IS calibration method is the preferred technique and is widely used in various types of analysis.

This paper investigates the stability of calibration factors under IS usage, with a comparison of the standard IS method verses the "Ethanol as IS" method for the quality control of alcoholic products by GC-MS. The "Ethanol as IS" method has been demonstrated on numerous occasions to be precise, accurate, robust, and simple when compared to the standard IS method [1].

The action of relative response factors (RRFs) on flame-ionization detectors (FID) has already been studied. A good correlation between RRFs and combustion enthalpies was identified as well as the possibility of using RRFs for predictive purposes [2]. Analysis using GC-MS is more complex and consequently, the prediction of RRF is more difficult. One of the main reasons for this difficulty is the large variety of types of GC-MS instruments and their greater complexity. In addition, the selection of ion registration mode such as, SIM or TIC would also have a dramatic influence on the RRF value.

The purpose of this work is to compare the stability of RRF values for the two calibration methods while sample parameters vary i.e. when simulating routine laboratory work. The GC-MS quality control of alcoholic products was selected as the model for this analysis.

2. Experimental

2.1 Reagents and chemicals

In this paper the following common volatile compounds stated in EC protocols [3] were analysed: acetaldehyde, methyl acetate, ethyl acetate, methanol, 2-butanol, 1-propanol, 2-methyl-1-propanol (isobutanol), 1-butanol, acetal (1,1-diethoxy-ethane), and 3-methyl-1-butanol (isoamylol). 1-Pentanol was used as a standard IS as stated in [3]. All chemicals mentioned above and ethanol with 96.4% alcohol by volume (ABV) were of more than 99.5% GC purity (Sigma-Aldrich or Merck). Deionised water (18 MΩ·cm) was used for the preparation of the calibration solution.

2.2 Preparation of solutions

Solutions were prepared in the following way. Firstly, water-ethanol solutions (WES) of 20 and 40% ethanol content were prepared by mixing 96.4% ethyl alcohol with deionized water and were used together with 96.4% ethanol as matrices. Each matrix was spiked with 1-pentanol, the standard IS to approximately 600 mg L^{-1} AA as required according to the protocol [3]. 20 mL of the prepared matrix was taken for further dilutions. Secondly, volatile compounds were added to the matrix to reach a concentration of approximately 5000 mg L^{-1} AA (solution 5000). The weight of every single added substance, including water and ethanol, was recorded with analytical balances. Solution 5000 was then diluted 5, 10, and 20 times with the respective matrix to achieve volatile compound concentrations of 1000, 500 and 250 mg L^{-1} AA.

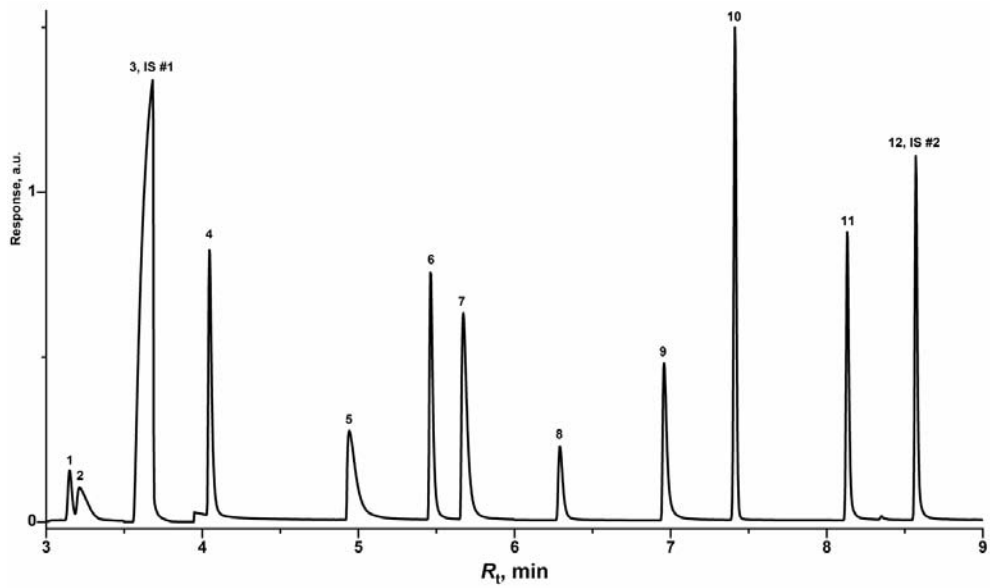

Fig. 1 Chromatogram of the solution 1000 in 40% matrix: (1) acetaldehyde, (2) methanol, (3) ethanol (IS #1), (4) methyl acetate, (5) 1-propanol, (6) ethyl acetate, (7) 2-butanol, (8)isobutanol, (9) 1-butanol, (10) acetal, (11) isoamylol, (12) 1-pentanol (IS #2).

2.3 Instrumentation

A Shimadzu GCMS-QP2010 Ultra equipped with a quadrupole type mass detector was used for chromatographic measurements. Prepared standard solutions of 0.5 µL volume were injected into the GC-MS system at 220 °C in the split (1:100) mode. Injection of solution 5000 could lead to saturation of the MS detector, therefore only 0.2 µL of each of the solution 5000 were injected. Rxi-1301 Sil MS capillary column (60 m length, 0.25 mm ID, and 0.25 µm phase thickness) was used with helium as the carrier gas (99.999% purity).

The following oven temperature program was used: 35 °C for 3 min, rising to 30 °C/min to 185 °C, hold for 4 min. The MS was used in electron ionization (EI) mode at 70 eV at an ion source temperature of 200 °C. The MS was operated in the single ion monitoring (SIM) mode. Example chromatogram of solution 1000 is presented in Fig. 1.

3. Results and discussion

3.1 Relative response factor variation for the same solution

If the solution is kept constant, any variation in measurement is a factor of the properties of the GC-MS instrument. Because RRF values for both methods were calculated from the same chromatogram we were able to assess the ability of the

instrument to achieve a constant A_{IS}/A_i ratio for 1-pentanol IS and ethanol IS (the C_i/C_{IS} ratio remains constant for the same solution). During four repeatable GC measurements the results showed (that without taking into account the exact matrix or concentration of volatile compound), the RRF value had a *RSD* of 0.9±0.3% and 0.6±0.2% for the "Ethanol as IS" method and standard IS method.

3.2 Relative response factor variation within the same matrix

It is important to understand how RRFs alter because of the variations in concentration of volatile compounds within the same matrix. By this test we revealed, if the selection of IS is significant when the concentration of a volatile compound is changed. Because in all matrices the solution 5000 was measured under different conditions, e.g., injected volume of 0.2 µL instead of 0.5 µL for the others, two concentration ranges were considered, 250–1000 mg L^{-1} AA and 250–5000 mg L^{-1} AA.

3.2.1 96% matrix

When using ethanol as the IS, *RSD* values of RRFs were, 0.9±0.4% for the 250–1000 mg L^{-1} AA range and 10.1±0.6% for the 250–5000 mg L^{-1} AA range. For the standard IS method, *RSD* values of RRFs were 0.9±0.4% for 250–1000 mg L^{-1} AA range and 0.9±0.5% for 250–5000 mg L^{-1} AA range. The results showed the same RRF variation in 250–1000 mg L^{-1} AA range for both methods. However, in case of a higher concentration range "Ethanol as IS" method showed a 25% increase in RRF values and thus 10% higher *RSD*. This occurred for all volatiles except acetaldehyde.

The above results do not include data for acetaldehyde because it exhibited an increase in up to 45% in RRF for both methods. The reason for this was the high reactivity of acetaldehyde and its disposition to form secondary products, e.g., oligomers and acetals. It is important that researchers and analytical laboratory technicians keep this fact in mind during their routine work.

3.2.2 40% matrix

For the "Ethanol as IS" method *RSD* values of RRFs were, 1.3±0.4% for the 250–1000 mg L^{-1} AA range and, 3.5±1.2% for the 250–5000 mg L^{-1} AA range. For the standard IS method *RSD* values of RRFs were, 1.9±0.6% for 250–1000 mg L^{-1} AA range and 3.2±1.2% for 250–5000 mg L^{-1} AA range. In this experiment the "Ethanol as IS" method showed comparable or slightly better results than the standard method.

Table 1
Summary of results of *RSD*s of relative response factors values.

Ethanol content in matrix	Concentration range			
	250–1000 mg L^{-1} AA		250–5000 mg L^{-1} AA	
	IS ethanol	IS 1-pentanol	IS ethanol	IS 1-pentanol
20%	6.9±0.7	5.7±0.5	10.1±1.3	10.2±1.7
40%	1.3±0.4	1.9±0.6	3.5±1.2	3.2±1.2
96%	0.9±0.4	0.9±0.4	10.1±0.6	0.9±0.5

3.2.3 20 % matrix

For the "Ethanol as IS" method *RSD* values of RRFs were, 6.9±0.7 % for the 250–1000 mg L^{-1} AA range and 10.1±1.3% for the 250–5000 mg L^{-1} AA range. For the standard IS method *RSD* values of RRFs were 5.7±0.5% for 250–1000 mg L^{-1} AA range and 10.2±1.7% for the 250–5000 mg L^{-1} AA range. The presented data does not include results for methanol (as results appeared anomalous); *RSD* of methanol within the 20% matrix was more than 40% for both IS methods. A summary of *RSD*s for all matrices is presented in Table 1.

3.3 Variation within different concentration and matrices

The generalized stability was assessed during the experiment and included all 12 RRF values obtained for standard solutions of different concentrations and matrices. By using this test we were able to reveal how RRF values change for a wide range of ABV and volatile concentrations. Within all prepared standard solutions *RSD* of RRF values of any volatile compound appeared to be 38.8±3.3% and 7.8±1.0% for both the "Ethanol as IS" method and the standard IS method. The results do not include data for acetaldehyde and methanol as their behaviour deviated significantly from the rest of the compounds.

4. Conclusions

The research in this paper recorded changes in RRF values during the analysis of alcoholic products using GC-MS with standard IS and ethanol IS methods. It was shown that within a 20–96% ABV and 250–5000 mg L^{-1} AA volatile concentration range, the resultant RRFs for the standard IS method (8% *RSD*) were more stable than those for the ethanol IS method (40% *RSD*). However, for 40% and 96% ABV matrices, the ethanol and standard IS methods showed nearly the same *RSD*s variation of no more than 1.5% within the 250–1000 mg L^{-1} AA volatile compounds concentration range. Similar RRF stability under a wider concentration range would be achieved only when injections are made under identical conditions, particularly, with the same injection volume.

It should be also noted that 1-pentanol was initially added to each matrix and the concentration was identical for all solutions within each ABV level. The additional errors and biases caused by manual addition of standard IS will certainly occur during routine usage of the standard IS method. The results presented in this paper demonstrated the better metrological properties of the standard IS method than they may show during use in the laboratory.

Although the ethanol IS method demonstrated poorer RRF stability than the standard IS method the former is still recommended as a worthwhile method in practice. The reasons for this are, the method requires no manual addition of IS, and there is no necessity to establish strength and density of the testing sample which is required in the standard IS method. Using ethanol as an IS method has the distinct advantage of being the more rapid than standard IS and is the cheapest method for analysis of alcoholic products, especially using GC-FID. For optimizing the use of ethanol as an IS with GC-MS, additional studies should be conducted so that RRF behaviour can be better predicted. This would enable the development of a more reliable application model for this type of instrumentation.

Acknowledgments

This work was financially supported by the Visegrad Fund.

References

[1] Charapitsa S., Sytova S., Korban A., Sobolenko L., Egorov V., Leschev S., Zakharov M., Čabala R., Busarova R., Shestakovich I., Tolstouhova A., Ondroušek S., Vávra J., Yilmaztekin M., Cabaroglu T.: Interlaboratory study of ethanol usage as an internal standard in direct determination of volatile compounds in alcoholic products. *BIO Web Conf.* **15** (2019), 02030.

[2] Tissot E., Rochat S., Debonneville C., Chaintreau A.: Rapid GC-FID quantification technique without authentic samples using predicted response factors. *Flav. Fragr. J.* **27** (2012), 290–296.

[3] Commission regulation (EC) No 2870/2000 laying down Community reference methods for the analysis of spirits drinks. *Official Journal of the European Communities* **L333** (2002), 20.

Analytical strategies for carotenoids determination in vegetables

Aliaksandra Kharoshka*, Tomáš Kouřimský, Věra Schulzová, Jana Hajšlová

University of Chemistry and Technology Prague, Faculty of Food and Biochemical Technology, Department of Food Analysis and Nutrition, Technická 3, 166 28 Prague 6, Czech Republic
✉ *kharosha@vscht.cz*

Keywords
carotenoids
certified reference material
HPLC-DAD
SFC-MS
vegetables

Abstract
Carotenoids are lipophilic bioactive compounds that can be challenging to analyse. Thus, it is very important to find correct extraction procedure, separation and detection techniques. In this study, we compared HPLC-DAD and SFC-MS methods on vegetable samples as well as certified reference material (CRM). It was found that the results of CRM analysis from both methods were close or in range of the reported values. Therefore, both techniques are applicable for carotenoids analysis, however, each has its advantages and drawbacks that were described in this work.

1. Introduction

Carotenoids are bioactive compounds that are widely found in nature as natural pigments with yellow to red colour. It is a group of lipophilic compounds with polyene backbone that can be divided into two main classes based on their chemical structures: carotenes and xanthophylls. The major representors of the carotenes are β-carotene and lycopene, xanthophylls – lutein or its isomer zeaxanthin. In nature there are around 700 carotenoids found mostly in plants, algae and microorganisms [1, 2].

The analysis of carotenoids can be challenging because these compounds are usually structural isomers or differ just in the number of hydroxyl groups. Carotenoids can be extracted from plants with or without hydrolysis. However, to ensure the analysis of all available carotenoids present in the sample hydrolysis is required. This results in release of carotenoids bound to proteins or fatty acids. However, such extraction procedure can result in losses because carotenoids are unstable compounds that degrade in the presence of light and heat [3]. As to analysis, the best separation of carotenoids can be achieved using liquid chromatography that is capable of isomers separation. Nevertheless, the result is based on the column chosen as well as mobile phase. The most used columns are reverse phase C18 and C30 columns. The most popular detectors in carotenoids analysis are UV-Vis detector, diode array detector and mass spectrometer. The first

one can be used in simple analysis of total carotenoid content as such detector does not allow one to obtain more information. Diode array detector (DAD) is considered as a simple and reliable option allowing precise measurements at relatively low concentrations. Application of MS opens new horizons in analysis allowing carotenoids profiling in samples. Possibly the best combination would be diode array detector coupled with mass spectrometer to ensure the most information about the analytes is available [1–6].

In this study we applied high-performance liquid chromatography with diode array detector (HPLC-DAD) and supercritical fluid chromatography coupled with mass spectrometer (SFC-MS) on several vegetable samples as well as certified reference material. The goal was to compare how two combinations of different separation techniques and detectors can be used for analysis of the same sets of samples.

2. Experimental

2.1 Reagents and chemicals

Lutein (purity 95%) was purchased from Labicom (Czech Republic), β-carotene (purity ≥ 99%), and *trans*-β-apo-8′-carotenal (purity ≥ 96%) were purchased from Sigma-Aldrich (Germany). Methanol, ethanol, and *n*-hexane were purchased from Merck (Germany), acetonitrile and *tert*-butyl-hydroxytoluene (*t*-BHT) from Sigma-Aldrich (Germany). Sodium hydroxide and sodium sulphate were obtained from Lach-Ner (Czech Republic), acetone from Penta Chrudim (Czech Republic). Water was purified using a Milli-Q Ultrapure water purification system (Millipore, Germany).

Certified reference material CRM BCR® 485 (mixture of lyophilized vegetables), European commission – Joint Research Centre from Sigma-Aldrich (Germany) was purchased to ensure the precision of the methods chosen.

2.2 Sample preparation

The first sample preparation procedure required alkaline hydrolysis. After samples were weighed to a plastic cuvette covered with aluminium foil to prevent photodegradation, internal standard *trans*-β-apo-8′-carotenal was added, then mixture of ethanol (0.2% *t*-BHT)/acetone = 6:4 (*v/v*) and pure *n*-hexane were added. After intense shaking next portion of solvents was added and sample was vortexed. The hydrolysis was started by adding appropriate amount of methanolic potassium hydroxide (concentration 20 g L^{-1}). Cuvettes were filled with nitrogen gas and left overnight at room temperature. The next day each sample was extracted with *n*-hexane until hexane layer became colourless. Hexane from each sample was evaporated following with the residue reconstitution in ethanol (0.2% *t*-BHT)/acetone = 6:4 (*v/v*). Sample was filtered through a centrifuge microfilter, and solution was transferred to an amber vial.

Sample preparation without hydrolysis was similar but with some exceptions. In the beginning, mixture of ethanol (0.2% *t*-BHT)/*n*-hexane = 1:1 (*v/v*) was added to the weighed sample. The cuvette was covered with aluminium foil and coated with parafilm. Each sample was shaken for 30 minutes. After that deionized water was added to separate the layers and the mixture was centrifuged. The rest of the procedure was the same as the one described above.

2.3 Instrumentation

2.3.1 HPLC-DAD determination

High-performance liquid chromatograph (Agilent Technologies 1200 series, USA) coupled with a diode array detector was used for sample analysis. The separation was done using reverse phase column Poroshell 120 EC-C18 (100×2.1 mm; 2.7 µm, Agilent Technologies, USA). Mobile phase was acetonitrile/water = 9:1 (*v/v*) (A) and pure acetonitrile (B) with gradient elution.

2.3.2 SFC-MS determination

Waters Acquity UltraPerfomance Convergence Chromatography (UPC^2) system (Waters, USA) coupled to hybrid mass spectrometer Q-TOF (SYNAPT G2-Si, Waters, USA) was applied to the analysis of the same sample sets. Separation was done using column Viridis HSS C18 SB (100×3 mm; 1.8 µm; Waters, USA). Mobile phase was carbon dioxide (A) and methanol/ethanol = 1:2 (*v/v*) (B) with gradient elution. Measurement was done using time-of-flight (TOF) analyzer.

For both analytical techniques the identification was based on comparison of *m/z* values or absorption spectra and retention times of the measured substances with the standards. Quantification was done using external calibration.

3. Results and discussion

In this study sets of vegetable samples were prepared and analysed using two analytical methods that utilize different separation principles and detectors. Spinach, green peas and carrots were chosen as vegetable samples. All the results were expressed on dry matter.

For both methods extraction procedure with hydrolysis was applied because the procedure without hydrolysis was not sufficient enough. Nevertheless, samples without hydrolysis can be analysed using SFC-MS to possibly determine bound forms of carotenoids.

Using HPLC-DAD method it was possible to quantitatively determine lutein and β-carotene. The limits of quantification were 1.8 mg kg^{-1} for lutein and 3.7 mg kg^{-1} for β-carotene. Using SFC-MS it was also possible to quantitatively determine lutein and β-carotene. Because mass spectrometer is more sensitive detector, limit

Table 1
Carotenoid content in mg kg^{-1} dry matter in vegetables determined using HPLC-DAD and SFC-MS.

Sample		Lutein		β-carotene	
		HPLC-DAD	SFC-MS	HPLC-DAD	SFC-MS
Spinach	Winter	530±50	455±40	682±66	379±35
	Spring	761±72	635±57	889±86	485±44
Green peas		52±6	55±6	41±5	52±6
Carrot	Orange	32±5	35±5	1877±94	1686±79
	Yellow	109±17	97±14	123±6	133±6
	Purple	41±6	32±5	43±2	26±1

Table 2
Carotenoid content in mg kg^{-1} dry matter in certified reference material determined using HPLC-DAD and SFC-MS.

	Lutein	β-carotene
CRM Certificate	12.5±0.8	25.6±1.2
HPLC-DAD	12.1±0.3	21.9±0.5
SFC-MS	11.8±0.1	29.7±0.5

of quantification (LOW) was 1 mg kg^{-1} for both analytes. Repeatability was expressed as relative standard deviation (in %) and was similar for both techniques. Relative standard deviations were from 5 to 15% depending on the natural content of the analyte in vegetable. Resulted content in analysed samples, expressed in mg kg^{-1} dry matter, is summarized in Table 1.

The results of CRM analysis from both methods were compared with the certificate. It can be said that both methods were proved as precise. The values in mg kg^{-1} dry matter are listed in Table 2.

Using HPLC-DAD four carotenoids were found. Besides lutein and β-carotene, lycopene and α-carotene were detected. When the measurement was done using SFC-MS, other carotenoids were observed in the sample. Those were before mentioned lycopene, zeaxanthin, and capsanthin. To prove their presence *m/z* values and retention times of analytes were monitored. Some other carotenoids were found but it was not possible to identify them. Possibly carotenoid astaxanthin was also present in the CRM. The chromatograms of CRM measured using HPLC-DAD and SFC-MS are presented in Fig. 1 and 2.

The main advantage of HPLC-DAD was availability of absorption spectra for each sample as well as overall work with the instrument. It can be said that such instrumentation is easier to work with for non-advanced users. On the other hand, SFC-MS method was faster and provided with information about all extracted compounds. Application of SFC-MS showed huge potential in possible profiling of carotenoids. However, it is impossible to identify the compound based on *m/z* value as many carotenoids are isomers, therefore, standards are needed. As a possibility for improvement, tandem mass spectrometry (MS/MS) can be used.

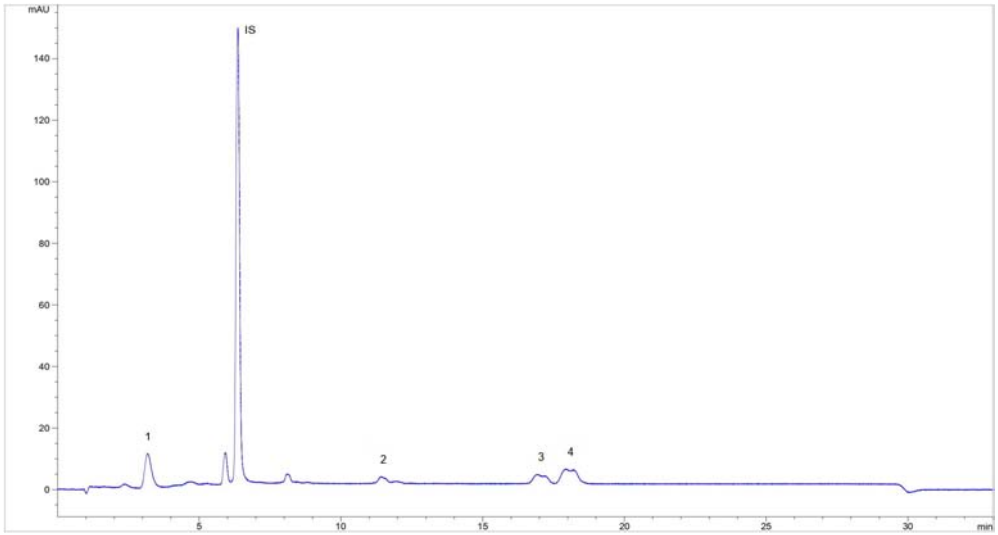

Fig. 1 Chromatogram of CRM obtained using HPLC-DAD measured at 450 nm: (1) lutein, (2) lycopene, (3) α-carotene, (4) β-carotene, (IS) *trans*-β-apo-8′-carotenal.

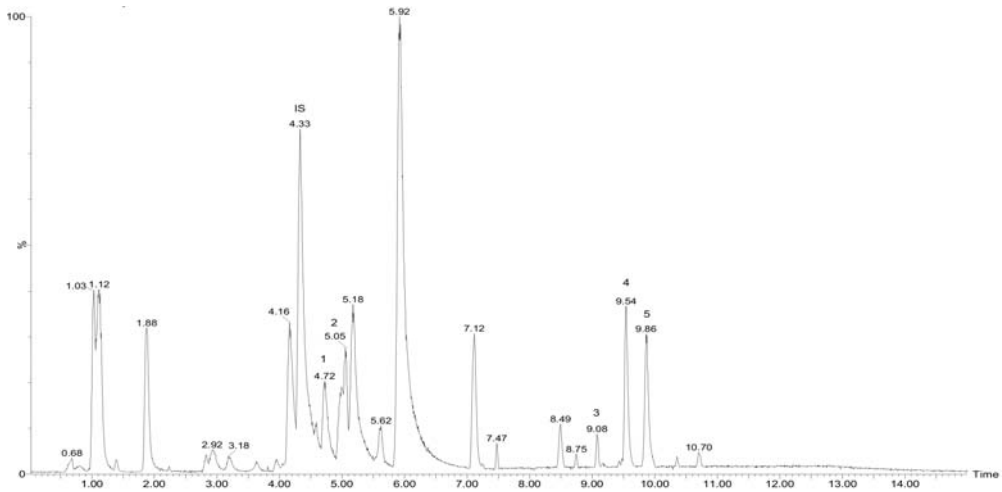

Fig. 2 Base peak chromatogram of CRM obtained using SFC-MS: (1) lycopene, (2) β-carotene, (3) capsanthin, (4) lutein, (5) zeaxanthin, (IS) *trans*-β-apo-8′-carotenal.

4. Conclusions

We have found that both HPLC-DAD and SFC-MS methods are good for routine analysis of several major carotenoids. Both methods were compared by the analysis of certified reference material and the results were similar to the certified ones. HPLC-DAD method was easy to use, analysis provided additional information for each compound. Limits of quantification were low enough for naturally

occurring carotenoids. However, there were some limitations. For example, lutein, and zeaxanthin were not separated using C18 column. In addition, the analysis takes almost 30 minutes. As to the second method, SFC-MS, the results were comparable to those from HPLC-DAD but the LOQs were lower. One sample run takes only 15 minutes which makes SFC-MS method faster with lower consumption of mobile phase. Usage of MS detector showed that other carotenoids were present. Overall, each method has its own advantages and disadvantages, but both give precise results.

Acknowledgments

This work was supported by student scientific research project "Impact of vegetable processing and storage on levels of bioactive substances, A2_FPBT_2021_033". The author thanks the Department of Food Analysis and Nutrition of UCT Prague for the contribution for the research.

References

[1] Amorim-Carrilho K.T., Cepeda A., Fente C., Regal P.: Review of methods for analysis of carotenoids. *TrAC, Trends Anal. Chem.* **56** (2014), 49–73.

[2] Saini R.K., Nile S.H., Park S.W.: Carotenoids from fruits and vegetables: Chemistry, analysis, occurrence, bioavailability and biological activities. Food Res. Int. **76** (2015), 735–750.

[3] Jumaah F., Plaza M., Abrahamsson V., Turner C., Sandahl M.: A fast and sensitive method for the separation of carotenoids using ultra-high performance supercritical fluid chromatography-mass spectrometry. *Anal. Bioanal. Chem.* **408** (2016), 5883–5894.

[4] Bhave A., Schulzová V., Mrnka L., Hajšlová J.: Influence of harvest date and postharvest treatment on carotenoid and flavonoid composition in French marigold flowers. *J. Agric. Food Chem.* **68** (2020), 7880i7889.

[5] Giuffrida D., Donato P., Dugo P., Mondello L.: Recent analytical techniques advances in the carotenoids and their derivatives determination in various matrixes. *J. Agric. Food Chem*. **66** (2018), 3302–3307.

[6] Regal P., Lamas A., Fente C.A., Franco C.M., Cepeda A.: Analysis and metabolomics of carotenoids. In: *Carotenoids: Properties, Processing and Applications*. C. Galanakis (ed.). London, Academic Press 2020, p. 189–222.

Author Index

Keyword Index

Proceedings of the 17th International Students Conference "Modern Analytical Chemistry"

Edited by Karel Nesměrák.
Published by Charles University, Faculty of Science.
Prague 2021.
1st edition – vi, 250 pages

ISBN 978-80-7444-089-2

ISBN 978-80-7444-089-2